FZD-459

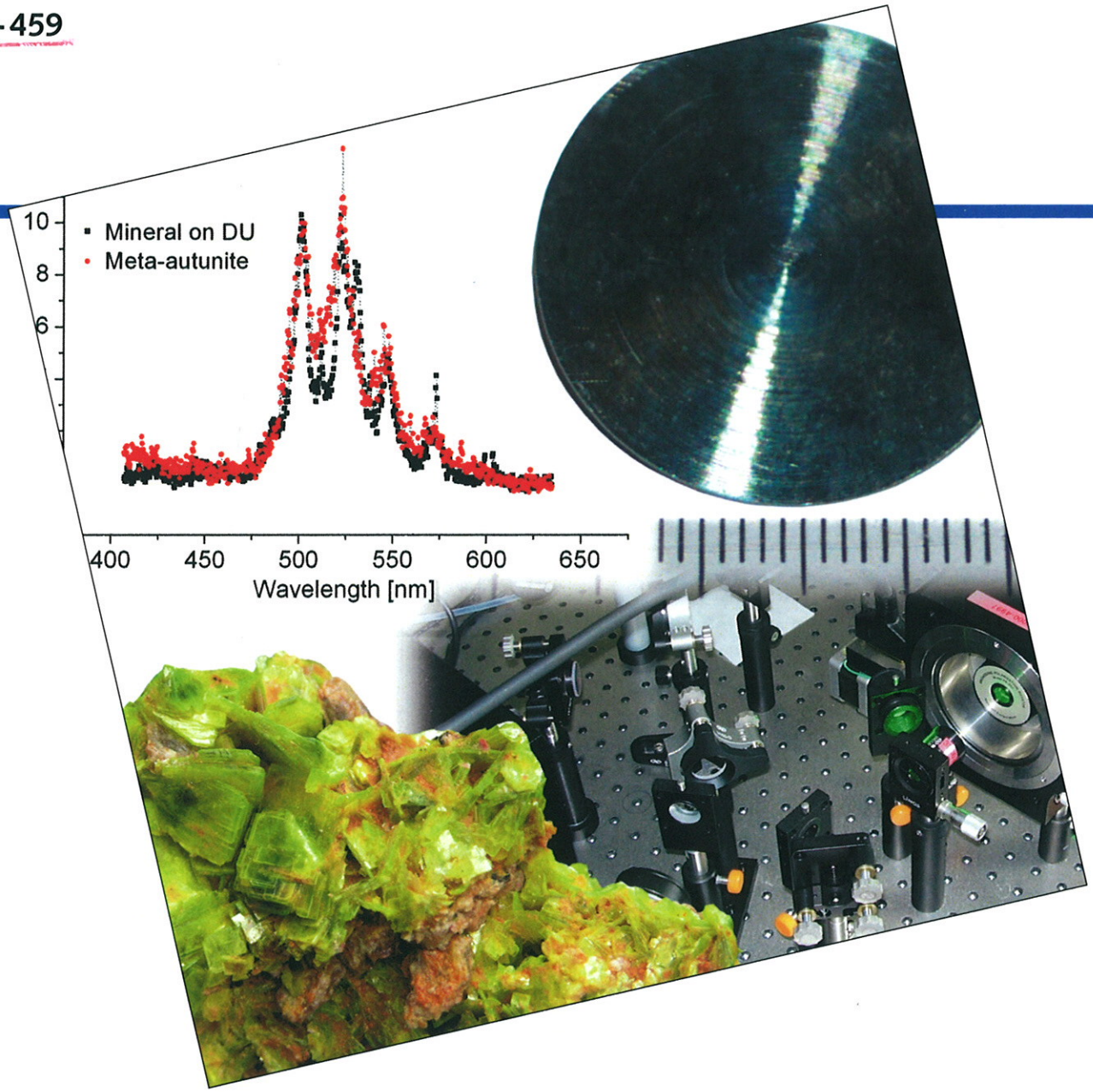

Wissenschaftlich-Technische Berichte
FZD-459 2007 · ISSN 1437-322X

ANNUAL REPORT 2006

INSTITUTE OF RADIOCHEMISTRY

Forschungszentrum
Dresden Rossendorf

Wissenschaftlich-Technische Berichte
FZD-459
2007

Annual Report 2006

Institute of Radiochemistry

Editor: **Prof. Dr. G. Bernhard**

Editorial staff: **Dr. H. Foerstendorf**
Dr. A. Richter
Dr. K. Viehweger

Forschungszentrum
Dresden Rossendorf

Contact

Forschungszentrum Dresden-Rossendorf
Institut für Radiochemie

Postal Address	*Address for visitors*
P.O. Box 51 01 19	Bautzner Landstraße (SW) 128
D-01314 Dresden	D-01328 Dresden
Germany	Germany

Phone: ++49 (0) 351 260 3210
Fax: ++49 (0) 351 260 3553
http://www.fzd.de/FWR
e-mail: contact.radiochemistry@fzd.de

This report is also available at http://www.fzd.de/FWR

Cover picture

The surface of a depleted uranium disc immersed in a calcium-phosphate solution – representing pore water concentrations of agricultural soils – was analyzed by time-resolved laser-induced fluorescence spectroscopy (TRLFS). The gained spectra were compared with fluorescence spectra from natural occurring uranium minerals and were identified as meta-autunite (see p. 68).

Preface

The Institute of Radiochemistry (IRC), one of the six institutes of the Forschungszentrum Dresden-Rossendorf (FZD) performs basic and applied research in the fields of radiochemistry and radioecology. Motivation and background of our research are environmental processes relevant for the installation of nuclear waste repositories, for remediation of uranium mining and milling sites, and for the assessment of radioactive contaminations caused by nuclear accidents and fallout. Because of their high radiotoxicity and long half-life the actinides are of special interest. The research is focused on a better understanding of the chemical behavior of actinides in the environment on a molecular level. We will increase our efforts to study both the speciation of actinides on bio-molecular interfaces and their transport in bio-systems.

Current topics of our research work are:

- Aquatic chemistry of actinides
- Actinides in bio-systems
- Interaction of actinides with solid phases

About 70 scientists, technicians and PhD students are employed at the IRC. We accomplished many new scientific results in the past year, which are presented in this annual report. Among them only a few can be highlighted in this preface.

Further progress was achieved in understanding the formation and characterization of uranium contaminated biofilms. For the first time we succeeded in the in-situ determination of different uranium oxidation states U(VI) and U(V) in a biofilm of a mixed bacterial culture.

Studies about the interaction of actinides with different bacterial strains improved our understanding about the different binding in biological systems. Pyoverdins excreted by especial bacteria are strong complexing agents for actinides.

We were very successful in the determination of formation pathways and structure of various actinides with bio-relevant ligands. These results contribute to a better understanding of actinide speciation during the transfer from geo- into bio-systems, especially with respect to the chemical processes on the interfaces and in biofluids.

We strengthened our research about behavior of depleted uranium ammunition in soils. It could be shown, that in dependence on soil composition and properties of pore water different secondary mineral phases were formed. By luminescence spectroscopy uranium phosphates, carbonates and hydroxides were identified.

Natural clay formations can serve as a host formation for nuclear waste repositories in the deep underground. Our investigations about interaction, sorption, and diffusion of actinides in clay demonstrated, that the presence of humics contained in clay influence the migration of different actinides in a variable way.

Furthermore we can report that our own radiochemical experimental facilities – the Rossendorf Beamline at ESRF (ROBL), the radiochemical laboratory at the Free-Electron Laser facility FELBE, and our various high-power laser systems – are continuously working on a high quantitative and qualitative level. These methods are the basis for excellent scientific results of our researchers and external users.

I would like to thank the visitors, German and international ones, for their interest in our research and for their participation in the institute seminars. We would also like to thank our scientific collaborators and the visiting scientists for coming to Dresden-Rossendorf in 2006 to share their knowledge and experience with us. We continue to strongly encourage the collaborations and visits by scientists in the future. Special thanks are due to the executive board of the Forschungszentrum Dresden-Rossendorf, the Ministry of Science and Arts of the State Saxony, the Federal Ministry of Education and Research, the Federal Ministry of Economics and Technology, the Deutsche Forschungsgemeinschaft, the European Commission, and other organizations for their support.

Prof. Dr. Gert Bernhard

Contents

SCIENTIFIC CONTRIBUTIONS

Part I: Aquatic chemistry of actinides

Part II: Actinides in bio-systems

Part III: Interaction of actinides with solid phases

PUBLICATIONS

SCIENTIFIC ACTIVITIES

Aquatic chemistry of actinides

Aqueous U(VI) species characterized by ATR-FTIR spectroscopy. Part I

K. Müller, H. Foerstendorf, V. Brendler

The aqueous hydroxo species of uranium(VI) at different concentrations (5 – 0.005 mM UO_2^{2+}) were studied by attenuated total reflectance Fourier-transform infrared (ATR-FTIR) spectroscopy. Upon lowering the UO_2^{2+} concentration at pH 4 the speciation of U(VI) in solution changes and the formation of hydroxo complexes is proposed.

The uranium(VI) ion bound in crystalline salts, minerals and dissolved in saturated solutions has been the subject of previous vibrational spectroscopic investigations [1,2]. Raman spectroscopy has mainly been used to study the uranyl complexation in aqueous systems, because of the difficulty to obtain IR spectra of aqueous solutions. ATR-FTIR spectroscopy allows the direct measurement of liquid samples and provides additional important spectral information. Current knowledge about aqueous U(VI) species is mainly based on thermodynamical calculations relying on data obtained by non-structural experiments such as potentiometric titration [3]. A spectroscopic verification of these U(VI) speciations is still lacking. In previous vibrational spectroscopic studies only UO_2^{2+} solutions with concentrations > 100 mM were investigated [4]. In this study we focus on the micromolar concentration range which is more relevant for environmental samples.

EXPERIMENTAL. The diluted U(VI) solutions were prepared from a 0.05 M stock solution using high purity double deionized water. Solution pH was adjusted to pH 4 by adding small amounts of 1 M and 0.1 M NaOH and NaCl, respectively. ATR-FTIR spectra of aqueous solutions were measured on a Perkin Elmer GX-2000 spectrometer. Spectral resolution was 4 cm^{-1} and spectra were averaged from 128 scans. The used ATR accessory (DURA SamplIR II, Smiths) is a horizontal diamond crystal with nine internal reflections. For adequate subtraction of the background a flow cell was used which allows an exchange of the sample solution with minimal external interference of the equilibrated system which was found to be an indispensable prerequisite for the detection of low absorption changes. Sample preparation and analysis were done under normal atmosphere.

RESULTS. In Fig. 1 the infrared spectra of aqueous U(VI) solutions at pH 2 (a) and at pH 4 (b-e) are shown. The uranyl concentration in solution at pH 4 ranged from 5 mM (Fig. 1b) to 5 µM (Fig. 1e), at pH 2 it was 10 mM. All spectra provide strong infrared absorption between 1000 and 880 cm^{-1}, which is related to the asymmetric stretching vibration (ν_3) of the UO_2^{2+}. At pH 2 a distinct band at 961 cm^{-1} is detected (Fig. 1a). At pH 4 and concentrations from 5 to 0.5 mM two partially overlapping bands with maxima at 961 and 935 cm^{-1} are observed (Fig. 1b,c). At concentrations below 0.5 mM the band at 961 cm^{-1} is no longer found whereas a band at 922 cm^{-1} is now observed. Simultaneously, in the spectra of the lower UO_2^{2+} concentrations two bands at 1460 and 1520 cm^{-1} become increasingly distinct (Fig. 1d,e).

DISCUSSION. In a previous IR study carried out at pH 4 and at higher UO_2^{2+} concentrations three U(VI) species

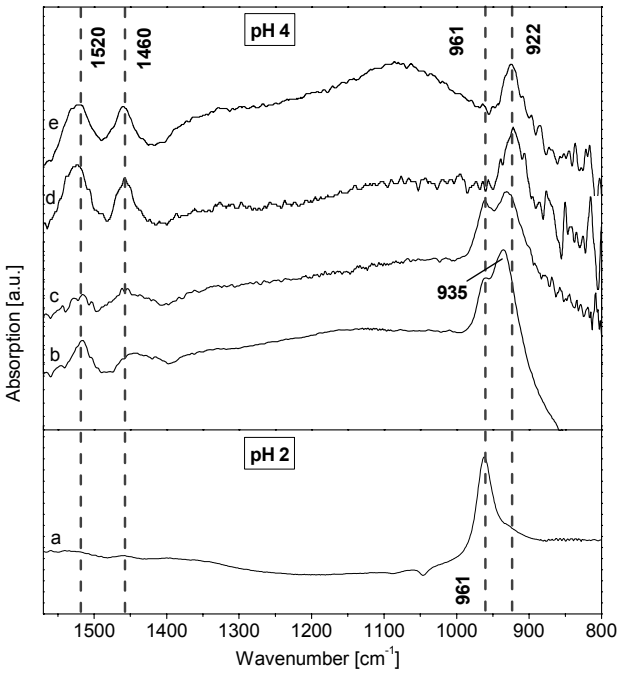

Fig. 1: ATR-FTIR spectra of U(VI) solutions at pH 2: (a) 10 mM, and at pH 4: (b) 5 mM, (c) 0.5 mM, (d) 0.05 mM, (e) 0.005 mM. Indicated values are in cm^{-1}.

showing overlapping absorption bands with maxima at 961, 943 and 923 cm^{-1} were identified [4]. The band at 961 cm^{-1} is assigned to the free UO_2^{2+} cation which is the only UO_2^{2+} species in solutions at very low pH values. The fraction of this species seems to be considerably reduced at concentrations lower than 50 µM since no band at 961 cm^{-1} can be detected (Fig. 1 upper traces). This is in clear contrast to aforementioned calculated U(VI) speciations [3].

An unequivocal assignment of the bands at 935 and 922 cm^{-1} to distinct uranyl species cannot be given so far. However, the spectra presented here clearly indicate the formation of two additional species. The appearance of the bands at 1460 and 1520 cm^{-1} correlates with the band at 922 cm^{-1} and is tentatively interpreted as a different hydroxo species of the uranyl cation compared to the species represented by the band at 935 cm^{-1}. This species contributes already to the spectra shown in Fig 1b,c, where the species with absorption maximum of 935 cm^{-1} is predominant.

The obtained spectral data constitute a reference to a modified speciation at different U(VI) concentrations in diluted aqueous solutions. Further IR spectroscopic investigations deal with the U(VI) hydrolysis species at higher pH levels [5].

ACKNOWLEDGEMENT. This work was supported by the Deutsche Forschungsgemeinschaft (Fo 619/1-1).

REFERENCES

[1] Brooker, M.H. et al. (1980) *J. Inorg. Nucl. Chem.* **42**, 1431-1440.
[2] Amayri, S. et al. (2004) *Can. Mineral.* **42**, 953-962.
[3] Guillaumont, R. et al. (2003) *Update on the Chemical Thermodynamics of U, Np, Pu, Am and Tc*, Elsevier, Amsterdam.
[4] Quiles, F. et al. (2000) *Vib. Spec.* **23**, 231-241.
[5] Müller, K. et al. this report, p. 12.

Aqueous U(VI) species characterized by ATR-FTIR spectroscopy. Part II

K. Müller, H. Foerstendorf, V. Brendler

The hydrolysis of uranium(VI) in aqueous solutions with a concentration of 20 µM in the pH range from pH 2 to 8.5 was studied by attenuated total reflectance Fourier-transform infrared (ATR-FTIR) spectroscopy.

The speciation of the uranium(VI) in aqueous solution in the micromolar concentration range is still lacking independent spectroscopic verifications. Referring to thermodynamical calculations predominantly based on potentiometric data, the uranyl ion is expected to form hydroxo- and carbonato-complexes at pH > 4 [1]. The aim of this study was to investigate the speciation of strongly diluted uranyl solutions over a wide pH range, using ATR-FTIR spectroscopy.

EXPERIMENTAL. The diluted 20 µM U(VI) solutions (0.1 M NaCl) were prepared and analyzed using ATR-FTIR spectroscopy as described in [2].
Additionally, a 5 mM $UO_2(CO_3)_3^{4-}$ model solution was prepared as a reference. Small aliquots of the 0.05 M uranyl stock were added to a 0.1 M $NaHCO_3$ solution (pH 8.8) with subsequent pH adjustment.

RESULTS. ATR-FTIR spectra of 20 µM uranyl solutions at distinct pH values are shown in Fig. 1. All spectra exhibit spectral features between 1000 and 880 cm^{-1} representing the asymmetric stretching vibration (ν_3) of the UO_2^{2+} cation. Below pH 3 one band at 961 cm^{-1} was observed. Between pH 3.2 and 6.5 a band at 922 cm^{-1} dominates. With increasing solution pH the band maximum shifts to lower wavenumbers and is found at 905 cm^{-1} at pH > 7.2. Furthermore, it is broadened with increasing pH. At pH > 2.5 additional bands are observed around 1520 and 1460 cm^{-1}. At pH > 7.2 another broad band is showing up at 1365 cm^{-1}.

DISCUSSION. The band at 961 cm^{-1} at very low pH (Fig. 1, upper traces) clearly represents the uncomplexed UO_2^{2+} species. In the spectrum obtained at pH 3.2 this band is not observed anymore, indicating that in the 20 µM solutions the free uranyl ion is dominant only at pH < 3. This is in contrast to calculated speciations. The strong shift of the uranyl band from 961 to 922 cm^{-1} as well as the appearance of additional bands at 1520 and 1460 cm^{-1} clearly indicate significant contributions of new UO_2^{2+} species at pH 3.2. We suggest the formation of not yet identified hydroxo complexes. Obviously, the ATR-FTIR spectra do not agree with the thermodynamical calculations concerning the pH predominant region of aqueous uncomplexed and hydroxo-complexed U(VI) species. One reason could be incorrect complexation constants, which constitute the base of the calculations and were only obtained by non-structural experiments [1]. It is also quite conceivable that we identified new U(VI) species in aqueous diluted solutions.
In the spectrum recorded at pH 7.2 the uranyl band undergoes a further shift to lower frequencies (905 cm^{-1}) indicating the formation of another uranyl species possibly with contributions of carbonate anions. For this reason a model spectrum of the pure $UO_2(CO_3)_3^{4-}$ complex at 5 mM UO_2^{2+} concentration is shown in Fig. 2. This spectrum supports the suggestion that the spectra at higher pH show contributions from uranyl species with carbonate ligands. The uranyl band is shifted to around 905 cm^{-1} and a band around 1365 cm^{-1} shows up possibly representing the υ_s CO_3^{2-} mode.

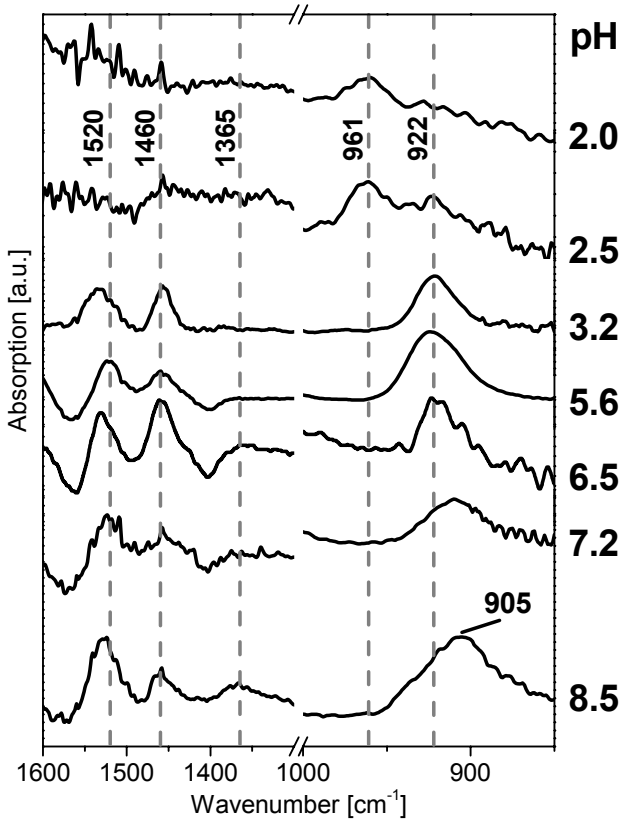

Fig. 1: ATR-FTIR-spectra of 20 µM U(VI) solutions at different pH values. Indicated values are in cm^{-1}.

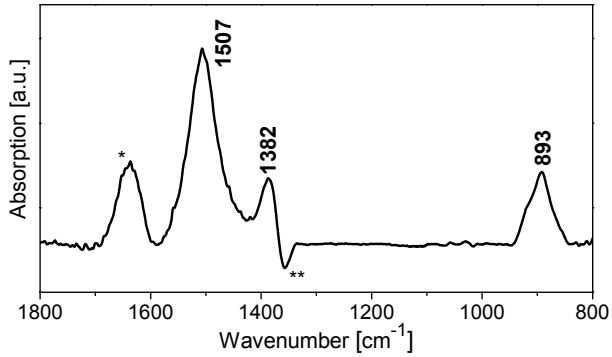

Fig. 2: ATR-FTIR-spectrum of 5 mM U(VI) solution in 0.1 M HCO_3^- at pH 8.8. * indicates water vibration, ** indicates excess of carbonate in solution.

ACKNOWLEDGEMENT. Financial support by the Deutsche Forschungsgemeinschaft (H.F.) is greatly acknowledged.

REFERENCES

[1] Guillaumont, R. et al. (2003) *Update on the Chemical Thermodynamics of U, Np, Pu, Am and Tc*, Elsevier, Amsterdam.
[2] Müller, K. et al. this report, p. 11.

Aqueous U(VI) hydrolysis species characterized by TRLFS

V. Brendler, S. Sachs

A new set of TRLFS experiments allowed the assignment of typical spectra to the major uranium(VI) hydrolysis species, taking into account the shift in speciation patterns triggered by the updated NEA thermodynamic database as of 2003.

In 2003 a major update of the NEA thermodynamic database for U, Np, Pu, and Am was issued [1]. With respect to the uranium(VI) hydrolysis important changes of some hydrolysis constants (namely that for the neutral $UO_2(OH)_2$(aq) species) were reported compared to the previous database release [2]. Considerable changes in the speciation pattern in the intermediate pH region result, as Fig. 1 illustrates.

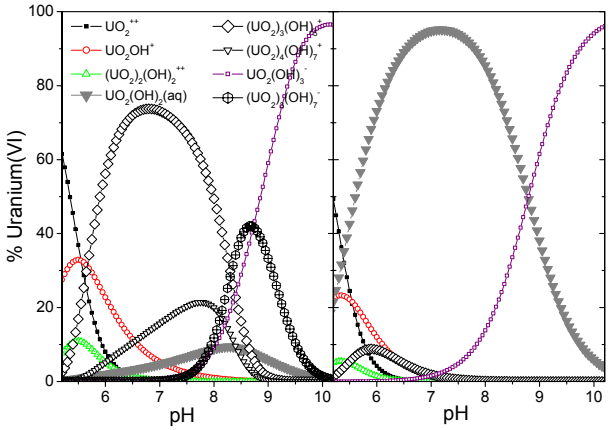

Fig. 1: Uranium(VI) speciation ($[U]_{total} = 1 \cdot 10^{-6}$ M, 0.1 M $NaClO_4$, N_2) based on the NEA TDB data as recommended by [1] (left) and [2] (right)

Thus doubts arose whether the assignment of typical TRLFS (time-resolved laser-induced fluorescence spectroscopy) spectra to the major hydrolysis species as published by Moulin et al. [3] may be biased, even though they already used an updated value for log β of $UO_2(OH)_2$(aq). This seemed to be an important task considering the wide-spread use of TRLFS to reveal U(VI) speciation in solution, in solid or on surfaces. To resolve this question, a new set of TRLFS experiments were planned, also taking advantage of the technological development of the TRLFS during the last decade.

Tab. 1: Averaged experimental conditions and theoretical speciation for the U(VI) TRLFS series samples (major species only).

#[1)]	pH	c_U[2)] [M]	Major species [%]
1 (7)	6.5	$1 \cdot 10^{-5}$	75 % $(UO_2)_3(OH)_5^+$; 10 % $(UO_2)_4(OH)_7^+$; 10 % UO_2OH^+
2 (9)	3.0	$5 \cdot 10^{-6}$	100 % UO_2^{2+}
3 (9)	5.5	$5 \cdot 10^{-7}$	50 % UO_2OH^+ ; 50 % UO_2^{2+}
4 (2)	10.0	$5 \cdot 10^{-6}$	100 % $UO_2(OH)_3^-$
5 (7)	6.0	$5 \cdot 10^{-6}$	70 % $(UO_2)_3(OH)_5^+$; 30 % $(UO_2)_4(OH)_7^+$
6 (4)	9.0	$1 \cdot 10^{-5}$	50 % $(UO_2)_3(OH)_7^-$; 50 % $UO_2(OH)_3^-$
7 (4)	8.0	$5 \cdot 10^{-7}$	30 % $(UO_2)_3(OH)_5^+$; 30 % $UO_2(OH)_3^-$; 30 % $UO_2(OH)_2$(aq)

[1)] in parentheses: number of repetitions. [2)] already taking into account the uranium sorption onto the container walls.

EXPERIMENTAL. Based on the NEA TDB update [1] speciation patterns were computed to elucidate those sample compositions most promising to give unambiguous spectra, cf. Tab. 1.
Sample preparation was performed at room temperature under pure N_2 atmosphere, excluding CO_2. Repetitions of sample 2 were partly prepared under ambient conditions. Aqueous U(VI) solutions were obtained by diluting a $1 \cdot 10^{-4}$ M $UO_2(ClO_4)_2$ stock solution (0.01 M $HClO_4$) with CO_2-free water. The ionic strength was set to 0.1 M using 1 M $NaClO_4$. pH values were adjusted with NaOH and $HClO_4$. Samples were excited at 266 nm (Nd:YAG diode laser with subsequent 4th harmonic generation) with 0.5 – 1.1 mJ pulse energies. Spectra were recorded by a diode array of 1024 intensified diodes, with a spectral resolution of 0.168 nm. The exposure time was 2 µs, the delay times (after laser) covered 50 ns up to 90 µs. Threefold measurements, cumulating 100 laser shots each, were averaged. For more details concerning the experimental procedure and the TRLFS set-up refer to [4].

RESULTS. Data processing started with pure-component samples. In a next step the samples of mixed composition were processed utilizing the single species information obtained before. The full 3D TRLFS information was used applying a wavelength specific fit of the fluorescence intensity to a sum of exponential decay terms, delivering simultaneously the decay time parameter and the individual spectra in case of species mixtures [5].
The fluorescence decay times and four most prominent peak maxima of important U(VI) hydrolysis species are summarized in Tab. 2.

Tab. 2: TRLFS parameters (fluorescence decay time τ and major peak maxima λ_i, i = 2..5) for important U(VI) hydrolysis species.

Species	τ [µs]	λ_2 [nm]	λ_3 [nm]	λ_4 [nm]	λ_5 [nm]
UO_2^{2+}	1.66 ± 0.07	488.6	510.0	533.3	558.9
UO_2OH^+	4.0 ± 0.1	496.4	511.5	533.1	557.8
$(UO_2)_3(OH)_5^+$	18.9 ± 0.3	497.9	513.8	534.0	556.8
$(UO_2)_3(OH)_7^-$	9.8 ± 1.3	494.9	507.6	527.6	549.4
$(UO_2)_4(OH)_7^+$	1.5 ± 0.3				
$UO_2(OH)_3^-$	2.9 ± 0.8	503.7	523.7	541.1	562.1

All hydrolysis species have TRLFS spectra shifted to higher wavelengths when compared to the pure uranyl cation, and mostly longer decay constants. These parameters are distinct enough to be used to aid speciation studies of complex mixtures. When compared to the results from [3], the most striking differences in fluorescence lifetimes are with respect to the species UO_2OH^+ and $(UO_2)_3(OH)_7^-$, where this work obtains substantially shorter values.

REFERENCES

[1] Guillaumont, R. et al. (2003) *Update on the Chemical Thermodynamics of U, Np, Pu, Am and Tc*, Elsevier, Amsterdam.
[2] Grenthe, I. et al. (1992) *Chemical Thermodynamics of Uranium*, Elsevier, Amsterdam.
[3] Moulin, Ch. et al. (1998) *Appl. Spectrosc.* **52**, 528-535.
[4] Sachs, S. et al. (2007) *Radiochim. Acta* **95**, 103-110.
[5] Brendler, V. et al. (1997) *Report FZR-180*, 13.

Comparative study of U(VI)- and U(V) carbonato complexes in aqueous solution

A. Ikeda, C. Hennig, S. Tsushima, K. Takao[1], Y. Ikeda[1], A.C. Scheinost, G. Bernhard
[1]Tokyo Institute of Technology, Tokyo, Japan

Uranyl(VI)- and uranyl(V) carbonato complexes were electrochemically prepared in aqueous Na_2CO_3 solution. Their complex structures were investigated by U L_{III}-edge EXAFS.

Due to its high solubility in aqueous solution, the carbonato complex of uranium is one of the most significant species for the migration study on nuclear waste repositories. Although uranium can change its oxidation state from U(III) to U(VI) in aqueous solution, only the species of U(VI) and U(V) are expected to be the soluble and migratory species under subsurface condition [1,2]. Although U(V) is unstable in a normal condition, it may play an important role if the solution from the repository sites undergoes a change in the redox condition. However, reliable information about the structure of uranyl(VI)- and uranyl(V) carbonato complexes is still missing. Hence, we have investigated the structure of these uranyl carbonato complexes in aqueous solution by EXAFS spectroscopy.

EXPERIMENTAL. Uranyl(VI) carbonate sample was prepared by dissolving $Na_4[U^{VI}O_2(CO_3)_3]$ in 1.4 M Na_2CO_3 solution. Uranyl(V) sample was obtained by the electrolysis of the uranyl(VI) carbonate solution [3]. U L_{III}-edge EXAFS measurements were performed at the Rossendorf beamline, Grenoble, France. Obtained data were treated on the software WinXAS (ver. 3.1) [4]. Theoretical phases and amplitude functions were calculated by the program FEFF 8.20 [5] on the basis of the reported crystal structure of $Na_2Ca[UO_2(CO_3)_3]\cdot nH_2O$ [6].

RESULTS. The uranyl(V) carbonate species is extremely sensitive to O_2 and reoxidizes promptly. Therefore, the uranyl(V) carbonate sample was placed in a glass cuvette under dry N_2 atmosphere in a glove box (O_2 concentration in the glove box was less than 1 ppm). The cuvette was then sealed up by hot melting. The sealed uranyl(V) sample was confirmed to be stable at least for two weeks by successive UV-visible absorption measurements, indicating that the measured XAFS spectrum for the uranyl(V) sample comprises the information only for the uranyl(V) carbonate species. Figure 1 shows the Fourier transforms (FTs) of the U L_{III}-edge EXAFS spectra for uranyl(VI)- and uranyl(V) carbonate species. It is obvious from the previous reports [7,8] that both uranyl(VI)- and uranyl(V) ions form a bidentate-coordinated tricarbonato complex, $[UO_2(CO_3)_3]^{n-}$ (n = 4 for uranyl(VI) and 5 for uranyl(V)), in the present basic Na_2CO_3 solution. The EXAFS structural parameters obtained from curve fits are summarized in Table 1. As a result of the reduction of U(VI) to U(V), U–O_{ax} and U–O_{eq} distances become 0.10 and 0.06 Å longer, respectively. Because the coordination arrangement is unchanged, the change in the bond length is affected only by the charge difference of uranium. Additionally, we succeeded in obtaining the detailed structural information about the outer coordination sphere. It should be noted that the U–O_{dist} distances show a relative small difference. These structural parameters are in good agreement with the results by DFT quantum calculation, assuring the validity of our EXAFS results.

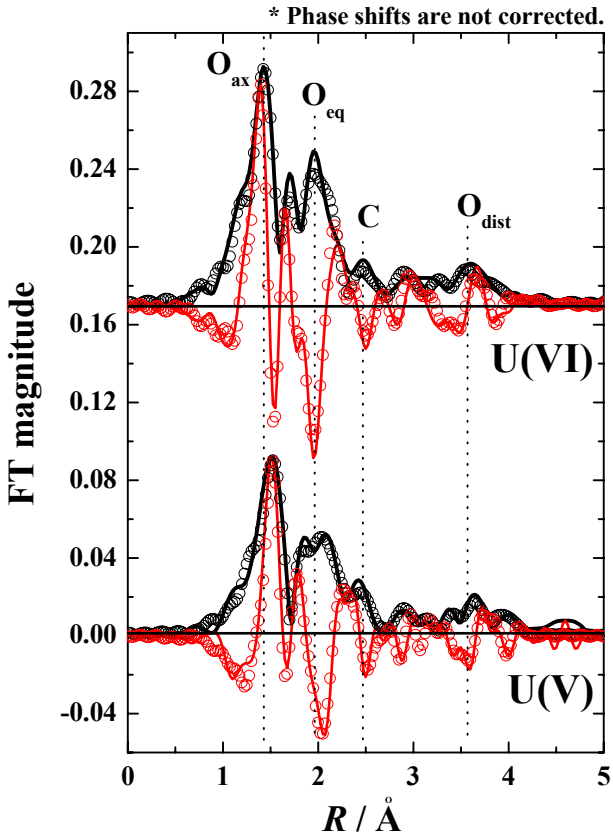

Fig. 1: Fourier transforms of U L_{III}-edge EXAFS for uranyl(VI)- and uranyl(V) carbonate species in 1.4 M Na_2CO_3 solution: –: experimental data, ○: theoretical curve fit, FT magnitude (black-colored data), imaginary part (red-colored data).

Tab. 1: EXAFS structural parameters obtained from curve fit.

	Shell	N (fixed)	R [Å][a]
U(VI)	O_{ax}	2	1.81
	O_{eq}	6	2.44
	C	3	2.92
	O_{ax}–MS	2	3.60
	O_{dist} & MS	3	4.17
U(V)	O_{ax}	2	1.91
	O_{eq}	6	2.50
	C	3	2.93
	O_{ax}–MS	2	3.83
	O_{dist} & MS	3	4.23

[a] Error: $R \leq \pm 0.01$ Å. Debye-Waller factors, σ^2, and the shift in threshold energy, ΔE_0, were varied in the range of 0.0015 – 0.01 Å^2 and 0 – 10 eV, respectively.

REFERENCES

[1] Ciavatta, L. et al. (1983) *Inorg. Chem.* **22**, 2088-2092.
[2] Grenthe, I. et al. (1992) *Chemical Thermodynamics of Uranium*, Elsevier, Amsterdam, p. 308 (2003 updated).
[3] Ikeda, A. et al. (2007) *Inorg. Chem.* (submitted).
[4] Ressler, T. (1998) *J. Synchrotron Rad.* **5**, 118-122.
[5] Ankudinov, A.L. et al. (1998) *Phys. Rev. B* **58**, 7565-7576.
[6] Coda, A. et al. (1981) *Acta Crystallogr.* **B37**, 1496-1500.
[7] Allen, P.G. et al. (1995) *Inorg. Chem.* **34**, 4797-4807.
[8] Docrat, T.I. et al. (1999) *Inorg. Chem.* **38**, 1879-1882.

Depleted uranium dissolution and determination of the formed uranium species

W. Schimmack[1], G. Geipel, R. Steudtner, M. Eilzer, U. Gerstmann[1], W. Schultz[1]
[1]GSF-National Research Center for Environment and Health, Institute of Radiation Protection, Neuherberg, Germany

The corrosion and leaching of depleted uranium (DU) was investigated for three years using DU munitions buried in a column with a soil core. The uranium species in the corrosion and leaching products were detected using TRLFS at room temperature as well as at 150 K. By comparison of the spectra with data in the uranium luminescence database three basic types of uranium species (phosphate, carbonates and hydroxides) can be assigned [1].

EXPERIMENTAL. The soil material was taken from the plough horizon of two fields with different soil types at the Klostergut Scheyern Experimental Station. Columns from plastic tubes of 190 mm diameter and 400 mm height were used; containing about 3.3 kg dry soil mass and 1 kg gravel for better drainage was filled on a plastic frit. The columns were installed in a laboratory with controlled temperature of 21 ± 1 °C and a relative humidity of 55 ± 10 %. According to the mean annual precipitation at Scheyern, the columns were irrigated weekly with 16 mm synthetic rainwater of pH 6 consisting mainly of 0.09 mM NH_4NO_3, 0.08 mM $(NH_4)_2SO_4$ and 0.05 mM $CaSO_4$. Three DU penetrators were located in the columns at different positions in depth. The mass of the used DU projectiles varied between 145 and 264 g. Before starting the experiment they were cleaned by nitric acid and aqua dest. The effluent of each column was collected weekly and passed through a filter of 0.45 µm pore size. The uranium speciation in the seepage water and the solid samples from the corrosion products was determined by time-resolved laser-induced fluorescence spectroscopy (TRLFS).

RESULTS. Each week they were irrigated and ^{238}U was determined in the effluents by Inductively Coupled Plasma Mass Spectrometry. In addition, ^{235}U was measured occasionally in order to assure that the origin of ^{238}U was predominantly the DU munitions. On average, 14.5 g corresponding to 7.9 % of the initial DU mass was corroded after three years indicating an acceleration of the corrosion as compared to the first year [1]. The leaching rates increased much stronger than the corrosion by factors of more than 100 resulting in a mean total amount of leached ^{238}U of 13 mg as compared to 0.03 mg after the first year. The uranium species identified by time-resolved laser-induced fluorescence spectroscopy were mainly hydroxo and carbonate compounds in the seepage water and phosphate compounds in the corroded material.
In Fig. 1 the luminescence spectrum of a yellow material is shown, which was crystallized at the soil surface. For comparison the spectrum of the mineral sabugalite $AlH(UO_2)(PO_4)_4{\cdot}16H_2O$ [3] has been added.
In contrast to the luminescence spectra of the solid material the spectra of the uranium species in the dissolved samples could only be obtained at temperatures below 220 K [4]. For better resolution the spectra were taken at 150 K. In Fig. 2 the luminescence spectrum of a seepage water sample is compared to a spectrum taken from a pure frozen $UO_2(CO_3)_3^{4-}$ solution. From the shape of the spectrum and the emission maxima of the luminescence of the

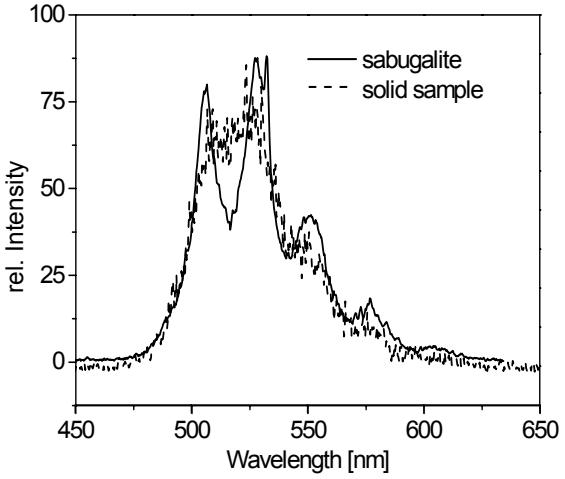

Fig. 1.: Luminescence spectra of the crystallized surface uranium species and the mineral sabugalite.

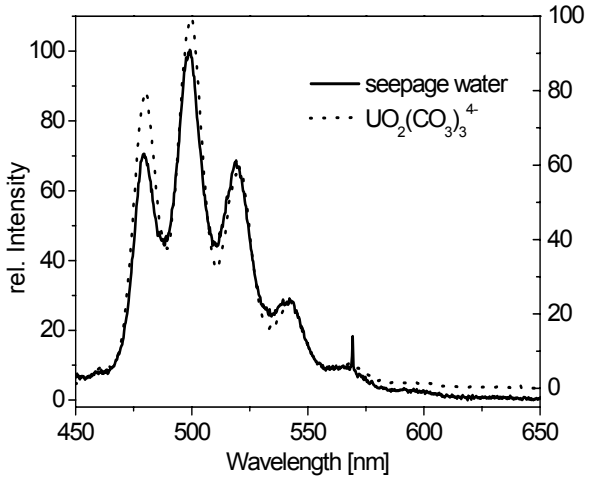

Fig.2.: Luminescence spectra of a seepage water sample and comparison with the spectrum of $UO_2(CO_3)_3^{4-}$.

seepage water sample it could be clearly concluded that the solution species is a uranyl carbonate species.
The seepage water of one of the six columns did show a different behavior. The measured luminescence spectrum was different from that of the $UO_2(CO_3)_3^{4-}$ species. The comparison with data previously observed from pure uranium hydroxo species lead to the conclusion that this seepage water contains mainly $(UO_2)_3(OH)_5^+$ species.
From the corrosion experiments it is concluded that the dramatic increase of the leaching and its large temporal and spatial variability do not allow any extrapolation into the future. However, the high level of the uranium concentrations in the seepage water demands further investigations on the transport of ^{238}U through the soil in order to estimate the concentration of ^{238}U from DU munitions in the groundwater for areas affected by DU weapons.

REFERENCES

[1] Schimmack, W. et al.(2007) *Radiat. Environ. Biophys.* (submitted).
[2] Schimmack, W. et al. (2005) *Radiat. Environ. Biophys.* **44**, 183-191.
[3] Geipel, G. et al. (2000) *Radiochim. Acta* **88**, 757-762.
[4] Geipel, G. (2006) in: *Handbook of Applied Solid State Spectroscopy*, 577-593, Springer, New York.

The influence of temperature at the uranyl(VI) luminescence

R. Steudtner, G. Geipel

The influence of temperature on the luminescence of the free uranyl ion (UO_2^{2+}) in 0.1 M aqueous solution of $HClO_4$ was studied. We investigated the temperature dependence of the lifetime and of the luminescence intensity of the excited uranyl ion in a temperature range from 278 – 318 K.

The luminescence lifetime and the luminescence intensity of a fluorophor are strongly temperature-dependent [1] and were intensively investigated for the free uranyl [2 - 4]. This work is a first part for the determination of thermodynamic constants (luminescence decay constant, enthalpy) of the uranyl ion.

EXPERIMENTAL. The luminescence spectra from the $5 \cdot 10^{-5}$ M $UO_2(ClO_4)_2$ solution in 0.1 M $HClO_4$ were measured in the temperature range from 278 – 318 K in 5 K steps. Time-resolved fluorescence spectra were recorded with an Inlite laser (Continuum; excitation wavelength: 266 nm, energy: ~1 mJ) and an intensified CCD camera (Roper-Scientific; delay time: varied, gate time: 2 µs). The cuvette were cooled and heated with a temperature-controlled cuvette holder (Temperature Control Quantum Northwest) connected to a water bath circulator (Lauda RM6). The temperature of the solution in the cuvette was controlled by a digital thermometer (Ama-Digit Precision).

RESULTS. The fluorescence intensities of the TRLFS spectra at time t_0 at various temperatures are shown in Fig. 1.

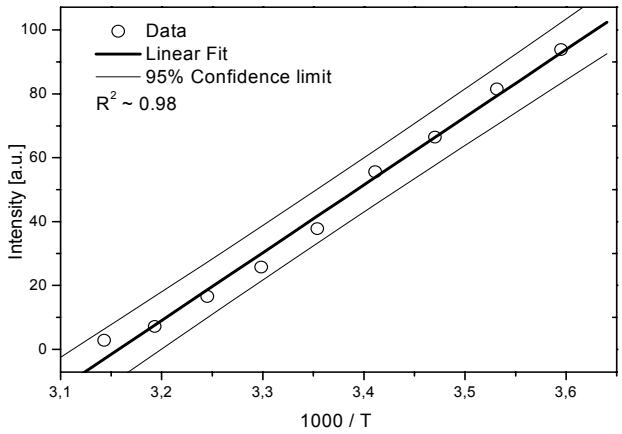

Fig. 1: Dependence of the luminescence intensity of the uranyl ion on temperature.

All data points are located within a confidence limit of 95 %. The linear fit of the measurement supports the observation, that an increase of the temperature of about 1 K results in a decrease of the fluorescence intensity of about 2.3 %.

The dependence of the luminescence decay constant of the uranyl ion on the temperature is shown in Fig. 2. All measured data are found within a confidence limit of 95 %. The equation of the luminescence decay constant is calculated from the linear fit of both series.

$$k_T = (7.42 \pm 0.56) \cdot 10^6 - (2.05 \pm 0.16) \cdot 10^{10} \cdot \frac{1}{T} \qquad (1)$$

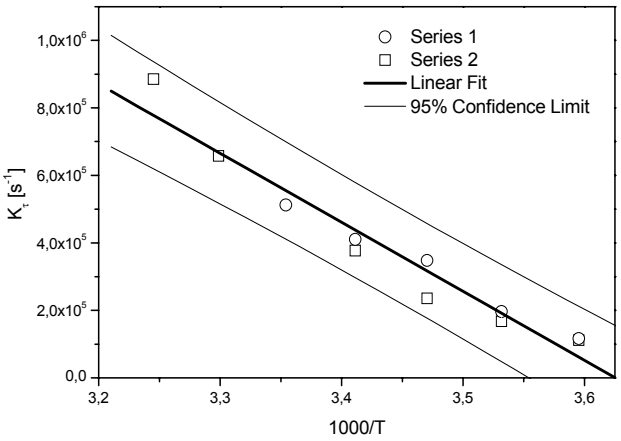

Fig. 2: Dependence of the luminescence decay constant of the uranyl ion on the temperature.

The luminescence decay constant describes the transition of the uranyl ion from the excited state to the ground state by emitted luminescence radiation.

$$UO_2^{2+*} \xrightarrow{k_T} UO_2^{2+} + h\nu \qquad (2)$$

For the determination of the activation energy (E_A) two procedures which base on the Arrhenius equation were applied. Both procedures allow the determination of k-T-pairs of variates. The first procedure represents the mathematical determination out of the luminescence decay constants (k_T) summarized in equation 3:

$$k_1 = A_1 \cdot e^{-E_A / RT_1}$$
$$k_2 = A_2 \cdot e^{-E_A / RT_2} \qquad (3)$$
$$E_A = (\ln k_2 - \ln k_1) \cdot \frac{T_1 \cdot T_2}{(T_2 - T_1)} \cdot R$$

The second procedure is realized by graphic analysis of the $\ln k / \frac{1}{T}$–diagram. The activation energy is obtained by the slope of the straight line.

The obtained activation energy of the luminescence decay of the uranyl ion in temperature range from 278 K to 318 K is 50.26 ± 0.55 kJ/mol.

REFERENCES

[1] Lakowicz, J.R. *et al.* (2006) *Principles of Fluorescence Spectroscopy,* Springer, Baltimore.
[2] Lotnik, S.V. *et al.* (2003) *Radiochemistry* **45**, 550-554.
[3] Lotnik, S.V. *et al.* (2003) *Radiochemistry* **45**, 555-558.
[4] Lotnik, S.V. *et al.* (2004) *Radiochemistry* **46**, 236-241.

Luminescence spectrum of uranyl(V) in 2-propanol perchlorate solution

R. Steudtner, T. Arnold, K. Großmann, G. Geipel, V. Brendler

The luminescence spectrum of uranyl(V) in aqueous perchlorate solution was detected for the first time at room temperature in the UV–vis region with a peak maxima at 440 nm and a fluorescence lifetime of 1.1 ± 0.02 µs using an excitation wavelength of 255 nm [1].

Absorption studies of tetravalent, pentavalent, and hexavalent uranium in solution have been performed by numerous scientists. However, only luminescence spectra of tetravalent [2] and in particular hexavalent aqueous [3] and adsorbed [4] uranium species have been reported. This is related to the fact that U(V) is unstable in solution due to disproportionation to U(IV) and U(VI) species [5 and reference therein]. Aqueous U(V) species are only stable in a very narrow pH range (pH 2–3) and only for a short time of approximately 1 h [6]. In addition, the only known stable uranyl(V) complex is a carbonate species formed in basic aqueous solution (pH > 11) [7].

EXPERIMENTAL. U(V) sample solutions were prepared by following a procedure described by Howes et al. [6]. A solution containing $4 \cdot 10^{-4}$ M uranium(VI), 0.2 M $NaClO_4$ and 0.5 M 2-propanol at pH 2.41 ± 0.1 ($HClO_4$ = 2 mM) was irradiated with a mercury-vapor lamp (λ_{max} = 254 nm; LOT-Oriel) for 3 – 10 min. The spectrum was recorded immediately at room temperature using a pulsed OPO laser system. The excitation wavelength was 255 nm with a pulse energy of 1 mJ.

RESULTS. In Fig. 1 the absorption spectra of U(VI) and acetone are shown. With increasing irradiation times uranyl(VI) is reduced to uranyl(V) while 2-propanol is oxidized to acetone (Fig. 1, inset). This is demonstrated by the increasing peaks at 255 nm and 265 nm which represent the absorption bands of the uranyl(V) cation and the acetone molecule, respectively. This is in agreement with earlier findings [6].
At that time about 80 – 90 % of the total uranium in the system is reduced to U(V). The time-resolved laser-induced fluorescence spectra and the respective fluorescence lifetime calculation are shown in Fig. 2, and revealed the presence of one species with a lifetime of 1.1 ± 0.02 µs.

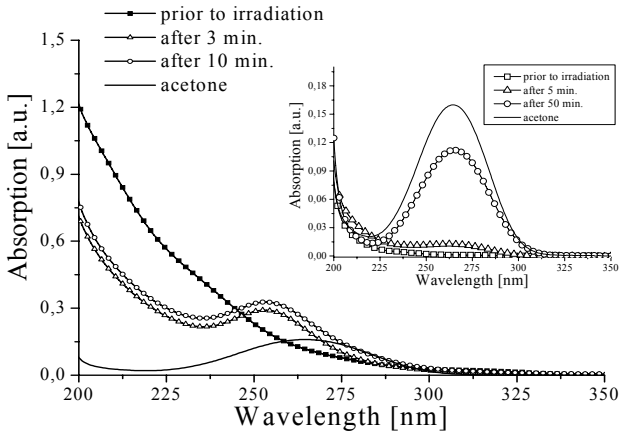

Fig. 1: Absorption spectra of the formation uranium(V) by irradiation with an Hg lamp. Inset: For comparison the absorption spectra of a corresponding 0.5 M 2-propanol solution which was also irradiated with the Hg lamp. Note the different scale of the y-axis.

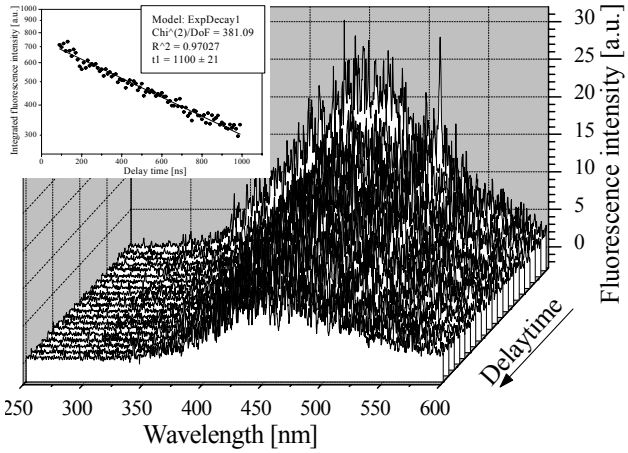

Fig. 2. Orginal TRLFS spectra of U(V) solution. Inset: Lifetime calculation of a fluorescent uranyl(V) species revealed a value of 1100 ns.

The fluorescence emission spectrum of this sample is shown in Fig. 3 and was fitted with a Lorentz-Gaussian function.

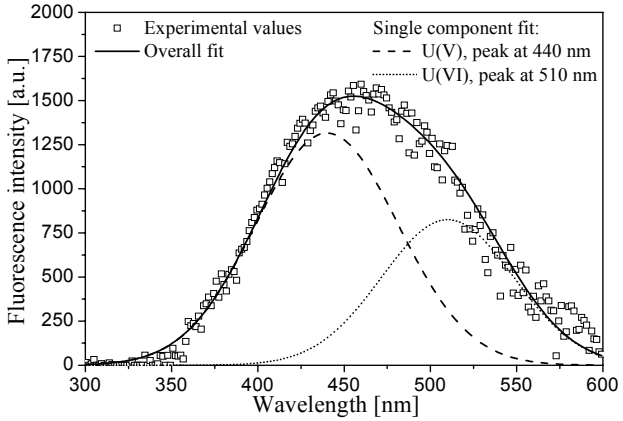

Fig. 3: Deconvoluted fluorescence emission spectrum of U(V).

A peak maximum at 440 ± 1.2 nm and a shoulder at about 510 ± 2.2 nm were detected. This shoulder is attributed to minor amounts of uranyl(VI) which was also excited by the 255 nm excitation wavelength.

ACKNOWLEDGEMENT. We thank Manuela Eilzer for technical assistance and the German Research Council (DFG) for financial support (Project No. AR 584/1-1)

REFERENCES

[1] Steudtner, R. et al. (2006) *Inorg. Chem. Commun.* **9**, 939-941.
[2] Kirishima, A. et al. (2003) *Chem. Commun.* **7**, 910-911.
[3] Geipel, G. et al. (2003) *J. Nucl. Mater.* **248**, 408-411.
[4] Baumann, N. et al. (2005) *J. Colloid Interface Sci.* **290**, 318-324.
[5] Mizuoka, K. et al. (2005) *Inorg. Chem.* **44**, 4472-4474.
[6] Howes, K.R. et al. (1988) *Inorg. Chem.* **27**, 791-794.
[7] Cohen, D. et al. (1970) *J. Inorg. Nucl. Chem.* **32**, 3525-3530.

Complexation of U(VI) with aromatic acids having different functionalities studied by UV-vis spectroscopy

M. Glorius, H. Moll, G. Bernhard

The complex formation of uranium(VI) with salicylhydroxamic (SHA), benzohydroxamic (BHA) and benzoic acid (BA) was investigated by UV-vis spectroscopy. The different U(VI) species are characterized by their individual absorption spectra and molar extinction coefficients. The formation constants of the identified uranium(VI) species, $M_pL_qH_r$, were determined.

To understand the actinide interaction processes in biological systems on a molecular level it is necessary to explore the complexation behavior of actinides with selected bioligands of relevant functionalities as model compounds. The three studied ligands are model compounds for pyoverdins, which are natural bioligands secreted from *Pseudomonas* ssp. possessing a high potential to bind actinides [1,2]. Furthermore, we want to explore if one could detect variations in the absorption spectra due to the different coordination environment of uranyl by using hydroxamic acids and benzoic acid.

EXPERIMENTAL. The absorption spectroscopy experiments were carried out at a total uranyl concentration of $1 \cdot 10^{-3}$ M as a function of the ligand concentration (10^{-4} M to $5 \cdot 10^{-3}$ M) at pH 3 and 4. The pH adjustments were made with $HClO_4$ or NaOH. The ionic strength was adjusted to 0.1 M ($NaClO_4$). The spectra were recorded from 350 to 500 nm using a CARY5G UV-vis-NIR spectrometer (Varian Co.) at 22 ± 1 ºC. The stability constants were determined using the factor analysis program SPECFIT. Details are summarized in [3].

RESULTS. Figure 1 shows the measured UV-vis spectra at a uranium concentration of 0.001 M at pH 3 as a function of the SHA (Fig. 1A) and BA (Fig. 1B) concentration.

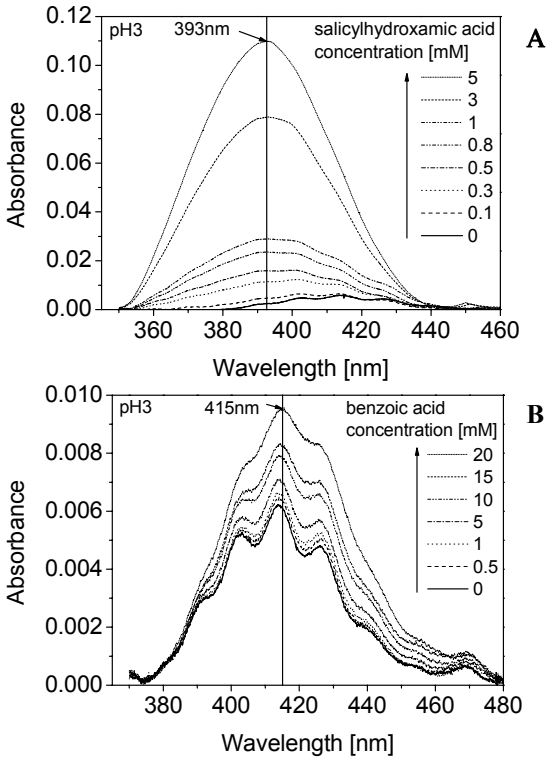

Fig. 1: Measured UV-vis spectra at 0.001 M UO_2^{2+} at pH 3 in the SHA- (A) and BA-system (B).

In the SHA- and BHA-uranyl system an increase in the absorbance combined with a blue shift of the absorption maxima of about 25 nm in comparison to the bands of the free uranyl ion was observed. In contrast to the SHA- and BHA-system the spectra of BA shows an increase in the absorbance and a red shift of the absorption maxima of about 2 nm (see Fig. 1).

The changes in the absorption spectra indicate in all three uranyl-ligand systems a formation of uranium(VI)-ligand complexes with a 1 : 1 stoichiometry. In the SHA-system indications for a 1 : 2 complex were found. The determined stability constants of the three systems extrapolated to infinite dilution are summarized in Tab. 1.

Tab. 1: Complex formation constants of the identified U(VI) complexes.

Ligand	Complex species $M_pL_qH_r$	*p*	*q*	*r*	log β^0
SHA	$UO_2HOC_6H_4CONHO^+$	1	1	1	16.22 ± 0.10
	$UO_2[HOC_6H_4CONHO]_2$	*1*	*2*	*2*	~ 30
BHA	$UO_2C_6H_4CONHO^+$	1	1	0	7.51 ± 0.05
	$UO_2[C_6H_4CONHO]_2$	1	2	0	14.58 ± 0.11
BA	$UO_2C_6H_4COO^+$	1	1	0	2.92 ± 0.14

The complex formation constants suggest that SHA forms more stable complexes compared to BHA. Both aromatic hydroxamate compounds form stronger uranyl species than BA. The strength of complex formation decreases generally from SHA via BHA to BA. This dependence is in agreement with results obtained with other metals, e.g., Fe(III) and Cu(II) [4,5].

Furthermore one can postulate different coordination modes of uranyl from the presented experimental findings. If uranyl is coordinated to hydroxamic acids this results in a blue shift of the absorption maxima. Whereas in the case of coordination to the carboxylic acid group of benzoic acid, a red shift of the absorption maxima was observed. So the uranyl ion is bound to benzoic acid over the oxygen atoms of the carboxylic group and to the hydroxamic acids probably via the oxygen atoms of the hydroxamic acid group. Theoretical calculations are in progress to get a further insight of the coordination environment of U(VI) in the three systems investigated. The differences in the coordination sphere of uranium cause the opposed displacements of the absorption maxima in comparison to the spectrum of the free uranyl ion.

The higher formation constants of uranyl with the aromatic hydroxamate compounds compared to benzoic acid points to the high potential of the pyoverdins to bind and mobilize uranium(VI) in the environment.

ACKNOWLEDGEMENT. This work was funded by the BMWi under contract number 02E9985.

REFERENCES

[1] Bouby, M. et al. (1999) *Czechoslovak. J. Phys.* **49**, 147-150.
[2] Moll, H. et al. this report, p. 39.
[3] Glorius, M. et al. (2007) *Radiochim. Acta* (in press).
[4] O'Brien, E. C. et al. (2000) *Inorg. Chem.* **79**, 47-51.
[5] Farkas, E. (2000) *J. Inorg. Biochem.* **79**, 205-211.

U(VI) complexation with aromatic acids having different functionalities investigated by TRLFS

M. Glorius, H. Moll, G. Bernhard

The complex formation of uranium(VI) with salicylhydroxamic (SHA), benzohydroxamic (BHA) and benzoic acid (BA) was investigated by time-resolved laser-induced fluorescence spectroscopy (TRLFS). In all three systems a static quench process of the uranyl fluorescence due to the complex formation was observed. The complex stability constants of the identified uranium(VI) species, $M_pL_qH_r$, were calculated.

In continuation of our studies [1] exploring the complexation of actinides with pyoverdin model compounds, this work is focused on the application of TRLFS in order to investigate the speciation of U(VI) with SHA, BHA and BA. One advantage of this technique is that the speciation investigations can be performed in the more environmentally relevant uranium(VI) concentration range compared to UV-vis studies [1]. We want to explore the fluorescence properties of the formed U(VI) species with SHA, BHA and BA. Moreover we want to compare the formation constants determined using TRLFS with those obtained by UV-vis.

EXPERIMENTAL. The TRLFS experiments were carried out at a total uranyl concentration of $5 \cdot 10^{-5}$ M as a function of the ligand concentration (10^{-5} M to 10^{-3} M) at pH 3 and 4. The pH adjustments were made with $HClO_4$ or NaOH. The ionic strength was adjusted to 0.1 M ($NaClO_4$). The spectra were recorded at 25°C using a pulsed Nd:YAG laser system. The excitation wavelength of the uranyl fluorescence was 266 nm with a pulse energy of 100 – 200 µJ. The stability constants at pH 3 were determined with a slope analysis and at pH 4 using the factor analysis program SPECFIT.

RESULTS. Figure 1 shows the measured fluorescence spectra at a uranium concentration of $5 \cdot 10^{-5}$ M at pH 3 as a function of the SHA concentration.

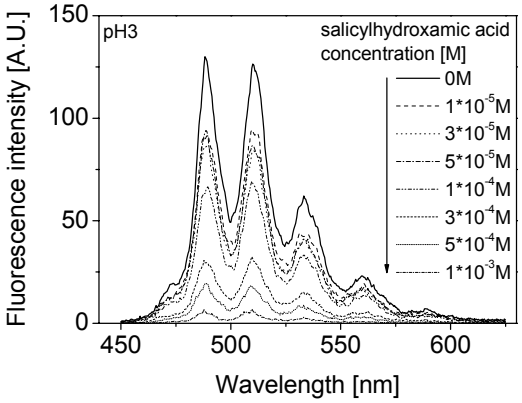

Fig. 1: Measured fluorescence spectra of the SHA-uranyl system at $5 \cdot 10^{-5}$ M UO_2^{2+} at pH 3.

In all three studied systems we observed a decrease in the fluorescence intensity with increasing ligand concentration at pH 3 and 4, which is typical for static fluorescence quenching due to the complex formation. The lifetimes decrease with increasing ligand concentration, indicating additional dynamic quenching. It follows, that all complexed ligand uranyl species emit no fluorescence light.

The determined lifetimes were used to calculate the fluorescence intensity if no dynamic quenching takes place. These corrected fluorescence intensities were then used to calculate the concentrations of the free uranyl ion as a function of the ligand concentration.

To determine the stability constants and to estimate the stoichiometry of the complexes a slope analysis was made using the logarithmic mass action law in its transformed linear form. Fig. 2 shows the result of the slope analysis of the U(VI)-SHA-system as an example.

The average slope of 0.9 ± 0.2 suggests in all three systems the formation of a 1:1 complex at pH 3. The intersection corresponds to the formation constant log k* of the complex. The stability constant log β was determined using log k* and the protonation constants of the ligands.

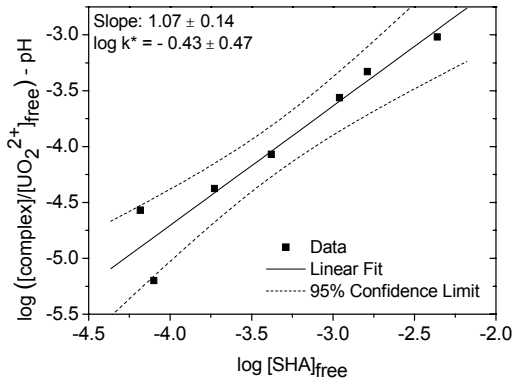

Fig. 2: Slope analysis of the complex formation of SHA.

In the SHA- and BHA-system a slope of 1.5 at pH 4 gives evidence for the formation of a second species most likely a 1 : 2 complex. Because of the occurrence of two complex species, the factor analysis program SPECFIT was used to evaluate the series measured at pH 4.

In Table 1 all determined complex formation constants extrapolated to infinite dilution are summarized.

Tab. 1: Complex formation constants of the identified U(VI) complexes.

Ligand	Complex species $M_pL_qH_r$	p	q	r	log β^0
SHA	$UO_2HOC_6H_4CONHO^+$	1	1	1	16.44 ± 0.06
	$UO_2[HOC_6H_4CONHO]_2$	*1*	*2*	*2*	33.43 ± 0.11
BHA	$UO_2C_6H_4CONHO^+$	1	1	0	7.47 ± 0.11
	$UO_2[C_6H_4CONHO]_2$	1	2	0	16.21 ± 0.49
BA	$UO_2C_6H_4COO^+$	1	1	0	3.11 ± 0.05

In general, for all ligands the stability constants determined by TRLFS are in agreement with the values measured using UV-vis spectroscopy and published in [2]. The U(VI) speciation determined in the BA-system is consistent also by applying different experimental methods like TRLFS, UV-vis [1] and potentiometry [3].

ACKNOWLEDGEMENT. This work was funded by the BMWi under contract number 02E9985.

REFERENCES

[1] Glorius, M. et al. this report, p. 18.
[2] Glorius, M. et al. (2007) *Radiochim. Acta* (in press).
[3] Vulpius, D. (2005) *Thesis,* Dresden University of Technology, Dresden.

Complex formation of U(VI) with *O*-phosphoethanolamine studied by TRLFS

A. Koban, G. Bernhard

The complex formation of the uranyl ion (UO_2^{2+}) in the aqueous system with *O*-phosphoethanolamine was investigated by time-resolved laser-induced fluorescence spectroscopy (TRLFS) at pH 2 to 6. A 1 : 1 complex was found with the stability constant of $\log K_{11} = 4.5 \pm 0.1$.

Phospholipids as important constituents of cell membranes are supposed to bind heavy metals. To predict the mobility and toxicity of actinides in biosystems, it is important to understand the binding mechanisms on the molecular level. *O*-phosphoethanolamine represents beside other phosphonates the polar head group of phospholipids.

O-phosphoethanolamine ($^+NH_3$-CH_2-CH_2-O-PO_3H^-) exists in solution in the zwitterionic form with the protonated amino group which may either coordinate the metal by deprotonation or also weaken the bond because of the positive charge.

EXPERIMENTAL. The TRLFS measurements with *O*-phosphoethanolamine were performed at total uranyl concentrations of 0.01 mM at various pH values between 2.0 and 6.0 and various ligand concentrations (0.05 to 75 mM). The spectra were recorded at room temperature using a pulsed Nd:YAG laser system.

RESULTS. The dependence of the fluorescence spectra of the uranyl ion on ligand concentration and pH value is demonstrated in Fig. 1 and 2. For comparison the uranyl spectra at pH = 2.0 and 6.0 are included.

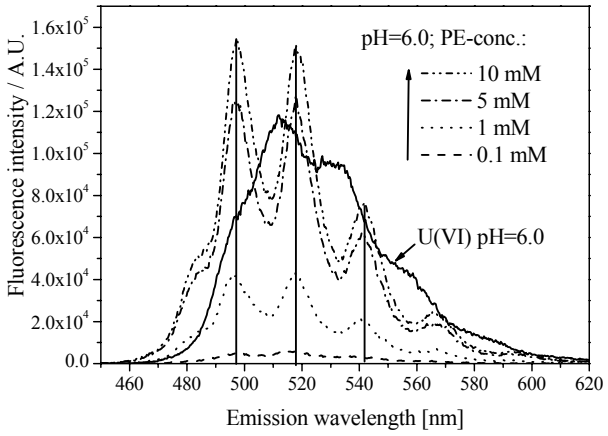

Fig. 1: Fluorescence spectra with *O*-phosphoethanolamine (PE) at fixed uranyl concentration (0.01 mM) and fixed pH (6.0) in dependence of the ligand concentration (0.1 – 10 mM).

We observed a strong increase of the fluorescence intensity with increasing ligand concentration (Fig. 1) and also with increasing pH (Fig. 2), combined with a red shift of the emission bands of about 8 nm, compared to the free uranyl ion. This suggests that uranyl is complexed by *O*-phosphoethanolamine even at low pH values. Up to pH 6.0 the predominance of the uranyl complex with *O*-phosphoethanolamine prevents the formation of uranyl hydroxide and carbonate species. The red shift of about 8 nm indicates a uranyl binding via the phosphate group.

The uranyl-phosphoethanolamine system shows mono-exponential decay from pH 2.0 to 4.0 and bi- or tri-exponential decay at pH higher than 4.0. The intensity of the first lifetime (averaged 3.1 ± 0.6 µs) increases with increasing ligand concentration and can be associated with a uranyl-phosphoethanolamine complex. The two larger lifetimes (9 ± 2 µs and 22 ±6 µs) of low intensity are generated by uranyl hydroxide species.

The spectra were analyzed with the program SPECFIT [1] to determine the stability constant of the uranyl-phosphoethanolamine complex. The necessary pK_a values of the ligand were taken from literature [2]. In addition, the stability constants of relevant uranyl hydroxide and carbonate species [3] were included in the calculation procedure. Possible species of the type $M_pH_qL_r$ were introduced in the data analysis procedure. As a result, the best fit for the *O*-phosphoethanolamine system was received with the 1 : 1 complex $UO_2[NH_3CH_2CH_2OPO_3]^+$. The complex stability constant was determined to be $\log K_{11} = 4.5 \pm 0.1$. From the calculations with SPECFIT it is clear that the amino group is not being deprotonated in the examined pH range. Thus, a participation of the amino group for the complexation can be ruled out. The stability constant of the uranyl complex with *O*-phosphoethanolamine is remarkable smaller than that of the uranyl *O*-phosphoserine complex ($\log K_{11} = 5.4 \pm 0.1$ [4,5]) and the uranyl-phosphoglycerol complex ($\log K_{11} = 6.2 \pm 0.1$ [6]). This is probably due to the positive charge of the protonated amino group in *O*-phosphoethanolamine, which may destabilize the complex.

The peak maxima of the complex species were calculated to be 483, 498, 518, 541, and 566 nm. [5]

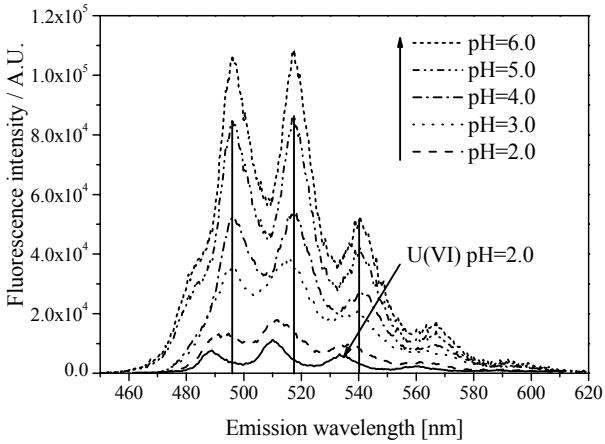

Fig. 2: Fluorescence spectra with *O*-phosphoethanolamine at fixed uranyl (0.01 mM) and ligand concentration (1 mM) in dependence of pH (2.0 – 6.0).

REFERENCES

[1] Binstead, R.A. et al. (2005) *SPECFIT Global Analysis System, Version 3.0.37*.
[2] Fölsch, G. et al. (1959) *J. Biol. Chem*. **234**, 2298-2303.
[3] Grenthe, I. et al. (1992) *Chemical Thermodynamics of Uranium*, Elsevier, Amsterdam.
[4] Koban, A. et al. this report, p. 21.
[5] Koban, A. et al. (2007) *J. Inorg. Biochem.* (accepted).
[6] Koban, A. et al. (2004) *Polyhedron* **23**, 1793-1797.

Complex formation of U(VI) with *O*-phosphoserine studied by TRLFS

A. Koban, G. Bernhard

The interaction of *O*-phosphoserine with the uranyl ion (UO_2^{2+}) in the aqueous system was investigated by time-resolved laser-induced fluorescence spectroscopy (TRLFS) at pH 2 to 6. Two complexes with a metal-to-ligand ratio of 1 : 1 and 1 : 2, respectively, were found with the stability constants of $\log K_{11} = 5.4 \pm 0.1$ and $\log K_{12} = 8.6 \pm 0.1$.

O-phosphoserine represents, beside other phosphonates, the polar head group of phospholipids. Phospholipids are important components of cell membranes and possibly constitute the binding sites for heavy metals. For a better understanding of the transport and binding mechanisms of radionuclides in the biosphere, studies on the molecular level are essential.

O-phosphoserine, in solution in the zwitterionic form ($^+NH_3(COO^-)CH\text{-}CH_2\text{-}O\text{-}PO_3H^-$), offers beside the phosphate group a carboxyl group as a potential metal binding site. The protonated amino group may either coordinate the metal by deprotonation or weaken the bond because of the positive charge.

EXPERIMENTAL. The TRLFS measurements were performed at a total uranyl concentration of 0.01 mM at various pH values between 2.0 and 6.0 and various ligand concentrations (0.05 to 75 mM). The spectra were recorded at room temperature using a pulsed Nd:YAG laser system.

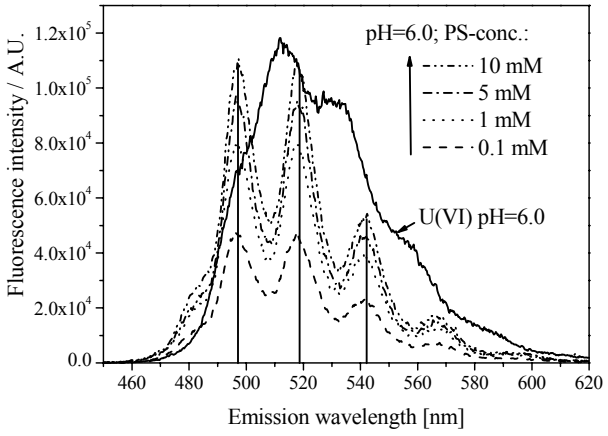

Fig. 1: Fluorescence spectra with *O*-phosphoserine (PS) at fixed uranyl concentration (0.01 mM) and fixed pH (6.0) in dependence of the ligand concentration (0.1 – 10 mM).

RESULTS. The fluorescence spectra of the uranyl-phosphoserine system depending on the ligand concentration and the pH value are shown in Fig. 1 and 2. For comparison the spectra of the free uranyl ion at pH 2 and the uranyl hydrolysis at pH 6 are included in the figures.

We observed a strong increase of the fluorescence intensity with increasing ligand concentration (Fig. 1) and also with increasing pH (Fig. 2). The emission bands are red-shifted of about 8-9 nm, compared to the free uranyl ion. This suggests that the uranyl ion is complexed by *O*-phosphoserine even at pH 2. The uranyl-phosphoserine complex species predominate up to pH 6.0 and prevent the formation of uranyl hydroxide and carbonate species. The red shift of about 8 – 9 nm clearly indicates a uranyl binding via the phosphate group.

The determination of the time-resolved spectra shows mono-exponential decay with an averaged lifetime of 1.6 ± 0.1 µs at lower pH range (2 – 4) and lower ligand concentration. At higher pH and higher ligand concentration a second lifetime of 3.5 ± 0.2 µs appears. In addition a further larger lifetime (about 27 ± 10 µs) with low intensity is present in nearly all systems at pH 4 to 6, which can assigned to uranyl hydroxide species. The lifetimes of 1.6 ± 0.1 µs and 3.5 ± 0.2 µs we assign to two different uranyl-phosphoserine species.

The spectra were analyzed with the program SPECFIT [1] to determine the stability constants of the uranyl-phosphoserine complexes. The necessary pK_a values of the ligand and the stability constants of relevant uranyl hydroxide and carbonate species were taken from literature [2,3]. As a result, two complexes, the 1 : 1 complex $UO_2[NH_3COOCHCH_2OPO_3]$ and the 1 : 2 complex $UO_2[NH_3COOCHCH_2OPO_3]_2^{2-}$, with the stability constants of $\log K_{11} = 5.4 \pm 0.1$ and $\log K_{12} = 8.6 \pm 0.1$, were found. The main peak maxima of these complexes were determined to be 496, 516, 539, and 564 nm (1 : 1 complex) and 497, 518, 541, and 565 nm (1 : 2 complex).

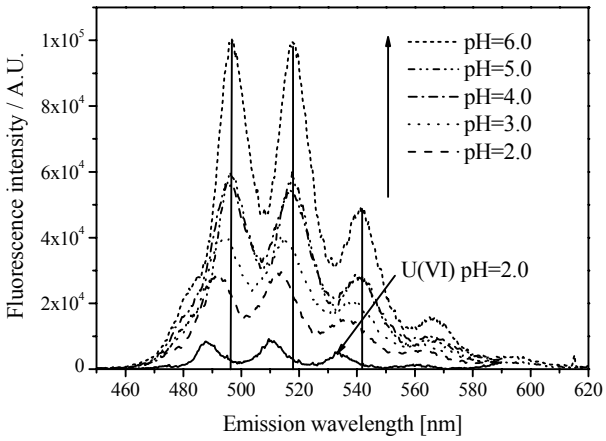

Fig. 2: Fluorescence spectra with *O*-phosphoserine at fixed uranyl (0.01 mM) and ligand concentration (1 mM) in dependence of pH (2.0 – 6.0).

From the calculations with SPECFIT it is obvious that the amino groups are not being deprotonated in the examined pH range. Thus, a participation of the amino groups for the complexation can be ruled out. Whether the carboxyl group is involved in complexation or not, cannot be decided exactly. The stability constants are not larger than with other phosphonates like phosphoglycerol [4], but rather smaller due to a destabilizing effect of the positive charged amino function. A participation of the carboxyl group is therefore not probable. [5]

REFERENCES

[1] Binstead, R.A. et al. (2005) *SPECFIT Global Analysis System, Version 3.0.37*.
[2] Yamauchi, O. et al. (1992) *Inorg. Chim. Acta* **198-200**, 749-761.
[3] Grenthe, I. et al. (1992) *Chemical Thermodynamics of Uranium*, Elsevier, Amsterdam.
[4] Koban, A. et al. (2004) *Polyhedron* **23**, 1793-1797.
[5] Koban, A. et al. (2007) *J. Inorg. Biochem.* (accepted).

Complex formation of U(VI) with L-phenylalanine (2-amino-3-phenylpropionic acid) and 3-phenylpropionic acid – Part I: TRLFS

A. Koban, S. Sachs

The uranyl complexes of 3-phenylpropionic acid and its 2-amino derivate L-phenylalanine were studied by TRLFS at acidic pH. Both complexes show no fluorescence. The amino group does not seem to influence the complex behavior.

The goal of investigation was to study the influence of amino groups in uranium(VI) complexation even at acidic pH ranges. Therefore TRLFS (time-resolved laser-induced fluorescence spectroscopy) measurements with uranyl and the model compounds L-phenylalanine (C_6H_5-CH_2-$CH(NH_2)$-COOH) and 3-phenylpropionic acid (C_6H_5-CH_2-CH_2-COOH) as complex ligands were carried out.

EXPERIMENTAL. The TRLFS measurements were performed at a total uranyl concentration of 10^{-5} M as a function of the ligand concentration (10 different concentrations from $1 \cdot 10^{-5}$ M to $2 \cdot 10^{-3}$ M each) at pH = 4.0 and an ionic strength of 0.1 M ($NaClO_4$). The spectra were recorded at room temperature using a pulsed Nd:YAG laser system.

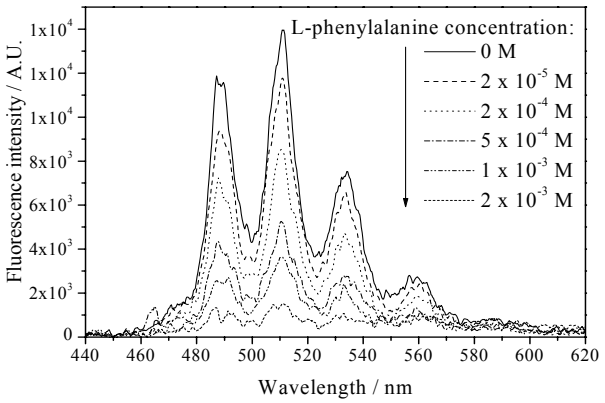

Fig. 1: Fluorescence spectra of uranium(VI) (10^{-5} M) at pH = 4.0 as a function of the ligand concentration of L-phenylalanine.

RESULTS. Figure 1 shows the fluorescence spectra of the uranyl ion as a function of the ligand concentration of L-phenylalanine at pH = 4.0. The spectra with 3-phenylpropionate as ligand look exactly the same. Both ligands caused a strong decrease of the fluorescence intensity with increasing concentration. We noticed no shift of the fluorescence peaks. This behavior is typical for static fluorescence quenching due to the complex formation.

With a modified logarithmic form of the mass action law the stoichiometry and the complex stability constant can be graphical determined via slope analysis, as demonstrated in Fig. 2 for the uranyl L-phenylalanine complex system. For both complex systems a slope near 1 was calculated, indicating a predominant 1 : 1 complex. The intersection offers the equilibrium constant log*K*', which can be converted under consideration of the pH and the pK_a of the ligands [1,2] into the stability constants logK_{ML} (see Table 1).

The fluorescence decay was mono-exponential in all samples. The lifetime, which belongs to the free uranyl ion, decreases with increasing ligand concentration. This indicates additional dynamic fluorescence quenching,

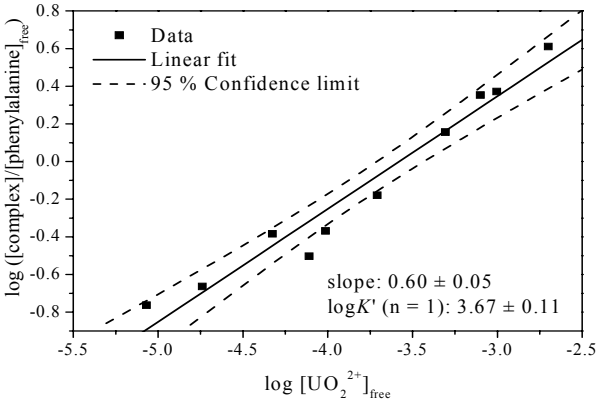

Fig. 2: Validation plot (slope analysis) of the complexation of uranium(VI) with L-phenylalanine.

caused by the free ligand. With the aid of the Stern-Volmer equation (Eq. 1) the lifetimes likewise can be used to calculate the complex stability constants.

$$\frac{\tau_0}{\tau} = 1 + K_{SV} \cdot [Q] \qquad (1)$$

τ_0 represents the fluorescence lifetime of the uranyl ion without quencher, and τ is the lifetime with quenching substance Q (free ligand). The Stern-Volmer plots (linear application of $(\tau_0/\tau)-1$ as function of c[ligand]) gave straight lines with an intersection of zero within the error limits. Their slope (K_{SV}) represents the complexation constant, which can be converted into the complex stability constant logK_{ML} as well, taking into account the pH and the pK_a values of the ligand (see Table 1). The complex stability constant of the uranyl L-phenylalanine complex is remarkable smaller than that of the uranyl 3-phenylpropionate complex. This indicates that the amino group, which appears in its protonated form R-NH_3^+ in acidic solution, is not involved in the complexation, but may rather destabilize the complex.

Tab. 1: Summary of the complex stability constants logK_{ML}.

UO_2-complex with	slope analysis	Stern-Volmer	average
L-phenylalanine[a]	1.91 ± 0.18	1.90 ± 0.07	1.9 ± 0.2
3-phenylpropionate[b]	4.06 ± 0.19	4.28 ± 0.08	4.2 ± 0.2

[a] pK_{a1}(COOH) = 2.24 ± 0.07; pK_{a2}(NH_3^+) = 9.16 ± 0.01 (pK_{a2} is not to be considered in the investigated pH range) [1].
[b] pK_a(COOH) = 4.40 ± 0.01 [2].

ACKNOWLEDGEMENT. This work was supported by the BMWi (No. 02 E 9673).

REFERENCES

[1] Ishimitsu, T. et al. (1977) *Talanta* **24**, 555-560.
[2] Hasegawa, Y. et al. (1990) *Bull. Chem. Soc. Jpn.* **63**, 2169-2172.

Complex formation of U(VI) with L-phenylalanine (2-amino-3-phenylpropionic acid) and 3-phenylpropionic acid – Part II: ATR FT-IR spectroscopy

A. Koban, H. Foerstendorf, K. Heim, S. Sachs

The uranyl complexes of phenylpropionic acid and its 2-amino derivate in aqueous solution were studied by FT-IR spectroscopy at acidic pH. As a result, the uranyl ion is complexed only by the carboxylate group and not by the amino group.

The involvement of functional amino groups in the molecular complexation of uranium(VI) with bioligands at acidic pH values is not well understood today. For this reason, vibrational spectroscopic investigations with model compounds were carried out. The complex behavior of L-phenylalanine (C_6H_5-CH_2-CH(NH_2)-COOH) and 3-phenylpropionic acid (C_6H_5-CH_2-CH_2-COOH) toward uranium(VI) at acidic pH values has been studied by ATR FT-IR spectroscopy.

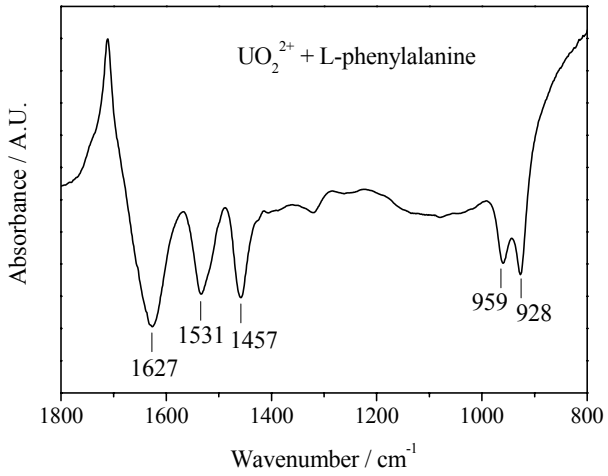

Fig. 1: FT-IR difference spectrum of a solution containing 10 mM UO_2^{2+} and 10 mM L-phenylalanine at pH 3.2.

EXPERIMENTAL. The measurements were performed with aqueous solutions containing a uranyl-to-ligand ratio of 1 : 1, a concentration of 10^{-2} M, an ionic strength of 1 M (NaCl), and pH = 3.2. At higher pH values precipitation of a not yet defined uranyl compound (either hydroxide and/or complex) was observed. The infrared spectra were recorded at room temperature with an FT-IR spectrometer (GX 2000, PerkinElmer) and a diamond ATR cell (crystal diameter: 4 mm, 9 reflections). For the experiments a flow cell (volume: 200 µL) with a constant flow rate of 200 µL/min was used. The spectra were calculated out of single beam spectra each co-added from 128 scans at a spectral resolution of 4 cm^{-1} as difference spectra between an aqueous solution of the free ligand and the related uranyl complex.

RESULTS. Fig. 1 and 2 show the difference IR spectra of the uranyl L-phenylalanine system and the uranyl 3-phenylpropionate system. The bands below 1000 cm^{-1} represent the antisymmetric stretching vibration ν_{as} of the uranyl cation. The bands at 959 and 957 cm^{-1} can be assigned to the free uranyl ion whereas the complexation of the uranyl cation causes a shift of the ν_{as} mode to 928 cm^{-1} (L-phenylalanine) and 926 cm^{-1} (3-phenylpropionate).
In the region between 1600 and 1400 cm^{-1} stretching vibrations of the carboxylate groups are normally observed. Therefore, the absorption peaks at 1457 and 1531 cm^{-1} (L-phenylalanine), and 1458 and 1533 cm^{-1} (3-phenylpropionate) are assigned to the symmetrical (ν_s) and antisymmetrical (ν_{as}) stretching vibration of the uranyl coordinating carboxylate group, respectively. The spectral region above 1600 cm^{-1} is characterized by the strong absorption band of the water solvent and therefore can not be interpreted accurately.
The spectra clearly demonstrate that the UO_2^{2+} cation is bound via the carboxylate groups to the ligands since the frequency of the uranyl band around 927 cm^{-1} is typically found for aqueous UO_2^{2+}-carboxylate complexes [1]. Additionally the degree splitting between the ν_{as} and ν_s mode of the carboxylate group indicates a bidentate binding to the actinide cation [1].

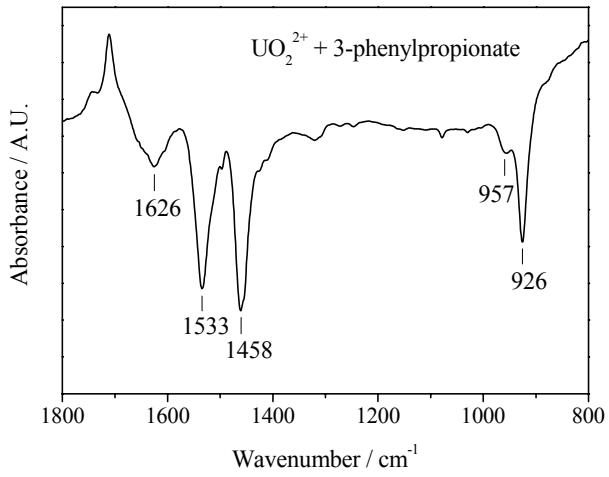

Fig. 2: FT-IR difference spectrum of a solution containing 10 mM UO_2^{2+} and 10 mM 3-phenylpropionate at pH 3.2.

In the uranyl L-phenylalanine system the ν_{as} mode of the free (959 cm^{-1}) and of the complexed (928 cm^{-1}) uranyl ion shows nearly the same intensity. In contrast, in the uranyl 3-phenylpropionate system the ν_{as} mode of the complexed uranyl ion (926 cm^{-1}) shows a considerably higher intensity compared to the band of the free uranyl ion (957 cm^{-1}). This is in accordance with the findings by TRLFS, that the 3-phenylpropionate is the stronger complexing agent for the UO_2^{2+} cation [2].
In the FT-IR spectrum of the uranyl L-phenylalanine complex system no bands can be assigned to a coordinating amino group. This underlines the conclusion made from TRLFS measurements, that the amino group is not involved in uranyl complexation under these experimental conditions, especially at acidic pH ranges [2]. However, contributions from amino groups to the spectra might be hidden under the strong difference band of the water solvent above 1600 cm^{-1} and therefore can not be ruled out entirely.

ACKNOWLEDGEMENT. This work was supported by the BMWi (No. 02 E 9673).

REFERENCES

[1] Kakihana, M. et al. (1987). *J. Phys. Chem.* **91**, 6128-6136.
[2] Koban, A. et al. this report, p. 22.

Interaction of U(VI) with phosphatidic acids studied by TRLFS

A. Koban, G. Bernhard

Uranyl complexes with two phosphatidic acids, which represent the nonpolar site of phospholipids, were studied by TRLFS at acidic pH. Two different species each were found by lifetime determination.

The study of the interaction of uranium with biosystems at a molecular level with the aid of model compounds is important for understanding the transport and metabolism of actinides in biosystems. Spectroscopic investigations at bacteria, who live in extreme habitats like uranium mining waste piles or deposits show that organic phosphate groups are mainly responsible for uranyl binding [1,2]. Other investigations with bacteria have ascertained that phospholipids are able to bind the uranyl ion [3,4].
Here we present the investigation of the interaction of the nonpolar sites of phospholipids, the phosphatidic acids, with uranyl at acidic pH, studied by TRLFS [5].

EXPERIMENTAL. The water-insoluble phosphatidic acids 1,2-dimyristoyl-sn-glycero-3-phosphate [H_3C-$(CH_2)_{12}$-COO-CH_2-(CH_3-$(CH_2)_{12}$-COO)CH-CH_2-OPO_3^{2-}; **DMGP**] and 1,2-dipalmitoyl-sn-glycero-3-phosphate [H_3C-$(CH_2)_{14}$-COO-CH_2-(CH_3-$(CH_2)_{14}$-COO)CH-CH_2-O-PO_3^{2-}; **DPGP**] were suspended (10 mM) in 0.01 mM UO_2^{2+} solutions at pH = 4.00 ± 0.05, stirred for 3 days, than centrifuged, and the soluble fraction was additionally filtrated. Fluorescence spectra were measured from the filtrate and the insoluble phase as suspension. The spectra were recorded at room temperature using a pulsed Nd:YAG laser system.

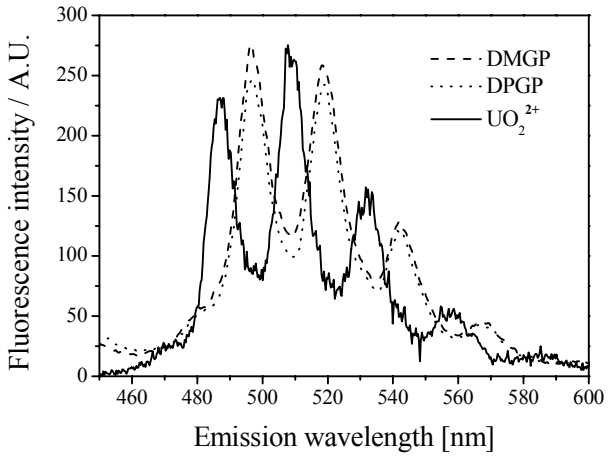

Fig. 1: Fluorescence spectra of uranyl with the phosphatidic acids 1,2-dimyristoyl-sn-glycero-3-phosphate (DMGP) and 1,2-dipalmitoyl-sn-glycero-3-phosphate (DPGP).

RESULTS. The two phosphatidic acids DMGP and DPGP were treated with an aqueous uranyl solution. After centrifugation and filtration no uranium could be detected in the aqueous solution, neither with fluorescence spectroscopy nor with ICP-MS. The fluorescence spectra of the wet solids are very similar among themselves. They are red-shifted of about 8 nm, compared with the free uranyl ion (see Fig. 1). This is caused clearly by the phosphate binding of the uranium. The peak maxima were determined to be 497, 519, 542, and 568 nm for both systems. Similar shifts were detected by uranyl complexes with several bacteria [1,6,7].

The evaluation of the time-resolved measurements of the uranyl phosphatidic acid systems show bi-exponential decay with a shorter lifetime of about 1 µs for both systems and a larger lifetime of 20 µs for the uranyl DMGP system and 13 µs for the uranyl DPGP system, respectively (see Fig. 2). This indicates that at least two uranyl complexes each have been formed. This is in accordance to the findings of uranyl bacteria complexes. Several studies of interaction of bacteria from uranium mining waste piles or deposits show also two groups of lifetimes [1,6,7]: one group with shorter lifetimes between 1.5 and 3.5 µs [1,6] and a second group with larger lifetimes between 24 and 45 µs [7].

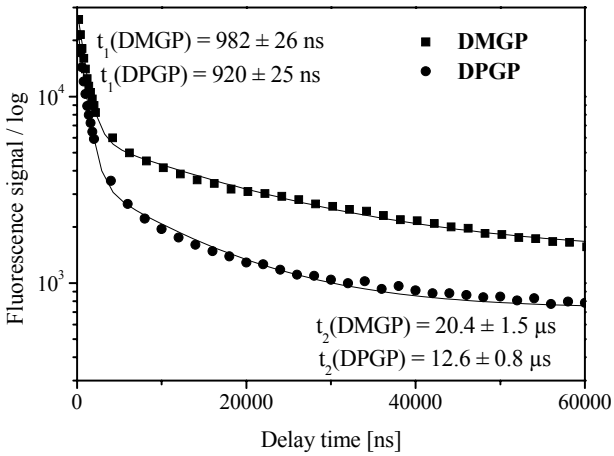

Fig. 2: Evaluation of the time-resolved fluorescence spectra to determine the lifetimes.

This study underlines the theory, that phospholipids are important components in biosystems for uranium complexation and that the complexation is carried out via the phosphate group. So far it is still unclear if deprotonated phosphate groups (R-PO_3^{2-}) or protonated phosphate groups (R-PO_3H^-) are involved in the uranyl binding. Also the formation of complexes with a metal-to-ligand ratio of 1 : 1 and 1 : 2 or dimeric or oligomeric structures have to be taken into account. Further investigations with additional methods such as EXAFS, ^{31}P NMR, or IR spectroscopy are required to clear up the complex types and their structures.

REFERENCES

[1] Panak, P. et al. (2000) *Radiochim. Acta* **88**, 71-76.
[2] Merroun, M. et al. (2003) *Radiochim. Acta* **91**, 583-591.
[3] Andres, Y. et al. (1994) *FEMS Microbiol. Lett.* **115**, 27-32.
[4] Macaskie, L.E. et al. (2000) *Microbiology* **146**, 1855-1867.
[5] Koban, A. et al. (2007) *J. Inorg. Biochem.* (accepted).
[6] Panak, P. et al. (1999) *Radiochim. Acta* **84**, 183-190.
[7] Merroun, M. et al. (2003) *BioMetals* **16**, 331-339.

Complex formation of Cm(III) with amino acids of different functionalities (L2-aminobutyric acid, L-threonine and O-phospho-L-threonine) studied by TRLFS

H. Moll, G. Bernhard

Curium species of the type $M_pH_qL_r$ were identified from the TRLFS spectra in all three systems. Depending on the substituent on the C3 atom, the strength of complexation decreases from phosphothreonine via threonine to L2-aminobutyric acid. The formed curium species influence the Cm(III) speciation at biologically important pH values.

Complexation studies of trivalent actinides with amino acids of different functionalities is challenging due to the importance of such biomolecules in the life cycle and because of the very limited knowledge in the literature about the speciation of e.g. Cm(III) in such biosystems. In particular, we want to determine how the substituent on the C3 atom (-H in the case of L2-aminobutyric acid, -OH in the case of threonine and $–OPO_3H_2$ in the case of phosphothreonine) influences the Cm(III) complexation.

EXPERIMENTAL. The detailed experimental parameters of the threonine (Thr)-, phosphothreonine (PThr)-, and aminobutyric acid (L) measurements are summarized in [1,2]. The experiments were performed under N_2 atmosphere at 25 °C. The [Cm(III)] was fixed to $3 \cdot 10^{-7}$ M. TRLFS spectra were recorded using a flash lamp pumped Ti:sapphire laser (Elight, Titania). Details on the experimental set-up are summarized in [3].

RESULTS. The TRLFS measurements indicated differences between the luminescence properties of the aqueous species formed in the phosphothreonine, threonine and aminobutyrate system. We could demonstrate that depending on the substituent on the C3 atom the strength of complexation decreases from phosphothreonine via threonine to L2-aminobutyric acid (see Fig. 1).

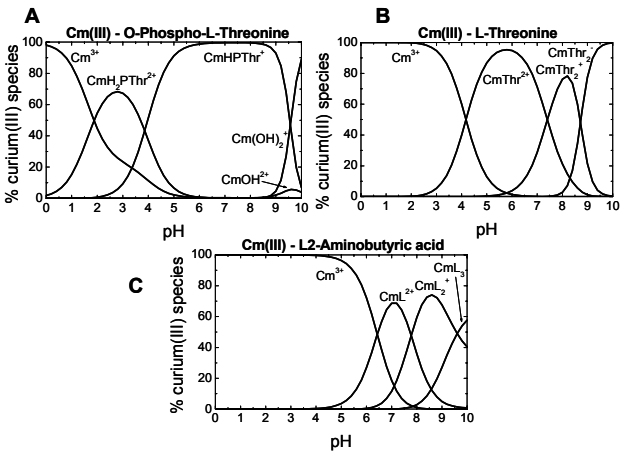

Fig. 1: Calculated species distribution in aqueous solution at [Cm(III)] $3 \cdot 10^{-7}$ M and ligand concentrations of 0.01 M.

The strongest species were formed in the presence of a phosphate group located at the C3 atom as in phosphothreonine. The complex CmH_2PThr^{2+} is characterized by a luminescence maximum at 597 nm and a luminescence lifetime of 77 µs. For the species $CmHPThr^+$ the largest red shift of the emission maxima for a 1:1 complex in this study of 7.2 nm compared to Cm^{3+} aqua ion was measured (see Fig. 2). Together with the luminescence

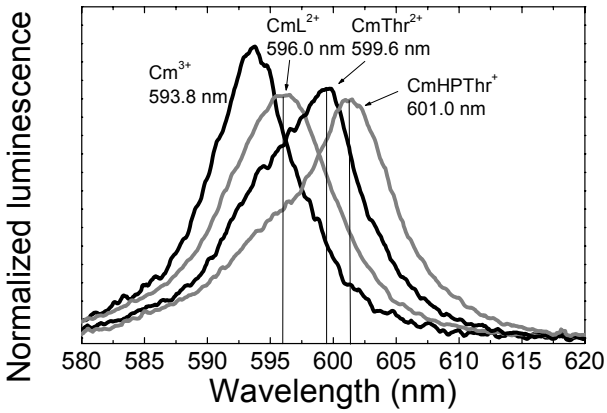

Fig. 2: Luminescence spectra of the single components, the 1:1 species, in the three systems as derived by peak deconvolution using SPECFIT; the spectra are scaled to the same peak area.

lifetime of 83 µs this points to the formation of a seven-membered chelate ring.

Three different Cm-threonine species could be identified [1]. In the complex, $CmThr^{2+}$, curium coordinates most likely in a monodentate way to the oxygen atom of the carboxylic group. The larger formation constant and red shift of the luminescence compared with the aminobutyrate 1:1 complex (see Fig. 2) suggest an incipient interaction with the $–NH_2$ group. The two Thr molecules in $CmThr_2^+$ are coordinated in a chelate fashion [1]. The findings for the third complex, $CmH_2Thr_2^-$, point to the formation of a stable chelate structure as described in [1].

The weakest tendency to form aqueous species with Cm(III) was observed in the L2-aminobutyrate system. The 1:1 complex, CmL^{2+}, shows with 596 nm the smallest red shift of all 1:1 species identified in this study (see Fig. 2). By taking all information [2] into consideration, the curium atom most likely interacts with the oxygen atom of the carboxylic group in a monodentate way. For the 1:2 species, CmL_2^+ (luminescence maximum: 600.8 nm; lifetime: 84 µs), follows that the two aminobutyrate molecules are coordinated monodentate via the oxygen atom of the carboxylic group to Cm(III). The largest red shift of the emission maxima, 603.8 nm, in the aminobutyrate system was detected for the CmL_3 complex. The lifetime of 118 µs suggests the coordination of two bidentate amino acid molecules, where the donors are the O from the $–COO^-$ group and the N from the $–NH_2$ group, and one monodentate amino acid molecule via the O from the carboxylic group.

It can be concluded that the formation of curium species with the three ligands influences the speciation of the curium ion at biologically important pH values between 4 and 7.

ACKNOWLEDGEMENT. This work was funded by the BMWi under contract number 02E9985.

REFERENCES

[1] Moll, H. et al. (2007) *J. Coord. Chem.* (in press).
[2] Moll, H. et al. (2007) *J. Radioanal. Nucl. Chem.* (accepted).
[3] Stumpf, T. et al. (2002) *J. Chem. Soc., Dalton Trans.* 3799-3804.

Nitrogen-containing humic acid model substances: Synthesis and characterization by ^{15}N-NMR spectroscopy

S. Sachs, E. Brendler[1]

[1]Institute of Analytical Chemistry, Faculty for Chemistry and Physics, TU Bergakademie Freiberg, Freiberg, Germany

A ^{15}N-labeled synthetic humic acid (HA) was synthesized and characterized by ^{15}N-NMR spectroscopy. Together with literature data for natural HA, the NMR results represent a base for the selection of model ligands to elucidate the impact of nitrogen functionalities on the metal ion complexation by HA.

Humic substances contain nitrogen, although in different and small amounts (HA: 0.8 – 4.3 % [1]). Whether nitrogen-containing functional groups contribute to the complexation between HA and metal ions is widely unknown. To get more detailed information on the kind of nitrogenous functionalities in HA, synthetic HA type M1 [2] was ^{15}N-labeled and characterized by ^{15}N-NMR spectroscopy.

EXPERIMENTAL. ^{15}N-labeled HA type M1 ([^{15}N]M1) was synthesized from 3.4 g xylose, 1.0 g [^{15}N]-L-phenylalanine, 0.5 g glycine, and 8 mL water. This mixture was refluxed in a N_2 stream for 10 h. The HA-like melanoidin fraction was separated from the reaction mixture as described in [2], dialyzed against water (dialysis tubes Thomapor®, MWCO < 1000, Roth), and dried.
Solid-state ^{15}N-NMR measurements were carried out using cross polarization with magic angle spinning (CP/MAS). The ^{15}N-NMR spectra were recorded on a Bruker Avance 400 MHz WB spectrometer equipped with a 7 mm probe head using ZrO_2 rotors. Chemical shifts are referred to nitromethane (= 0 ppm). The peak assignment is based on data collections for ^{15}N-NMR chemical shifts of organic compounds and humic substances [3,4].

RESULTS. Compared to an unlabeled HA type M1, HA [^{15}N]M1 shows a similar elemental composition, functional group content and IR spectrum [5]. Figure 1 shows the ^{15}N-NMR spectrum of HA [^{15}N]M1. It exhibits signals between −150 and −350 ppm indicating the presence of various N-containing functionalities in the HA structure.

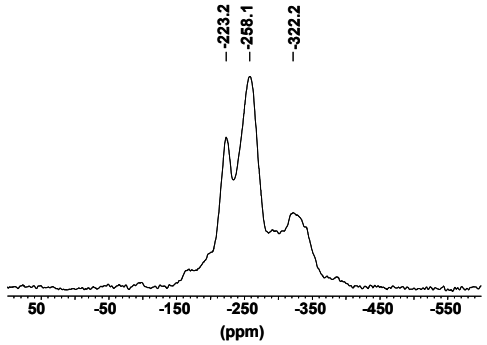

Fig. 1: ^{15}N-NMR spectrum of HA [^{15}N]M1 (rotation frequeny: 5 kHz; contact time: 1 ms; repetition rate: 3 s).

Recording ^{15}N-NMR spectra by CP/MAS is an indirect method. Protons of the sample are excited and their magnetization is transferred to the ^{15}N nuclei by simultaneously irradiating the resonance frequencies of ^{1}H and ^{15}N during a contact time τ_{CP} at a certain ratio of radio frequency field strength. This results in an enhancement of the ^{15}N-signal. In general the enhancement maximum for H-free environments is found at longer τ_{CP} than for H-carrying groups. Figure 2 shows the NMR spectra of HA [^{15}N]M1 recorded with different τ_{CP}. The increase of τ_{CP} from 1 to 5 ms results in a slight intensity increase of the signals between −150 and −200 ppm. The signals at −255 and at about −315 ppm have higher intensities at shorter τ_{CP}. From that and reference data it is concluded that the chemical shifts up to −200 ppm are due to H-free and heterocyclic bound structural elements.

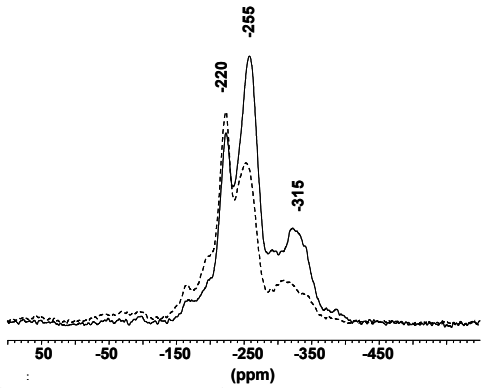

Fig. 2: ^{15}N-NMR spectra of HA [^{15}N]M1 measured at different contact times (solid: 1 ms, dashed: 5 ms; rotation frequency: 5 kHz; repetition rate: 3 s).

The main resonances in the spectrum of HA [^{15}N]M1 can be attributed to NH in heterocyclic structures (−220 ppm), NH in amide structures (−255 ppm), and to primary and secondary amines (NH, NH_2, −315 ppm). The shoulders between −150 and −200 ppm are ascribed to N-substituted pyrroles and/or indoles or heterocyclic –N= sites in these compounds. Free NH_2 groups of amino acids exhibit resonance signals between −325 and −350 ppm [4]. The spectrum of [^{15}N]M1 shows a broad unresolved signal in this range, which is more intensive at lower τ_{CP}. This signal could be a result of overlapping chemical shifts of primary and/or secondary amines and terminal amino acid groups. The obtained data agree with N structures for natural organic matter discussed in [1].
Thus NH_2 groups of [^{15}N]-L-phenylalanine are for the most part transformed into heterocyclic and amide nitrogen functions. There are, however, also primary and/or secondary amine groups, and possibly terminal amino acid groups in the HA structure. First studies on the impact of amino acid NH_2 groups on the U(VI) complexation by HA are described in [6,7].

ACKNOWLEDGEMENT. This study was funded by the German Federal Ministry of Economy (02 E 9673).

REFERENCES

[1] Stevenson, F.J. (1994) *Humus Chemistry. Genesis, Compositions, Reactions*, 2nd ed., Wiley, New York.
[2] Pompe, S. et al. (1996) *Radochim. Acta* **74**, 135-140.
[3] Berger, S. et al. (1992) *NMR-Spektroskopie von Nichtmetallen. Band 2: ^{15}N-NMR-Spektroskopie*, Thieme, Stuttgart.
[4] Bortiatynski, J.M. et al. (1996) in*: ACS Symposium Series 651 (Humic and Fulvic Acids)*, American Chemical Society, p. 57-77.
[5] Sachs, S. et al. (2006) *Final Report BMWi-Project No. 02 E 9673.*
[6] Koban, A. et al. this report, p. 22.
[7] Koban, A. et al. this report, p. 23.

Binding properties of nucleosides with a phosphonate substituted clip using TRLFS

B. Raditzky, H. Stephan[1], G. Geipel, J. Polkowska[2], F.-G. Klärner[2]

[1]Institute of Radiopharmacy, FZD, Dresden, Germany; [2]Institute of Organic Chemistry, University of Duisburg-Essen, Germany

The interaction of nucleosides with a molecular clip was studied by TRLFS at neutral pH. All ligands quench the fluorescence of the clip. Association constants around log K_a = 4 were determined for all 1:1 complexes.

Molecular recognition and self-assembly, based on weak non-covalent interactions, are significant processes in chemical and biological systems [1], e.g. in enzyme-substrate binding or formation of protein complexes. So, the development of efficient synthetic receptors with the ability to bind substrates selectively is important. The water-soluble naphthalene clip with substituted phosphonate groups (Fig. 1) offers electron-rich side walls, which are suitable to bind electron-poor guests [2]. The complexation behavior of this clip toward nucleosides has been studied by time-resolved laser-induced fluorescence spectroscopy with ultrafast pulses (fs-TRLFS).

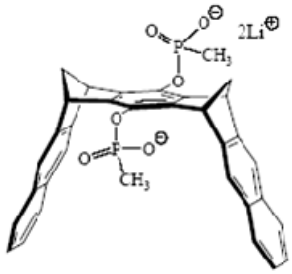

Fig. 1: Structure of the phosphonate substituted clip.

EXPERIMENTAL. The water-soluble benzene-naphthalene-spaced clip was prepared according to published procedure [3,4]. The experiments were accomplished in phosphate buffer solution with an ionic strength of 0.8 M at pH 7.4. The samples were prepared under following conditions: $[clip]_0$: $1 \cdot 10^{-5}$ M, [nucleoside]: 8 different concentrations between $5 \cdot 10^{-6}$ M to $1 \cdot 10^{-4}$ M. The spectra were measured at room temperature using a pulsed Nd:YVO_4-Laser system (delay time: 20 ns, excitation wavelength: 266 nm). The results are means of two independent experiments.

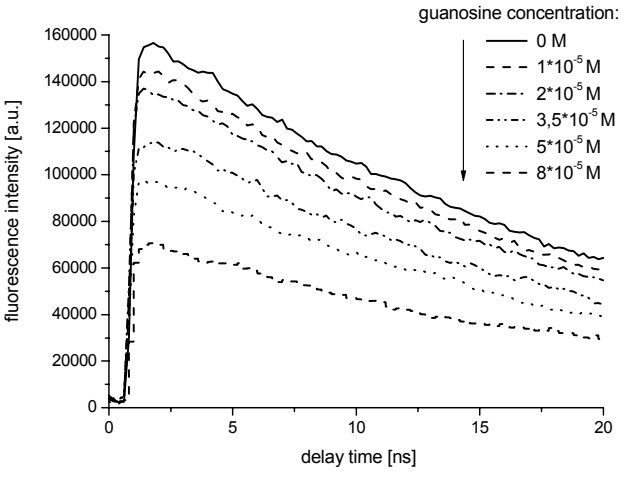

Fig. 2: TRLFS spectra of the phosphonate-clip at pH 7.4 as a function of guanosine concentration.

RESULTS. The phosphonate-substituted clip showed fluorescence in the wavelength range between 320 and 440 nm. The spectra hold a decrease of the fluorescence intensity with increasing ligand concentrations. Figure 2 depicts the spectra of guanosine as an example for fluorescence-quenching as a function of the nucleoside concentration. With the mass action law the association constant can be determined. To characterize the binding properties of the formed complexes, a validation plot was performed. Via slope analysis the binding constant log K_a was graphical determined. Figure 3 shows the validation plot for the complexation of guanosine with the phosphonate clip.

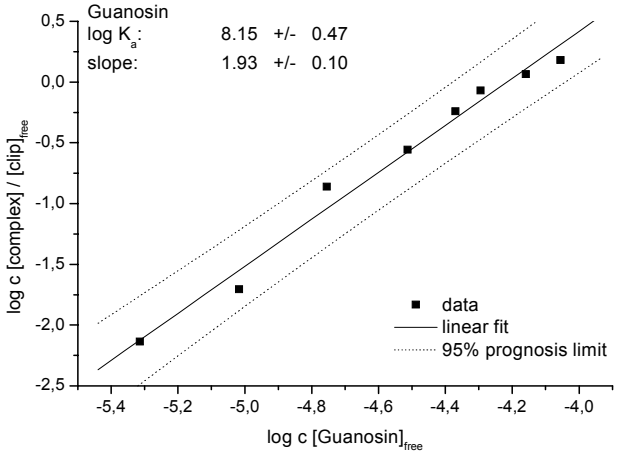

Fig. 3: Validation plot (slope analysis) of the association of guanosine with the phosphonate-clip.

A slope near 1 was calculated for the complexation of adenosine, cytidine, thymidine and uridine, resp., with the clip investigated advising a 1:1 complexation. Only for guanosine a 2:1 complex (two nucleoside molecules bind to one clip molecule) was acquired. The measured stability constants were shown in Tab. 1. All stability constants, except the log K_a for the guanosine-clip complex, are comparable (log $K_a \approx 4$).

Tab. 1: Complexation data for the interaction of the phosphonate-clip with nucleosides at pH 7.4.

clip with	slope analysis	complex	log K_a
guanosine	1.93 ± 0.10	2:1	8.15 ± 0.47
adenosine	1.02 ± 0.05	1:1	4.25 ± 0.07
cytidine	0.73 ± 0.05	1:1	4.15 ± 0.06
thymidine	1.09 ± 0.05	1:1	3.99 ± 0.11
uridine	1.03 ± 0.06	1:1	4.05 ± 0.10

ACKNOWLEDGEMENT. This work is part of D31 Cost action "Organizing Non-Covalent Chemical Systems with Selected Functions".

REFERENCES

[1] Vögtle, F. (1997) *Supramolekulare Chemie,* Teubner Verlag, Stuttgart.
[2] Jasper, C. et al. (2002) *Angew. Chem.* **114**, 1411-1415.
[3] Fokkens, M. et al. (2005) *Chem. Eur. J.* **11**, 477-494.
[4] Klärner, F.-G. et al. (2006) *J. Am. Chem. Soc.* **128**, 4831-4841.

Investigation and identification of the silicous uranyl minerals sodium boltwoodite $Na[UO_2SiO_3(OH)]\cdot 1.5H_2O$ and uranophane $Ca[(UO_2)_2(SiO_3)_2(OH)_2]\cdot 5H_2O$ introducing TRLFS fingerprinting

S. Lehmann, G. Geipel

To establish TRLFS as an almost non-invasive and non-destructive analytical method for identification of uranium(VI) mineral phases in environmentally relevant concentration ranges, sodium boltwoodite and uranophane were synthesized for reference purposes, and their spectroscopic features were determined by recording their time-resolved laser-induced fluorescence spectra and characterizing these two minerals by means of their positions of peaks and their time of fluorescence decay.

In the environment, not only the primary compounds of uranium have a sustainable impact, but also the secondary minerals, which are formed while uranium is passing through solid and aqueous phases and mainly determining the contamination of soils and groundwater by processes such as precipitation and dissolution, co-precipitation, adsorption and desorption [1]. TRLFS allows direct measurements of such samples in very low concentration ranges. Hence, for identification of natural occurring uranium(VI) complexes, in particular uranyl silicates, sodium boltwoodite and uranophane as substrates for silicious uranyl minerals were synthesized and characterized introducing TRLFS, and thus, add to a better understanding of the chemical coordination of adsorbed silicious uranium(VI) phases.

EXPERIMENTAL. Sodium boltwoodite was synthesized applying the method described in [2] for the synthesis of sodium weeksite. Verification of the successfully obtained mineral was carried out by means of XRD and FT-IR measurements. Uranophane was prepared out of synthetic boltwoodite. Instructions for the syntheses of both minerals are provided in [3]. The success of the reaction was again verified by XRD and FT-IR measurements. The TRLFS system applied is described in [4]. Fluorescence spectroscopic investigations were carried out with the solid samples. The excitation wavelength used was 266 nm.

RESULTS. Evaluation of the TRLFS recordings provides sharp emission bands and defined peak position for sodium boltwoodite and uranophane. Results can be found in Tab. 1. Values are compared to peak positions of the free uranyl ion (aq.). Fluorescence peaks of sodium boltwoodite are shifted to lower wavelengths whereas the peak maxima characterizing uranophane show a shift towards higher wavelengths. Furthermore, based on the TRLFS spectra obtained the time of fluorescence decay of both minerals was determined. Sodium boltwoodite as well as uranophane show two lifetimes. For sodium boltwoodite, they are $t_1 = 6400$ ns $\pm$ 580 ns and $t_2 = 147000$ ns $\pm$ 7400 ns with $R^2 = 0.942$. For uranophane, with $R^2 = 0.997$, $t_1 = 2200$ ns $\pm$ 130ns and $t_2 = 7400$ ns $\pm$ 1700ns were determined.
The presence of varying contents of water molecules, partly quenching the fluorescence, and small quantities of impurities might provide an explanation for the occurrence of the second lifetime in sodium boltwoodite and uranophane.

Tab. 1: Position of TRLFS peak maxima of sodium boltwoodite and uranophane in comparison to peak maxima of UO_2^{2+}(aq.):

Free uranyl [nm]	Sodium boltwoodite [nm]	Uranophane [nm]
470.1	458.6	484.5
486.7	477.6	493.8
507.9	499.2	512.3
531.0	521.3	533.2
556.0	543.2	555.6
584.2	567.2	580.1

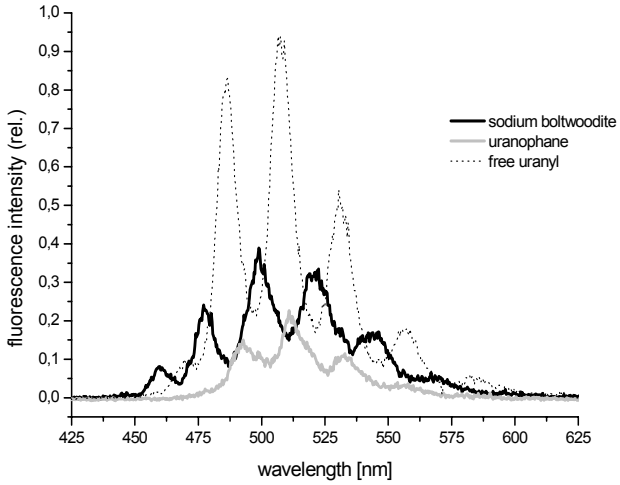

Fig. 1: Deconvoluted fluorescence spectra of sodium boltwoodite and uranophane in comparison to free uranyl.

REFERENCES

[1] Lottermoser, B. (2003) *Mine Wastes: Characterization, Treatment and Environmental Impacts,* Springer, Berlin/Heidelberg.
[2] Vochten, R. et. al. (1997) *N. Jb. Miner. Mh.* **12**, 569-576.
[3] Vochten, R. (1997) *Can. Mineral.* **35**, 735-741.
[4] Geipel, G. (2000) *Radiochim. Acta* **88**, 757-762.

DFT calculations of uranyl(VI) hydrate

S. Tsushima, A.C. Scheinost

Hydration number and water exchange rate and mechanism of uranyl(VI) was studied by density functional theory (DFT) calculations.

In a number of previous publications, it has been shown that quantum chemical calculations can be used to estimate the hydration number of UO_2^{2+} ions and also their water exchange mechanisms. We followed the same procedure as previous works to study the stable hydration number and water exchange mechanism of the UO_2^{2+} ion, but searched the potential energy surface more carefully. Geometry optimization was performed in solvent at the B3LYP level. The small core effective core potential was used for U and O with the corresponding basis set. All calculations were performed using Gaussian 03. Precursors, intermediates, and transition states were confirmed to be the real states through vibrational frequency analysis with no or just single imaginary frequency present.

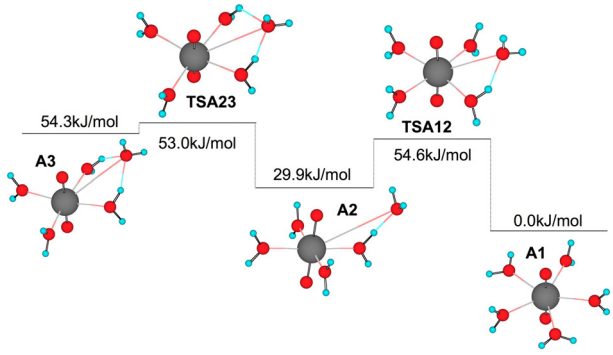

Fig. 1: Geometries and Gibbs energies of 4-fold, 5-fold uranyl(VI) hydrate and transition states between them. Gibbs energy value is relative to complex A1.

The structures of $UO_2(H_2O)_5^{2+}$ and $UO_2(H_2O)_4(H_2O)^{2+}$ were optimized (Fig. 1). The transition states between intermediates were also identified. 4-fold uranyl(VI) (A2) was found to be 29.9 kJ/mol above 5-fold (A1), and its activation Gibbs energy was determined to 54.6 kJ/mol. The Gibbs energy difference between the two "4+1" models, A2 and A3, is 24.4 kJ/mol and is surprisingly large. In contrast to this, the gas phase energy difference between A2 and A3 is only 0.3 kJ/mol. The large Gibbs energy difference between A2 and A3 comes from the entropy term (*ST*) and also from the solvation energy. These two factors make A2 to be much more stable than A3. There is a problem with the A2 model, however, since the $H_I\cdots O_{II}$ bond distance is 1.561 Å and is much shorter than a normal hydrogen bond distance. The $U\text{-}O_{II}$ distance of 4.427 Å in A2 is also much shorter than experimentally obtained $U\text{-}O_{II}$ distance of 4.50 Å by high-energy X-ray scattering (HEXS) [1]. DFT calculation is known to overestimate the hydrogen bond strength, and thereby tends to underestimate the hydrogen bond distance. Siboulet et al. optimized the structure of UO_2^{2+} with complete first and second hydration shells at the B3LYP level and obtained the $H_I\cdots O_{II}$ bond distance of 1.70 – 1.79 Å [2]. Therefore, it is not a DFT problem that we encountered, but due to a strong electrostatic attraction of "+1" water by UO_2^{2+} cation by using an "ill-shaped" model which lacks the rest of the second hydration sphere. The problem with the A2 model is that a short $H_I\cdots O_{II}$ bond distance can overestimate the stability of the "4+1" complex by decreasing the cavity of the solute thereby increasing the absolute solvation energy. We roughly estimate that this type of model can overestimate the stability of 4-fold uranyl(VI) hydrate by ~10 kJ/mol.

There is also a problem in the A3 model in so far as this is not the symmetric point of the water exchange reaction. To make A3 to be the symmetric point, one needs to add another second-shell water molecule that also has two hydrogen bonds to the first shell waters. This results in an extremely low coordination number for the second shell, and such complex cannot stay as a stable intermediate. Clearly, A2 is a more reasonable model as an intermediate of dissociative (*D*-) water exchange pathway, but short $H_I\cdots O_{II}$ bond distance causes its energy to be less precise.

Similar calculations were performed to test the "5+1" against the "6" model. It was found that the 6-fold uranyl(VI) is 42.9 kJ/mol above the 5-fold coordination, and there is virtually no activation barrier; the transition states being very close to the intermediate. There is the same "*n*+1" model problem here and the $H_I\cdots O_{II}$ distance is too short, suggesting that the stability of "5+1" is overestimated. Therefore, although the calculated energy difference between "5+1" and "6" is 42.9 kJ/mol, the actual energy difference between 5-fold and 6-fold uranyl(VI) is estimated to be smaller.

The activation Gibbs energies of water exchange reaction via dissociative (*D*-) and associative (*A*-) pathway obtained in this study are $\Delta G^{\ddagger} = 54.6$ kJ/mol and $\Delta G^{\ddagger} = 42.4$ kJ/mol, respectively. The experimental number for the same reaction obtained by ^{17}O NMR is 38.1 kJ/mol [3] and is in reasonable accord with the theoretically obtained number for the *A*-mechanism.

Our results suggest that although the 4-fold intermediate is energetically favorable over the 6-fold intermediate, the activation energy of the water exchange reaction is lower to pass through the *A*-mechanism than through the *D*-mechanism. However, we point out again that the "*n*+1" model tends to overestimate the stability of the complex, and stability of both "5+1" and "4+1" complexes are hence most likely overestimated. We therefore conclude that 6-fold uranyl(VI) is perhaps more stable than 4-fold uranyl(VI) both at its intermediate and transition states.

In summary, precursors, intermediates, and transition states identified for 4-, 5-, and 6-fold uranyl(VI) hydrate suggest 5-fold uranyl(VI) to be the most stable. It was found that the "*n*+1" model underestimates the $An\text{-}O_{II}$ distance and thereby overestimates its energetic stability. 6-fold uranyl(VI) stays closer to 5-fold complex than the 4-fold uranyl(VI) does. The water exchange reaction of 5-fold uranyl(VI) takes place through the *A*-mechanism, and this process is very rapid. No evidence was found that 4- or 6-fold uranyl(VI) hydrate would stay in solution at a detectable level.

ACKNOWLEDGEMENT. S. Tsushima was supported by a stipend from Alexander-von-Humboldt foundation.

REFERENCES

[1] Soderholm, L. et al. (2005) *J. Anal. Bioanal. Chem.* **383**, 48.
[2] Siboulet, B. et al. (2006) *Chem. Phys.* **326**, 289.
[3] Farkas, I. et al. (2000) *Inorg. Chem.* **39**, 799.

TRLFS: Analyzing spectra with an expectation-maximization (EM) algorithm

A. Steinborn[1], S. Taut[2], V. Brendler, G. Geipel, B. Flach[1]

[1]Artificial Intelligence Institute, Dresden University of Technology, Dresden, Germany; [2]Radiation Safety Group, Dresden University of Technology, Dresden, Germany

A new approach for fitting models to time-resolved laser-induced fluorescence spectroscopy (TRLFS) spectra is presented, based on an expectation-maximization (EM) algorithm. It allows to partition the spectrum into its components and peaks using the revealed hidden attributes of the emitted photons drawn from a probability density distribution.

Assuming fluorescence spectra result from counting emitted photons in defined intervals, a photon can be described by emission time and wavelength as observable attributes and by component and peak affiliation as hidden ones. Understanding the attribute values of the emitted photons as drawn from a probability density distribution, the model estimation problem can be described as a statistical problem with incomplete data. Solutions based on well known least squares method often had convergence problems or did deliver inconsistent parameter sets. Therefore an expectation-maximization (EM) algorithm was derived and tested to solve the maximum-likelihood task. The advantage of the new approach is the ability to partition the spectrum simultaneously into its components and peaks using the revealed hidden attributes of the photons.

MODEL. The emitted photons are the elementary events of the statistical model. Each photon can be described by emission time and wavelength as observable attributes and by component and peak affiliation (k and g) as hidden ones. The probability density function

$$p(t,\lambda) = \sum_{k \in K} p(k) \cdot p(t \mid k) \cdot \sum_{g \in G_k} p(g \mid k) \cdot p(\lambda \mid k,g)$$

describes the probability that a photon with wavelength λ will be emitted at time t. To model TRLFS spectra based on actinide species the use of exponentials for the temporal distribution $p(t \mid k)$ and of Gaussians or Lorentzians for the spectral distributions $p(\lambda \mid k,g)$ seem appropriate. The best model parameters M^* are calculated by the maximum-likelihood estimator

$$M^* = \arg\max_M \prod_{t,\lambda} p(t,\lambda)^{\phi_{t\lambda}}$$

which maximizes the probability of the measured data $\phi_{t\lambda}$. The maximum-likelihood estimator is realized as an hierarchical expectation-maximization algorithm [1,2,3]. This is an iterative algorithm and performs in each iteration an expectation (E) and a maximization (M) step. The E step calculates the hidden parameters using the actual model parameters and the M step uses this parameters to refine the model parameters. The revealed hidden parameters can be used to partition the spectra into its components and peaks.

RESULTS. The investigation of the developed EM algorithm for simulated spectra shows that the estimation of the parameters is a bit biased for reasons unknown so far. However, the algorithm is still applicable in practice because the bias is smaller than 10 % of the standard deviation. Figure 1 shows the partition of an experimental uranyl spectrum (10^{-5} M U total, pH 2, I = 0.1 mol/L NaClO$_4$) into the two significant components: UO_2^{2+} as the dominant species under these conditions and a smaller one of unknown stoichiometry, most probably UO_2HPO_4(aq) caused by the use of phosphate containing detergents for vessel cleaning. The pictures shows the spectral distributions of the first (bottom) and second (top) components with the six major peaks typical for the uranyl cation. This possibility to simultaneously partition a spectrum into its components and peaks is a great advantage in contrast to least squares methods because an acceptable partition implies reliable model parameters. This facilitates new possibilities for evaluation of the resulted models. The simultaneous detection of time and spectral model parameters results in a mutually consistent description of TRLFS spectra. This is essential for the projected applications such as to catalogue and to compare TRLFS spectra using model based similarity measures. Furthermore the statistical aspect of TRLFS is considered.

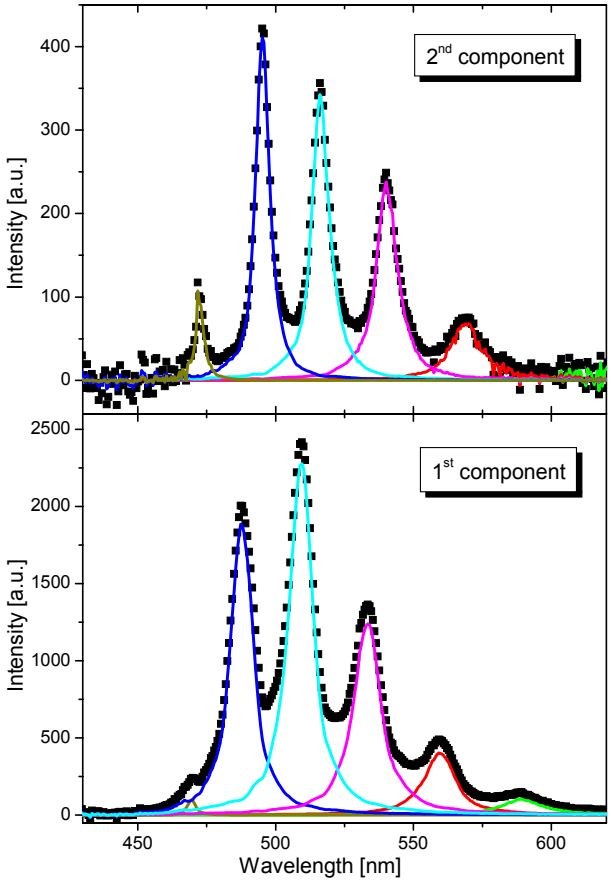

Fig. 1: First and second component (each with six peaks) of TRLFS spectrum of a 10^{-5} M uranium(VI) solution at pH 2.

REFERENCES

[1] Dempster, A.P. et al. (1977) *Proc. Royal Stat. Soc.* **B-39**, 1-38.
[2] Schlesinger, M.I. et al. (2002) *Ten lectures on statistical and structural pattern recognition*, Kluwer Academic Publishers, Dordrecht.
[3] Steinborn, A. (2006) *Untersuchung der Ähnlichkeit von TRLFS-Spektren*, *Diploma thesis*, Dresden University of Technology, Dresden.

Development of a database for TRLFS: Experimental raw data and model parameters

M. Rentzsch[1], V. Brendler, S. Taut[2], G. Geipel, M. Eilzer

[1]Faculty of Mechanical and Process Engineering; University of Applied Science, Dresden, Germany; [2]Radiation Safety Group, Dresden University of Technology, Dresden, Germany

A relational database has been developed to promote a uniform storage of TRLFS spectra including all meta data related to the experimental set-up and the subsequent data processing. The approach also provides retrieval features and is designed to allow an easy transfer to other spectroscopic methods.

TRLFS (time-resolved laser-induced fluorescence spectroscopy) as a valuable speciation tool for highly sensitive non-invasive in-situ experiments has been used since many years now. The generated large amount of spectra, their background information and the data processing results are distributed over several physical locations in varying formats so far. This significantly hampers an efficient use of the available information, renders quality assurance very difficult and complicates comparison and generalization. Thus, the authors drafted a database for storage and retrieval of spectroscopic data. This was done in a generic way to allow for an easy transfer of the concept to other methodologies later, such as X-ray absorption or infrared spectroscopy.

IMPLEMENTATION. A relational database was designed, it is currently implemented in MS Access 2000. The major content blocks and their mutual relationship are illustrated in Fig. 1. Namely this concerns data records for

– the specification of an experiment and experimental conditions, such as the amount of accumulated laser shots, the gate time width, temperature, extraordinary conditions of atmosphere, or the usage of a cryostat,
– the physico-chemical (and biological, if applicable) specification of the investigated sample, such as concentration ranges, pH-value, ionic strength, sample composition with regard to pure components, grain size, usage type of components (e.g., electrolyte, solvent),
– the instrumental set-up, such as system configuration, technical specification of single devices (laser, spectrograph, detector, grating, delay generator).

To restrict access to sensitive parts of the database three major categories of users are defined:

The Searchers are able to use the archive of spectra with all metadata about measurements. They will be able to retrieve spectra based on several obligatory query attributes (e.g., biological keywords).

The Experts have the same permissions as the above group, but in addition are allowed to input new spectra with all metadata about the respective experiment. As a rule, this user group are the experimenters themselves.

The Administrators have no restrictions in running user applications at all, including changes in the data base design itself.

An online manual is in development, which will also be accessible within the database interface. The spectra itself can be stored in different ways: as pure (structured) ASCII table, as file with formats imposed by the original detector system, or as graph (binary data / image).

A part of the database still to be incorporated is the storage of model parameters obtained from the data processing of the original spectra. In the case of TRLFS this means the number of components, with peak maxima, fluorescence decay lifetimes, and peak areas associated to each component.

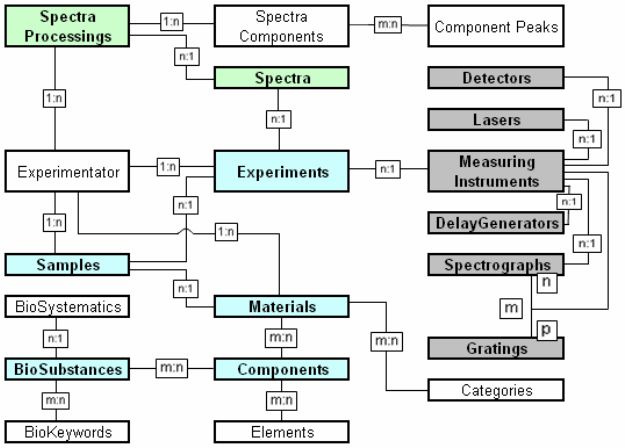

Fig. 1: Schematic entity-relationship diagram for the TRLFS database.

USER INTERFACE. The user interface starts with a menu offering buttons for the following actions:

– *Data Input / Assembly.* A subsequent filling of these input forms guarantees the uniformity of the most important experimental metadata, simultaneously preventing redundancy. This menu option ensures the referential integrity of the spectra/metadata pool.
– *Data Query & View.* Here, direct access to the spectra and meta data pool itself is provided. It provides professional users the opportunity of a targeted query by defined criteria, e.g., solution composition or involved metal. The possibility of an easier and faster comparison will make evaluations more efficient.
– *Administration.* This option allows for maintenance and statistical data evaluation. This includes backup tasks, data export and adaptation to local requirements.
– *Online Help.* In case of problems the user will find detailed explanations about the meaning and format requirements of the various tables and fields therein, including hints how to fill them.

ACKNOWLEDGEMENT. Special thanks to all colleagues from the IRC at FZD for their helpful suggestions and data supply, especially to Dr. N. Baumann.

REFERENCES

[1] Brendler, V. et al. (2004) *Report FZR-409.*
[2] Baloui, S. (2001) *Access 2002.* Markt+Technik Verlag, München.

Actinides in bio-systems

Microsensor analysis of oxygen in uranium contaminated and well aerated multi-species biofilms

E. Krawczyk-Bärsch, K. Großmann, T. Arnold, K. Flemming, S. Diessner[1]
[1]Institute of Microbiology, Dresden University of Technology, Dresden, Germany

Oxygen concentration profiles were measured in a multispecies biofilm and in biofilms, which were exposed to different concentrations of uranium. The results of the microsensor profiling of O_2 were completely different. While the biofilm, which was not exposed to uranium showed a relatively high concentration of O_2 from the top to the bottom, the O_2 concentrations in the uranium contaminated biofilms decreased very quickly, depending on the uranium concentration. These decreases of O_2 could be due to changes in microbial communities as well as changes in microbial activities within the biofilms, induced by the addition of uranium.

EXPERIMENTAL. Oxygen microsensor studies were carried out in multispecies biofilms, which were cultured in a standard culture medium (Sifin; TN 1171) with a pH of approximately 7.2, and in air atmosphere condition at room temperature (20 °C). The culture medium was pumped through three annular reactors [1] for two months with a flow-rate of 15.2 mL/min, and an inner cylinder rotation speed of 14 rpm. Inside the reactors biofilms were grown on glass slides to a thickness of approximately 600 µm. They were removed from the first reactor (A) for microsensor studies in a flow cell. Reactor (B) and (C) were fed with $UO_2(ClO_4)_2$ to adjust the total uranium concentration in the culture medium to $1 \cdot 10^{-5}$ mol/L and $1 \cdot 10^{-6}$ mol/L, respectively. These biofilms were then exposed to the uranium for three weeks before they were removed for microsensor studies in a flow cell. Concentration profiles of oxygen versus biofilm depths were measured in each biofilm by electrochemical microsensors. These sensors have a tip diameter of 10 µm, a stirring sensitivity of < 1 to 2 %, and a response time of < 1 s [2]. Profiles of oxygen were measured at different X-Y positions. For each X Y position, the microsensor was slowly moved downward in 20 or 50 µm steps in the x-axis by a motor-driven micromanipulator while the oxygen concentration was read out using the software Profix from Unisense.

RESULTS. The biofilm cultured in reactor [A] showed relatively high concentrations of O_2 from the top to the bottom of the biofilm (see Fig. 1) showing well aerating conditions within the biofilm. In contrast, the O_2 concentration profiles in the biofilm of reactor (B) revealed a very low O_2 concentration. The O_2 concentration decreased very quickly from the top to the bottom of the biofilm. Already in a depth of already 360 µm no oxygen was detectable. In biofilm (C) the O_2 concentration was lower than the one measured in reactor (A), but higher than the one measured in reactor (B). Overall, in reactor (C) the O_2 values decreased slower than the one in reactor (B), but never reached 0 µmol/L. Near the bottom of the biofilm 33 µmol/L O_2 were still measured.
The microsensor results clearly demonstrate that the O_2 concentration is significantly dependent on the concentration of uranium.
Since the biofilm is well aerated, it is presumably composed of aerophile microbes. Consequentially, the O_2 concentration will not decrease as expected unless the biofilm is fed with a substance, which could act as a stress factor for the microbes, like uranium. Since metals have a strong effect on oxygen consumption, decreases in oxygen concentration could be due to changes in microbial activities [3] as well as on the activation of microbial communities induced by the addition of uranium [4]. Some dominating microbes will die off due to the toxic effect of uranium, whereas other inactive microbes will be activated. In addition, the bioenergetics within the biofilm will change since the bacteria, which were died off, will provide food for others and thereby influencing the O_2 concentrations. For a detailed interpretation and a confirmation of our assumption, the composition of the microbial community of the biofilms will be determined by 16S rDNA gene sequence retrieval and FISH in the near future.

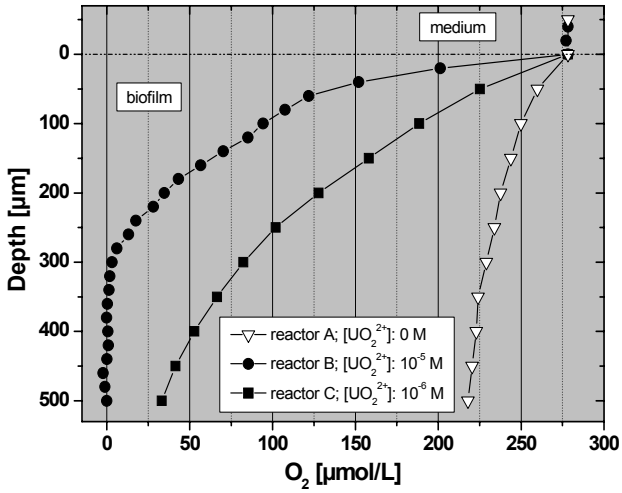

Fig. 1: Oxygen concentration profiles in well aerated multispezies biofilms, containing different uranium concentrations.

ACKNOWLEDGEMENT. We thank the DFG for founding the project (Contract No. AR 584/1-1).

REFERENCES

[1] Lawrence, J. R. et al. (2000) *J. Microbiol. Methods* **42**, 215-224.
[2] Revsbech, N. P. (2005) *Methods Enzymol.* **397**, 147-166.
[3] Viret, H. et al. (2006) *Sci. Total Environ.* **367**, 302-311.
[4] Geissler, A. et al. (2005) *Geobiology* **3**, 275-285.

Identification of U(V) in a mixed culture biofilm by confocal laser scanning microscopy (CLSM)

K. Großmann, T. Arnold, E. Krawczyk-Bärsch

Fluorescent uranium(V) particles were observed by confocal laser scanning microscopy (CLSM) in a 43 µm thick living mixed culture biofilm. The fluorescent particles were 1 – 5 µm in diameter and were located at the bottom of the biofilm, i.e. the mineral biofilm interface. They were not in contact with the microbial cells, but rather embedded in extracellular polymeric substances (EPS).

The influence of microbes on the mobility and immobilization of radionuclides in surface and subsurface environments so far, in contrast to the inorganic influence, lacks a profound understanding. This situation makes it very difficult to assess their influence on the migration behavior of actinides in surface and subsurface environments despite knowing that biofilms can provide a sink for dissolved heavy metals [1]. The presence of fracture associated biofilms and their associated extracellular matrix alters the adsorption behavior of the rock. This is due to changes in the reactive surface area associated with organic matter and different adsorptive properties [2].

EXPERIMENTAL. A mixed culture biofilm was cultured in a standard culture medium (Sifin; TN 1171; pH ~7.2) in air atmosphere using a rotating annular biofilm reactor. The biofilm was grown on biotite platelets, (approximately 10x10x5 mm) which were glued on glass slides (76x26x1 mm). For the first 3 – 4 weeks, the biofilms were grown without U(VI). Then the medium inside the reactor was fed with $UO_2(ClO_4)_2$ ($1 \cdot 10^{-3}$ M) to a total uranium concentration of $5 \cdot 10^{-6}$ mol/L. No sterile conditions were applied during the whole time of running the experiment leading to the mixed culture biofilm. The flow-rate was 15.2 mL/min and the inner cylinder rotated with 14 rpm. After a contact time of three days with U(VI) the biofilm was studied by CLSM using a Leica TSC-SP2. The autofluorescence of the mixed culture biofilm and the EPS was excited by the mercury-vapour lamp. To visualize uranium(VI) and uranium(V) in the biofilm an excitation wavelength of 408 nm, generated by a cw diode laser (Coherent, Vioflame [407 nm, 25 mW]), was used. The CLSM investigation of the biofilm specimens were carried out without using fluorescently labeled lectins or fluorochromes.

RESULTS. Bacterial agglomerates surrounded by extracellular polymeric substances (EPS) (light grey region) were detected in the mixed culture biofilm, as shown in Fig. 1. In addition, bright particles of approximately 1 to 5 µm in diameter were observed within the EPS of the biofilm. These particles were located at the bottom of the biofilm, i.e. the mineral (biotite surface) biofilm interface. Our results are consistent with previously published results. *Pseudomonas* EPS 5028 has been described to sequester uranium from solution (3). Accumulated uranium evident as a yellow precipitate was also observed by Pons and Fusté in *Pseudomonas* EPS 5028 (4). The observed particles in our biofilms were not in contact with the microbial cells, but rather embedded in EPS. The measured fluorescence spectra of various particles showed the signal displayed in Fig. 2. This signal obtained for three different region of interest (ROI) of one particle (bright spot on the left side of Fig. 1) showed a fluorescence spectrum in the range of 415 to 475 nm. This signal was attributed to U(V), since it showed the same U(V) fluorescence spectrum as described by Steudtner et al. (5). We attribute our findings to redox processes taking place within the biofilm. Obviously, some of the U(VI) was reduced to U(V) and probably to U(IV).

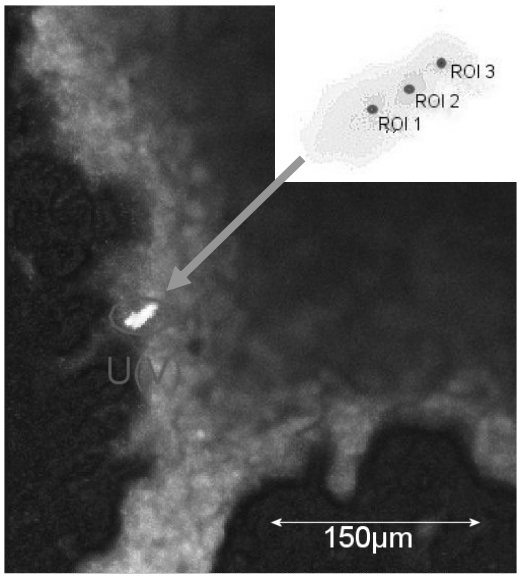

Fig. 1: Autofluorescence image of the biofilm. Dark grey upper right region represents bacterial agglomerates and the surrounding light grey region was attributed to EPS. Right upper side shows the three different region of interests (ROIs) of the encircled U(V) particle.

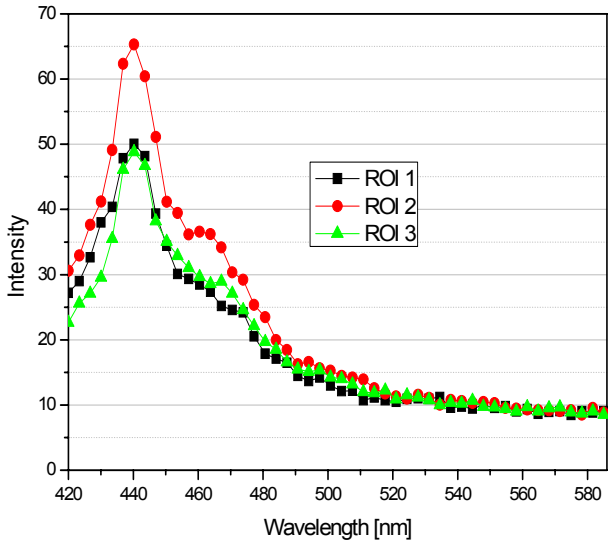

Fig. 2: The respective fluorescence spectra of the three different ROIs of the bright particle shown in Fig. 1.

REFERENCES

[1] Späth, R. et al. (1998) *Water Sci. Technol.* **37**, 207-210.
[2] Anderson, C.R. et al. (2003) *Geobiology* **1**, 169-178.
[3] Marqués, A.M. et al. (1991) *Appl. Microbiol. Biotechnol.* **35**, 406-410.
[4] Pons, M.P. et al. (1993) *Appl. Microbiol. Biotechnol.* **39**, 661-665.
[5] Steudtner, R. et al. (2006) *Inorg. Chem. Commun.* **9**, 939-941.

Isolation of bioligands secreted by cells of *Pseudomonas fluorescens* (CCUG 32456 A) and their characterization by mass spectrometry

H. Moll, A. Johnsson[1], M. Schäfer[2], H. Budzikiewicz[2], K. Pedersen[1], G. Bernhard
[1]Göteborg University, Göteborg, Sweden; [2]University of Cologne, Cologne, Germany

Bioligands secreted under aerobic conditions by *P. fluorescens* (CCUG 32456 A) were isolated and characterized by mass spectrometry. The cells secrete a mixture of siderophores consisting of ferribactins and pyoverdins in a ratio of 2 : 1. A structural model of one produced pyoverdin could be drawn.

Pyoverdins are special bacterial siderophores produced by fluorescent *Pseudomonas* species. This unique class of bioligands possess a high potential to bind and therefore to transport actinides in the environment. These water-soluble, fluorescent pigments are characterized by their high efficiency in complexing and transporting iron(III) ions [1]. The structure of pyoverdins can be divided into three different parts a) a chromophore, b) a peptide chain, composed of 6 to 12 mainly hydrophilic amino acids, bound via its N-terminus to the carboxyl group of the chromophore, and c) an acyl chain, attached to the NH_2 group of the chromophore, consisting of dicarboxylic acid residues (e.g. succinate or its amide form), the type of which depends on the growth conditions [1].

EXPERIMENTAL. *P. fluorescens* (CCUG 32456 A) was grown in batch cultures under aerobic conditions in the standard succinate medium at room temperature. After one week the cultures were pooled and the pooled material was centrifuged at 8000 g for 10 minutes. The supernatants were then suction-filtered (0.2 µm). The pH of the filtered supernatant was lowered to 6 and the solution was frozen pending purification. Purification was done using uncomplexed pyoverdin, as outlined in [2]. Columns packed with XAD-4 Amberlite resin were loaded with pyoverdin solution, rinsed with Milli-Q water (MQ) and eluted with 50 % methanol (MetOH). The resulting pulverized pyoverdin mixtures were used for the mass spectrometric studies.
Mass spectra were obtained with a MAT 900 ST instrument with an EB-QIT (quadrupol ion trap) geometry and equipped with an ESI II ion source (Finnigan MAT, Bremen, Germany); spray voltage 3.4 – 3.6 kV, capillary temperature 230 °C. Collision activation (CA) in the octapole unit in front of the QIT with He diffusing from the QIT as collision gas was followed by product ion analysis in the QIT.

RESULTS AND DISCUSSION. Figure 1 shows the molecular ion region ($[M+2H]^{2+}$) of a pyoverdin sample from *P. fluorescens*. Comparison of the fragmentation patterns of the various species obtained by collision activation with data from literature [3] demonstrated the presence of siderophores corresponding to those produced by *P. fluorescens* ATCC 17400 [4]. Specifically, the following species were observed: *m/z* 650.24 pyoverdin with succinamide side chain (Fig. 2), *m/z* 650.74 pyoverdin with succinic acid side chain, *m/z* 644.25 ferribactin with succinamide side chain (cf. [5]), *m/z* 659.27 ferribactin with glutamic acid side chain, *m/z* 653.27 and 668.27 are probably the open chain analogs of *m/z* 644.25 and 659.27 (Gln-Dab, glutamine and 2,4-diaminobutanoic acid instead of their tetrahydropyrimidine condensation product) (cf. [6]). This is evidenced because the ions B_7^{++} (cleavage after Dab) at *m/z* 509 (side chain succinic acid amide (Suca)) and *m/z* 524 (glutamic acid (Glu) side chain), respectively, are of high abundance especially in the MS^n-QIT product ion mass spectra while analogous ions of the analogs with the tetrahydropyrimidine condensation product are missing in the spectra. The free Dab stabilizes the second ionizing proton.

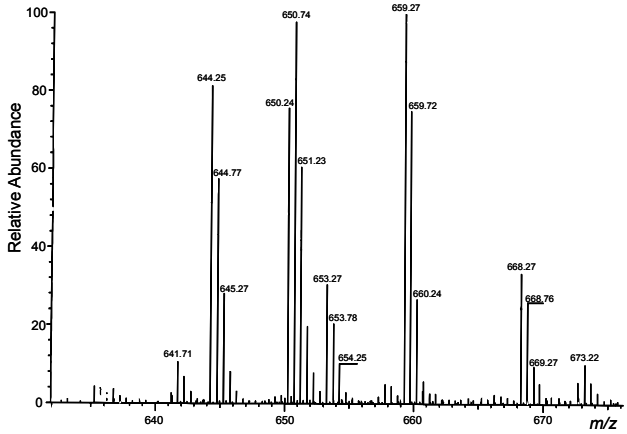

Fig. 1: Molecular ion region ($[M+2H]^{2+}$) of a sample of a pyoverdin preparation from *P. fluorescens* (CCUG 32456 A).

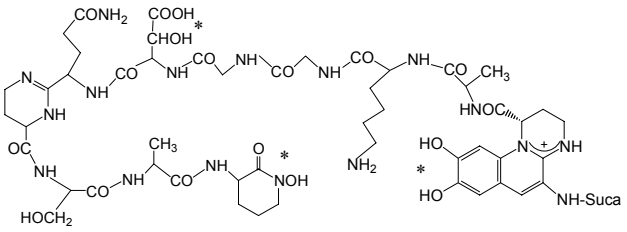

Fig. 2: Proposed structure of the pyoverdin from *P. fluorescens* (CCUG 32456) with a succinamide (Suca) side chain (Suca-Chr-Ala-Lys-Gly-Gly-OHAsp-(Gln-Dab)-Ser-Ala-cOHOrn). Asterisks indicate the complexation sites. The amino acids Ala, Lys, and Gln (underlined) are D-configured.

These open forms are probably no artifacts since the tetrahydropyrimidine ring can be hydrolyzed only under drastic conditions as described in [7]. As frequently observed for a succinate culture the production of ferribactin (biogenetic precursors of the pyoverdin [1]) prevails over that of pyoverdin [8], here in a ratio of 2 : 1.

ACKNOWLEDGEMENT. This work was funded by the BMWi under contract number 02E9985.

REFERENCES

[1] Budzikiewicz, H. (2004) *Fortschr. Chem. Org. Naturst.* **87**, 83-237.
[2] Meyer, J.M. et al. (1978) *J. Gen. Microbiol.* **107**, 319-328.
[3] Baysse, C. et al. (2002) *FEBS Lett.* **523**, 23-28.
[4] Demange, P. et al. (1990) *Tetrahedron Lett.* **31**, 7611-7614.
[5] Budzikiewicz, H. et al. (2007) *BioMetals* (in press).
[6] Boukhalfa, H. et al. (2006) *Inorg. Chem.* **45**, 5607-5616.
[7] Gipp, S. et al. (1991) *Z. Naturforsch.* **46c**, 534-541.
[8] Budzikiewicz, H. et al. (2006) *Z. Naturforsch.* **61c**, 815-820.

Aqueous pyoverdin species of *Pseudomonas fluorescens* (CCUG 32456 A) investigated by UV-vis and fs-TRLFS

H. Moll, A. Johnsson[1], M. Glorius, G. Geipel, K. Pedersen[1], G. Bernhard
[1]Göteborg University, Göteborg, Sweden

The pyoverdin absorption spectra were strongly pH dependent. These characteristic changes were used to determine the different pyoverdin deprotonation species. Using time-resolved laser-induced fluorescence spectroscopy with ultrafast pulses (fs-TRLFS) two components in the pyoverdin mixture could be distinguished on the bases of their different fluorescence lifetimes (690 ± 85 and 4850 ± 30 ps).

In order to understand the mobilizing potential of pyoverdins towards actinides it is essential to explore their speciation in aqueous solution in the absence of actinides. We studied the protonation equilibria of *P. fluorescens* (CCUG 32456 A) pyoverdins within a pH range of 3 to 10 by UV-vis spectroscopy. The fluorescence properties of the bioligand mixtures were investigated by applying fs-TRLFS.

EXPERIMENTAL. The preparation and characterization of the pulverized pyoverdin mixtures are summarized in [1]. The pyoverdin concentration [LH_4] was fixed to $5.8 \cdot 10^{-5}$ M and the pH was varied between 3 and 10. All experiments were made in an ionic medium where the sodium concentration was kept constant at 0.1 M by adding $NaClO_4$. The absorption spectroscopy experiments were performed using a CARY5G UV-vis-NIR spectrometer (Varian Co.) at 22 ± 1 ºC. The spectra were evaluated using the factor analysis program SPECFIT. Details are summarized in [2]. Experimental details of the fs-TRLFS setup are given in [3].

RESULTS AND DISCUSSION. The pH sensitivity of the absorption spectra of the pyoverdin sum fraction is depicted in Fig. 1.

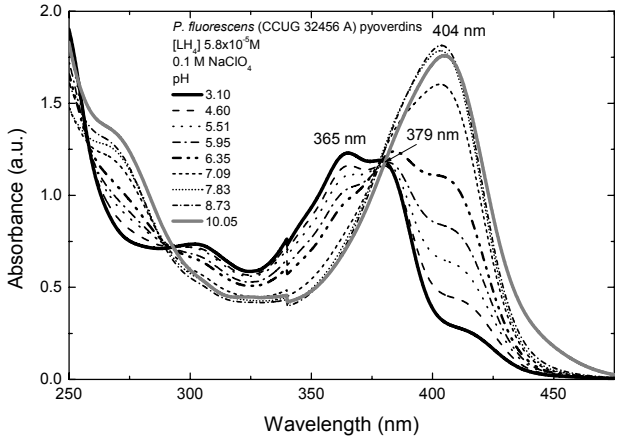

Fig. 1: Absorption spectra of the *P. fluorescens* (CCUG 32456 A) pyoverdin sum fraction as a function of pH at an ionic strength of 0.1 M ($NaClO_4$).

At pH values below 5 the absorption spectra are characterized by a double peak at 365 and 379 nm. Whereas the maximum at 365 nm decreases with increasing pH the maximum at 379 nm remains nearly unchanged up to pH 6. In the pH region above 7 one single absorption band at 403 nm dominates the interesting wavelength region. The visible absorption bands shown in Fig. 1 are dominated by the pyoverdin chromophore even if the pyoverdin mixture contains ⅓ pyoverdins and ⅔ ferribactins.

The pyoverdin molecule will be denoted as LH_4 according to the general approach that pyoverdin molecules can liberate four labile protons from the complexing sites most likely responsible for metal binding [4,5]. Three pK values could be determined using SPECFIT. The absorption spectrum of the deprotonated catechol-type moiety, L^{4-}, could not be characterized with sufficient accuracy due to indications of a sample decomposing at pH > 10. The following formation constants were calculated:
$\log \beta_{012} = 22.67 \pm 0.15$ ($pK_1 = 4.40$),
$\log \beta_{013} = 29.15 \pm 0.05$ ($pK_2 = 6.48$) and
$\log \beta_{014} = 33.55 \pm 0.05$ ($pK_3 = 10.47$), respectively.

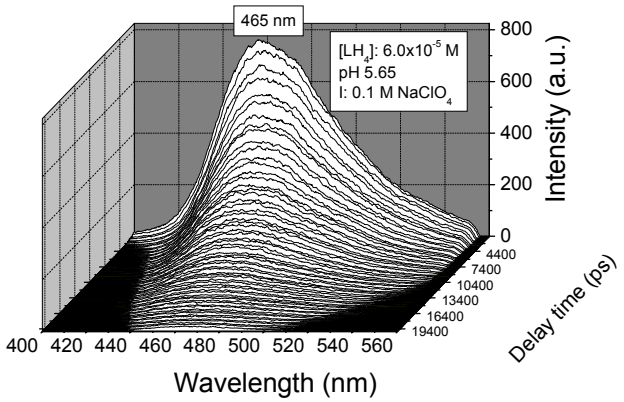

Fig. 2: TRLFS spectra of *P. fluorescens* (CCUG 32456 A) pyoverdins as a function of the delay time.

The excellent fluorescence properties of the pyoverdin sum fraction after excitation with a monochromatic laser-beam at 266 nm is shown in Fig. 2. The broad emission spectrum with a maximum at 465 nm could by fitted by applying two species at 456 and 487 nm. The evaluation of the fluorescence decay showed again two main components having different fluorescence lifetimes of 690 ± 85 and 4850 ± 30 ps. This can be explained by the identification of two major constituents, ferribactins (biogenetic precursors of the pyoverdin) and pyoverdins, of the pyoverdin sum fraction by mass spectrometry [1]. To our knowledge this is the first detailed characterization of aqueous pyoverdin species by fs-TRLFS.

ACKNOWLEDGEMENT. This work was funded by the BMWi under contract number 02E9985.

REFERENCES

[1] Moll, H. et al. this report p. 37.
[2] Moll, H. et al. (2007) *Inorg. Biochem.* (submitted).
[3] Geipel, G. et al. (2004) *Spectrochim. Acta* **60**, 417-424.
[4] Teintze, M. et al. (1981) *Biochemistry* **20**, 6446-6457.
[5] Bouby, M. et al. (1999) *Czechoslovak J. Phys.* **49**, 147-150.

The interaction of U(VI) with pyoverdins secreted by a subsurface strain of *Pseudomonas fluorescens* investigated by UV-vis spectroscopy

H. Moll, A. Johnsson[1], M. Glorius, K. Pedersen[1], G. Bernhard
[1]Göteborg University, Göteborg, Sweden

UO_2^{2+}-containing species of the type $M_pL_qH_r$ were identified from the dependencies observed in the UV-vis spectra at pyoverdin concentrations below 0.1 mM. These complexes are characterized by their individual absorption spectra and molar extinction coefficients. The following formation constants were determined: log β_{112} = 30.50 ± 0.40 and log β_{111} = 26.60 ± 0.40 at ionic strength I = 0.1 M.

In continuation of our studies exploring the isolation and characterization of pyoverdins secreted by a subsurface strain of *P. fluorescens* (CCUG 32456 A) [1,2], we are reporting here the complexation of these bioligands with uranium(VI) investigated by UV-vis spectroscopy. The cells were isolated from groundwater from borehole KR0013, 70 m underground in the Äspö HRL tunnel [3]. The interaction of U(VI) with these particular bioligands is unknown so far.

EXPERIMENTAL. The preparation and characterization of the pulverized pyoverdin mixtures are summarized in [1]. The experiments were performed a) at fixed pyoverdin concentrations [LH_4] of $5.8\cdot10^{-5}$ M by varying [UO_2^{2+}] between $1\cdot10^{-6}$ and $1\cdot10^{-3}$ M at pH 3 and 4; and b) at fixed [UO_2^{2+}] and [LH_4] of $1\cdot10^{-5}$ M and $5.8\cdot10^{-5}$ M, respectively, as a function of the pH. 0.1 M $NaClO_4$ was used as background electrolyte. The UV-vis experiments were performed using a CARY5G UV-vis-NIR spectrometer (Varian Co.) at 22 ± 1 ºC. The spectra were evaluated using the factor analysis program SPECFIT. Details are summarized in [4].

RESULTS AND DISCUSSION. Figure 1 summarizes the absorption spectra of the *P. fluorescens* (CCUG 32456 A) pyoverdins in the UO_2^{2+} system in dependence of the varied physico-chemical parameter.

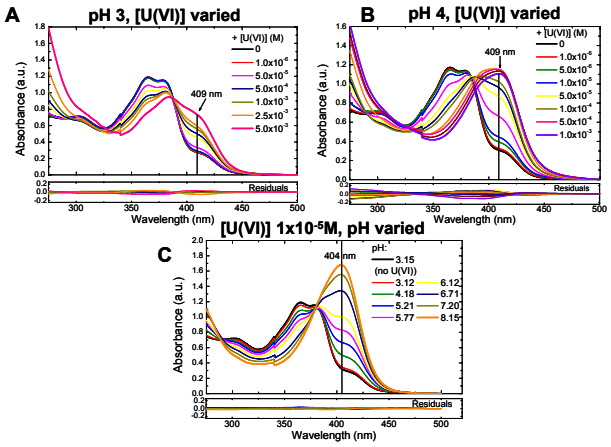

Fig. 1: Absorption spectra of the *P. fluorescens* pyoverdins measured in the UO_2^{2+} system at [LH_4] $5.8\cdot10^{-5}$ M and an ionic strength of 0.1 M. The residual spectra after the SPECFIT analysis are included.

The formation of pyoverdin – UO_2^{2+} species is indicated by the increased absorption band at 409 nm as shown in Fig. 1A and 1B. Figure 1C depicts the pH dependence of the UO_2^{2+} pyoverdin complex formation equilibria at fixed concentrations of UO_2^{2+} and LH_4. This study shows that UV-vis spectroscopy in combination with the factor analysis software SPECFIT is a sensitive tool to investigate the speciation of UO_2^{2+} in the aqueous *P. fluorescens* (CCUG 32456 A) pyoverdin system. Four different pyoverdin species LH_4, LH_3^-, LH_2^{2-}, LH^{3-} and two uranyl pyoverdin complexes UO_2LH_2 and UO_2LH^- could be identified by their individual absorption spectra (see Fig. 2).

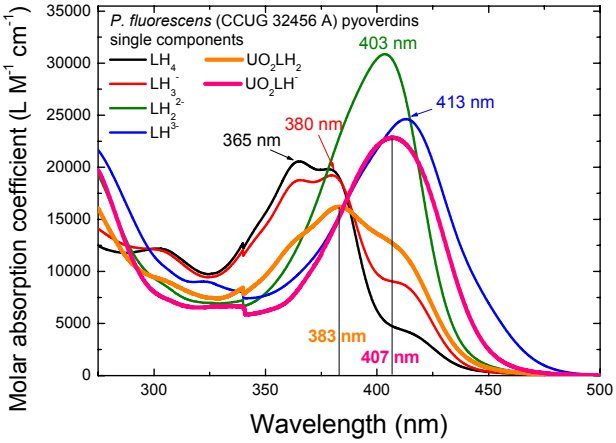

Fig. 2: Absorption spectra of the single components in the aqueous *P. fluorescens* pyoverdin system with and without UO_2^{2+} as derived by peak deconvolution using SPECFIT.

Formation constants of the uranyl species were calculated by applying SPECFIT to be log β_{112} = 30.50 ± 0.40 and log β_{111} = 26.60 ± 0.40, respectively. The large magnitudes of these formation constants reflect the potential of such bioligands to bind and transport actinides in the environment. We have noticed close similarities of the UV-vis spectra in different pyoverdin-metal systems in general and the close similarities of UO_2^{2+} species with pyoverdins produced by different pseudomonads [5-8]. This might indicate that UO_2^{2+} has a similar coordination environment in pyoverdins of different origin. The results of the present work contribute to a better understanding of the UO_2^{2+} coordination chemistry with natural siderophores of the pyoverdin type in aqueous solution.

ACKNOWLEDGEMENT. This work was funded by the BMWi under contract number 02E9985.

REFERENCES

[1] Moll, H. et al. this report p. 37.
[2] Moll, H. et al. this report p. 38.
[3] Pedersen, K. (1997) *FEMS Microbiol. Rev.* **20**, 399-414.
[4] Moll, H. et al. (2007) *Inorg. Biochem.* (submitted).
[5] Albrecht-Gary, A.M. et al. (1994) *Inorg. Chem.* **33**, 6391-6402.
[6] Teintze, M. et al. (1981) *Biochemistry* **20**, 6446-6457.
[7] Bouby, M. et al. (1998) *Radiochim. Acta* **80**, 95-100.
[8] Bouby, M. et al. (1999) *Czechoslovak J. Phys.* **49**, 147-150.

Response of nitrate-reducing bacterial populations of the uranium mining waste pile Haberland to treatments with uranyl or sodium nitrate

A. Geissler, S. Selenska-Pobell

Significant changes were induced in the indigenous nitrate-reducing bacterial community of the uranium mining waste pile Haberland by treatments with uranyl or sodium nitrate. These changes were estimated by using the *nar*G gene as a functional marker. Stimulation of different bacterial groups was observed depending on the type of the used solutions and also on the aeration conditions.

Nitrate is often a cocontaminant of uranium in the uranium mill tailings and strongly influences its mobility [1]. Nitrate can serve as a favorable electron acceptor for many microorganisms [2] and in this way it may postpone the reduction of U(VI). It can be even involved in a direct oxidation of U(IV) by some bacteria [3]. In addition, it was demonstrated that the Fe(III) oxides, produced by the anaerobic nitrate-dependent Fe(II) oxidizing bacteria, are involved in a rapid absorption of U(VI) from solutions [4]. In this work we present results on the capability of the natural bacterial community of the uranium mining waste pile Haberland to reduce nitrate in the presence or in the absence of uranium under different aeration conditions. For this, a direct molecular approach based on the membrane-bound nitrate reductase gene *nar*G [5] was used.

EXPERIMENTAL. The original soil sample (JG35-2) was collected from a depth of 2 m from the studied uranium waste. The sub-sample JG35+U4 was prepared by adding 5.0 mL of a filter-sterilized 1 mM uranyl nitrate solution to 20 g of the original sample to achieve a final concentration of 100 mg U kg^{-1}. The sample was fumigated through a sterile filter with an anaerobic gas mixture containing N_2 and CO_2 (80 : 20) and then incubated for 4 weeks without shaking at 10 °C in the dark in an anaerobic jar with Anaerocult®-A (Merck, Darmstadt, Germany). In parallel, under the same conditions another 3.6 g of the original sample were incubated with 0.9 mL of a filter-sterilized 2 mM sodium nitrate solution (sub-sample JG35-K4). The sub-samples JG35+U1 and JG35-K1 were treated under aerobic conditions as described earlier [6]. The *narG* gene clone libraries were prepared by using the primers na3F and narG5'R as described in [7].

RESULTS. Most of the sequences found in the original untreated sample JG35-2 were related to the NarG of the alphaproteobacterium *Brucella suis* and formed distinct clusters with the sequences of not yet cultured bacteria retrieved from other not contaminated with uranium environments (Fig. 1). In addition, two small groups of sequences clustered with NarG of the betaproteobacterial species *Thiobacillus denitrificans* and *Polaromonas naphthalenivorans*. The incubation of the sub-sample JG35+U1 with uranyl nitrate under aerobic conditions induced the following changes: No sequences related to the "*Brucella*"-like clusters were found and only a few sequences shared relatedness with the above mentioned "*Polaromonas*"-like NarG. Instead, several sequences were retrieved which formed a compact cluster, distantly related to the NarG of the betaproteobacterium *Chromobacterium violaceum*. Most sequences in this sub-sample were related to the NarG of *Geobacter metallireducens*. One additional group shared a high identity with the NarG of *Arthrobacter* spp. and another one was identical with the NarG of *Pseudomonas fluorescens*. The changes in the nitrate-reducing community induced by the treatment with sodium nitrate under aerobic conditions (sub-sample JG35-K1) were less drastic but also significant. In this case most of the NarG sequences formed novel subclusters within the "*Brucella*"-like and in the "*Polaromonas*"-like clusters found in the untreated sample, or formed novel clusters distantly related to them. The rest of the clones formed a tight cluster with the "*Arthrobacter*"-like NarG sequences found in the already mentioned uranyl nitrate treated sub-sample JG35+U1. The changes in the *narG*-gene harboring bacterial populations in the sub-samples treated under anaerobic conditions were notably different. In a strong contrast to the above described treatment under aerobic conditions, no "*Brucella*"-like or "*Arthrobacter*"-like NarG sequences were found in the sub-sample JG35-K4 treated anaerobically with sodium nitrate. This treatment led to a propagation of bacterial groups carrying "*Bacillus*"-like NarG, not expressed in any of the other samples studied. NarG sequences were also predominant which were related with the "*Chromobacterium*"-like cluster retrieved from the sub-sample JG35+U1. In the anaerobically with uranyl nitrate treated sub-sample JG35+U4, in contrast, the most predominant group of NarG sequences was closely related to the above mentioned "*Polaromonas*"-like cluster. However, the size of this cluster was ten times larger then in the other samples. Remarkable for this sub-sample was that more than 80 % of the NarG sequences were closely related to the NarG of particular *Alpha-* or *Betaproteobacteria* found in small numbers in the original sample.

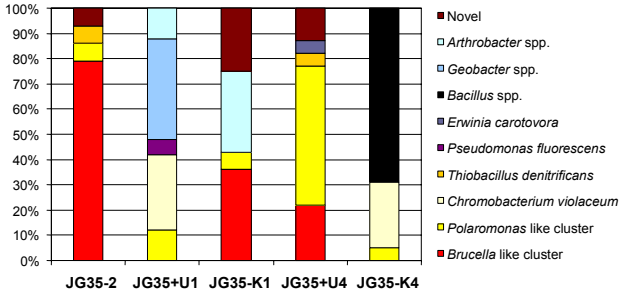

Fig. 1: Size of the predominant nitrate reducing bacterial populations (given in percentages) in the studied samples.

To our knowledge, this is the first analysis which demonstrates changes in natural nitrate-reducing bacterial community induced by sodium or uranyl nitrate treatments. We demonstrated that the nitrate-reducing populations indigenous to the uranium mining waste Haberland are able also to interact with and to tolerate uranium.

REFERENCES

[1] Senko, J.M. et al. (2005) *Geomicrobiol. J.* **22**, 371-378.
[2] Finneran, K.T. et al. (2002) *Environ. Microbiol.* **4**, 510-516.
[3] Beller, H.R. (2005) *Appl. Environ. Microbiol* **71**, 2170-2174
[4] Lack, J.G. et al. (2002) *Appl. Environ. Microbiol* **68**, 2704-2710.
[5] Philippot, L. et al. (2002) *Appl. Environ. Microbiol* **68**, 6121-6128.
[6] Geissler, et al. (2005) *Geobiology* **3**, 275-285.
[7] Goregues, C.M. et al. (2005) *Microb. Ecol.* **49**, 198-208.

Interactions of *Arthrobacter* isolates from the uranium mining waste pile Haberland with U(VI) and Pb(II)

A. Geissler, M. Merroun, S. Selenska-Pobell

The cellular localization of U(VI) and Pb(II) accumulated by two *Arthrobacter* strains recovered from the uranium mining waste pile Haberland was studied by transmission electron microscopy (TEM) and energy-dispersive X-ray (EDX) analysis. The results demonstrated that at pH 4.5 U(VI) was accumulated as intracellular needle-like fibrils, while Pb(II) was mainly precipitated on the bacterial cell surfaces.

Microorganisms have evolved the following mechanisms to interact with U(VI): biosorption by cell surface polymers [1], biological oxidation [2] and reduction [3], and intracellular accumulation [4,5]. Studies on bacterial tolerance and resistance to soluble Pb have revealed two general mechanisms. The first of them is an active efflux [6] and the second one appears to be precipitation of Pb, mainly as lead phosphates [7]. In this paper the interactions of two natural Gram-positive *Arthrobacter* isolates with U(VI) and Pb(II) were studied.

EXPERIMENTAL. Bacterial cells grown to mid-exponential phase were harvested by centrifugation at 10000 x g for 15 min at 4 °C and washed twice with 0.9 % NaCl to remove the interfering ingredients of the growth medium. The pellets of the washed cells were resuspended in 30 mL $Pb(NO_3)_2$ or $UO_2(NO_3)_2$ solutions (0.5 mM, pH 4.5) and incubated by shaking for 48 h. The metal treated cells were harvested and washed as above described. The resulted pellets were fixed in 2.5 % glutaraldehyde solved in 0.1 M cacodylate buffer (pH 7.2) for 2 h at 4 °C and then washed three times with the same buffer. The cell pellets were fixed for 60 min. at 4 °C in 1 % OsO_4 solved in cacodylate buffer before being hydrated with ethanol and embedded in a Spurr resin. The samples were analyzed by using TEM and EDX as described in [1].

RESULTS. As shown in Fig. 1 the cells of the two *Arthrobacter* strains, JG37-Iso2 and JG37-Iso3, exposed to uranyl nitrate solutions at pH 4.5 accumulated U(VI) in a form of needle-like fibrils. The EDX spectra of uranium deposits showed that they are composed of oxygen (O), phosphorus (P), and uranium (U). Our results are concurrent with the observations of Suzuki and Banfield [5] who found an intracellular accumulation of uranium closely associated with polyphosphate granules by another natural isolate closely related to *Arthrobacter liticus*.

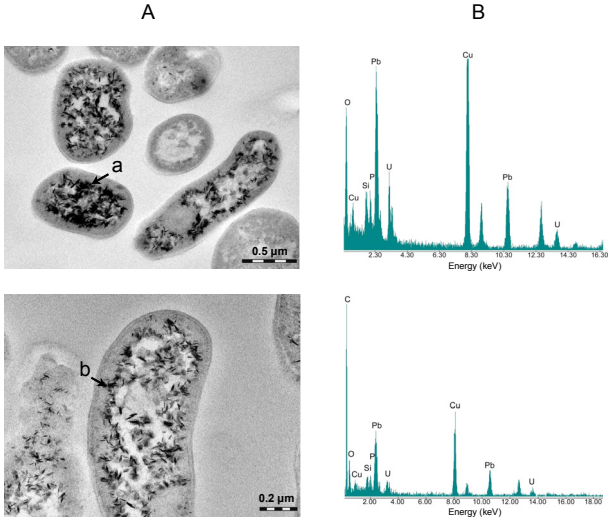

Fig. 1: TEM micrographs (A) of a thin section of *Athrobacter* sp. JG37-Iso2 (above) and *Arthrobacte*r sp. JG37-Iso3 (at the bottom) cells containing intracellular uranium accumulates and EDX spectra (B) of the points (a and b) marked with arrowheads.

In the case of Pb(II) the precipitates were mainly located at the cell surface and only a few of them were localized intracellularly (Fig. 2A). The EDX spectra derived from the Pb precipitates (Fig 2B) showed that they were composed of oxygen (O), phosphorus (P), and lead (Pb). The electron diffraction (Fig. 2C) revealed a crystalline nature of the precipitates. The electron diffractogram showed a strong reflection with a spacing 4.3 and 2.94 Å, which are in a good agreement with the spacing 4.33 and 2.959 Å reflections for pyromorphite ($Pb_5(PO_4)_3Cl$) (JCPDS, File 19-0701). Formation of pyromorphite phases ($Pb_5(PO_4)_3OH$) was also demonstrated for suspensions and biofilms of the Gram-negative bacterial species *Burkholderia cepacia* [8]

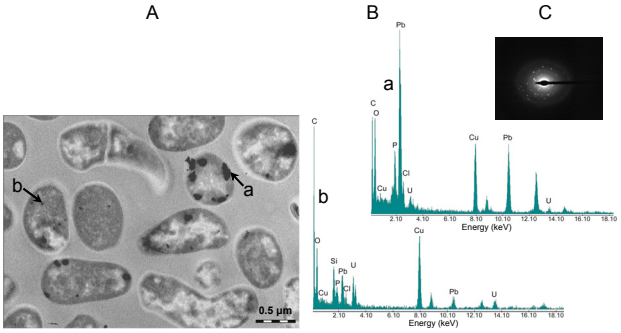

Fig. 2: TEM micrograph (A) of a thin section of *Arthrobacter* sp. JG37-Iso2 cells treated with 0.5 mM $Pb(NO_3)_2$ at pH 4.5 and EDX spectra (B) of the points marked with arrowheads. The metal accumulated was localized at the cell surface (a) and intracellularly (b). Electron diffraction of the Pb precipitate marked with arrowhead (a) is shown in (C).

As evident from the results presented in Fig. 2, not all cells of the Arthrobacter culture are able to form pyromorphite. Moreover, by using a Live/Dead staining (not shown) we demonstrated that about 60 % of the Pb-treated Arthrobacter cells were alive after 48 h of contact time. This indicates that the mineralization of the cells is dependent on their viability and that only a fraction of the bacterial culture is involved in the interactions with Pb(II).

REFERENCES

[1] Merroun, M. et al. (2005) *Appl. Environ. Microbiol.* **71**, 5532-5543.
[2] Beller, H.R. (2005) *Appl. Environ. Microbiol.* **71**, 2170-2174.
[3] Lovley, D. et al. (1993) *Arch. Microbiol.* **159**, 336-344.
[4] Francis, A.J. et al. (2004) *Radiochim. Acta* **92**, 481-488.
[5] Suzuki, Y. et al. (2004) *Geomicrobiol. J.* **21**, 113-121.
[6] Borremans, B. et al. (2001) *J. Bact.* **183**, 5651-5658.
[7] Mire, C.E. et al. (2004) *Appl. Environ. Microbiol* **70**, 855-864.
[8] Templeton, A.S. et al. (2003) *Environ. Sci. Technol.* **37**, 300-307.

Changes in archaeal community of the waste pile Haberland induced by uranyl nitrate treatments

T. Reitz, A. Geissler, S. Selenska-Pobell

Changes in the archaeal community of the uranium mining waste pile Haberland caused by the addition of uranyl or sodium nitrate were investigated by using the 16S rRNA gene retrieval. A significant shifting from subgroup 1.1a to subgroup 1.1b of the mesophilic *Crenarchaeota* was observed in all treated sub-samples of a particular site, independently on the aeration conditions and the amount of the added salt solutions.

Archaea represent the third domain of life beside *Bacteria* and *Eukarya*. These microorganisms are phylogenetically more closely related to eukaryotes than bacteria. Thus they can be used to study the origin of some complex eukaryotic functions and reaction mechanisms in a simple microbial cell system. Similarly to bacteria they interact effectively with metals and radionuclides [1,2] and can therefore influence the fate and the migration of uranium in contaminated sites.

EXPERIMENTAL. The studied soil sample (JG35-2) was collected from a depth of 2 m from the uranium mining waste pile Haberland located near the town of Johanngeorgenstadt, Germany. The uranium content of the sample was 26 mg U/kg. Four portions of the sample were supplemented with 1 mM uranyl nitrate (pH 4.0) to achieve final concentrations of 86 mg U/kg (sub-samples U1 and U4) and of 300 mg U/kg (sub-samples U2 and U3). The latter two samples were incubated for 14 weeks at 10 °C in the dark, under aerobic (U2) and anaerobic (U3) conditions. The sub-samples U1 and U4 were incubated for only 4 weeks under aerobic and anaerobic conditions. To investigate the influence of the added nitrate on the archaeal community, parallel samples (K1 and K4) were supplemented with 2 mM sodium nitrate (pH 4.0) and incubated under aerobic and anaerobic conditions. The archaeal diversity was estimated via the 16S rRNA gene retrieval as described earlier [3].

RESULTS. As evident from the results presented in Fig. 1 the archaeal diversity of the untreated sample JG35-2 was limited to only a few lineages of mesophilic *Crenarchaeota* predominantly assigned to the subgroup 1.1a (89 of 142 clones). Some of the closely related 16S rRNA gene sequences (Sh765B-AG-A11, Gitt-GR-27) were recovered from other uranium contaminated sites [3]. The addition of 60 mg U/kg uranyl nitrate to the soil subsamples U1 and U4 induced a significant shifting to mesophilic *Crenarchaeota* of subgroup 1.1b (see the corresponding clone numbers in Fig. 1). Very similar results were obtained by increasing the uranium concentration to 300 mg U/kg and extending the incubation time to 14 weeks under anaerobic conditions (data not shown). No *Crenarchaeota* of the subgroup 1.1a were detected in the uranyl nitrate treated samples.

The same shifting of the archaeal populations was observed in the control sub-samples which were supplemented with sodium nitrate and incubated for 4 weeks aerobically (K1) or anaerobically (K4) (Fig. 1), and also in those incubated for 14 weeks (not shown). On the basis of these results we concluded that the added nitrate is the reason for the shifting in the archael community. Furthermore, a high uranium tolerance for the stimulated lineages could be presumed, due to the fact that they survive concentrations of up to 300 mg U/kg.

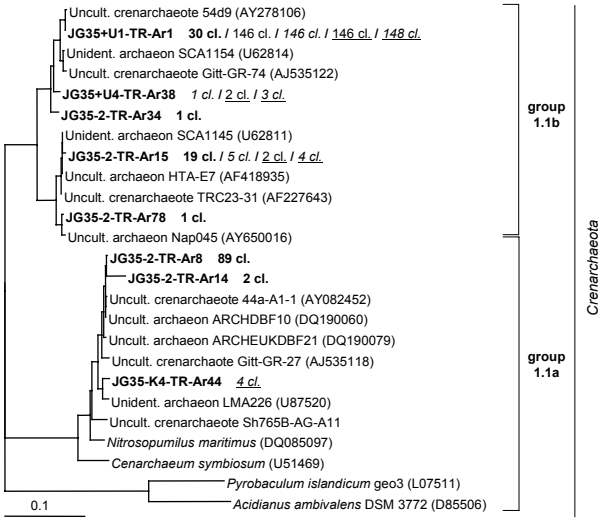

Fig. 1: Phylogenetic classification and frequency of the recovered 16S rRNA gene sequences in the clone libraries of the samples **JG35-2**, U1, *U4*, K1 and *K4*.

The retrieved 16S rRNA sequences of the 1.1b *Crenarchaeota* stimulated by the treatments are identical or almost identical with the 16S rRNA gene localized on a fosmid clone 54d9 (Fig. 1). This clone contains 43 putative protein-encoding genes in addition to the 16S rRNA one [5]. Interestingly, one of these genes is homologous to a copper-containing nitrite reductase. Two other genes show significant similarities to subunits of bacterial ammonia-mono-oxygenases. The authors proposed that the not yet cultured *Crenarchaeota*, represented by the fosmid 54d9, are most possibly capable to couple ammonia oxidation with nitrite reduction. Based on the 16S rRNA sequential identity between the fosmid clone 54d9 and the stimulated 1.1b-*Crenarchaeota* in our study, we suppose that the latter probably possess the same activities. Our prediction is supported by the fact that the above mentioned treatments induced in the studied sub-samples along with the 1.1b *Crenarchaeota* a large variety of nitrate reducing and denitrifying bacteria, including also ammonifying species [5]. These bacteria might provide the stimulated 1.1b *Crenarchaeota* populations with ammonia and nitrite and support in this way a metabolism similar to the predicted. Such metabolism would be concurrent with the recently discovered strong predominance of *Archaea* among ammonia-oxidizing prokaryotes in soil [6]. Efforts to isolate strains of this yet to be cultured archaeal lineage are in progress in our laboratory.

REFERENCES

[1] Kashefi, K. et al. (2000) *Appl. Environ. Microbiol.* **66**, 1050-1056.
[2] Francis, A.J. et al. (2004) *Radiochim. Acta* **92**, 481-488.
[3] Radeva, G. et al. (2003) *Report FZR-373*, p. 29.
[4] Treusch, A.H. et al. (2005) *Environ. Microbiol.* **7**, 1985-1995.
[5] Geissler, A. et al. this report, p. 40.
[6] Leininger, S. et al. (2006) *Nature* **442**, 806-809.

EXAFS structural parameters of U(VI) species in algal biomass at low temperature

A. Günther, A. Rossberg, A.C. Scheinost, G. Bernhard

Algae are increasingly recognized as important for metal and actinide biosorption and bioaccumulation processes. *Chlorella* species accumulate relatively high quantities of uranium. The EXAFS spectra recorded at 30 K show a monodentate binding of uranium on phosphate groups at pH 5 and 6. The structural parameters are similar to those obtained for m-autunite at the same temperature. At pH 3 no uranyl-phosphate interactions were found in the monocellular algal samples. For this pH the obtained structural parameters are similar to those of uranyl hydrate.

EXPERIMENTAL. For the sorption experiments the stored algal biomass was re-suspended in a solution of 0.9 % $NaClO_4$ and contacted for 72 h with $UO_2(ClO_4)_2$. In each reaction solution the concentration of algal biomass was 0.75 g dry mass/L. The uranium concentration was $1 \cdot 10^{-4}$ M. The pH values of the solutions were adjusted with $HClO_4$ or NaOH to pH 3, 5 or 6. After separation of the washed algal biomass by centrifugation, the fresh samples were transferred to polyethylene sample holders. The EXAFS spectra of the uranium containing algal biomass were recorded at the Rossendorf Beamline (ROBL) at the ESRF in Grenoble. The U L_{III}-edge spectra were measured in fluorescence mode at 30 K using a closed-cycle He-cryostat. The EXAFS spectra were analyzed using the suite of program EXAFSPAK [1]. Theoretical scattering phases and amplitudes were calculated by using X-ray structural data of m-autunite with the scattering code FEFF8 [2].

RESULTS. Figure 1 shows the raw U L_{III}-edge k^3-weighted EXAFS spectra and their corresponding Fourier transforms (FT) of algal cells (samples A – C) at 30 K. The changes in the EXAFS spectra are attributed to structural changes in the equatorial plane of uranium(VI) (Fig. 1). The corresponding structural parameters are summarized in Table 1.

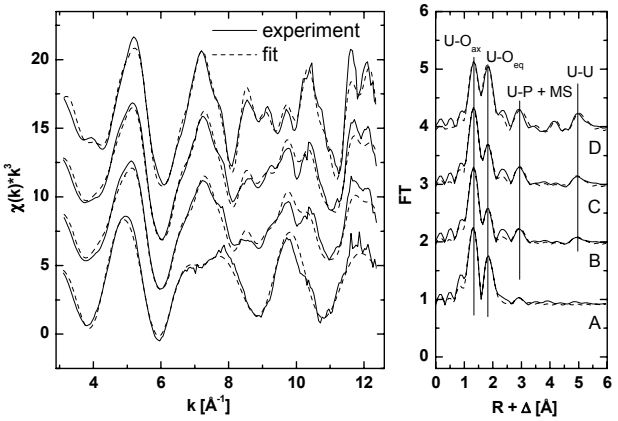

Fig. 1: U L_{III}-edge EXAFS spectra and their corresponding Fourier Transformations (FT) of uranium containing different algal samples (A – C) and m-autunite (Vo21) at 30 K (D).

The spectrum of the algae contaminated at pH 3 is well reproduced by taking only backscattering of O atoms into account. We obtained for the axial (ax) oxygen a radial U-O_{ax} distance of 1.77 Å and for the equatorial (eq) oxygen a radial U-O_{eq} distance of 2.39 Å. The spectrum is similar to the spectrum of uranyl hydrate (data not shown), and the obtained structural data are accordingly also similar (Tab. 1). After thawing of the algal cells and measurement at room temperature the spectrum and the corresponding structural parameters did not change significantly.

Tab. 1: EXAFS structural parameters at 30 K for U(VI) species sorbed on algal cells at different pH and of reference samples.

Sample	Shell	N	R[Å]	σ^2 [Å^2]
(A) Algae (pH 3)	U–O_{ax}	2*	1.77	0.0018
	U–O_{eq}	4.7	2.39	0.0077
	U–P	–	–	–
	U–U	–	–	–
(B) Algae (pH 5)	U–O_{ax}	2*	1.77	0.0023
	U–O_{eq}	4*	2.29	0.0079
	U–P	4*	3.57	0.0057
	U–U	4*	5.22	0.0090
(C) Algae (pH 6)	U–O_{ax}	2*	1.77	0.0022
	U–O_{eq}	4*	2.28	0.0056
	U–P	4*	3.57	0.0038
	U–U	4*	5.22	0.0070
(D) m-autunite (Vo21)	U–O_{ax}	2*	1.77	0.0039
	U–O_{eq}	3.8	2.29	0.0020
	U–P	3.8	3.59	0.0030
	U–U	4.0	5.27	0.0030
Uranyl hydrate	U–O_{ax}	2*	1.76	0.0014
	U–O_{eq}	4.9	2.41	0.0046

N-coordination number with an uncertainty of 25 %, R-radial distance with an uncertainty of ± 0.02 Å, σ^2 – Debye-Waller factor,
* fixed during the shell fitting.

In case of the algal samples at pH 5 and 6 a short U–O_{eq} bond distances of 2.28 or 2.29 Å and a U–P interaction were found in the formed uranyl species. The radial U–P distance of 3.57 Å indicates a monodentate binding of uranium on phosphate groups. In addition both samples show a U–U interaction with a radial distance of 5.22 Å (Fig. 1 (B,C), Tab. 1). The EXAFS structural parameters of these samples agree with those of m-autunite (Fig. 1 (D) and Tab. 1). The U–U radial distance and the Debye-Waller factors of the biological samples B and C are slightly different compared to the corresponding data of m-autunite.
To exclude the possibility of a change in the uranyl speciation during freezing the algal cells samples to 30 K in comparison to the uranyl speciation in the original samples we plan future EXAFS studies at room temperature.

ACKNOWLEDGEMENT. The authors thank R. Vochten (University of Antwerp) for providing the m-autunite sample.

REFERENCES

[1] George, G.N. et al. (1995) *EXAFSPAK A Suite of Computer Programs for Analysis of X-Ray Absorption Spectra.* Stanford Synchrotron Radiation Laboratory, Stanford, USA.
[2] Ankudinov, A.L. et al. (1998) *Phys. Rev. B* **58**, 7565-7576.

Transmission electron microscope analysis of Eu(III) accumulated by *Bacillus sphaericus* JG-A12 cells

M. Merroun, S. Selenska-Pobell

The cellular localization of Eu(III) accumulated by cells of *Bacillus sphaericus* JG-A12 was investigated using Transmission Electron Microscope (TEM) and Energy-Dispersive X-ray (EDX) analysis. The results indicated that Eu is mainly accumulated at the cell surface of the bacterium, particularly on the S-layer protein.

In addition to uranium, radioactive waste contains many fissions products including the 4f rare elements (lanthanides) and trivalent actinides such as Cm. Because trivalent actinides and trivalent lanthanides have similar cation radii and both are hard cations, their coordination chemistry is nearly indistinguishable for many ligands [1]. To understand the chemical behavior of these elements in geological and environmental context for future nuclear waste disposals, it is necessary to study their interaction mechanisms with natural bacteria. In this work, the cellular localization of the accumulated europium, as inactive analogue of the trivalent actinide (Cm), by the cells of *B. sphaericus* JG-A12, a bacterium isolated from a uranium mining waste pile, was studied using TEM and EDX analysis. The cells of this strain are enveloped by a surface (S)-layer protein.

EXPERIMENTAL. After incubation with europium, the bacterial cells were fixed in 2.5 % glutaraldehyde in 0.1 M cacodylate buffer (pH 7.2) for 2 h at 4 °C and then washed three times with the same cacodylate buffer. The cell pellets were fixed for 60 min at 4 °C in 1 % OsO_4 in cacodylate buffer before being dehydrated with ethanol gradients (50, 70, 90, and 100 %) and embedded in EM bed 812 epoxy resin. The samples were thin sectioned (90 nm) using a diamond knife on a Reichert Ultracut S ultramicrotome, and the sections were supported on copper grids and coated with carbon. Samples were examined with a high resolution Philips CM 200 transmission electron microscope at an acceleration voltage of 200 kV.

RESULTS. TEM observation of the cells exposed to Eu(III) solution at pH 4.5 revealed the presence of electron dense accumulations mainly at the level of the S-layer protein and on the cell wall. Some intracellular Eu deposits were also detected. EDX analysis of these deposits indicated the presence of Eu and phosphorus.
In summary, preliminary results using TEM analysis demonstrated that this bacterial strain accumulates europium as metal phosphate precipitates mainly at the cell surface. The precipitation mechanism of this lanthanide is unknown. In addition, we speculate that the S-layer protein of this bacterium play a protective role against this heavy metal.

ACKNOWLEDGEMENT. This work is supported by grant D/04/39988 from DAAD.

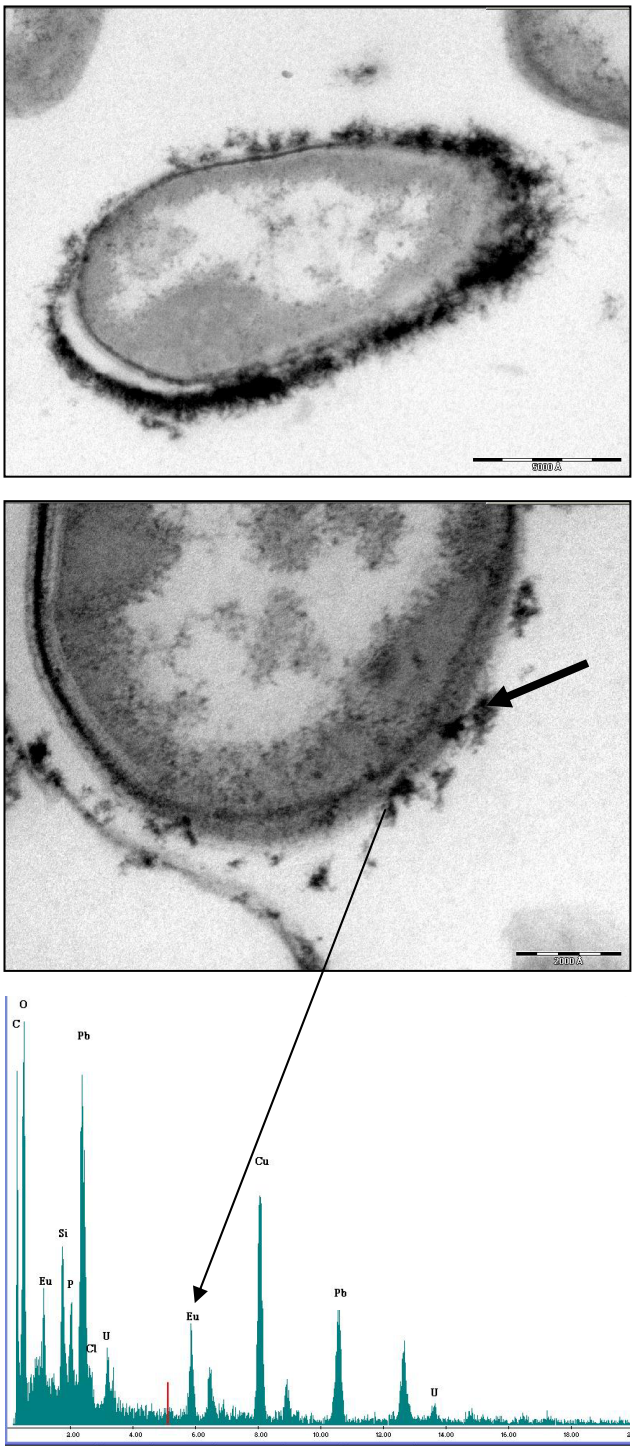

Fig. 1: Transmission electron micrographs of thin sections of *B. sphaericus* JG-A12 treated with europium and EDX spectra of the Eu accumulates.

REFRENCES

[1] Jensen, M.P. et al. (2002) *J. Am. Chem. Soc.* **124**, 9870-9877.

Uranium binding by cells and S-layer proteins of two *Bacillus* isolates and their corresponding reference strains

J. Raff, A. Heller, M. Dudek, T. Raff, K. Pollmann

The uranium binding of cells and S-layers of the *Bacillus* strains *B. sphaericus* JG-A12, *B.* sp. JG-B7, *B. sphaericus* NCTC 9602 and *B. fusiformis* DSM 2898 were compared in dependence of pH and uranium concentration. Highest uranium binding capacities were observed at pH 6. At low pH values, cells bind more uranium than S-layers whereas with increasing pH, S-layer proteins bind more uranium than cells. At pH 8 only S-layer proteins bind significant amounts of uranium.

Former studies demonstrated, that S-layer proteins from different bacterial isolates or reference strains vary in their interaction with uranium, concerning capacity and affinity. Thus S-layers from isolates recovered from sites with higher uranium contents (JG-B isolates) are able to bind more uranium than those ones obtained from bacteria living in environments with less (JG-A isolates) or no uranium (reference strains) [1,2]. In contrast to that, the uranium binding by different bacterial cells show no analog correlation. To complete the uranium binding experiments, the influence of the metal concentration and the pH on sorption was investigated by using the uranium mining waste pile isolates *B. sphaericus* JG-A12 and *B.* sp. JG-B7 and their corresponding reference strains, *B. sphaericus* NCTC 9602 and *B. fusiformis* DSM 2898.

EXPERIMENTAL. All *Bacillus* strains were grown in nutrient broth (5 g/L peptone, 3 g/L meat extract) containing 10 mg/L $MnSO_4 \cdot H_2O$. After harvesting the cells at late logarithmic growth phase, cells were washed and the biomass was split into two parts, one for the uranium binding experiments with entire cells and one for the preparation of S-layer proteins. The S-layers were extracted with a protocol according to reference [2]. Sorption experiments were carried out in triplicates with 2.5 mg dry weight (dw) biomass. The biomass was equilibrated to pH 4, 5, 6, 7 and 8. After transferring the biomasses into 84 mL 10^{-5} M $UO_2(NO_3)_2 \cdot 6H_2O$ in 0.9 % $NaClO_4$ with a corresponding pH, the samples were shaken for 48 h at 30 °C. Finally all samples and controls were centrifuged at 12.000 g for 10 min and the uranium content of all supernatants was measured by inductive coupled plasma mass spectroscopy (ICP-MS).

RESULTS. In all four cases the S-layer proteins were purified until homogeneity (see Fig. 1). As known from N-terminal sequencing, the double band in lane four (JG-B7) arises from one S-layer protein existing in a monomeric and dimeric structure after denaturation and results not from posttranslational modifications, e.g. glycosylation [3]. Moreover, all S-layer proteins are not glycosylated but phosphorylated. Highest phosphorus (P) content was determined for the S-layer protein of the strain DSM 2898 with 1.01 ± 0.20, followed by JG-A12 with 0.94 ± 0.35, NCTC 9602 S-layer with 0.83 ± 0.04, and JG-B7 S-layer with 0.72 ± 0.14 mol P per mol protein. As obvious from sorption experiments (see Fig. 2), the optimum for uranium binding is at pH 6. In addition, at pH 6 or below, cells possess higher binding capacities than S-layer proteins. This is not surprising, as especially cell wall components of Gram positive bacteria, e.g. peptidoglycan, teichoic or teichuronic acids and proteins, carry large amounts of carboxyl and phosphate groups, which are evidentially responsible for the binding of cationic uranyl species at low pH values [4]. In contrast to that, JG-B7 S-layer bind equal or higher amounts of uranium compared to cell biomass. This refers to a relation between the binding capacity of the bacterial S-layers and the uranium content of the environment, where the bacteria were recovered from [1]. Interestingly, at pH 7 the *Bacillus* cells show decreasing and significant lower uranium binding capacities compared to those of all tested S-layer proteins. Furthermore, at pH 8 only S-layer proteins are able to bind uranium. As the uranium speciation at pH 7 or above is dominated by negatively charged uranium species, one explanation might be the higher number of positively charged functional groups in S-layer proteins, originating from side chains of Lys and Arg. On the other hand one may speculate, that the lattice structure itself plays a crucial role in the uranium complexation or that the complexes formed with bioligands, like S-layer proteins, are more stable than the inorganic uranyl complexes. Which explanation is the appropriate one has to be addressed with further studies. Differences between S-layers of the two waste pile isolates and of their corresponding reference strains only occur at low pH values ($\leq$ pH 5) and high uranium concentrations (≥ 100 µM) and are not as distinctive as originally expected.

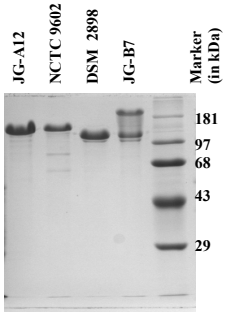

Fig. 1: Stained SDS gel of purified S-layers.

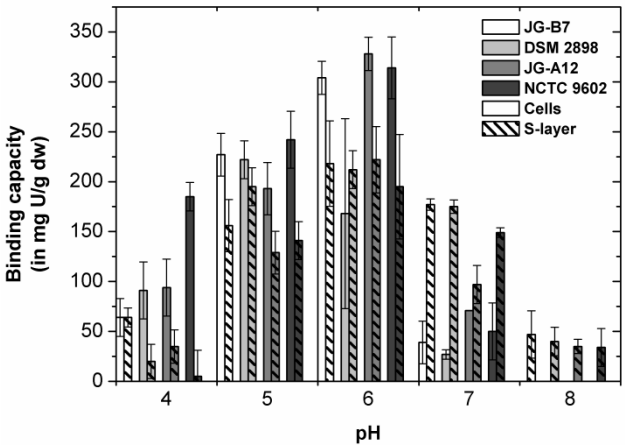

Fig. 2: Uranium binding capacities of cells and S-layer proteins in dependence of pH.

ACKNOWLEDGEMENT. We thank R. Getzlaff and I. Plumeier (GBF Braunschweig) for the N-terminal sequencing of the S-layer proteins.

REFERENCES

[1] Raff, J. et al. (2005) *Report FZR-443*, p. 29.
[2] Raff, J. et al. (2003) *Chem. Mater.* **15**, 240-244.
[3] Heller, A. (2006) *Diploma thesis*, Univ. Appl. Sci. Dresden.
[4] Merroun, M. et al. (2005) *Appl. Environ. Microbiol*. **71**, 5532-5543.

EXAFS characterization of the Pt nanoparticles formed on S-layer sheets of *Bacillus sphaericus* JG-A12

M. Merroun, K. Pollmann, J. Raff, A. Rossberg, S. Selenska-Pobell

S-layer sheets of *Bacillus sphaericus* JG-A12 were used as templates for the deposition of metallic platinum nanoclusters using dimethyl amino borane (DMAB) as reducing agent. XAS analysis indicated that the formed Pt nanoparticles have a mean diameter of about 2.5 to 3.5 nm.

The fabrication of patterned arrays of nanoparticles whose electronic, optical and magnetic properties will find technological applications, such as ultra-high-density memories, is currently one of the most important objectives of inorganic material research. In this study, the size of the Pt nanoparticles formed on the S-layer protein of *B. sphaericus* JG-A12 was estimated using a combination of X-ray absorption spectroscopy (XAS) and iterative target test factor analysis [1].

EXPERIMENTAL. *B. sphaericus* JG-A12 was routinely grown in NB medium. The preparation of S-layer protein was performed as described in [2]. For sorption of Pt(II), 10 mg of dialyzed protein was incubated in 100 mL of a solution of 2 mM K_2PtCl_4 overnight at room temperature in the darkness. Pt(II) was reduced by the addition of a few drops of 100 mM DMAB to produce Pt(0)-nanoparticles. The metallized protein samples were centrifuged (20 min, 10000×*g*) and dried in a vacuum oven (48 h, 30 °C).

RESULTS. Figure 1 shows the XANES regions of the EXAFS spectra obtained with Pt-treated S-layer after addition of DMAB and for reference compounds containing three oxidation states of platinum: Pt(II) (solution of 2 mM K_2PtCl_4), Pt(IV) and metallic Pt (platinum foil). Comparison of the experimental spectra to the reference spectra clearly shows that Pt is present as metallic Pt and Pt(II) in the Pt-treated S-layer. To determine the relative amounts of Pt(0) and Pt(II) present in the biological sample, we applied Iterative Transformation Factor Analysis. The calculation revealed a mixture of 52 % metallic Pt and 48 % Pt(II) for the S-layer sample.

Pt L_{III}-edge EXAFS spectrum of the Pt/S-layers of *B. sphaericus* JG-A12 in presence of DMAB is shown together with Pt foil in Fig. 2. In this sample, Pt is present mainly as metallic phase where the interatomic distances found are comparable with the one of metallic foil. The coordination number (N) is different from the bulk ones, showing the presence of small metal particles. The reduction of the coordination number of the first shell is used to estimate the average particle [3]. The coordination number value of the Pt-Pt found in this work (5.5 ± 0.4) is not the real coordination number of the Pt per nanoparticle. This value correspond to the coordination number of Pt-Pt per sample. The coordination number of latter bond per nanoparticle is weighted by the atomic percentage of Pt atoms in the metallic phase [3]. It was found that the nanoparticles deposited on the S-layer protein have a mean diameter of about 2.5 – 3.5 nm.

These results are in agreement with those found using synchrotron-based X-ray diffraction studies (v. Borany, personal communication).

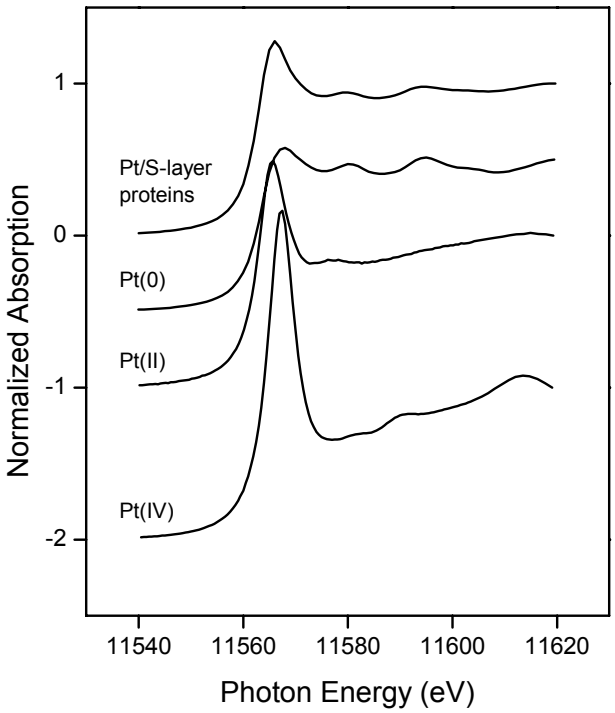

Fig. 1: XANES region of EXAFS spectra of the Pt L_{III}-edge in reference compounds and for Pt-loaded S-layer of *B. sphaericus* JG-A12.

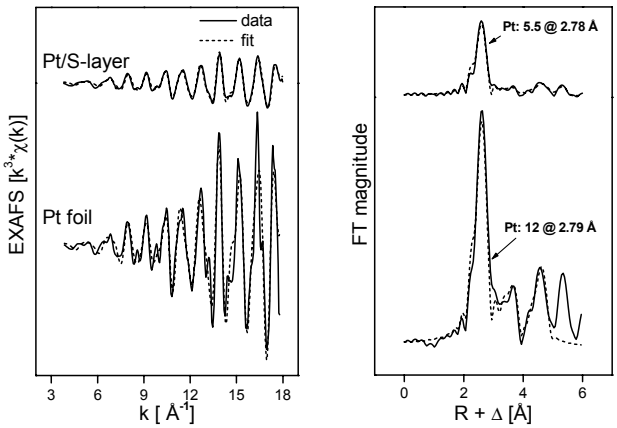

Fig. 2: Pt L_{III}-edge EXAFS spectra and their corresponding fourier transforms of Pt- treated S-layer of *B. sphaericus* JG-A12 and Pt foil.

ACKNOWLEDGEMENT. This work is supported EU grant GRD1-2001-00750.

REFERENCES

[1] Rossberg, A. et al. (2003) *Anal. Bioanal. Chem.* **376**, 631-638.
[2] Raff, J. (2002) *FZR Report-358*.
[3] Sun, Y. et al. (2006) *Langmuir* **22**, 807-816.

Reduction of Cr(VI) by S-layer supported Pd(0) nanoparticles

K. Pollmann, J. Raff, A. Mücklich[1], S. Selenska-Pobell
[1]Institute of Ion Beam Physics and Materials Research, FZD, Dresden

Pd-nanoparticles were used to reduce toxic Cr(VI) to Cr(III). S-layer supported nanoparticles showed a significantly higher catalytic activity in comparison to cell supported Pd(0) or bulk Pd(0).

Nanoparticles have attracted much attention for the development of new materials since their properties usually differ significantly from those of the bulk material. Their magnetic and superconducting behavior can be changed and the catalytic activity can be significantly enhanced due to the high volume/surface ratio. The use of self-assembling organic templates such as the regular structured proteinaceous surface layers (S-layers) of bacteria is a promising approach to produce a wide range of discrete, size-selected inorganic nanoparticles in a simple way.
Mostly S-layers comprise protein monomers with the ability to self-assemble into 2-D arrays. The regular distributed pores of these paracrystalline arrays work as binding sites for various metals and offer ideal structures for the formation of regular distributed nanoclusters of a defined size. S-layers have been used as templates for the fabrication of Pt, Pd, and Au nanocrystals [1,2] (Fig. 1).

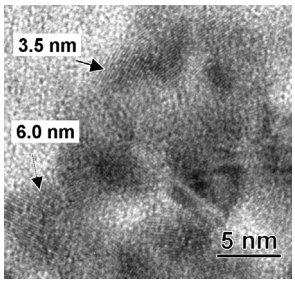

Fig. 1: TEM micrograph of S-layer supported Pd-nanoclusters (dark areas); the data indicate the size of the clusters.

The reduction of Cr(VI) to the less toxic Cr(III) has been shown to be a suitable system to test the catalytic activity of nanoparticles in a simple way [3]. Previous results (EU-project Bio-CAT) demonstrated the ability of *B. sphaericus* supported Pd-particles to reduce Cr(VI) [4]. In this study, up to 46 % of applied Cr(VI) was reduced by cell supported Pd(0) and about 90 % of applied Cr(VI) was reduced by SL-Pd(0). However, kinetic data were not investigated and the catalytic activity of cell-Pd(0) and Sl(JG-A12)-Pd(0) were not directly compared. In the present study we investigated the time dependent Cr(VI) reduction by S-layer produced nanoparticles (Sl-Pd(0)) in comparison with those of Pd(0) produced on cells of *Bacillus sphaericus* JG-A12 (cell-Pd(0)) or bulk Pd(0) produced by the reduction of Pd(II) in the absence of a biological template.

EXPERIMENTAL. *Preparation of Pd-catalysts.* Cells of *B. sphaericus* JG-A12 were routinely grown on NB medium. Harvested cells were washed two timesein Seralpur-H_2O. S-layer of *B. sphaericus* JG-A12 was prepared as described previously [5]. For production of Pd(0) nanoparticles, 30 mg of cell biomass or 10 mg of S-layer protein were incubated in 100 mL of a solution of 2 mM Na_2PdCl_4, respectively. After 24 h biomass was centrifuged and washed 2 times with Seralpur-H_2O. Bound Pd(II) was reduced by the addition of H_2 as reducing agent. As control, Pd(II) of a solution of 2 mM Na_2PdCl_4 was reduced by H_2. The resulting Pd(0) and Bio-Pd(0) were centrifuged, washed with Seralpur-H_2O and dried at 80 °C. The Bio-Pd(0) was grinded to fine powder using a swing mill.

Reduction of Cr(VI). All experiments were done in triplicate samples. Catalytic tests were carried out in 10 mL sealed serum bottles in a total volume of 5 mL containing 20 mM MOPS-NaOH buffer (pH 7.0), 450 µM Na_2CrO_4 and 25 mM formate. Reactions were initiated by the addition of Pd(0) or Bio-Pd(0), comprising 1 mg Pd(0), each. Suspensions were incubated at room temperature. Timed samples (200 µl) were taken and analyzed for residual Cr(VI).
Assay of Cr(VI). Cr(VI) was assayed using diphenylcarbazide reagent (DPC) [3]. DPC stock solution was prepared by dissolving 100 mg DPC reagent in 10 mL acetone plus 0,4 mL phosphoric acid. Supernatant samples (200 µl) were mixed with 8 µl DPC-reagent and allowed to stand at room temperature for 10 min. Cr(VI) was determined by measuring of $A_{\lambda=540}$ versus standards of CrO_4^{2-}.

RESULTS. No loss of Cr(VI) was observed in cell free controls (Fig. 2). In the case of Sl-Pd(0), cell-Pd(0), and Pd(0), an initially rapid rate of Cr(VI) reduction was followed by a slower rate. The initial reduction rates within the first 30 min were determined as 464 ± 11 µM/h (Sl-Pd(0)), 294 ± 32 µM/h (cell-Pd(0)), and 146 ± 30 µM/h (Pd(0)). Within the first 6 hours, 86 % of Cr(VI) was reduced in the case of Sl-Pd(0), whereas only 69 % or 36 % of Cr(VI) was reduced by cell-Pd(0) and Pd(0), respectively, within the same time period. The specific rates of reduction determined over the first 2 hours show a 1,5-fold higher Cr(VI)-reduction rate using Sl-Pd(0) as catalyst (162,5 ± 9 µM/h) compared with cell-Pd(0) (109 ± 5 µM/h) and even a 2,3-fold enhanced reduction rate compared with Pd(0) (72 ± 4 µM/h). These results demonstrate a significantly enhanced catalytic activity of Bio-Pd(0) in comparison with the larger Pd(0) particles. The S-layer was shown to be a suitable biological template for the production of highly catalytically active metallic nanoclusters.

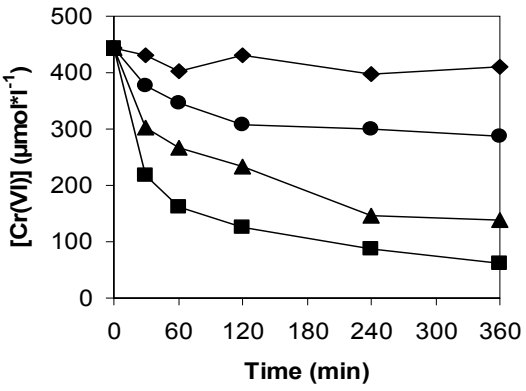

Fig. 2: Reduction of 450 µM Cr(VI) using 25 mM sodium formate (♦) without catalyst, (●) by 1 mg chemical Pd(0), (▲) by 1 mg cell-Pd(0) (prepared on cells of JG-A12), (■) or by 1 mg S-layer-Pd(0) prepared on S-layer proteins of JG-A12.

REFERENCES

[1] Wahl, R. et al. (2001) *Adv. Mater.* **13**, 736-740.
[2] Merroun, M. et al. (2007) *Mater. Sci. Eng.* (in press).
[3] Mabbett, A.N. et al. (2002) *Biotechnol. Bioeng.* **79**, 389-397.
[4] BIO-CAT (2005) *Final Report, EU-Project GRD1-2001-00750.*
[5] Raff, J. (2002) *Report FZR-358.*

Interaction of actinides with solid phases

U(VI) sorption on sandstone

C. Nebelung, V. Brendler

The sorption of U(VI) on natural sandstone was investigated in batch sorption experiments. Sorption maximum was found between pH 5.5 and 7. The linear sorption isotherm indicates only one binding type.

EXPERIMENTAL. Three series of batch sorption experiments were carried out: variation of mass - volume ratios (m/V), pH and U(VI) concentrations (each value from three parallel samples). The surface area of sandstone, fraction 63 - 200 µm, was 0.69 m^2/g (N_2-BET). XRD measurements show mainly quartz and a small content of orthoclase. ICP-MS after chemical digestion gave 92.9 % Si, 3 % Al, 1.7 % K, 1.2 % Ca, 0.6 % Fe and 0.6 % Na. The sandstone in 0.1 M $NaClO_4$ was conditioned for 4 - 5 weeks under air atmosphere with pH adjustment. After uranium addition the samples were shaken for five days and subsequently centrifuged (30 min, 3500 rpm). An aliquot of the supernatant was prepared for direct liquid scintillation (LS) measurement and a part after filtration through a 30 kD-filter to separate potentially existing colloids. The samples for the variation of m/V ratio from 0.25 to 50 g/L were prepared at pH 8 and 10^{-6} M U(VI). The samples for studying the pH-dependence were conditioned between 3 and 11 (in 0.5 steps). The m/V was 12.5 g/L, the U(VI) concentration 10^{-6} M (two samples each with 9.52 µg ^{238}U and one sample with 2155 Bq ^{234}U in 40 mL). In case of the variation of the uranium concentration m/V was set to 12.5 g/L and the pH to 5. The added U(VI) concentrations were between 10^{-9} M and 10^{-3} M uranium, whereas the natural uranium concentration dissolved from the sandstone at low concentrations ($5.3 \cdot 10^{-9}$ M), has to be considered. For the samples with uranium concentrations 10^{-9} M to 10^{-7} M pure ^{233}U was used, for the samples containing 10^{-6} M to 10^{-3} M uranium were added 1000 Bq ^{233}U to the adequate amount of ^{238}U.

RESULTS. By variation of the mass to volume ratio (Fig. 1) a sorption of 50 % between 5 and 12.5 g/L was found. We used m/V = 12.5 g/L (0.5 g in 40 mL) for the further measurement, to get the possibility to observe changes in the sorption.
The pH dependence (Fig. 2) shows a maximal sorption between pH 5.5 - 7.5. The sorption edge was at pH 5. Only a small colloidal fraction was observed. The difference between centrifuged and ultra filtrated samples was below 4 %.

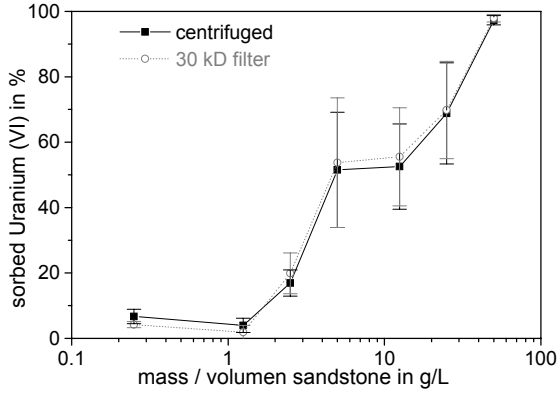

Fig. 1: Sorption of U(VI) as function of mass to volume ratio.

The main component in sandstone is quartz. The U(VI) sorption results on quartz [1] at similar conditions show only a maximum of 50 % sorption between pH 6 - 7. The higher sorption in sandstone caused by the higher surface area or by other minerals, e.g., muscovite [1], orthoclase [2], ferrihydrite [3] or hematite [4,5]. The sorption on these minerals was up to 100 %.

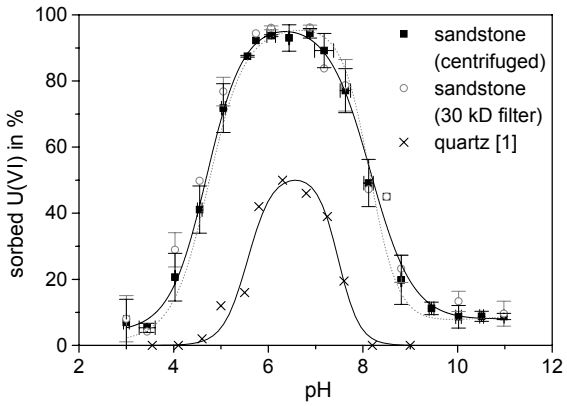

Fig. 2: pH dependence of U(VI) sorption on sandstone and quartz.

The sorption isotherms give a better characterization than only K_D-values. In this study the Freundlich isotherm was used to describe the sorption:

$$\log \frac{c_{sorb}}{m} = \log k + \frac{1}{n} \log c_{eq} \qquad (1)$$

where c_{sorb} = concentration of sorbed U(VI) in mol/kg
m = mass of the solid in kg
c_{eq} = equilibrium concentration of dissolved U(VI) in mol/L

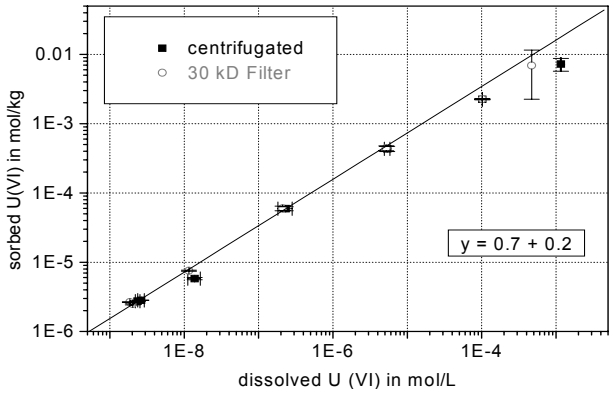

Fig. 3: Freundlich sorption isotherm at pH 5.

The linear sorption isotherm with a slope of 0.7 indicates one binding type (Fig. 3).

ACKNOWLEDGEMENT. Funding by the BMBF and BMWA (02C1144) is gratefully acknowledged.

REFERENCES

[1] Arnold, T. et al. (1998) *Chem. Geology* **151**, 129-141.
[2] Zorn, T. et al. (1997) *Report FZR-180*, p. 5-6.
[3] Zänker, H. et al. (2001) *Report FZR-343*, p. 30.
[4] Hsi, C.K.D. et al. (1985) *Geochim. Cosmochim. Acta* **49** 1931-1941.
[5] Lenhart, J.J. et al. (1999) *Geochim. Cosmochim. Acta* **63**, 2891-2901.

Differences in U(VI) sorption on natural and synthetic sandstone

C. Nebelung, V. Brendler

The sorption of U(VI) on sandstone was investigated in batch sorption experiments. Sorption maxima were found between pH 5.5 and 7.5 on natural sandstone, and pH 6 to 7 on synthetic sandstone. The linear sorption isotherms indicate one binding type.

EXPERIMENTAL. Two batch sorption experiments were carried out: variation of pH and U(VI) concentrations. The synthetic sandstone was a mixture (I) of 95 % quartz and 5 % muscovite for the pH dependence and (II) 90 % quartz, 5 % muscovite and 5 % hematite for the concentration dependence. The surface area (N_2-BET) of quartz was 0.047 m^2/g, of muscovite 0.88 m^2/g, of hematite 0.89 m^2/g and of natural sandstone 0.69 m^2/g. XRD measurements of the single minerals show pure quartz and pure muscovite and in the hematite spectrum also some goethite. By ICP-MS after chemical digestion also 0.77 % Ca in quartz, 5.85 % Fe in muscovite, 1.5 % Ca, and 1 % Si in hematite were found. The experimental conditions for the sorption are described in [1].

Tab. 1: Main components in weight % (> 0.1 %)

element	natural sandstone[1)]	synthetic sandstone I[2)]	synthetic sandstone II[2)]
Na	0.33	--	--
Al	1.67	1.22	1.24
Si	52.20	49.85	46.99
K	0.97	0.59	0.58
Ca	0.67	0.75	0.79
Fe	0.34	0.30	3.50

[1)] measured by ICP-MS after digestion.
[2)] calculated from ICP-MS results of single minerals.

RESULTS. The pH dependence (Fig. 1) shows the maximal sorption of U(VI) on natural sandstone at 95 % between pH 5.5 - 7.5, and on synthetic sandstone only 70 % sorption between pH 6 - 7. The sorption edge was at pH 5 on natural sandstone and at pH 5.5 on synthetic sandstone. The colloidal fraction was higher for synthetic sandstone with its maximum of 35 % at pH 6.

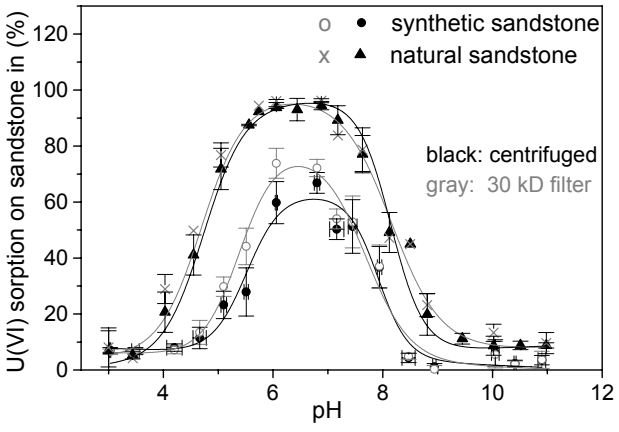

Fig. 1: pH dependence of U(VI) sorption.

For each pH step also samples with uranium but without sandstone were measured. At pH 5.5 to 8 also differences between direct measurement, centrifuged and ultrafiltrated were observed. Thus the retention of U(VI) was caused not only by sorption but also by precipitation.

Figure 2 shows the comparison of natural (red) and synthetic sandstone (black) with single components (at similar conditions) quartz (green) [2], muscovite (blue) [2], and hematite (cyan) [3]. More U(VI) were adsorbed on natural (95 %) and on synthetic sandstone (70 %), than on quartz (only 50 %) as the main component. The higher sorption are caused by the other components muscovite and hematite, and by the higher surface area.

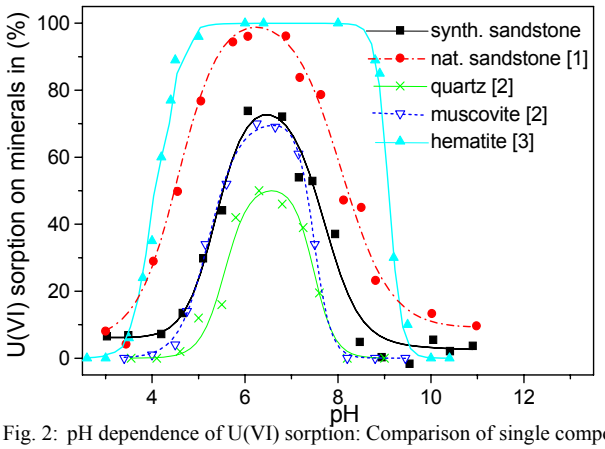

Fig. 2: pH dependence of U(VI) sorption: Comparison of single components of synthetic sandstone with the mixture.

The Freundlich sorption isotherms at pH 5 show a slope of 0.7 for natural and synthetic sandstone (Fig. 3). The U(VI) sorption on natural sandstone varied between 95 % (10^{-9} M) and 7 % (10^{-3} M). The sorption of synthetic sandstone is smaller: 80 % sorption at an addition of 10^{-9} M U(VI) and 2 % at 10^{-4} M. Precipitation was observed when 10^{-3} M U(VI) were added.

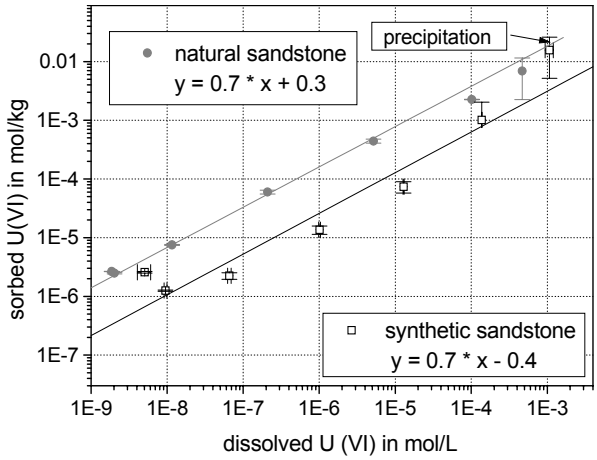

Fig. 3: Freundlich sorption isotherms at pH 5.

ACKNOWLEDGEMENT. Funding by the BMBF and BMWA (02C1144) is gratefully acknowledged.

REFERENCES

[1] Nebelung, C. et.al. this report, p. 51.
[2] Arnold, T. et al. (1998) *Chem. Geology* **151**, 129-141.
[3] Lenhart, J.J. et al. (1999) *Geochim. Cosmochim. Acta* **63**, 2891-2901.

Surface speciation of uranyl(VI) on gibbsite: A combined spectroscopic approach

T. Arnold, A.C. Scheinost, N. Baumann, V. Brendler

Three adsorbed U(VI) surface species on gibbsite were identified by TRLFS and EXAFS. These species were a dimer, a bidentate inner-sphere surface complex and a uranium carbonate species.

Time-resolved laser-induced fluorescence spectroscopy (TRLFS) and extended X-ray absorption fine-structure (EXAFS) spectroscopy were applied to study the species of uranyl(VI) adsorbed onto gibbsite particles. This system is important as a model for the characterization of the edge sites of aluminosilicates, relevant as potential host rock and as part of engineered barrier systems.

EXPERIMENTAL. Synthetic gibbsite (γ-$Al(OH)_3$) with a specific surface area of 49.5 m^2/g (BET) was used in this study. The experiments were performed in air atmosphere, in the pH range 5.5 to 8.5, an ionic strength of 0.01 M ($NaClO_4$), a solid concentration of 4.15 g/L, and using a grain size of 100 – 300 nm. The gibbsite suspension was pH adjusted until it became stable. Then U(VI) was added to obtain a concentration of 10 µM. After that a contact time of two to three days was applied during which the samples were placed in an overhead mixer. Then the samples were centrifuged at 3500 rpm, the supernatant decanted and the residue was re-suspended in a solution of the same pH and ionic strength. These samples were then studied by TRLFS and EXAFS. TRLFS measurements were carried out at room temperature and under cryogenic conditions as well.

RESULTS. TRLFS at room temperature provided evidence for two adsorbed uranium(VI) surface species. The two species showed similar positions of the fluorescence emission bands and different fluorescence lifetimes indicating a different coordination environment for the two species [1]. All EXAFS spectra could be fitted with 2 axial oxygen atoms at a distance of 1.80 Å, and approximately 6 O atoms in the equatorial plane (Tab. 1).

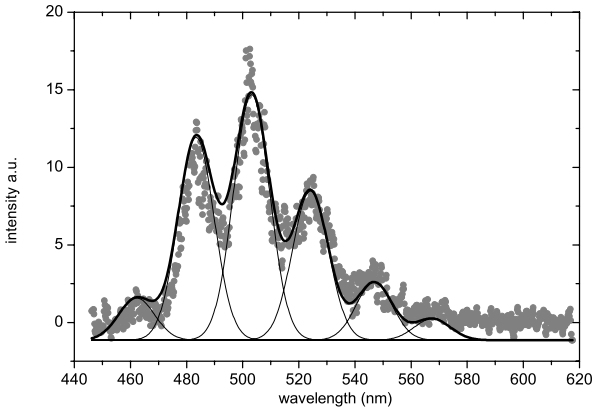

Fig. 1: TRLFS measurement of a U(VI) gibbsite sample conducted at 10 K. The total U(VI) concentration was 10^{-5} M and pH 6.45.

For all but sample U6-27, inclusion of a U–U backscattering shell greatly improved the fit. Coordination numbers varied between 0.8 and 1.1, and distances between 4.21 and 4.22 Å. The coordination numbers of approximately one suggest formation of dimeric sorption species. The formation of edge-sharing, hexagonal uranyl dimers, as shown in Fig. 2, is the most likely arrangement for the fitted U–U distance of 4.2 Å. For all samples except of U6-27, inclusion of a U-Al path slightly improved the total fit result. The distance of this U–Al path varied between 3.33 and 3.34 Å. The distance is in line with a bidentate inner-sphere sorption complex to $Al(O,OH)_6$ octahedra, e.g. that on imogolite with 3.3 to 3.35 Å [2], but slightly shorter than the 3.40 to 3.44 Å found for montmorillonite [3].

Tab. 1: U L_{III}-edge EXAFS multishell fit results of U(VI) gibbsite sorption samples.

	pH	CN	R [Å]	σ^2 [Å^2]
U6-24	5.46	2.0^f O_{ax} 5.8 O_{eq} 2.0^c MS 0.7 Al 0.8 U	1.80 2.39 3.60^c 3.33 4.22	0.0023 0.0062 0.0046^c 0.0100 0.0010
U6-25	6.46	2.0^f O_{ax} 6.2 O_{eq} 2.0^c MS 1.0 Al 0.9 U	1.80 2.40 3.60^c 3.33 4.21	0.0028 0.0076 0.0056^c 0.0100 0.0010
U6-26	7.53	2.0^f O_{ax} 5.6 O_{eq} 2.0^c MS 0.7 Al 0.8 U	1.80 2.42 3.60^c 3.33 4.22	0.0028 0.0069 0.0056^c 0.0100 0.0010
U6-27	8.22	2.0^f O_{ax} 5.5 O_{eq} 2.0^c MS	1.80 2.42 3.60^c	0.0027 0.0069 0.0054^c

^{f}: fixed parameter, ^{c}: correlated parameter, MS: multiple scattering.

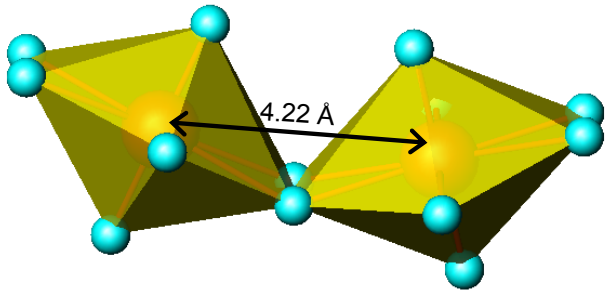

Fig. 2: Edge-sharing hexagonal uranyl dimers.

Cryogenic TRLFS experiments carried out at 10 K implied the presence of a third surface species. The significant shift of the fluorescence emission bands to shorter wavelength (approximately 16 nm) points to a ternary uranyl carbonato surface species. Such a shift is indicative for uranyl carbonate species [4]. The results obtained in this study will help to formulate more realistic surface reactions on aluminosilicates.

ACKNOWLEDGEMENT. The synthetic gibbsite was provided by T. Rabung and J. Lützenkirchen from INE FZK.

REFERENCES

[1] Baumann, N. et al. (2005) *J. Colloid Interface Sci.* **290**, 318-324.
[2] Arai, Y. et al. (2006) *Geochim. Cosmochim. Acta* **70**, 2492-2509.
[3] Hennig, C. et al. (2002) *Radiochim. Acta* **90**, 653-657.
[4] Wang, Z. (2004) *Environ. Sci. Technol.* **38**, 5591-5597.

New TRLFS measurements of U(VI) sorption onto gibbsite

A. Křepelová, V. Brendler, N. Baumann, G. Bernhard

The time-resolved laser-induced fluorescence spectroscopy (TRLFS) was applied to investigate the species of U(VI) sorbed onto gibbsite. The experiments were carried out at different pH values.

Batch experiments were combined with spectroscopic measurements to obtain the molecular-level information on the interaction of U(VI) with gibbsite. Gibbsite was chosen as a model system for aluminol binding sites of kaolinite, see [1].

EXPERIMENTAL. The experiments were performed according to [2] using commercially available gibbsite from Merck with no special pre-treatment. U(VI) was adsorbed under the following conditions: $[U(VI)]_0 = 1 \cdot 10^{-5}$ M, solid / liquid ratio: 12.5 g/L, I: 0.1 M $NaClO_4$, pH: 5-8.5, $p(CO_2)$: $10^{-3.5}$ atm, for details see [2]. After completed U(VI) sorption, the supernatant solutions were removed by centrifugation. Gibbsite samples with adsorbed U(VI) were re-suspended in 40 mL of a $NaClO_4$ solution with pH and ionic strength identical to the original solution (without U(VI)). A Nd:YAG diode laser (Spectron) was used. Time-resolved spectra were recorded with a ICCD-camera (Spectron) in the wavelength range between 446 nm and 617 nm (delay times: 0.03 - 50.03 µs, pulse energy: 0.3 mJ, excitation wavelength: 266 nm).

RESULTS. The results of U(VI) sorption onto gibbsite at different pH values are summarized in Tab. 1.
As an example, the original spectrum of U(VI) sorbed onto gibbsite at pH 6 is shown in Fig. 1.

Tab. 1: U(VI) content in the solutions after sorption and percentage of U(VI) sorbed onto gibbsite.

pH	$U(VI)_{supernatant}$ (µg/L)	$U(VI)_{supernatant}$ (mol/L)	$U(VI)_{adsorbed}$ (%)
5	1470	$6.18 \cdot 10^{-6}$	38.24
5.5	302	$1.27 \cdot 10^{-6}$	85.85
6	127	$5.34 \cdot 10^{-7}$	94.66
6.5	35.6	$1.50 \cdot 10^{-7}$	97.12
7	63.9	$2.68 \cdot 10^{-7}$	97.32
7.5	73.9	$3.11 \cdot 10^{-7}$	96.18
8	707	$2.97 \cdot 10^{-6}$	70.29
8.5	1940	$8.15 \cdot 10^{-6}$	17.87

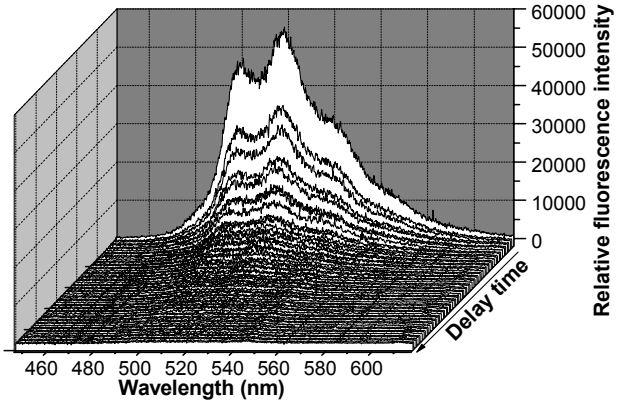

Fig. 1: TRLFS spectrum of U(VI) adsorbed onto gibbsite at pH 6.

Based on the TRLFS spectra, the fluorescence decay function was determined. First of all, a background value was calculated for each sample as the mean value of fluorescence intensities in the wavelength ranges, where no signal was detectable, multiplied by the number of evaluated spectra. The fluorescence lifetime analysis was performed in the wavelength range 470 – 600 nm. For that, the calculated background values were kept fixed during the fitting. The lifetimes of the species were calculated from exponential decay function, which has for i species the following form:

$$Y = \sum_n A_i \cdot e^{-\frac{x}{\tau_i}} \quad (1)$$

The best approximation was a bi-exponential decay function yielding one short (τ_1) and one significant longer (τ_2) fluorescence lifetime for the samples prepared at pH 5 - 7. In all cases, assuming only a mono-exponential decay gave significant worse fittings. However, for the samples prepared at pH ≥ 7.5, a three-exponential decay function gave the best fitting results. It means that at higher pH values, at least two long-lived fluorescence species are formed on gibbsite surface simultaneously. The measured fluorescence lifetimes for all measured samples are summarized in Tab. 2.

Tab. 2: Fluorescence lifetimes of U(VI) species sorbed onto gibbsite, errors represent 1σ. τ_1 and τ_2 of the sample at pH 8.5 were kept fixed by lifetime analysis to obtain τ_3.

pH	τ_1 (ns)	τ_2 (ns)	τ_3 (ns)
5	2320 ± 180	15000 ± 110	–
5.5	2240 ± 90	12900 ± 330	–
6	2310 ± 420	9500 ± 560	–
6.5	2730 ± 100	15800 ± 370	–
7	2180 ± 90	12800 ± 230	–
7.5	1510 ± 20	7700 ± 140	37600 ± 140
8	2100 ± 60	11200 ± 650	51800 ± 700
8.5	2360	13200	51000 ± 230

The obtained values of fluorescence lifetimes differ from the results of recent TRLFS measurements of U(VI) sorption on gibbsite reported by Baumann et al. [2]. Although, the samples were prepared under comparable conditions, differences in obtained results can be caused by using of another measuring laser system. Also, the overall measurement duration was significantly longer than that in [2] (50.03 µs vs. 6.5 µs). The longer the measurement the more accurate values of lifetimes of the long-lived species can be obtained. We assume that we measured true values of τ_2 and τ_3. However, the values of τ_1 measured in this work are maybe overestimated due to long measurement duration.

ACKNOWLEDGEMENT. This work was financially supported by BMWi under contract No. 02E9673.

REFERENCES

[1] Křepelová, A. et al. this report, p. 59.
[2] Baumann, N. et al. (2005) *J. Colloid Interface Sci.* **290,** 318-324.

TRLFS measurements of U(VI) sorbed on CSH phases under alkaline conditions

J. Tits[1], G. Geipel, R. Steudtner, M. Eilzer
[1]Waste Management Laboratory, Paul-Scherrer-Institute, Villigen, Switzerland

The uranium speciation was studied under alkaline conditions. The data were used to compare the spectra with sorption species from Calcium Silicate Hydrate (C-S-H) phases.

EXPERIMENTAL. The first part of the TRLFS measurements consisted of the analysis of 10^{-3} M U(VI) perchlorate precipitated in 0.3 M NaOH, 0.3 M KOH, 0.015 M $Ca(OH)_2$ and artificial cement pore water (ACW). This pore water contains 0.114 M NaOH, 0.18 M KOH and $1.6 \cdot 10^{-3}$ M $Ca(OH)_2$.
In a second part, the fluorescence emission of U(VI) sorbed on C-S-H phases synthesized in H_2O was analyzed. After one day contact time two samples were analyzed: 1) U(VI): $5 \cdot 10^{-5}$ M, 2) U(VI): $2 \cdot 10^{-6}$ M. These suspensions are initially supersaturated w.r.t. Na-uranate and K-uranate, but it is known from batch sorption experiments that the sorption process is faster than the precipitation and more than 99 % of the U(VI) should be sorbed on the C-S-H phases [1].
The fluorescence emission was measured using a cryostat at −120 °C. Fluorescence emission spectra were recorded in the range from 350 nm to 650 nm using delay times between 0.04 µs and 1000 µs after application of the laser pulse (101 spectra). The gate time was set to 2 µs. 50 laser shots were collected for each single spectrum for the sample containing $5 \cdot 10^{-5}$ M U(VI) and 100 laser shots for the sample containing $2 \cdot 10^{-6}$ M U(VI).

RESULTS. At room temperature, no usable fluorescence emission signal could be detected.
The resulting fluorescence emission spectra recorded at −120 °C are shown in Fig. 1. It is well known that lowering the sample temperature increases both the fluorescence spectral intensity and the luminescence decay time as well [2]. In the case of the U(VI) suspensions in NaOH, KOH and ACW, five peaks could be detected three of which were well resolved. The peak maxima were identified with the help of the Origin-Pro™ peak-fitting procedure and are summarized in Table 1. The spectra of these three suspensions were nearly identical suggesting that the Na-uranate and K-uranate precipitated in these suspensions have a very similar structure. The fluorescence decay of the three U(VI) suspensions could be described with a mono-exponential function suggesting the presence of only one fluorescing species. The lifetimes of the U(VI) species were very similar in the three suspensions and were calculated to be in the range of 139 – 154 µs (Tab. 1). It is well known that the fluorescence lifetime increases with decreasing temperature. Therefore these lifetimes cannot be compared with fluorescence lifetimes obtained at room temperature. In the further course of the present project it will be necessary to evaluate the influence of the temperature on the fluorescence lifetime.
The U(VI) suspension in $Ca(OH)_2$ did not exhibit any fluorescence signal. This unexpected result could not be explained yet and should be repeated to confirm the absence of fluorescence emission.
The resulting fluorescence emission spectra of the C-S-H phases are also shown in Fig. 1. Although the total U(VI) concentration in the samples was at least a factor 50 lower than in the U(VI) precipitates, the fluorescence intensity was significantly higher. The resolution was not as good as in the case of the U(VI) precipitates. In most cases two to three peaks were observed together with two to three more or less clearly defined shoulders. The peak maxima are summarized in Tab. 1. Note that the maxima for peak 4 and 5 have a quite high uncertainty. The peak maxima of the U(VI) sorbed species are clearly shifted to higher wavelengths compared to the peaks in the spectra of the U(VI) precipitates. The U(VI) concentration did not seem to have an influence on the spectral characteristics. The fluorescence decay of the two U(VI) suspensions could be described with a mono-exponential function suggesting the presence of only one fluorescing species. The fluorescence lifetime of the U(VI) sorbed species was significantly higher (~200 µs) compared to the fluorescence lifetime of the U(VI) precipitates (139 – 154 µs).

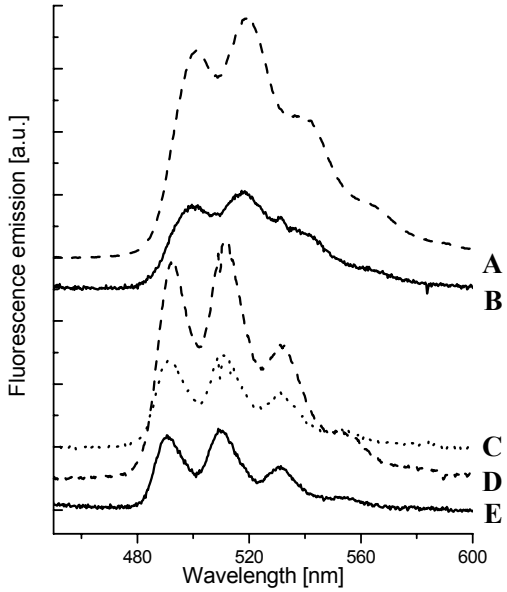

Fig. 1: U(VI) fluorescence emission spectra under alkaline conditions (T = −120 °C). $5 \cdot 10^{-5}$ M U(VI) on CSH in H_2O, S : L = 1.0 g/L (A); $2 \cdot 10^{-6}$ M U(VI) on CSH in H_2O, S : L = 1.0 g/L (B); ACW (C); 0.3 M NaOH (D); 0.3 M KOH (E).

Tab. 1: Luminescence data of the uranium species.

Sample	Peak maxima [nm]					Lifetime [µs]
0.3 M KOH	491.3	510.3	530.7	551.5	579.4	154
0.3 M NaOH	492.6	511.4	531.8	552.9	577.5	139
ACW	491.9	511.2	531.1	551.4	579.0	153
$5 \cdot 10^{-5}$ M U(VI) /CSH/H_2O	500.3	518.9	540.1	562.6	589.6	198
$5 \cdot 10^{-5}$ M U(VI) /CSH/H_2O (repetition)	500.4	519.0	540.0	562.1	589.9	215
$2 \cdot 10^{-6}$ M U(VI) /CSH/H_2O	498.7	516.8	536.7	561.1	589.3	202

REFERENCES

[1] Tits, J. et al. (2006) *J. Colloid Interface Sci.* **300**, 78-87.
[2] Geipel, G. (2006) in: *Handbook of Applied Solid State Spectroscopy*, 577-593, Springer, New York.

TRLFS properties of uranium(VI) sorbed onto silica gel

P. Trepte[1], V. Brendler

[1]Faculty of Mechanical and Process Engineering, University of Applied Sciences, Dresden, Germany

Silica gel serves as a model system for the silanol surface binding sites offered by alumo silicates. Here, the TRLFS properties were obtained for at least three U(VI) surface complexes with fluorescence decay constants of 47 µs, 185 µs and 299 µs. Also peak maxima as a function of pH are available, which are red-shifted by 10-16 nm compared to the free uranyl cation.

The U(VI) binding to complex systems such as clays, which play an important role in nuclear waste disposal design, is still to be clarified. An efficient tool to study the relevant speciation in-situ is required, thus TRLFS (time-resolved laser-induced fluorescence spectroscopy) is applied. Silica gel is used as a model substance for the investigation of silica binding sites in clays. It was preferred to quartz due to its high specific surface area (BET: 505 m^2/g for grain size < 40 µm) compared to quartz (BET: 0.66 m^2/g for grain size < 20 µm) [1]. Thus significantly better signal-noise ratios could be realized.

EXPERIMENTAL. Batch experiment series with silica gel (Merck) were performed. All measurements were using 10 mg silica gel in 40 mL 0.1 M $NaClO_4$ and a uranium concentration of $5 \cdot 10^{-6}$ mol/l. The pH was varied between 4.5 and 9. For the TRLFS measurements the solid phase was centrifuged and resuspended with a $NaClO_4$ solution with pH and ionic strength identical to the original but without uranium. A Nd:YAG diode laser with an excitation wavelength of 266 nm was used to study the sorbed species. Spectra were recorded by a diode array in the wavelength range between 460 and 620 nm. The exposure time was 20 µs; the delay times covered 30 ns up to 200 µs. For further details of the experimental set-up see [2]. All measurements were performed under oxygen atmosphere and at room temperature.

RESULTS. The sorption of U(VI) onto silica gel increases up to pH 5.5 (approx. 96 %) and remains at this level until pH 9. This behavior is a result of the high specific surface area of the assigned silica gel and the strong specific interactions to U(VI). Using TRLFS measurements studying the silica gel samples in the pH range 4.5 - 6 two and for pH values above 6.5 three uranium silica surface species could be identified (Fig. 1). The fluorescence decay lifetime (τ-values) of the short-lived species with a lifetime less than 100 µs (grey hatched range) is rather uncertain. The fluorescence measurements had to cover a relatively long measuring time, due to the long fluorescence lifetimes of the other species. So the measuring intervals had to be selected rather large (here 10 µs). Thus the indicated average value with $\tau_1 = 47$ µs is only an estimate for an existent but not exactly assignable short-lived species. Over the entire pH range two further species with $\tau_2 = 185$ µs and $\tau_3 = 299$ µs (average values) could be determined, but were not coexistent in each sample. Further τ-values > 450 µs could be determined. However it could not be clarified so far, whether this indicates a further species or a pH-dependent drift of the fluorescence lifetime.

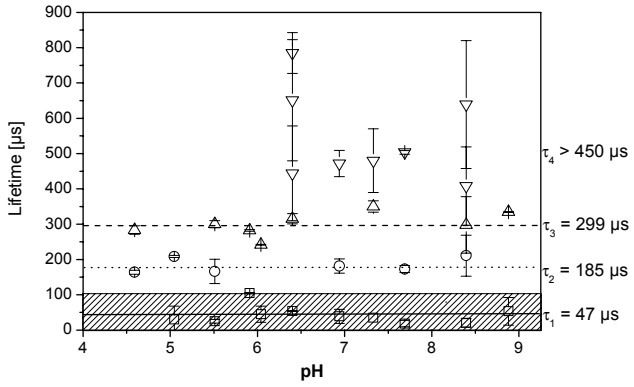

Fig. 1: Uranium sorption on silica gel: pH dependence of the fluorescence lifetimes.

The fluorescence spectra of the silica gel samples showed six characteristic emission bands. Their peak maxima are shifted to higher wavelengths compared to the free uranyl ion in perchlorate medium. The shift increases with pH from about 10 nm at pH 4.5 to about 16 nm at pH 9. See also the shift of the three most distinctive peak maxima in Fig. 2.

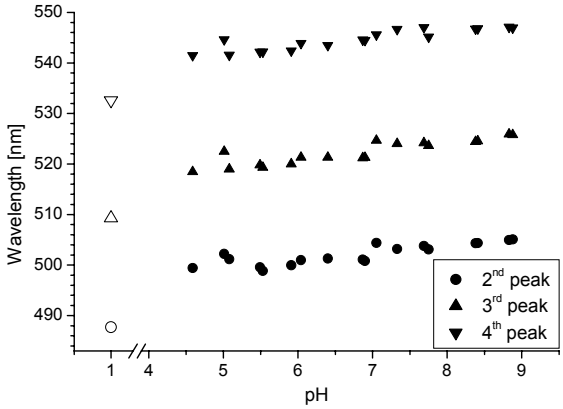

Fig. 2: Uranium sorption on silica gel: pH dependence of the peak maxima; empty symbols: free UO_2^{2+}.

A deconvolution of the fluorescence spectrum has been carried out exemplarily at pH 5.5 and 6.0 and will be continued for the full pH range. The deconvoluted spectra showed different emission bands for the single species. The determined values for the fluorescence lifetime showed a pH dependence different to the values for quartz as determined in [1]. There no peak positions and only one similar lifetimes could be determined, probably due to the shorter measuring time (37 µs compared to 200 µs in the present work). The new results are more reliable, combined with those from the gibbsite system [3] they provide parameters essential for the description of the uranium sorption on alumo silicates.

REFERENCES

[1] Brendler, V. et al. (2004) *Report FZR-419,* p. 52.
[2] Sachs, S. et al. (2007) *Radiochim. Acta* **95**, 103-110.
[3] Baumann, N. et al. (2005) *J. Colloid Interface Sci.* **290**, 318-324.

Np(V) sorption onto kaolinite in the absence and presence of humic acid

K. Schmeide

The Np(V) sorption onto kaolinite as a function of pH, Np and humic acid (HA) concentration as well as of ionic strength is studied in batch experiments.

EXPERIMENTAL. The reference clay kaolinite KGa-1b (Washington County, Georgia) [1] was obtained from the Clay Minerals Society Source Clay Repository. Conditions of batch experiments: $[NpO_2^+] = 1 \cdot 10^{-5}$ or $1 \cdot 10^{-6}$ M, [HA] = 50 mg/L (synthetic HA type ^{14}C-M42 [2]), I = 0.01 or 0.1 M $NaClO_4$, solid / solution ratio 4 g/L, pH 6-10.5, aerobic conditions. ^{233}Pa was separated from ^{237}Np using Dowex-50 prior to each sorption step. Np was added instantly after HA to the preconditioned kaolinite. After a contact time of 72 h [Np] and [HA] were determined by means of LSC (α/β-discrimination).

RESULTS. In Fig. 1, the Np sorption onto kaolinite is shown as a function of pH and the initial Np concentration. At $1 \cdot 10^{-5}$ M Np, the Np sorption increases with pH up to pH 9 and decreases again at higher pH values. At pH 9, $NpO_2CO_3^-$ dominates the Np speciation in solution. Between pH 9 and pH 10, neptunyl carbonate complexes with a higher negative charge are formed in solution ($(NpO_2(CO_3)_2)^{3-}$, $NpO_2(CO_3)_2(OH)^{4-}$ and $(NpO_2(CO_3)_3)^{5-}$). The surface charge of kaolinite in the considered pH range is also negative (e.g., p.z.n.p.c. = 5.1 ± 0.2 [3]). Thus, the electrostatic repulsion between these neptunyl carbonate complexes and kaolinite decreases the Np sorption onto kaolinite above pH 9. The decrease of $[NpO_2^+]_{init}$ from $1 \cdot 10^{-5}$ to $1 \cdot 10^{-6}$ M leads to a shift of the Np adsorption edge to lower pH values by a half pH unit.

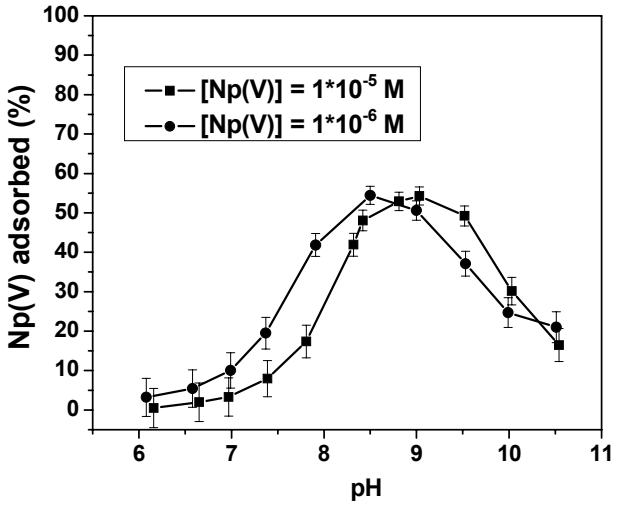

Fig. 1: Np sorption onto kaolinite in the absence of HA. ($[NpO_2^+] = 1 \cdot 10^{-5}$ or $1 \cdot 10^{-6}$ M, I = 0.01 M $NaClO_4$).

Fig. 2 shows the influence of HA on the Np sorption onto kaolinite as a function of pH. No effect of HA on the Np sorption is detectable between pH 6 and pH 7.3. At higher pH values up to pH 10.5 the amount of Np adsorbed onto kaolinite is decreased by HA. On the one hand, this can be attributed to the formation of dissolved neptunyl humate complexes which are formed in solution between pH 6 and pH 9 with a maximum of 11.2 % near pH 8 (accord. to Np speciation calculation - not shown). On the other hand, the mixed ternary neptunyl carbonate humate complex (expected for the alkaline pH region, but presently not quantified thermodynamically) would explain the reduction of the Np sorption by HA at pH > 9. The mobilizing effect of HA on Np is more strongly pronounced in sorption experiments with the higher initial Np concentration of $1 \cdot 10^{-5}$ M (not shown).

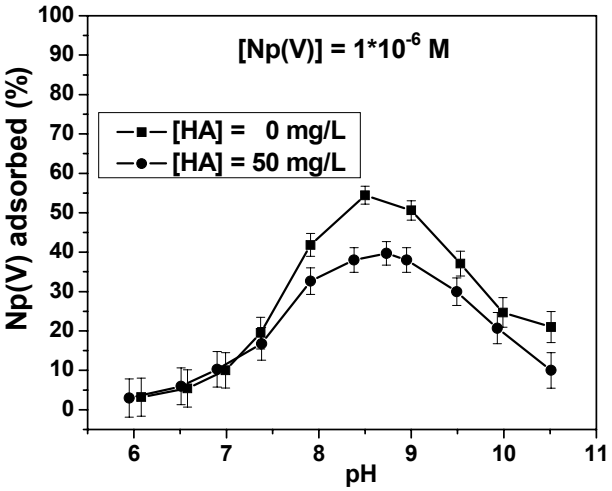

Fig. 2: Influence of HA on the Np sorption onto kaolinite. ($[NpO_2^+] = 1 \cdot 10^{-6}$ M, [HA] = 0 or 50 mg/L, I = 0.01 M $NaClO_4$).

The influence of the ionic strength on the Np sorption onto kaolinite in the absence of HA is shown in Fig. 3. Compared to the sorption experiments performed with an ionic strength of 0.01 M ($NaClO_4$), the Np sorption is increased between pH 7.4 and pH 10 when a higher ionic strength of 0.1 M ($NaClO_4$) is applied.

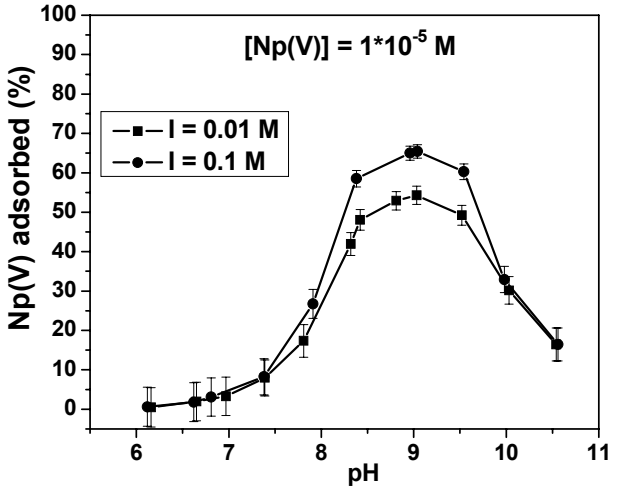

Fig. 3: Influence of ionic strength on the Np sorption onto kaolinite. ($[NpO_2^+] = 1 \cdot 10^{-5}$ M, I = 0.01 or 0.1 M $NaClO_4$).

ACKNOWLEDGEMENT. The German Federal Ministry of Economics and Labor funded this work (02E9673).

REFERENCES

[1] Pruet, R.J. et al. (1993) *Clays Clay Miner.* **41**, 514-519.
[2] Sachs, S. et al. (2004) *Report FZR-399*, p. 4.
[3] Sutheimer, S.H. et al. (1999) *Amer. Mineral.* **84**, 620.

Influence of humic acid on Am(III) sorption onto kaolinite

A. Křepelová, S. Sachs, G. Bernhard

In the present work, results of first batch experiments to study the influence of humic acid (HA) on Am(III) sorption onto kaolinite as a function of pH value are interpreted.

Understanding the migration behavior of actinides is important for the reliable long-term risk assessment of potential nuclear waste repositories. HA can affect the speciation of actinide ions, and therefore, their migration in the environment. Kaolinite was selected as the model mineral and representative of clay formations.

EXPERIMENTAL. The sorption experiments were performed at room temperature under ambient atmosphere in a glove box. Synthetic HA type M42 [1] and kaolinite KGa-1b [2] from the Clay Minerals Society Source Clay Repository were applied. Kaolinite suspensions were equilibrated for 72 h. The final concentrations of Am(III) and HA were $1 \cdot 10^{-6}$ M and 10 mg/L, respectively. The ionic strength was 0.01 M $NaClO_4$ and the solid / liquid ratio was 4 g/L. The pH values were adjusted between pH 3 and pH 10. The contact time of Am(III), HA and kaolinite was 60 h. The samples were analyzed by LSC for the final Am(III) concentration. The experimental conditions were similar to U(VI) sorption experiments, as given in detail in [3].

RESULTS. The sorption behavior of actinides is affected by their speciation in solution. Therefore, the aqueous distribution of Am(III) species was calculated for Am(III) concentration $1 \cdot 10^{-6}$ M in 0.1 M $NaClO_4$ in CO_2 presence using the code EQ3/6 [4]. From Fig. 1 it can be seen that Am(III) prevails in solution as the free Am^{3+} cation up to pH 7, between pH 6 and pH 8.5 also the $AmOH^{2+}$ cation is important. $AmCO_3^+$ prevails between pH 7.5 and pH 8.5 and at higher pH values (pH > 8.5), the negatively charged Am(III)-carbonato complexes $Am(CO_3)_2^-$, and $Am(CO_3)_2^{3-}$ dominate. Moreover, $AmOHCO_3$(am) can precipitate between pH 8 and pH 8.7 under the given experimental conditions.

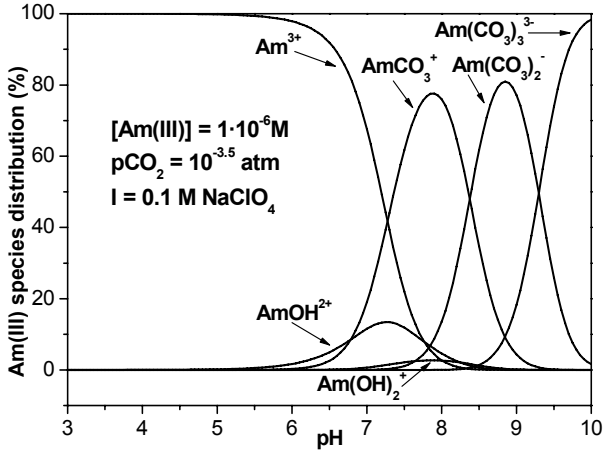

Fig. 1: Am(III) speciation in solution.

First, kinetic experiments were conducted to evaluate the time, which Am(III) requires to reach the sorption equilibrium (experimental conditions as in sorption experiments, pH 5). The sorption equilibrium was achieved very fast. 98 % of Am(III) was adsorbed already after half an hour and the amount of Am(III) adsorbed did not change significantly within the time [3].

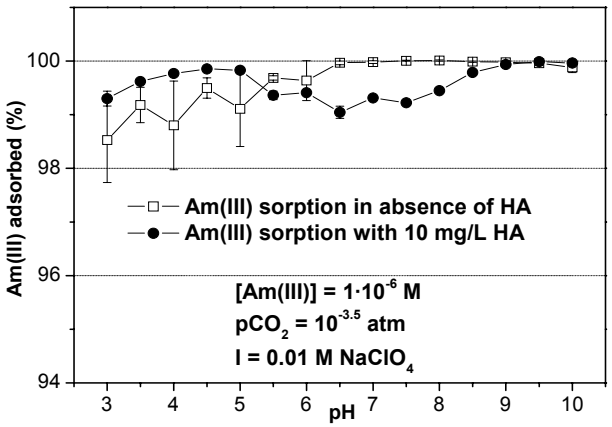

Fig. 2: Am(III) adsorption onto kaolinite in the presence and absence of HA.

The results of batch experiments are depicted in Fig. 2. Am(III) shows a very strong sorption onto kaolinite, which is almost independent on the pH value in the HA-free system. The percentage of adsorbed Am(III) amounts to 98 % at pH 3 and to almost 100 % at higher pH values. Occurrence of the sorption edge at lower pH values was expected as in the case of U(VI) [3] or in comparison to literature [5,6]. However, no sorption edge was observed in the studied system. The reasons for this can be the high solid/solution ratio used in the sorption experiments or the influence of ionic strength.

In the presence of HA, there are small changes in Am(III) sorption in comparison to the HA-free system. At pH < 5, HA enhances very slightly the sorption of Am(III). Conversely, at pH ≥ 5.5, HA decreases the sorption of Am(III) in comparison to the HA-free system because of formation of americium-humate complexes. The formation of binary Am(III)-humate and ternary Am(OH)HA or $Am(OH)_2$HA complexes was reported by Kim et al. [7] and Morgenstern et al. [8], respectively. However, the drop of Am(III) sorption onto kaolinite observed in this study is very small, just around 2 %. One can assume that the Am(III) sorption will further decrease with increasing HA concentration similarly to the system U(VI)-HA-kaolinite [3]. At pH > 8.5, the HA has no influence on Am(III) sorption onto kaolinite.

ACKNOWLEDGEMENT. We thank V. Brendler for the speciation calculation and C. Nebelung for the LS-spectra deconvolution. This work was financially supported by BMWi under contract No. 02E10156 and EU project FUNMIG.

REFERENCES

[1] Sachs, S. et al. (2004) *Report FZR-399*.
[2] Pruett, R.J. et al. (1993) *Clays Clay Miner.* **41**, 514-519.
[3] Křepelová, A. (2007) *Thesis*, Dresden University of Technology, Dresden.
[4] Wolery, T.J. (1992) *UCRL-MA-110662 Part 1,* Lawrence Livermore National Laboratory.
[5] Samadfam, M. et al. (2000) *Radiochim. Acta* **88**, 717-721.
[6] Takahashi, Y. et al. (1998) *J. Radioanal. Nucl. Chem.* **234**, 277-282.
[7] Kim, J.I. et al. (1989) *Radiochim. Acta* **48**, 135-143.
[8] Morgenstern, M. et al. (2000) *Radiochim. Acta* **88**, 7-16.

A continuation in TRLFS study of the influence of HA on U(VI) sorption onto kaolinite

A. Křepelová, V. Brendler, S. Sachs, N. Baumann, G. Bernhard

Time-resolved laser-induced fluorescence spectroscopy (TRLFS) was applied to study the kind of U(VI) surface complexes onto kaolinite. These investigations were carried out at different pH values in the absence and presence of humic acid (HA). Updated results are presented in this paper.

EXPERIMENTAL. The experiments were performed using kaolinite KGa-1b [1] and synthetic HA M42 [2]. Four samples of U(VI) adsorbed onto kaolinite in the absence of HA and four of U(VI) adsorbed in the presence of HA were prepared under the following conditions: $[U(VI)]_0$: $1 \cdot 10^{-5}$ M, $[HA]_0$: 10 mg/L, solid / liquid ratio: 4 g/L, I: 0.1 M $NaClO_4$, pH: 5, 6, 7, 8, $p(CO_2)$: $10^{-3.5}$ atm. For TRLFS measurements a Nd:YAG diode laser (Spectron) was used. Time-resolved spectra were recorded with an ICCD-camera (Spectron) in the wavelength range between 446 nm and 617 nm (delay times: 0.03 – 100.03 µs, pulse energy: 0.3 mJ, excitation wavelength: 266 nm). For the details and measuring conditions see [3].

RESULTS. HA quenches the fluorescence of the samples. This is obvious from the comparison of the fluorescence intensities and the amounts of U(VI) adsorbed onto kaolinite of the samples prepared, for example, at pH ~ 7 in the presence and absence of HA. The difference in the U(VI) adsorption amounts to 7 % (91 % vs. 98 %), while the relative fluorescence intensity (12000 vs. 2500) is almost five times lower in the presence of HA than in its absence. This points out to differences in surface speciation induced by HA.

In both cases, the TRLFS spectra of the adsorbed U(VI) surface species on kaolinite suspensions indicated at least two surface species with two different fluorescence lifetimes, i.e., one short- and one long-lived species. The comparison of the mean values of the respective fluorescence lifetimes obtained in the presence and absence of HA is given in Tab. 1. In the presence of HA, the fluorescence lifetimes of both species are significantly shorter. Shorter fluorescence lifetimes indicate HA in the coordination environment of the adsorbed U(VI) surface species, because HA quenches the fluorescence lifetime. This means that in the presence of HA the hydration shell of uranyl ions is partly displaced with HA.

Tab. 1: Comparison of mean values of obtained fluorescence lifetimes of the samples in the absence and presence of HA. Errors represent 1σ.

pH 5 – 8	τ_1 (ns)	τ_2 (ns)
HA-absence	5900 ± 700	42500 ± 1700
HA-presence	4400 ± 600	30900 ± 3600

Six fluorescence emission bands were obtained for the fluorescence spectra of all measured samples of U(VI) adsorbed onto kaolinite in absence of HA. The positions of peak maxima of short- and long-lived species show no difference, but they are shifted significantly relative to the values for free UO_2^{2+} ion in perchlorate medium [4], see Tab. 2. Due to coincidence of all fluorescence peaks, the short- and the long-lived U(VI) surface species are assumed to be similar in coordination environment throughout the investigated pH range. In presence of HA, only five peaks were found due to lower quality of the measured spectra. Similarly to the binary system, there is no difference in the peak maxima positions of the short- and the long-lived species. Furthermore, no changes in peak positions of the samples in absence and presence of HA were observed. It can be concluded that HA does not influence the peak positions of both species. Also changes in pH have no significant influence on the fluorescence lifetimes of U(VI) surface species.

Tab. 2: Comparison of peak positions maxima of four main peaks of the samples in the absence and presence of HA and of UO_2^{2+} ion in perchlorate medium [4].

pH 5 – 8	2nd peak	3rd peak	4th peak	5th peak
HA-absence	501.8	520.6	541.7	567.8
HA-presence	501.1	520.5	542.2	566.7
UO_2^{2+}-perchlorate	487.8	509.3	532.6	558.1

To identify, on which of possible binding sites of kaolinite U(VI) would prefer to adsorb, TRLFS measurements of the system U(VI)-kaolinite were compared with the systems U(VI)-gibbsite [5] and U(VI)-silica gel [6]. Table 3 compares the mean values of fluorescence lifetimes.

Tab. 3: Comparison of mean values of fluorescence lifetimes for the system U(VI)-kaolinite with model systems. Errors represent 1σ.

System	τ_1 (ns)	τ_2 (ns)	Ref.
Gibbsite[1]	2360 ± 220	13200 ± 2500	[5]
Silica gel[2]	138400 ± 52900	361800 ± 103200	[6]
Kaolinite[2]	5900 ± 700	42500 ± 1700	This work

[1]pH 5 – 7; [2]pH 5 – 8.

The fluorescence lifetimes of both species on kaolinite lie in the range between values obtained for gibbsite and for silica gel, however, the fluorescence lifetimes of species on kaolinite are closer to those on gibbsite than those on silica gel. It seems that U(VI) adsorbs on both kinds of available sites but not equal. Aluminol binding sites are assumed to control the sorption of U(VI). From SEM of kaolinite particles, the ratio between planes and edges of kaolinite particles was calculated to be about 0.72, which indicates a higher amount of edges relative to basal planes. Similarly, Brady et al. [7] reported higher percentage of edges relative to basal plane of the kaolinite KGa-1. They also reported elevated reactivity of Al edge sites, relative to Si, and a weak sorption on basal planes resulting from their molecular modeling. Moreover, an excess of Al_2O_3 in kaolinite was found by chemical analysis [3].

ACKNOWLEDGEMENT. This work was financially supported by BMWi under contract No. 02E9673.

REFERENCES

[1] Pruet, R.J. et al. (1993) *Clays Clay Miner.* **41**, 514-519.
[2] Sachs, S. et al. (2004) *Report FZR-399.*
[3] Křepelová, A. (2007) *Thesis*, Dresden University of Technology, Dresden.
[4] Bell, J.T. and Biggers, R.E. (1968) *J. Mol. Spectr.* **25**, 312-329.
[5] Křepelová, A. et al. this report, p. 54.
[6] Trepte, P. (2006) *Diploma thesis*, University of Applied Sciences, Dresden.
[7] Brady, P.V. et al. (1998) in: *Adsorption of Metals by Geomedia*, p. 371-382, Academic Press, San Diego.

Diffusion of U(VI) in a compacted humic substance-kaolinite-sorbate

S. Sachs, J. Mibus

The migration of U(VI) in a compacted humic substance-kaolinite-sorbate, representing a model substance for clays rich in organic matter, was studied. It was compared to the U(VI) migration in kaolinite in absence and presence of humic acid (HA) in solution. Generally, in presence of humic material U(VI) is immobilized in association with humic matter. A slightly deeper intrusion of U(VI) into the clay layer was observed for the humic substance-kaolinite-sorbate.

Clay minerals and mélanges of organic substances are common components of many soils, sediments, and rocks. HA strongly influences the migration of U in compacted kaolinite [1]. Compared to the HA-free system, U was significantly immobilized. In the present study, the diffusion behavior of U(VI) in a synthetic humic substance-kaolinite sorbate [2] was studied. The results were compared to the U diffusion in kaolinite in the absence as well as in the presence of separately added HA in solution which is described in detail in [2].

EXPERIMENTAL. A synthetic humic substance-kaolinite-sorbate that was obtained by synthesis of HA type M42 in presence of kaolinite (R1/06KS, total organic carbon content (TOC): 5.1 mg/g) [2] was compacted in a diffusion cell [3] to a dry bulk density of 1.56 g/cm³. The clay plug was equilibrated with 0.01 M $NaClO_4$ solution (1 mM NaN_3) at pH 7. The diffusion of U(VI) was studied at ambient air. The tracer concentration C was kept constant at the boundaries ($C(0,t) = C_0$; $C(L,t) = 0$) with $C_{0,U} = 1 \cdot 10^{-6}$ mol/L ($^{238}U + ^{234}U$). The high and low concentration reservoir was analyzed periodically using liquid scintillation counting with α/β separation. After 79 d the cell was opened and the clay was cut into slices of 0.5 or 1 mm thickness. After drying, U was extracted from the clay by 1 M HNO_3 and analyzed as described above.

RESULTS. Figure 1 presents the U distribution in the synthetic humic-substance-kaolinite-sorbate after 79 d in comparison to that of U in kaolinite in absence of HA [2]. It becomes clear that U is not able to migrate deep into the humic substance-kaolinite sorbate. U is immobilized at the solution-clay boundary most likely in association with humic substances.

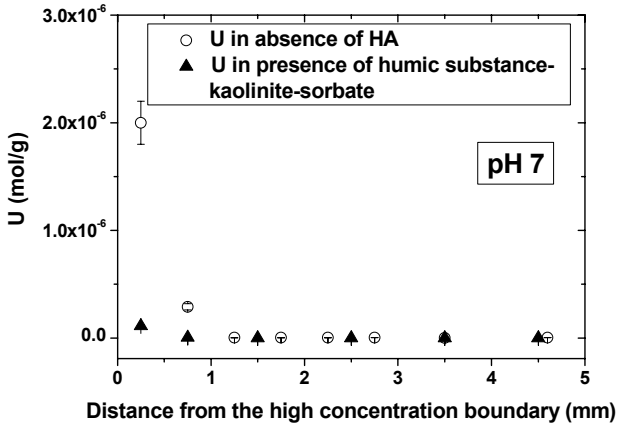

Fig. 1: U distribution in the humic substance-kaolinite sorbate after 79 d in comparison to the U distribution in absence of HA (64 d; [2]).

The comparison of the present results with those of the U migration in kaolinite in presence of HA in solution [2] (Fig. 2) shows that U penetrates slightly more into the humic substance-kaolinite-sorbate.

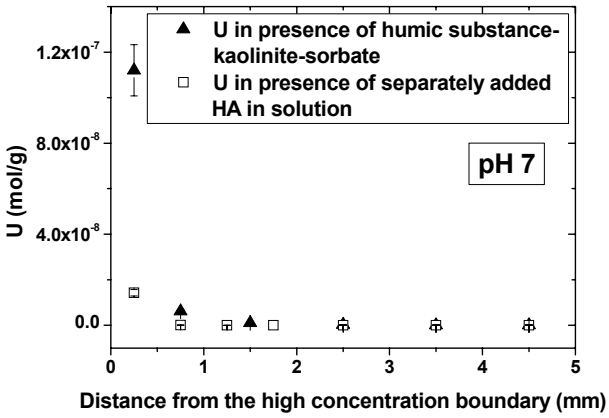

Fig. 2: U distribution in the clay plug after the experiment with the humic substance-kaolinite sorbate (79 d) and with kaolinite and HA in solution (78 d; [2]).

At the start of the experiment with the humic substance-kaolinite-sorbate, U exists in a HA-free solution. With access to the sorbate, U can interact with the immobilized humic material as well as with the kaolinite surface which is not homogeneously covered by a humic substance layer [4]. Simultaneously, HA-like substances diffuse from the clay into the high and low concentration reservoir solutions, whose TOC concentrations steadily increase during the experiment. After the end of the experiment, the TOC content in the high and low concentration reservoir amounted to about 1.8 and 0.8 mg C respectively, representing about 3.2 and 1.5 mg of mobilized HA-like substances. These HA-like substances are able to complex increasing amounts of U in form of the UO_2(OH)HA(I) complex [5]. Thus, the diffusion of U(VI) is increasingly influenced by this complex. Hence, U is probably immobilized at the solution-clay boundary in association with humic matter as already found for the U migration in kaolinite in presence of separately added HA in solution [1,2].

The slightly deeper intrusion of U into the humic substance-kaolinite-sorbate (Fig. 2) may be attributed to the first stage of the experiment, when no HA-like substances were present in solution and U was allowed to diffuse as non-HA-complexed species (cf. Fig. 1).

As many natural sediments and soils contain considerable amounts of organic matter, this model system is expected to reflect migration processes in the environment more realistically than the pure clay system originally free from organic matter.

ACKNOWLEDGEMENT. The German Federal Ministry of Economy funded this study (02 E 9673).

REFERENCES

[1] Mibus, J. et al. (2006) *Report FZR-443*, p. 60.
[2] Sachs, S. et al. (2006) *Final Report BMWi-Project No. 02 E 9673*.
[3] Van Loon, L.R. et al. (2003) *J. Contam. Hydrol.* **61**, 73-83.
[4] Reich, T. et al. (2006) *Report FZR-443*, p. 46.
[5] Sachs, S. et al. (2007) *Radiochim. Acta* **95**, 103-110.

Zeta potential of UO_2(am) by laser Doppler velocimetry

S. Weiß, H. Zänker, A. Potthoff[1]

[1]Fraunhofer Institute for Ceramic Technologies and Systems, Dresden, Germany

The Smoluchowski zeta potential of freshly precipitated UO_2(am) was determined as a function of pH. For the first time this was done by laser Doppler velocimetry. The UO_2(am) particles showed a relatively high surface charge at pH > 4. A point of zero charge (pzc) of pH 6.9 was found.

EXPERIMENTAL. The surface charge of a mineral oxide influences its ability to sorb ions and its colloidal stability. High surface charge results in high repulsion forces and in the formation of stable colloids. Low charge leads to attraction and flocculation of colloids. The zeta potential is a measure of the surface charge. Laser Doppler velocimetry determines the zeta potential by detecting the electrophoretic mobility of particles using laser light scattering in an alternating electrical field.

There have been only few publications concerning the zeta potential of UO_2 [1-4]. The authors of these publications applied other methods of measurement different from ours and used minerals [3] or material synthesized by thermal reduction [4]. The results are and also the influence of oxidized layers on the surface is not clear.

In this work, the zeta potential of colloidal and freshly flocculated microcrystalline UO_2 was measured for the first time. Our measuring conditions are representative of tetravalent uranium in deep anoxic s. The results can provide information on mobilization (colloidal transport) and immobilization flocculation processes of particulate UO_2.

EXPERIMENTAL. All experiments were prepared in a glove box under nitrogen atmosphere with < 1 ppm O_2 in order to avoid surface oxidation of the precipitates. For the preparation of U(IV) precipitate see [5]. The solutions contained 1 mM uranium in 0.2 M $HClO_4$/$NaClO_4$. The precipitated UO_2(am) was characterized by XRD and EXAFS [6]. The zeta potential of the precipitations was measured in two series: titration of colloidal UO_2(am) with NaOH from pH 2.2 to 11.5 (serial A) and titration of flocculated UO_2(am) with $HClO_4$ from pH 11.0 to 2.2 (serial B). The titrated samples were equilibrated for 20 minutes at each titration step. Samples of 1-2 mL were removed at each step and filled into sealed cuvettes for measurement of the zeta potential (Zetasizer Nano ZS, Malvern Instruments) at different pH values. These measurements were done outside the glove box but within a time span (5 min) during which the ingress of oxygen into the sealed cuvettes is still negligible.

RESULTS AND DISCUSSION. The distribution of the zeta potentials was found to be monomodal at each pH, indicating chemical homogeneous surfaces. The results are shown in Fig. 1. Both experimental series yielded approximately the same pH dependency of the zeta potential. The values for pH < 4 are relatively high (30 – 40 mV). These high zeta potentials are in accordance with the observed stability of the colloids at pH 2 – 4: colloidal UO_2(am) solutions remained stable for > 1.5 years. At pH > 4 the zeta potential decreased rapidly and the point of zero charge (pzc) was reached at pH 6.9. This pzc is slightly higher than the value found by Olsson et al. (pH 5 – 5.5) [2] using potentiometric titration and Pravdic et al. using streaming potential measurements (pH 5.8 ± 0.2) [4]. It is well known [2,4] that discrepancies and falsification of the zeta potential can occur due to the oxidation affinity of UO_2, i.e. due to the formation of a layer of higher uranium oxides at the surface of the UO_2 particles. However, it is still not even clear if such layers result in too high [2] or too low [1] points of zero charge. In our experiments the exclusion of O_2 was ensured more carefully than in the previous studies [2-4]. There is also a lack of knowledge about possible influences of crystallinity or of the washing procedures applied by Olsson et al. [2].

Our results indicate that UO_2(am) colloids can be very stable in acidic solutions. On the other hand, they tend to be immobilized at near-neutral pH values, i.e. in the range of typical natural waters.

Points of zero charge of other tetravalent metal oxides have been published. For ThO_2 Olsson et al. found a pzc of pH 8.4 – 8.8 at I = 0.1 M $NaClO_4$ [2]. For ZrO_2 Kagawa et al. reported a pzc of pH 6.5 [7] which is close to the value for UO_2 measured in this work.

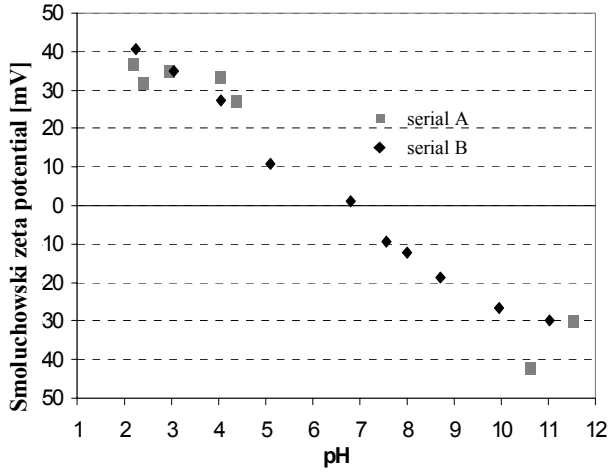

Fig. 1: Measured Smoluchowski zeta potential vs. pH for serial A (titration started at pH 2.2) and serial B (titration started at pH 11.0).

ACKNOWLEDGEMENT. The authors thank S. Teichert (IKTS) for performing titrations and zeta potential measurements.

REFERENCES

[1] Parks, G.A. et al. (1965) *Complex Systems Chem. Rev.* **65**, 177-198.
[2] Olsson, M. et al. (2002) *Journal Colloid Interface Sci.* **256**, 256-261.
[3] Parreira, H.C. et al. (1960) *An. da Acad. Brasileira de Ciencias* **32**, 35-42.
[4] Pravdic, V. et al. (1963) *Croatica Chemica Acta* **35**, 247-261.
[5] Weiß, S. et al. (2004) *Report FZR-419*, p. 13.
[6] Ulrich, K.U. et al. (2005) *Report FZR-443*,p. 17.
[7] Kagawa, M. et al. (1987) *J. Am. Ceram. Soc*. **70**, C-212.

Adsorption of U(VI) onto colloids produced by the weathering of rock material

H. Zänker, S. Weiß

Iron-rich colloids produced by the weathering of rock can adsorb significant amounts of uranium(VI) which transforms the uranium in a colloid-borne form. However, this adsorption of U is significantly influenced by background solutes such as dissolved $CaSO_4$.

In [1] we showed that Fe(III)-rich secondary mineral colloids produced by the weathering of rock can influence the behaviour of U(VI) in natural waters such as seepage waters from mine waste rock piles. Here we test the influence of the dissolved background solutes $NaHCO_3$ and $CaSO_4$ on the fraction of colloid-borne uranium.

EXPERIMENTAL. The weathering of phyllite from an abandoned uranium mine (for the chemical and mineralogical composition see [2]) was simulated. The phyllite was jaw-crushed and sieved. The ground phyllite was suspended in MilliQ water (40 g/L). The material was "prewashed" twice by centrifugation and re-suspension. For the "weathering" the suspension was shaken for 90 h during which period the colloids were formed (oxic conditions, pH 8.4). Thus, the ground phyllite was used as a "colloid generator". The bulk of the ground phyllite was separated from the colloids by centrifugation at 1000×g. The particle size cut-off of this particle separation is about 10^2 nm (cf. [3]). The centrifugate (supernatant) was used as the colloidal suspension for the sorption experiments. A uranium concentration of 50 µg/L and a series of pH values between 8.2 – 4.7 were adjusted (acidification with H_2SO_4). The following background solutes were added: (a) 105 mg/L $NaHCO_3$ or (b) 150 mg/L $CaSO_4 \cdot 2H_2O$ or (c) no additions apart from the presence of CO_2 from the air. The samples were allowed to equilibrate for one day. Finally, the major fraction of the colloids was removed by ultracentrifugation (170000×g, separation by pipetting again). The maximum hydrodynamic diameter of the particles still present in the supernatant after this centrifugation is about 10^1 nm (cf. [3]). The supernatant solutions from the 1000×g and 170000×g centrifugations were analyzed by ICP-MS and/or AAS.

RESULTS. Information on the inventories of colloids of the size class 10^1 to 10^2 nm and the chemical composition of the colloids of this size class can be derived from the differences of the ICP-MS/AAS results after the 1000×g and the 170000×g centrifugations, $c_{1000\times g} - c_{170000\times g}$. It follows from the differences $c_{1000\times g} - c_{170000\times g}$ that the colloidal solution produced by the weathering of the phyllite contained a total of > 10 mg/L of colloids of the size class 10^1 to 10^2 nm. The colloids consist primarily of secondary minerals. They contain significant amounts of ferric iron (the complete chemical composition of the colloids is given in [2]). Figure 1 demonstrates the adsorption of the uranium(VI) onto the colloids and the influence of the background solutes on this adsorption. The figure shows the colloid-borne U fraction (percentage of the total U) as determined by the differences $c_{1000xg} - c_{170000xg}$ for uranium as a function of pH. Note that U(VI) is truly dissolved in these simulated natural waters in the absence of colloids which can be seen from the blank experiment in Fig. 1 (dotted line). However, the presence of the colloids

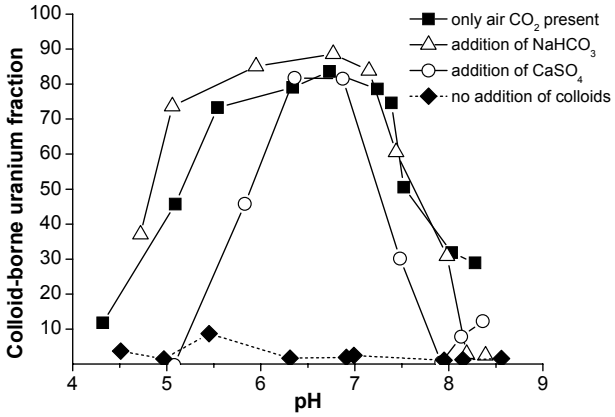

Fig. 1: Fraction of colloid-borne U as a function of pH in the presence of colloids from the „colloid generator" (■), after addition of background solutes (Δ: $NaHCO_3$, ○: $CaSO_4$) and without the addition of colloids (♦: blank).

makes most of the uranium colloid-borne in the middle pH region.

We expect the most important sorbent for the U(VI) to be the ferrihydrite component of the colloids (cf. [4]). The background solute $CaSO_4$ causes a "narrowing" of the pH region in which colloid-borne uranium occurs. We assume that soluble complexants can suppress the formation of colloid-borne surface complexes due to a competition between uranyl surface complexation at the colloid / water interface and uranyl complexation in solution (see also [5]). In the slightly acidic region, surface complexation may be suppressed by the formation of dissolved complexes such as $UO_2(SO_4)^0$ (aq). In the slightly alkaline region, surface complexation may be counteracted by the formation of complexes such as $Ca_2UO_2(CO_3)_3^0$(aq).

CONCLUSIONS. Colloids produced by the weathering of phyllite are able to keep large fractions (up to 90 %) of the uranium(VI) in a colloid-borne form in the pH region of 5.0 to 7.5. In the absence of colloids, this U(VI) would be truly dissolved. Background solutes can significantly influence the surface complexation of U on the colloids.

REFERENCES

[1] Zänker, H. et al. (2006) *Report FZR-443*, p. 18.
[2] Zänker, H. et al. (2006) *Aquatic Geochem.* **12**, 299-325.
[3] Zänker, H. et al. (2003) *Report FZR-400*, p. 48.
[4] Arnold, T. et al. (2001) *J. Contam. Hydrol.* **47**, 219-231.
[5] Fox, P.M. et al. (2006) *Geochim. Cosmochim. Acta* **70**, 1379-1389.

Determination of diffusion coefficients of humic acid in bulk water

J. Mibus, C. Müller, S. Sachs, R. Küchler[1]
[1]Institute of Safety Research, FZD, Dresden, Germany

Diffusion coefficients of humic acid in bulk water have been determined using the capillary method. These macroscopic coefficients agree with spectroscopic results from the literature.

The diffusion of humic acid (HA) in compacted clay depends on their diffusion properties in bulk water and the sterical hindrance in the pores. Spectroscopically determined diffusion coefficients of HA in water are reported in [1], however, no macroscopic coefficients have been measured so far. We used a modified capillary method to determine diffusion coefficients of HA and a conservative tracer in bulk water and present a mathematical model for interpretation.

EXPERIMENTAL. ^{14}C-labeled HA type M42 [2] of a concentration of C_0 = 12 mg/L (200 Bq/mL) in a 0.01 M $NaClO_4$ medium of pH 7 and tritiated water (HTO, 530 Bq/mL) were used as tracer. Teflon® tubes of 1.6 mm diameter and 100 mm length were filled with tracer or tracer-free solution from each side (Fig. 1a).

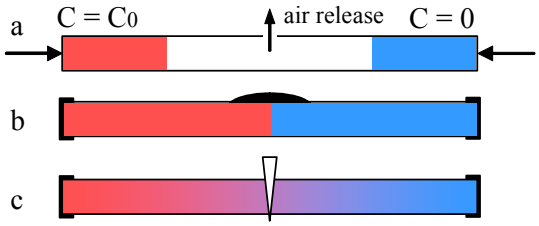

Fig. 1: Experimental set-up.

A bore of 0.1 mm in the middle releases encased air. After sealing the tube with silicon resin (Fig. 1b), the tracer was allowed to diffuse for various time periods (T = 22 ºC). Then, the tubes were cut (Fig. 1c), and the tracer activities in both solutions were measured by liquid scintillation counting. The size distribution of HA was analyzed by ultrafiltration (Microsep, Pall, 1 - 1000 kD).

MODELING. The diffusion coefficient D [m^2/s] is estimated by an analytical solution of Fick's second law

$$C_{high}(t) = \frac{C_0}{2}\left(1 - 2\sum_{i=1}^{n}(-1)^i \frac{\sin^2\left(i\frac{\pi}{2}\right)\exp\left(-\left(i\frac{\pi}{L}\right)^2 Dt\right)}{\left(i\frac{\pi}{2}\right)^2}\right) \quad (1).$$

C_{high} [Bq/m^3] is the integral concentration over the high concentration side, L [m] is the tube length, and t [s] is the time. The corresponding C_{low} equals the difference to C_0.

RESULTS. The observed tracer distribution normalized to the total tracer amount as a function of time is plotted in Fig. 2. The fitted diffusion coefficient of HTO underestimates the reported value only slightly (Tab. 1). Mixing in the tube is governed by diffusion and the influence of thermal convection and mechanical vibration is negligible. The HTO recovery indicates a very low loss of tracer. The estimated D_w value of HA agrees with spectroscopically determined values (^{1}H NMR) from [1]. The reported range in D_w is due to the polydisperse nature of HA as the diffusivity depends on the molecular size.

Tab. 1: Tracer recoveries and diffusion coefficients.

Tracer	HTO	HA
Recovery	0.98 ± 0.01	0.89 ± 0.04
D_w in 10^{-9} m^2/s	2.07 ± 0.02	0.36 ± 0.01
Reported D_w in 10^{-9} m^2/s	2.2 [3]	0.11 to 0.37 [1]

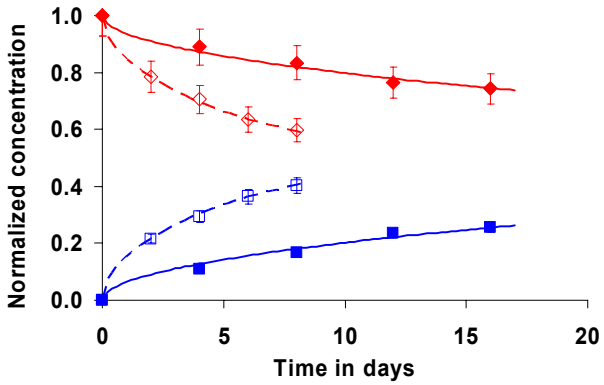

Fig. 2: Measured and fitted concentration curves vs. time (open symbols: HTO, closed symbols: HA, lines: corresponding model).

This trait causes a slight shift of the HA size distribution in the low concentration reservoir to a lower molecular size (Fig. 3). This effect, however, is too weak to derive diffusion parameters for single size fractions. Thus, the fitted D_w in Tab. 1 represents a mean value of the polydisperse matter.

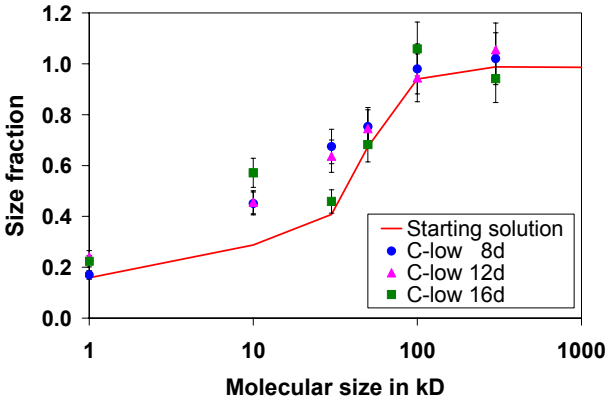

Fig. 3: Size distribution of HA in the starting solution and the low concentration reservoir after various diffusion times.

CONCLUSIONS. Macroscopic diffusion coefficients of humic acid are consistent with spectroscopic results. A slight molecular size fractionation can be observed.

ACKNOWLEDGEMENT. The German Federal Ministry of Economics funded this study (02 E 9673).

REFERENCES

[1] Morris, K.F. et al. (1999) *Anal. Chem.* **71**, 5315-5321.
[2] Sachs, S. et al. (2004) *Report FZR-399*.
[3] Li, Y.H. et al. (1974) *Geochim. Cosmochim. Acta* **38**, 703-714.

Abiotic selenium reduction by ferrous iron at the solid/water interface: The Se(IV)-Fe^{2+}-montmorillonite system

A.C. Scheinost, L. Charlet[1], A. Géhin[1]
[1]Geochemistry Group, LGIT, Université Joseph Fourier, Grenoble, France

Selenite ($Se(IV)O_3^{2-}$) sorbed to the Fe^{2+}-equilibrated montmorillonite surface as outer-sphere complex is slowly reduced to Se(0) and precipitates as nanosized metal clusters.

The fission product ^{79}Se is commonly considered as one of the key risks of nuclear waste disposal sites due to its long half-live of 65 ka and due to the suspected predominance as anionic aqueous species ($Se(IV)O_3^{2-}$ and $Se(VI)O_4^{2-}$) with high environmental mobility. This mobility may decrease by formation of reduced Se species (oxidation states 0, −I, −II) through biotic as well as abiotic reduction mechanisms. For instance, Myneni et al. have demonstrated that the mixed Fe(II)/Fe(III) mineral green rust reduces selenite . Since aqueous Fe(II) species may be far more ubiquitous in the near-field and far-field of nuclear waste disposal sites, and are efficient reducers of a range of toxic metals like As and U, we investigated the reduction of selenite by Fe^{2+}-equilibrated montmorillonite.

EXPERIMENTAL. Using a Jacomex inert-gas glovebox (< 1 ppm O_2), a suspension containing 20 g/L of a synthetic, strictly Fe-free montmorillonite was equilibrated for one week with 5 mM Fe^{2+} in 50 mM $CaCl_2$ at pH 6. At t = 0, 500 µM Se(IV) was added. Samples were collected at selected time intervals up to one month (Fig. 1), then shock-frozen, stored and transported in LN_2 to stop the redox reactions and to maintain an O_2-free environment. Se-K edge XAS spectra were collected at the Rossendorf beamline (ESRF, Grenoble, France) within a few hours after sample preparation using a He-filled closed-cycle cryostat running at 15 K. Following this protocol, we prevented O_2 diffusion to the sample, photo-reduction (or -oxidation) of Se by the intense X-ray beam, and excluded the thermal contributions of the Debye-Waller factor.

RESULTS. The time-resolved Se-K edge XANES spectra (Fig. 1) show with time the growth of a shoulder at 12657 eV, corresponding to Se(0), and the decline of the main white-line peak at 12662 eV, corresponding to Se(IV). The first indication of a reduction is visible after 6 hours, and the reduction is not completed within one month. All spectra can be reconstructed with two components by PCA, suggesting the presence of only one reaction product in addition to the initial Se species, which was measured under the same experimental conditions, but without Fe^{2+} in suspension. Even after including the spectrum of gray Se(0), all spectra are well reconstructed by two spectral components, suggesting the formation of this zero-valent species (Fig. 1).
The spectral deconvolution of the EXAFS spectra with iterative transformation factor analysis resulted in the EXAFS spectra of the two components, i.e. of the two species (Fig 2). As expected, component 1 corresponds to the selenite anion (3 O atoms at 1.70 Å), while the absence of any backscatters beyond the coordination sphere demonstrates that it is sorbed to the montmorillonite surface as an outer-sphere complex. The local structure of component/species 2 is similar but not identical to gray (trigonal) Se(0). While the spectrum of a gray Se(0) reference was fitted with 2.3 Se atoms at 2.39 Å, and with 4.8 Se at 3.39 Å, component/species 2 was fitted with 2.7 Se at 2.36 Å and 1.4 Se at 3.26 Å, including significantly enhanced Debye-Waller factors. These structural data suggests that nano-sized Se(0) clusters with large structural disorder formed during the reduction.
Formation of this reduced species may greatly diminish the amount of soluble Se on one hand; on the other hand it cannot be excluded that this species remains mobile due to its colloidal nature.

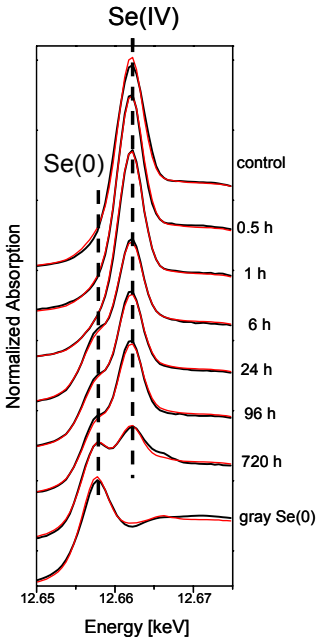

Fig. 1: Time-resolved Se-K edge XANES spectra of the Se(IV)-Fe^{2+}-montmorillonite system (black lines) and spectral reconstruction with two components (ITFA). As references, the spectra of a control without Fe^{2+} and of gray Se(0) are shown.

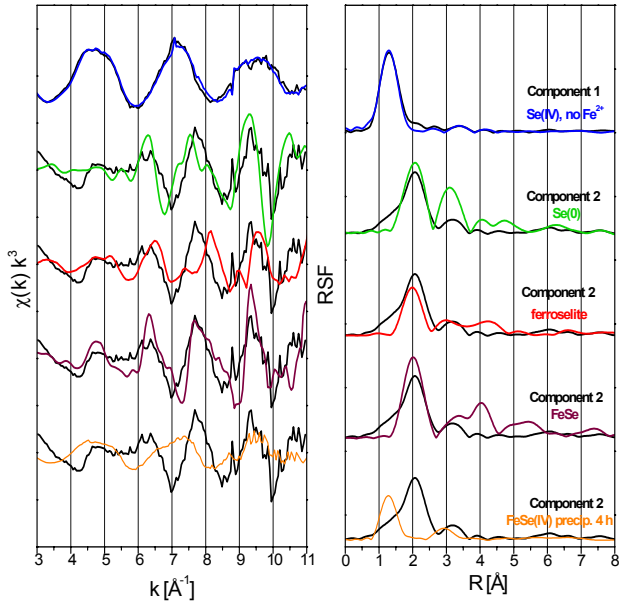

Fig. 2: Se-K edge EXAFS spectra of ITFA-derived spectral components of component/species 1 and 2 (black lines) in comparison to selected references (colored lines).

REFERENCES

[1] Myneni, S.C.B. et al. (1997) *Science* **278**, 1106-1109.
[2] Rossberg, A. et al. (2003) *Anal. Bioanal. Chem.* **376**, 631-638.

Carbonate effects on surface speciation of uranyl at the ferrihydrite-water interface: Application of factor analysis on EXAFS spectra.

A. Rossberg, S. Tsushima, A.C. Scheinost, K.-U. Ulrich

The mobility of U(VI) in aqueous environments is commonly controlled by the formation of aqueous U(VI)-carbonato species and by sorption on mineral surfaces, both processes competing with each other in the above-neutral pH range. Here we employ factor analysis of EXAFS spectra [1] to determine the number of the structurally different U(VI) species and their relative concentration as a function of pH and $pCO_{2(g)}$.

EXPERIMENTAL. We prepared solutions of a) 1 mM $Fe(NO_3)_3 \cdot 9H_2O$ with 12 µM $UO_2(NO_3)_2 \cdot 6H_2O$ and 15 mM $NaNO_3$ and b) 1 mM $FeCl_3 \cdot 6H_2O$ with 12 µM UO_2Cl_2 and 15 mM NaCl in i) CO_2-free atmosphere, ii) in equilibrium with air ($[CO_2]$ = 0.038 vol. %) and iii) in atmosphere with increased $[CO_2]$ = 1.0 vol. %. The precipitation of ferrihydrite and sorption of U(VI) were controlled by using 0.1 or 1 M NaOH. The final pH was adjusted to 5.5, 7.0, or 8.0. After centrifugation the wet pastes were frozen in liquid N_2 to avoid sample alteration. In addition the aqueous $UO_2(CO_3)_3^{4-}$ complex was prepared at pH 11 using solutions with 50 mM U(VI) and 1 mM Na_2CO_3. The fluorescent U L_{III} EXAFS of the sorption samples was measured at 30 K using a closed cycle He-cryostat. The $UO_2(CO_3)_3^{4-}$ complex was measured at room temperature in transmission mode.

RESULTS. Figure 1 shows the raw U L_{III} k^3-weighted EXAFS spectra and their corresponding Fourier transforms. All spectra are closely matched by abstract reproductions based on two components. Furthermore, the indicator function [1] shows a minimum at two components, hence the spectra can be considered as representing only two structurally different uranyl species. By using the VARIMAX procedure the qualitative concentration distribution of the two components were calculated (Fig. 2, top). According to the VARIMAX result component 1 is attributed to the spectrum at pH 8.0 with $[CO_2]$ = 0 vol. % and component 2 is the $UO_2(CO_3)_3^{4-}$ complex at pH 11. The relative concentration distribution of components 1 and 2 are calculated using the iterative target test (Fig. 2, bottom). According to the VARIMAX result we fixed the relative concentration of spectrum 1 (component 1) and spectrum 9 (component 2) to 100 %. The error in the rel. concentrations can be estimated using the spectra 1-3. For these samples the content of $UO_2(CO_3)_3^{4-}$ has to be zero because they were prepared in the absence of carbonate. The arrow in Fig. 2 (bottom) is hence an indicator of the maximum error (8 %) in the relative concentrations of the components.

The structure of the inner-sphere sorption complex (component 1) was determined using MCTFA [2]. In this sorption complex U(VI) coordinates in a bidentate arrangement to the edge of an $Fe(O,OH)_6$ octahedron. The spectra of component 2, representing the aqueous $UO_2(CO_3)_3^{4-}$ complex, reveals no contribution from Fe backscattering, hence remains as an outer-sphere complex at the ferrihydrite surface.

CONCLUSIONS. At atmospheric conditions ($[CO_2]$ = 0.038 vol. %) and in the pH range from 5.5 to 7.9, inner-sphere surface complexation to $Fe(O,OH)_6$ octahedra is complemented by a small amount (15 ± 8%) of outer-sphere uranyl-carbonato surface species. Only if $[CO_2]$ is increased to 1.0 vol. %, formation of uranyl-carbonato complexes becomes more important or even predominant, in contrast to the results by Bargar et al. [3]. The formation of these outer-sphere carbonato complexes maintains uranyl sorption to ferrihydrite even at above-neutral pH and at elevated CO_2-concentration typical for aqueous environments with enhanced microbial activity.

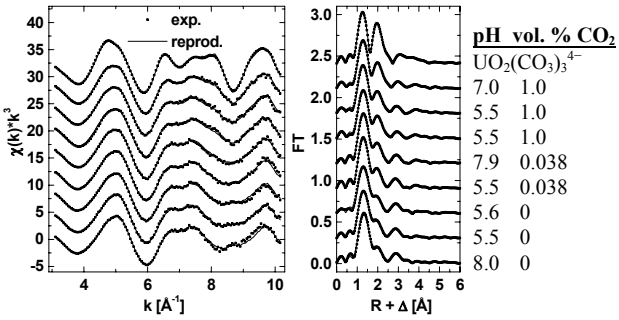

Fig. 1: U L_{III} EXAFS spectra and their abstract reproductions using two components. # Ferrihydrite precipitate was equilibrated with $CO_{2(g)}$ before U(VI) was added.

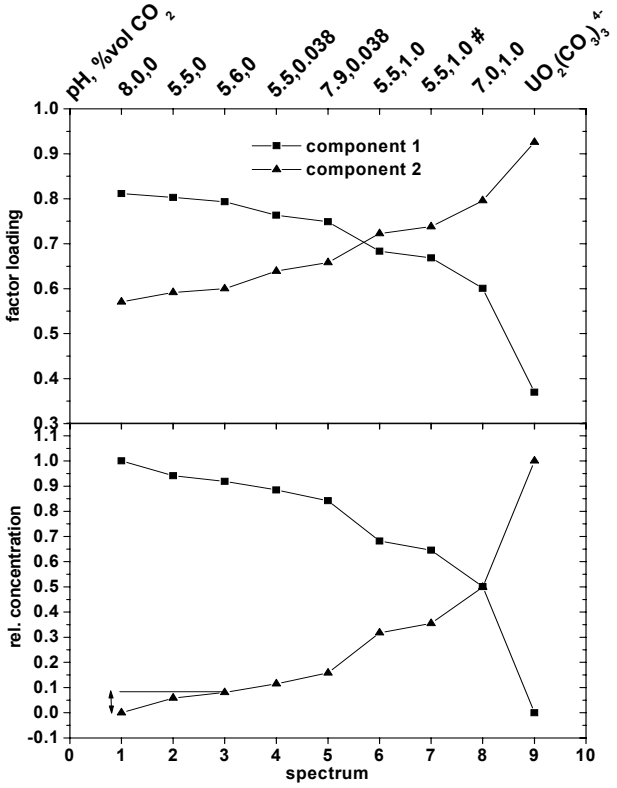

Fig. 2: Component distribution calculated by VARIMAX procedure (top), rel. concentrations of the components calculated by iterative target test. # Ferrihydrite precipitate was equilibrated with $CO_{2(g)}$ before U(VI) was added. Arrow – see text.

REFERENCES

[1] Rossberg, A. et al. (2003) *Anal. Bioanal. Chem.* **376**, 631-638.
[2] Ulrich, K.-U. et al. (2006) *Geochim. Cosmochim. Acta* **70**, 5469-5487.
[3] Bargar, J. R. et al. (2000) *Geochim. Cosmochim. Acta* **64**, 2737-2749.

Particle size and particle size distribution of chitosan / $[Ti_2W_{10}PO_{40}]^{7-}$ associates

H. Zänker, W. Richter, T. Meißner[1], H. Stephan[1]
[1]Institute of Radiopharmacy, FZD, Dresden, Germany

Associates of the cluster anion $[Ti_2W_{10}PO_{40}]^{7-}$ with chitosan were studied by three different methods of particle size determination. The associates proved to be nanoparticles of a size range of about $5 \cdot 10^1$ to $5 \cdot 10^2$ nm.

In the past decade, polyoxomethalates (POMs) based on V(V), Mo(VI) and W(VI) were found to be attractive candidates for medical applications. Such polynuclear metal compounds show unique transport properties and abilities to get into cells and may act as antiviral and antitumoral agents. Our efforts are aimed at the deposition of sufficiently high transition metal concentrations in target cells as the prerequisite for applying Photon Activation Therapy, a way of cancer treatment [1]. Here we report on the preparation and colloid-chemical characterization of associates formed by the biopolymer chitosan and the Keggin type cluster anion $[Ti_2W_{10}PO_{40}]^{7-}$. The colloid-chemistry of the associates is crucial for their transport behavior. Photon correlation spectroscopy (PCS), filtration, centrifugation and scanning electron microscopy (SEM) were employed for the colloid-chemical characterization.

EXPERIMENTAL. The experiments were carried out on the following solutions:
Solution A: 50 mg/L chitosan + $1 \cdot 10^{-4}$ M POM, diluted with water by a factor of 10,
Solution B: 50 mg/L chitosan + $1.25 \cdot 10^{-5}$ M POM and,
Solution C: 100 mg/L chitosan + $2.5 \cdot 10^{-5}$ M POM.
There is an excess of POM in solution A. Solution B and C have an excess of chitosan. The concentration of the associates in solution C was twice as high as in solution B.

RESULTS. Filtration experiments on the solutions suggested that all particles were smaller than 1 µm. SEM micrographs of the deposits on 100 nm filters showed particles of a size of less than 100 nm (cf. [1]). Figure 1 gives the PCS particle size distribution of solution A as calculated from the autocorrelation function by the CONTIN deconvolution method. Figure 1a shows the light-intensity weighted particle size distribution which is the primary information of PCS. Note that such distributions are strongly biased towards large particles due to the strong dependence of scattered light intensity on particle radius [2,3]. Therefore, the right peak in Fig. 1a, even though being the highest peak in the diagram, represents only a minor fraction of the total particle concentration. This can be seen from Fig. 1b which gives an estimation of the mass weighted particle size distribution as derived from the light-intensity weighted distribution using the Brookhaven BI-90 routine software and assuming that all particles have the same particle density. Furthermore, centrifugation experiments were performed to analyze the particle size. Two preparative centrifuges were used as "analytical" centrifuges as described in [4]. The maximum conceivable hydrodynamic diameters of the chitosan-$[Ti_2W_{10}PO_{40}]$ associates still present in the supernatant after one-hour centrifugations at different angular speed were calculated. The particle size distribution of the chitosan-$[Ti_2W_{10}PO_{40}]$ associate diameters in solutions A, B and C resulting from these calculations for the different centrifugal accelerations according to [4] is given in Tab. 1 (for details see [1]). As one can see from this table, similar size distributions of the particles have been found in the diluted solutions A and B, i.e. 70 – 90 % of the particles are smaller than 100 nm which is in agreement with the PCS results given in Fig. 1b. In solutions of higher concentrations (solution C) the particle size increases - the majority of the particles is then larger than 100 nm (aggregation).

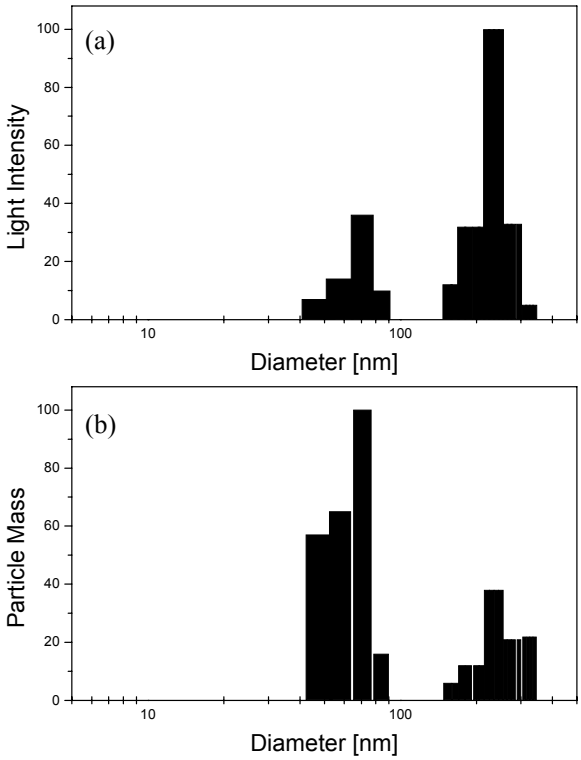

Fig. 1: Light-intensity (a) and mass (b) weighted particle size distribution as obtained by PCS.

Tab. 1: Estimated particle size distribution according to centrifugation experiments.

Particle size class [nm]	Frequency (w.t. %) Solution A	Solution B	Solution C
> 350	1	–	28
100 – 350	28	10	41
50 – 100	26	50	22
< 50	45	40	9

CONCLUSIONS. It can be concluded that three methods of particle size determination based on three different physical principles (SEM, PCS and centrifugation) consistently provide a particle size range of about $5 \cdot 10^1$ to $5 \cdot 10^2$ nm for the chitosan-$[Ti_2W_{10}PO_{40}]$ associates. This is within the size range desirable for medical application.

REFERENCES

[1] Meißner, T. et al. (2006) *Transition Metal Chem.* **31**, 603-610.
[2] Schurtenberger, P. et al. (1993) *Environmental Particles Vol. 2*, Boca Raton, p. 37.
[3] Plaschke, M. et al. (2001) *Anal. Chem.* **73**, 4338-4347.
[4] Zänker, H. et al. (2004) *Report FZR-400*, p. 48.

EXAFS studies of Zn–Al and Ni–Al Layered Double Hydroxides

H. Funke, A.C. Scheinost, M. Chukalina[1], A. Voegelin[2]

[1]Institute of Microelectronics Technology RAS, Chernogolovka, Russia; [2]Institute of Terrestrial Ecology, Swiss Federal Institute of Technology (ETH) Zurich, Switzerland

LDH phases containing Zn, Ni or both 3d-metals show an unexpected variation in solubility. By studying the short-range structure of these phases by low-temperature EXAFS spectroscopy supplemented by wavelet analysis, we are able to exclude structural causes for this solubility variation.

Layered Double Hydroxides (LDH) are a group of minerals (hydrotalcites) and synthetic solids. They consist of layers of edge-sharing metal hydroxide octahedra hosting divalent metal cations like, Ni^{2+}, Zn^{2+}, Co^{2+} and Cr^{2+}. In up to ⅓ of the cationic centers, the divalent cations are replaced by Al^{3+} [1,2].
The resulting net positive charge of the hydroxide sheets is counterbalanced by hydrated anions in the aqueous interlayers, responsible for the anion exchange properties.
In comparison with simple metal hydroxides, LDH phases have a significantly lower solubility at relevant geochemical conditions. Therefore, formation of such phases plays an important role in reducing the toxicity of metals and radionuclides in e.g., soils, sediments and nuclear waste repositories [3].
Voegelin et al. examined the solubility of pure Zn and Ni LDHs as well as of mixed Zn–Ni LDH phases in column experiments under acidic conditions [4]. When only Zn was present, 95 % of the retained Zn was leached at pH 3. In contrast, only 23 % of the retained Ni was leached in experiments with Ni alone. When both Zn and Ni were present, 90 % of the retained Zn and 87 % of the retained Ni were released. EXAFS analysis performed at room temperature revealed that the LDH phases in the Zn experiment had been completely dissolved, while the LDH phase formed in the Ni experiment was still present.
The intention of our study was to investigate whether or not differences in the short-range structure are responsible for these differences in solubility.

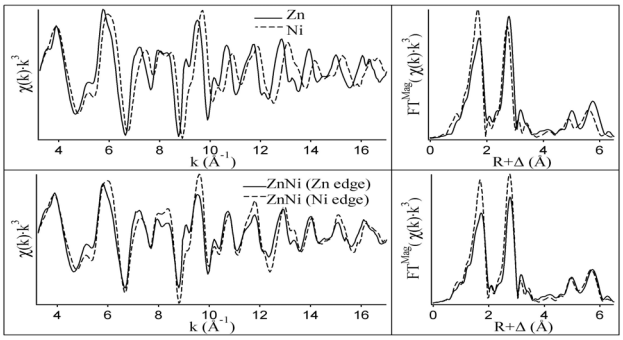

Fig. 1: EXAFS spectra and corresponding Fourier transform of the pure Zn–Al and Ni–Al LDH (above) and of the mixed ZnNi–Al LDH (below) measured at Zn–K and Ni–K edges, respectively.

EXPERIMENTAL. Three samples were prepared:
1) pure Zn^{2+} LDH with ⅓ Al^{3+} inclusion
2) pure Ni^{2+} LDH with ⅓ Al^{3+} inclusion
3) mixed LDH with ⅓ Zn^{2+}, ⅓ Ni^{2+}, ⅓ Al^{3+}
The Zn and Ni K-edge spectra were collected in transmission mode at the Rossendorf beamline at the ESRF, Grenoble, F, at 20 K using a closed-cycle He cryostat.

RESULTS. The measured EXAFS spectra had a much lower noise than previously published LDH spectra due to the reduction of the thermal components of the Debye Waller factor (Fig. 1). For the pure ZnAl and NiAl LDH the difference of metal distances is in line with the ionic radii of Zn^{2+} (0.74 Å) and Ni^{2+} (0.69 Å) (Tab. 1). For the mixed ZnNiAl LDH the coordination distances around Ni and around Zn are again in line with the respective ionic radii. The shell distances, however, are intermediate between those of pure NiAl and ZnAl LDH, suggesting an even distribution of Ni and Zn in the hydroxide layers and the absence of a significant clustering of ZnAl hydroxide or NiAl hydroxide regions (Fig. 1).
The Al backscattering atoms fitted for the first metal shell are confirmed by the Morlet wavelet method [5]. Using the refined FEFF-Morlet method [6], we could also confirm that Al atoms are present in the third metal shell (~6.2 Å), but not in the second metal shell (~5.2 Å), suggesting an even, charge-balanced distribution of Al^{3+} in the mixed-metal hydroxide layers for all investigated LDH phases.

CONCLUSIONS. All structures revealed an even distribution of 3d-metals and Al. No significant structural differences were found between the binary Ni–Al and Zn-Al LDH on one hand, and ternary Zn/Ni–Al LDH on the other hand. Hence, the differences in solubility are not caused by structural differences.

ACKNOWLEDGEMENT. This work is supported by the NATO Collaborative Linkage Grant CBP.NR,CLG 981353.

REFERENCES

[1] Bellotto, M. et al. (1996) *J. Phys. Chem.* **100**, 8527-8534.
[2] d'Espinose de la Caillerie, J.-B. et al. (1995*) J. Am. Chem. Soc*. **117**, 11471-11481.
[3] Voegelin, A. et al. (2002) *Environ. Sci. Technol.* **36**, 3749-3754.
[4] Voegelin, A. et al. (2005) *Environ. Sci. Technol.* **39**, 5311-5318.
[5] Funke, H. et al. (2005) *Phys. Rev B* **71**, 094110.
[6] Funke, H. et al. (2006) *Report FZR-443*, p. 47.

Tab. 1: EXAFS fit result of ZnAl LDH, NiAl LDH, and a mixed ZnNiAl LDH phase.

Sample	Edge	O			1st metal			1st Al			2nd metal			3rd metal + MS		
		CN	R	σ^2	CN	R	σ^2	CN	R	σ^2	CN	R	σ^2	CN	R	σ^2
Zn	Zn	6.0	2.08	0.0072	3.6	3.07	0.0048	2.8	3.06	0.0036	4.6	5.32	0.0062	12.8	6.21	0.0095
ZnNi	Zn	5.7	2.08	0.0070	3.1	3.05	0.0050	1.9	3.03	0.0023	4.9	5.30	0.0063	11.5	6.18	0.0093
ZnNi	Ni	5.7	2.05	0.0042	5.4	3.07	0.0040	3.9	3.11	0.0028	2.2	5.29	0.0027	9.4	6.15	0.0083
Ni	Ni	5.6	2.05	0.0045	1.6	3.04	0.0027	1.0	2.91	0.0020	1.9	5.23	0.0036	8.4	6.10	0.0092

TRLFS fingerprints of uranium phosphate minerals

N. Baumann, T. Arnold, A. Massanek[1]
[1]Mineralogical Collection, Geoscientific Collections, TU Bergakademie Freiberg

A thin film of a uranium mineral grows on the surface of metallic uranium which has been in contact with a Ca-phosphate solution – representing pore water concentrations of agricultural soils. This mineral was identified by Time-Resolved Laser-Induced Spectroscopy (TRLFS) as meta-autunite. However, since the fluorescence signal was very weak, we have repeated the investigations with better equipment. The sample was a disc of depleted uranium (DU) obtained from a pristine tank shell. The gained spectra were compared with fluorescence spectra from natural occurring uranium minerals (fingerprints), which could be formed under these conditions. Such minerals were provided by the Mineral Collection of the Mining Academy Freiberg, Germany.

DU is a byproduct in the production of nuclear fuel. It is used also for military purposes in projectiles for attacking armored vehicles. Concerns about the ecological consequences following the use of DU as ammunition in wars in Iraq and in the former Yugoslavia DU have received much public attention.

EXPERIMENTAL. The samples for our investigations were discs from DU with 0.5 mm in thickness and 25 mm in diameter. These discs were obtained from a pristine British military tank shell (CHARM 3 penetrator). One sample was placed in a solution containing 20 cm^3 $2.5 \cdot 10^{-3}$ M $Ca(NO_3)_2$ with $1.05 \cdot 10^{-3}$ M $(NH_4)_3PO_4$. After a contact time of 360 days the sample was taken out of the solution. TRLFS measurements were made on the surface of the sample, immediately after rinsing with deionised water and drying. TRLFS spectra for 5 different spots on the DU disc were recorded. The results were compared with measurements performed under the same conditions (first delay time, laser energy) of the natural minerals meta-autunite $Ca(UO_2)_2(PO_4)_2 \cdot 2–6H_2O$, autunite $Ca(UO_2)_2(PO_4) \cdot 10–12H_2O$ and chernikovite $(H_3O)_2(UO_2)_2(PO_4)_2 \cdot 6H_2O$. An Nd:YAG diode laser with subsequent fourth harmonic generation (wavelength 266 nm) was used for the excitation of all samples. In contrast to the measurements reported in [1], the resulting spectra were measured by a charge coupled device (CCD) camera (model 7476-0008 by Princeton Instruments), with 1024 intensified diodes. Gate width was set to 2000 ns, delay times ranged from 30 to 10030 ns in steps from 100 ns for one time-resolved spectrum. To obtain the fluorescence life times the spectroscopic data were evaluated with in-house software [2]. Generation of all graphics and the peak deconvolution of the obtained single spectra utilized the Origin v7.5 software (Origin Lab Inc.). An optical filter was used to avoid the so-called laser dispersion peak in the time resolved spectra.

RESULTS. The detected uranyl emission bands in the TRLF spectra obtained from the altered DU sample shown in Fig. 1 have a high resolution with exceptional low noise. Six distinct peaks are visible, and four of them are very sharp. To calculate the life times from the fluorescence signal a bi-exponential decay function gave the best approximation, yielding two fluorescence decay

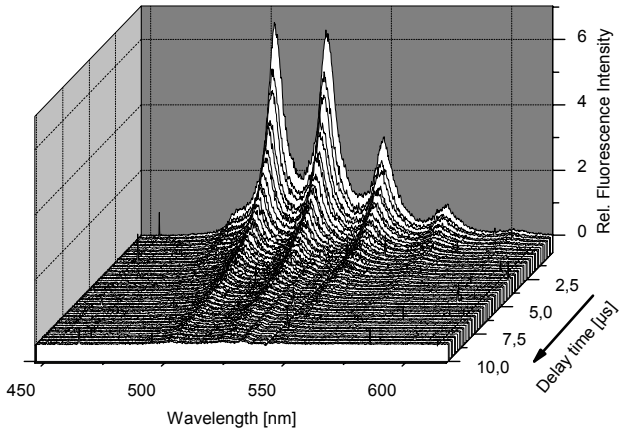

Fig. 1: Time-resolved fluorescence spectra of altered DU as a function of delay time.

times: 500 ± 90 ns and 2200 ± 300 ns. The best match for the spectra observed on the DU sample in the most intense spectra was found with the reference spectra of meta-autunite. For the comparisons of the spectra the first and therefore most intense spectra were used. This match is striking when focusing on the ratio of the peak heights from the 2nd and the 3rd peak – counted from the left side. Both peaks have almost the same size. The 2nd peak in the spectra of autunite and of chernikovite is distinctively lower than the 3rd peak. The comparison of the newly-formed unknown uranium altered phase on the DU disc with well-known uranium reference compounds clearly showed the presence of meta-autunite. These results verify the results published in [1].

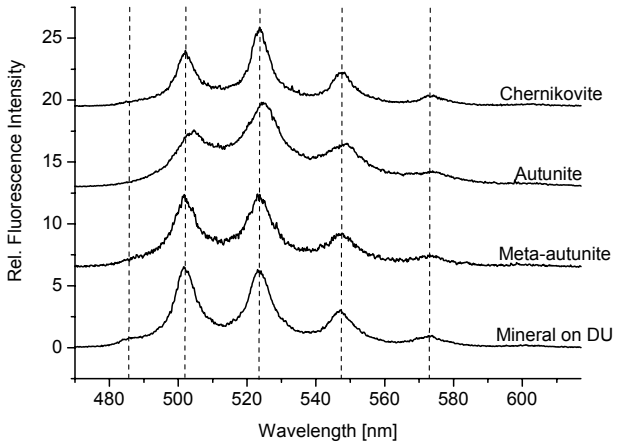

Fig. 2: Fluorescence spectra of mineral on DU, meta-autunite, autunite and chernikovite. All spectra are normalized curves and offset along the vertical axis.

ACKNOWLEDGEMENT. The DU samples were provided by David Read from Enterpris, University of Reading and University of Aberdeen, U.K.

REFERENCES

[1] Baumann, N. et al. (2006) *Sci. Total Environ.* **366**, 905-909.
[2] Brendler, V. et al. (1997) *Report FZR-180*, p. 13.

Identification of actinide molecule complexes by vibrational photothermal beam deflection spectroscopy

H. Foerstendorf, K. Heim, W. Seidel[1], G. Bernhard
[1]Institute of Radiation Physics, FZD, Dresden, Germany

Photothermal beam deflection (PTBD) spectroscopy using a free-electron laser (FEL) as a coherent pulsed pump source was applied for recording infrared spectra of actinide molecule complexes. The obtained spectra were verified by FT-IR spectroscopy. We tried to evaluate the minimum content of actinide ions which can still be detected by our setup of the PTBD experiment. It was found that the limit is obviously given by the background absorption of the KBr matrix.

Photothermal Beam Deflection (PTBD) spectroscopy in the infrared region combines the low detection limits, the surface selectivity of photothermal methods [1, 2] and vibrational spectroscopic information of the sample under investigation [3]. We present first results of model samples containing actinide molecule complexes obtained by PTBD using an FEL as a coherent pump source. The spectra are compared with those obtained by Fourier-transform Infrared (FT-IR) spectroscopy.

EXPERIMENTAL. The setup of the PTBD-FEL experiment is described elsewhere [4]. All samples were prepared as KBr pellets as typically used for FT-IR spectroscopy. PTBD absorption spectra and FT-IR transmission spectra represent the average of 128 scans for each data point and spectrum, respectively. Spectral resolution was 2 – 3 cm^{-1} for PTBD (depending on wavelength) and 4 cm^{-1} for FT-IR spectroscopy.

RESULTS. The infrared spectra of a Np(V)nitrate test sample in the spectral region (880 – 680 cm^{-1}) where the ν_3 mode of the NpO_2^+ cation can be expected are shown in Fig. 1. A comparison of the spectra demonstrates the high accuracy which can be achieved by the PTBD technique in the infrared region. In this spectral range the ν_2 and ν_4 modes of the nitrate group generally show up as well. In fact, the spectra show three partially overlapping bands at 839, 820 and 755 cm^{-1}. Today only a tentative assignment of the bands can be given. From Raman spectroscopic investigation [5] we assign the band at 820 cm^{-1} to the ν_3 mode of the NpO_2^+ cation. Consequently, the bands at 839 and 755 cm^{-1} have to be assigned to the ν_2 and ν_4 mode of the nitrate group, respectively.

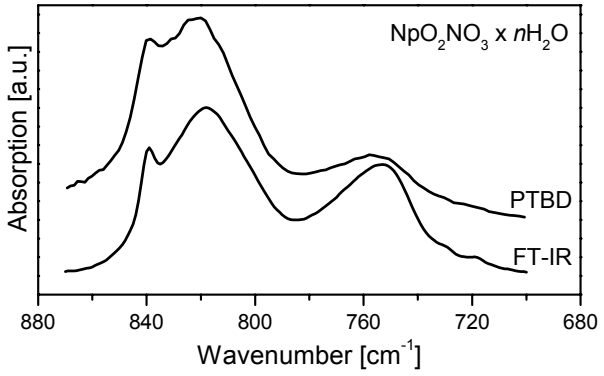

Fig. 1: Infrared spectra of the ν_3 mode region of the neptunyl(V) cation measured by PTBD (upper trace) and FT-IR (lower trace).

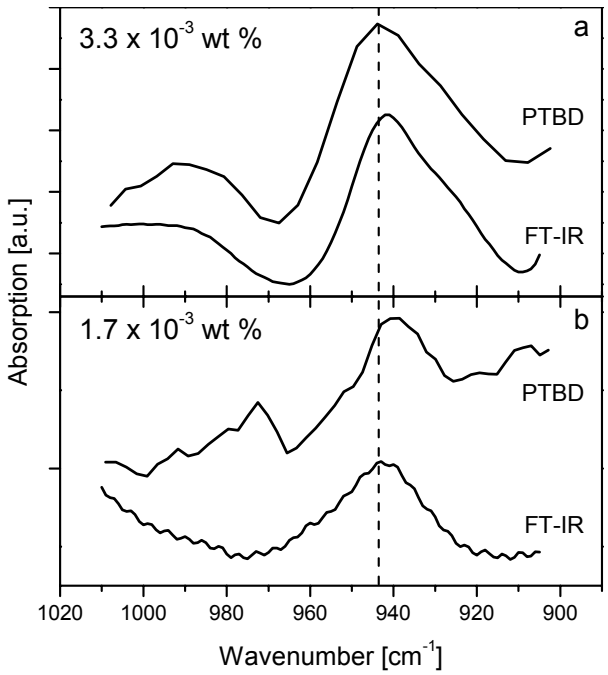

Fig. 2: PTBD (upper traces) and FT-IR (lower traces) spectra of the ν_3 mode region of the uranyl(VI) cation at different concentrations of $UO_2(NO_3)_2 \cdot 6H_2O$. (a): $3.3 \cdot 10^{-3}$ wt % (~150 µM); (b): $1.7 \cdot 10^{-3}$ wt % (~75 µM).

Figure 2 presents the spectra of the KBr pellets containing the lowest concentrations of $UO_2(NO_3)_2 \cdot 6H_2O$ which provide a clear vibrational UO_2^{2+} band obtained by PTBD and FT-IR spectroscopy. Again the high accuracy of the spectra demonstrates the applicability of the PTBD technique to identify actinide molecule complexes in solid samples. Although it has been shown that photothermal spectroscopy is capable of measuring absorptions below 10^{-6} [1] the dynamic reserve of the PTBD technique in our FEL experiment is in the same order of magnitude as for FT-IR spectroscopy since no well-defined absorption bands of the ν_3 uranyl mode were observed at lower concentrations (data not shown). The limitations are obviously set by residual water and other possible impurities of the KBr matrix which result in a background absorption over the whole spectral range. Therefore, the KBr matrix turned out to be inappropriate to elucidate accurately the detection limit of the PTBD technique in the infrared region of light. However, the quantity of the actinide and the dimension of the sample necessary for generating a significant deflection signal is considerably reduced by a factor of approximately 250 in the PTBD experiment due to its geometrical setup. The generation of the thermal wave and of the deflection signal occurs next to the surface of the sample. This potentially provides access to investigations of natural mineral surfaces.

REFERENCES

[1] Harris, T.D. et al. (1985) *Appl. Spectrosc.* **39**, 28-32.
[2] Commandré, M. et al. (1996) *Appl. Optics* **35**, 5021-5034.
[3] Seidel, W. et al. (2004) *Eur. Phys. J.-Appl. Phys.* **25**, 39-43.
[4] Foerstendorf, H. et al. (2007) *J. Nucl. Mater.* (in press).
[5] Gregoire-Kappenstein, A.C. et al. (2003) *Radiochim. Acta* **91**, 665-672.

Double-electron excitation in X-ray absorption spectra of actinides

C. Hennig

Double-electron excitation in L_3 edge X-ray absorption spectra of actinides has been observed for the first time. The double-electron excitation has been identified as a $L_3N_{6,7}$ shake up effect [1].

Inner-shell photoexcitation is often accompanied by the excitation of secondary electrons with lower binding energies. These electrons can be excited into unoccupied states (shake up) or ejected into the continuum (shake off). Such processes are revealed as satellite lines in X-ray fluorescence and photoelectron spectra. Multielectron resonances have been observed in the absorption spectra of noble gases [2], liquids [3], solids [4] and metal vapor [5]. Up to now it has not been investigated whether the actinides show also multielectron excitations. The low vapor pressure and radioprotection aspects prevent investigations in the gas phase. In the last decade, several EXAFS data of actinides in aqueous solution have been published with the aim to reveal their near-order structure. A part of these spectra were reinvestigated with regard to multielectron features.

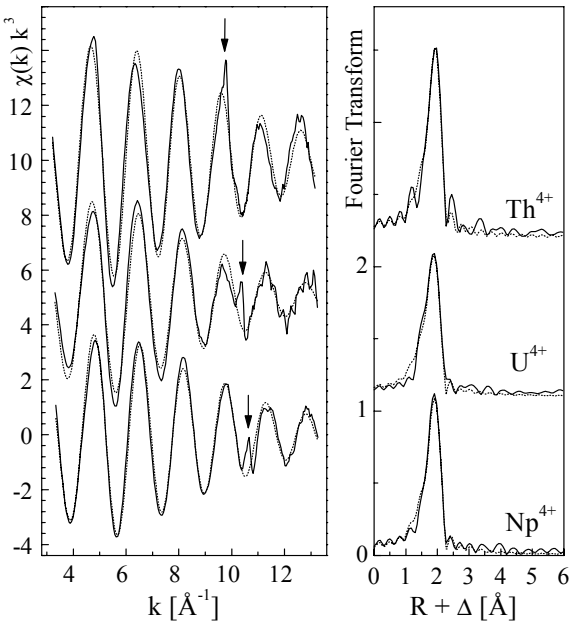

Fig. 1: L_3-edge k^3 weighted EXAFS data (left) of Th^{4+}, U^{4+}, Np^{4+} and their corresponding Fourier transforms (right). The arrow indicates the double-electron excitation.

The L_3-edge k^3 EXAFS spectra of Th^{4+}, U^{4+} and Np^{4+} hydrates in aqueous solution are shown in Fig. 1. The signal is formed by a single-frequency sinusoidal oscillation. In the k range 9.8 – 11.2 $Å^{-1}$ small anomalous features appear superimposed to the main oscillations. These features are indicated individually by arrows. Their position appears shifted to higher k values with increasing atomic number Z. All features show a relative sharp maximum. Sharp, resonance-like absorption features appear if the core electron excitation is accompanied by a shake up of the second electron to a bound state. In contrast, the cross section appears gradually increased with increasing photon energy, if both electrons are excited to the continuum. Therefore, the sharp features in Fig. 1 originate from a shake up process. In order to assign the experimental features to a specific electron excitation channel with the energy E_S, the difference between the energy of the anomalous maximum E_f and the energy of the absorption edge threshold, E_0, was estimated. The relaxation of an atom due to core-hole creation is usually described in the frame of the $Z+1$ approximation. Evidence was found between E_S and the $Z+1$ $4f_{5/2}$ and $4f_{7/2}$ energy level. E_S and related $Z+1$ energies, taken from reference [6], are shown in Fig. 2. The E_S values for Pu^{3+} and Am^{3+} were taken from reference [1]. There is actual no experimental value available for Pa, Z = 91. The comparison allows to assign the spectral feature to an excitation of a core $2p_{3/2}$ electron accompanied by the autoionization of a $4f$ electron. This process creates a $[2p_{3/2}4f_{5/2}/4f_{7/2}]$ double hole configuration, or, in the edge terminology, a $L_3N_{6,7}$ resonance. The shake up of one of the 14 $4f$ electrons to the lowest unoccupied MO results in a feature strong enough to be detectable.

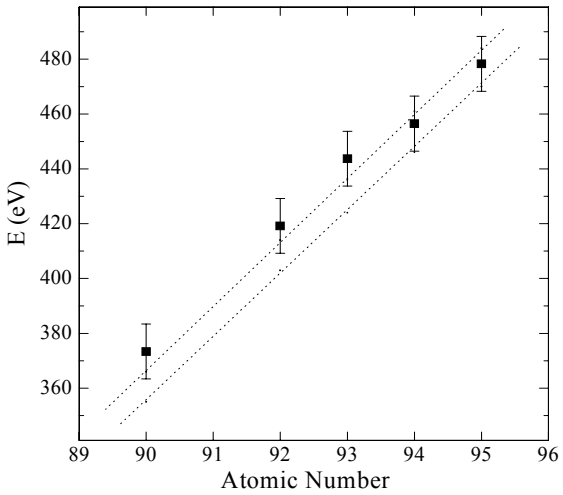

Fig. 2: Experimental energy (E_S) for the double-electron excitation (square dots) in comparison with the $Z+1$ $4f_{5/2}$ and $4f_{7/2}$ energy (dotted line). The error bars represent absolute errors, while the relative errors are in the dimension of the data points.

The double-excitation affects the EXAFS signal and can influence the data analysis. An excitation of a second electron reduces the transition probability in the main scattering path and opens a new one. This may affect especially the integral scattering amplitude for $E \geq E_f$. Therefore, the coordination numbers N_{ij}, extracted from the amplitude function, are expected to be influenced. In contrast, there is no correlation of the double-electron excitation to the origin of the wave vector $E_{k=0}$. Therefore, the influence on R, which is extracted from the scattering phase contribution, is not expected to be significant. A second effect may occur in the data extraction process. The atomic background signal $\mu_0(E)$ is usually approximated by a spline function. Deviations between $\mu_0(E)$ and the spline function, affected from a double-electron excitation, may lead to artificial peaks at $R \leq 1.2$ Å.

REFERENCES

[1] Hennig, C. (2007) *Phys. Rev. B* (in press).
[2] Deutsch, M. et al. (1992) Phys. Rev. A 45, 2112-2115.
[3] D'Angelo, P. et al. (2004) J. *Phys. Chem. B* **108**, 11857-11865.
[4] Filipponi, A. et al. (1988) *Phys. Rev. B* **38**, 3298-3304.
[5] Padežnik Gomilšek, J. et al. (2003) *Phys. Rev. A* **68**, 042505.
[6] Porter F.T. et al. (1978) *J. Phys. Chem. Ref. Data* **7**, 1267-1284.

THEREDA – Development of a thermodynamic reference database for performance assessment of waste disposal sites

A. Richter, V. Brendler, S. Hagemann[1], H. Moog[1], V. Neck[2], C. Marquardt[2], W. Voigt[3]

[1]Gesellschaft für Anlagen- und Reaktorsicherheit mbH, Braunschweig, Germany; [2]Institute for Nuclear Waste Disposal, Forschungszentrum Karlsruhe, Karlsruhe, Germany; [3]Institute for Inorganic Chemistry, TU Bergakademie Freiberg, Freiberg, Germany

A new cooperative project was started which aims at the development of a consistent and quality secured thermodynamic reference database for all safety relevant elements and for the relevant temperature and pressure range. This database THEREDA is due to fulfill the specific German quality requirements for modeling geochemical processes in waste disposal sites.

Reliable predictions of the migration of toxic impurities in the biosphere are of particular importance to assure the security of a waste disposal site. There, site-independent thermodynamic data for speciation and solubility calculations are significant input data of the respective codes. At present, the data are restricted in their implementation due to incomplete coverage of main and trace elements, inconsistency of considered species and respective formation constants, limitations concerning the solution composition and limited variation ranges of intensive parameters (temperature, pressure, density). The requirement for comparable and traceable results of geochemical model calculations is a consistent and bindingly used standard database. Until now, such a specific database for the application in waste repository and remediation projects of Germany does not exist. Hence, a joint venture of qualified institutions was initiated and started. The goal of this project is the development of a consistent, quality assured thermodynamic reference database that is applicable for performance assessment studies for existing or potential underground waste disposal sites which fulfills the specifically German quality requirements.

THE THEREDA-PROJECT. The project THEREDA – **The**rmodynamic **Re**ference **Da**tabase – aims at making long-time performance assessment trustier, more comparably and more comprehensibly.
The work will be done jointly by the members of the "Working Group Thermodynamic Reference Database", including besides the Institute of Radiochemistry, the Gesellschaft für Anlagen- und Reaktorsicherheit Braunschweig (GRS), the Forschungszentrum Karlsruhe, Institute for Nuclear Waste Disposal (FZK-INE), TU Bergakademie Freiberg, Institute for Anorganic Chemistry (TU-BAF), and Colenco Power Engineering, Baden (Switzerland).
Main parameters of the database are:
– Data relating to chemical elements (most stable modification in standard state, formation enthalpy, function of heat capacity)
– Stoichiometry factors / reaction equations
– Reaction data including phase transitions
– Parameters of ion interaction models (Pitzer, SIT)
– If available: confidence interval and validity limits

As secondary information will be gathered inter alia:
– Bibliographical information of the original references
– Quality criteria for data evaluation.

Error estimations and propagations will be made possible by comprehensive documentation of basis species and interpretation algorithms. These are essentially for uncertainty and sensitivity analyses. Support and upgrading of the database will be provided and facilitated by a panel of experts beyond the duration of the project.
A website (www.thereda.de) will be created parallel to the database development. This homepage enables potential users the access to the database via commonly available web-browsers and provides a platform for information and discussion regarding the database.
Figure 1 demonstrates the database schema with the access possibilities.

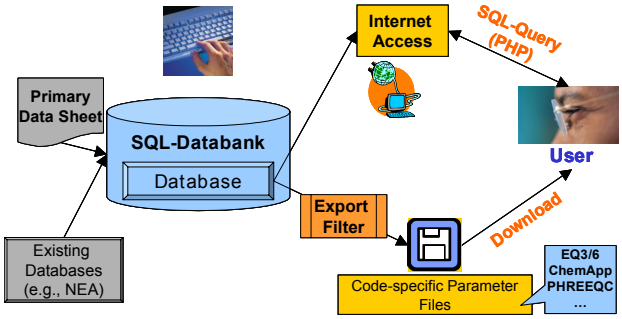

Fig. 1: Scheme of the database with access possibilities.

The Institute of Radiochemistry will contribute to the following work packages:
– Binding guidelines for data analysis and evaluation (e.g. extrapolation of literature data to zero ionic strength and standard temperature, quantitative and qualitative specification of data rating, consistency tests, validations)
– Safe-guarding of uniformity and retraceability to enable a uniform utilization of the gathered data: design and development of filters for the code PHREEQPITZ
– Accomplishment of consistency tests
– Gathering, analysis and critical selection of data for the systems uranium, radium, arsenic and iron (particularly oxidation state III)
– Transfer of the data in ASCII-files for the subsequent upload in the database
– Creation, test, support and adaptation of the database interface
– Support of the THEREDA-intranet
– Identification of critical data gaps
– Preparation of the future integration of the sorption databases RES^{3}T/ISDA in the reference database.

ACKNOWLEDGEMENT. Financial support by the BMWi (contract No. 02E10136), the BMBF (contract No. 02C1436) and the GRS (contract No. VA3252-AN550550-UA2671), which is gratefully acknowledged.

Gap Scan – A new software tool for infrared spectroscopic applications at the FELBE facility

K. Heim, R. Jainsch[1], K.-W. Leege[1], H. Foerstendorf
[1]Department of Research Technology, FZD, Dresden, Germany

A software tool was developed which provides full automatic acquisition of continuous wavelength scans by varying the gap of the undulator of the free electron laser (FEL). This was realized by a routine connecting the ELBE software control system and a data acquisition system of an FEL user laboratory.

The undulator U27 of the FEL of the electron linear accelerator with high brilliance and low emittance (FELBE) is a source of pulsed, coherent light which is continuously tunable over the infrared wavelength range from 4 to 20 µm [1]. The wavelength adjustment is done by varying the ELBE electron beam energy, as well as the gap and distance length (i.e. the phase) of the undulator via five separately controllable motor gears [2].
For spectroscopic applications a software tool named GapScan was embedded at the ELBE software control system which is based on a SIMATIC™ S7 system and on a WinCC™-Userinterface [3]. This tool provides scanning of the FEL wavelength within a user defined wavelength range by setting the start and end values and the step width of the undulator's gap drive (Fig. 1). The emitted FEL wavelength has to be verified by a calibration for each parameter set of the accelerator at distinct gap positions of the undulator. The wavelength range which can be scanned without changing the energy of the electron beam can span up to 3.5 µm and spectral resolution up to approximately 0.5 cm^{-1} can be achieved depending on the average wavelength and line width.
For data acquisition and pre-evaluation on the Photothermal Beam Deflection experiment [1,4] a LabView™ interface on a PC equipped with a PCI card (National Instruments) was developed (Fig. 2). The deflection and reference signal are recorded simultaneously and are displayed on the screen for visual control. For recording infrared spectra it is necessary to automate the data acquisition and alternately setting the FEL wavelength by varying the undulator's gap by GapScan.

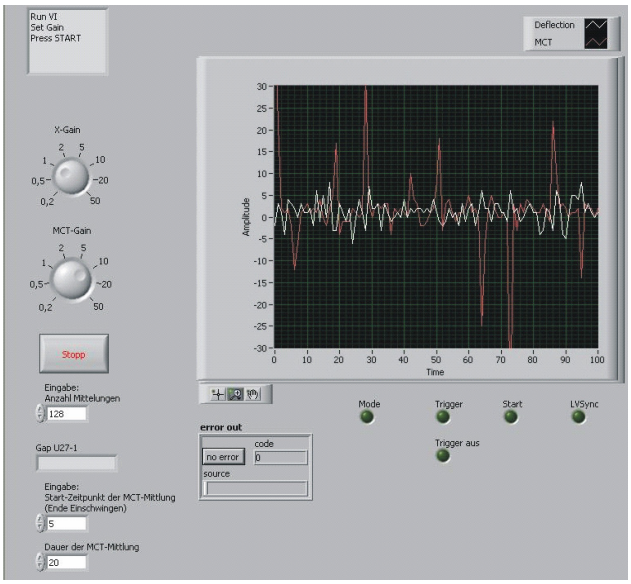

Fig. 2: LabView™ data acquisition program.

The communication and synchronization between the FEL-Control-System, based on WinCC™ and SIMATIC™ S7, and the LabView™ data acquisition system is done by network functions accessing the ELBE-OCP-TCP-Gateway [3]. Thus the acquisition of whole absorption spectra has become as time effective as possible. First results in spectroscopic actinide research were obtained using this software solution [4]. The GapScan tool including the interface FEL-Control-System is available for all users of the FELBE facility.

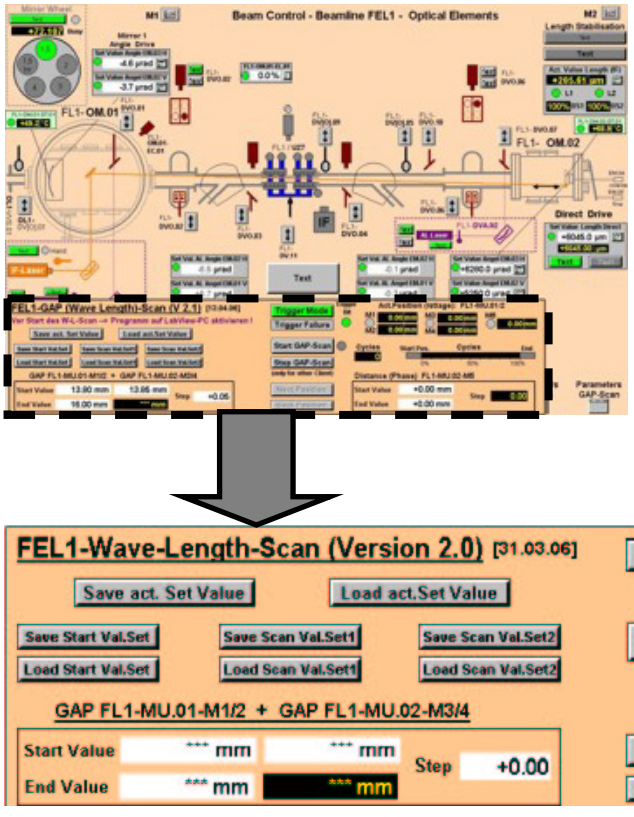

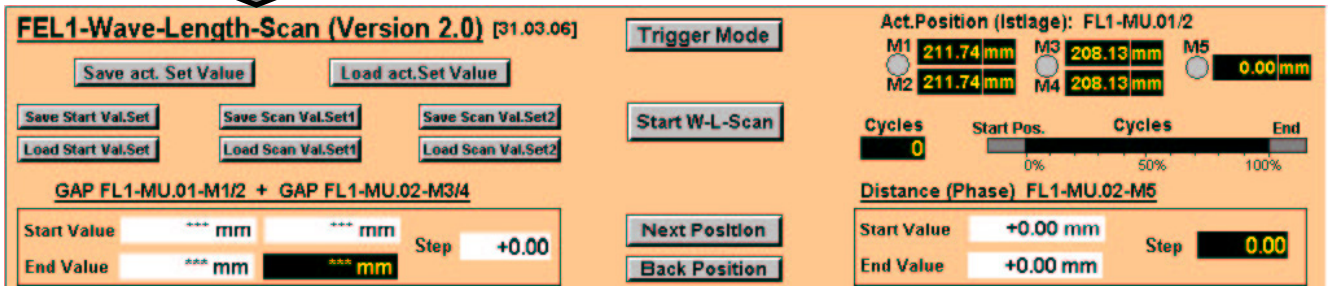

Fig. 1: WinCC™ -Userinterface of the FELBE beam control (upper panel). Display of the GapScan tool (lower panel).

REFERENCES

[1] Foerstendorf, H. et al. (2006) *Report FZR-443*. p.49.
[2] http://www.fzd.de/db/Cms?pNid=471.
[3] Wagner, A. et al. (2005) *Report FZR-428*, p.49.
[4] Foerstendorf, H. et al. this report, p. 69.

- Articles (peer-reviewed)
- Invited review
- Proceedings, reports
- Lectures, oral presentations
- Posters
- Theses
- Diploma
- Awards / Research fellowships
- Work placements

▸ Articles (peer-reviewed)

Arnold, T.; Utsunomiya, S.; Geipel, G.; Ewing, R. C.; Baumann, N.; Brendler, V.
Adsorbed U(VI) surface species on muscovite identified by laser fluorescence spectroscopy and transmission electron microscopy
Environmental Science & Technology 40, 4646-4652 (2006).

Baumann, N.; Arnold, T.; Geipel, G.; Trueman, E.R.; Black, S.; Read, D.
Detection of U(VI) on the surface of altered depleted uranium by time-resolved laser-induced fluorescence spectroscopy (TRLFS)
Science of the Total Environment 366, 905-909 (2006).

Bhatt, A. I.; Kinoshita, H.; Koster, A. L.; May, I.; Sharrad, C.; Steele, H. M.; Volkovich, V. A.; Fox, O. D.; Jones, C. J.; Lewin, B. G.; Charnock, J. M.; Hennig, C.
Actinide, lanthanide, and fission product speciation and electrochemistry in ionic melts
ACS Symposium Series 933, 219-231 (2006).

Cachia, J. N.; Deschanels, X.; Den Auwer, C.; Pinet, O.; Phalippou, J.; Hennig, C.; Scheinost, A.
Enhancing cerium and plutonium solubility by reduction in borosilicate glass
Journal of Nuclear Materials 352, 182-189 (2006).

Deschanels, X.; Picot, V.; Glorieux, B.; Jorion, F.; Peuget, S.; Roudil, D.; Jegou, C.; Broudic, V.; Cachia, J. N.; Advocat, T.; Den Auwer, C.; Fillet, C.; Coutures, J. P.; Hennig, C.; Scheinost, A.
Plutonium incorporation in phosphate and titanate ceramics for minor actinide containment
Journal of Nuclear Materials 352, 233-240 (2006).

Ender, V.; Schumann, T.; Sachs, S.; Bernhard, G.
On the uptake mechanisms of organics from natural water - Investigations with strong and weak base ion exchangers and their corresponding copolymers
PowerPlant Chemistry 8, 541-549 (2006).

Fahmy, K.; Merroun, M.; Pollmann, K.; Raff, J.; Savchuk, O.; Hennig, C.; Selenska-Pobell, S.
Secondary structure and Pd(II) coordination in S-layer proteins from *Bacillus sphaericus* studied by infrared and X-ray absorption spectroscopy
Biophysical Journal 91, 996-1007 (2006).

Geipel, G.
Some aspects of actinide speciation by laser induced spectroscopy
Coordination Chemistry Reviews 250, 844-854 (2006).

Geipel, G.; Bernhard, G.
Alkaline earth uranyl compounds – From solution to mineral phases
Geochimica et Cosmochimica Acta 70, A196 (2006).

Günther, A.; Geipel, G.; Bernhard, G.
Complex formation of U(VI) with the amino acid L-threonine and the corresponding phosphate ester O-phospho-L-threonine
Radiochimica Acta 94, 845-851 (2006).

Hennig, C.
Structure analysis of actinide compounds in solution by X-ray absorption spectroscopy
Acta Crystallographica A 62, 61 (2006).

John, J.; Filipská, H.; Cernochová, K.; Benes, P.; Geipel, G.; Kubecek, V.; Semelová, M.; Bocan, J.
New TRLFS laboratory at the CTU in Prague
Journal of Physics D 56, D565-D568 (2006).

Křepelová, A.; Sachs, S.; Bernhard, G.
Uranium(VI) sorption onto kaolinite in the presence and absence of humic acid
Radiochimica Acta 94, 825-833 (2006).

Meißner, T.; Bergmann, R.; Oswald, J.; Rode, K.; Richter, W.; Zänker, H.; Kraus, W.; Emmerling, F.; Reck, G.; Stephan, H.
Chitosan-encapsulated Keggin anion $[Ti_2W_{10}PO_{40}]^{7-}$: Synthesis, characterization and cellular uptake studies
Transition Metal Chemistry 31, 603-610 (2006).

Merroun, M.; Nedelkova, M.; Rossberg, A.; Hennig, C.; Selenska-Pobell, S.
Interaction mechanisms of bacterial strains isolated from extreme habitats with uranium
Radiochimica Acta 94, 723-729 (2006).

Moll, H.; Merroun, Mohamed L.; Hennig, C.; Rossberg, A.; Selenska-Pobell, S.; Bernhard, G.
The interaction of *Desulfovibrio äspöensis* DSM 10631^T with plutonium
Radiochimica Acta 94, 815-824 (2006).

Montavon, G.; Hennig, C.; Janvier, P.; Grambow, B.
Comparison of complexed species of Eu in alumina-bound and free polyacrylic acid. A spectroscopic study
Journal of Colloid and Interface Science 300, 482-490 (2006).

Poineau, F.; Fattahi, M.; Den Auwer, C.; Hennig, C.; Grambow, B.
Speciation of technetium and rhenium complexes by in situ XAS-electrochemistry
Radiochimica Acta 94, 283-289 (2006).

Pollmann, K.; Merroun, M.; Raff, J.; Hennig, C.; Selenska-Pobell, S.
Manufacturing and characterization of Pd-nanoparticles formed on immobilized bacterial cells
Letters in Applied Microbiology 43, 39-45 (2006).

Pollmann, K.; Raff, J.; Merroun, M.; Fahmy, K.; Selenska-Pobell, S.
Metal binding by bacteria from uranium mining waste piles and its technological applications
Biotechnology Advances 24, 58-68 (2006).

Raff, J.; Selenska-Pobell, S.
Toxic avengers
Nuclear Engineering International 51, 34-36 (2006).

Sabirova, J.; Ferrer, M.; Regenhardt, D.; Timmis, K.; Golyshin, P.
Proteomic insights into metabolic adaptations in *Alcanivorax borkumensis* induced by alkane utilization
Journal of Bacteriology 188, 3763-3773 (2006).

Scheinost, A.C.; Rossberg, A.; Vantelon, D.; Xifra, I.; Kretzschmar, R.; Leuz, A.-K.; Funke, H.; Johnson, C.A.
Quantitative antimony speciation in shooting-range soils by EXAFS spectroscopy
Geochimica et Cosmochimica Acta 70, 3299-3312 (2006).

Schmeide, K.; Reich, T.; Sachs, S.; Bernhard, G.
Plutonium(III) complexation by humic substances studied by X-ray absorption fine structure spectroscopy
Inorganica Chimica Acta 359, 237-242 (2006).

Schneiker, S.; Martins Dos Santos, V.A.P.; Bartels, D.; Bekel, T.; Brecht, M.; Buhrmester, J.; Chernikova, T.N.; Denaro, R.; Ferrer, M.; Gertler, C.; Goesmann, A.; Golyshina, O.V.; Kaminski, F.; Khachane, A.N.; Lang, S.; Linke, B.; McHardy, A.C.; Meyer, F.; Nechitaylo, T.; Pühler, A.; Regenhardt, D.; Rupp, O.; Sabirova, J.S.; Selbitschka, W.; Yakimov, M.M.; Timmis, K.N.; Vorhölter, F.-J.; Weidner, S.; Kaiser, O.; Golyshin, P.N.
Genome sequence of the ubiquitous hydrocarbon-degrading marine bacterium *Alcanivorax borkumensis*
Nature Biotechnology 24, 997-1004 (2006).

Steudtner, R.; Arnold, T.; Großmann, K.; Geipel, G.; Brendler, V.
Luminescence spectrum of uranyl(V) in 2-propanol perchlorate solution
Inorganic Chemistry Communications 9, 939-941 (2006).

Stumpf, S.; Stumpf, T.; Dardenne, K.; Hennig, C.; Foerstendorf, H.; Klenze, R.; Fanghänel, T.
Sorption of Am(III) onto 6-line-ferrihydrite and its alteration products: Investigations by EXAFS
Environmental Science & Technology 40, 3522-3528 (2006).

Ulrich, K.-U.; Paul, L.; Meybohm, A.
Response of drinking-water reservoir ecosystems to decreased acidic atmospheric deposition in SE Germany: Trends of chemical reversal
Environmental Pollution 141, 42-53 (2006).

Ulrich, K.-U.; Rossberg, A.; Foerstendorf, H.; Zänker, H.; Scheinost, A.
Molecular characterization of uranium(VI) sorption complexes on iron(III)-rich acid mine water colloids
Geochimica et Cosmochimica Acta 70, 5469-5487 (2006).

Vulpius, D.; Geipel, G.; Baraniak, L.; Bernhard, G.
Complex formation of neptunium(V) with 4-hydroxy-3-methoxybenzoic acid studied by time-resolved laser-induced fluorescence spectroscopy with ultra-short laser pulses
Spectrochimica Acta Part A 63, 603-608 (2006).

Vulpius, D.; Geipel, G.; Baraniak, L.; Rossberg, A.; Bernhard, G.
Complex formation of uranium(VI) with 4-hydroxy-3-methoxybenzoic acid and related compounds
Journal of Radioanalytical and Nuclear Chemistry 270, 661-667 (2006).

Zänker, H.; Hüttig, G.; Arnold, T.; Nitsche, H.
Formation of iron-containing colloids by the weathering of phyllite
Aquatic Geochemistry 12, 299-325 (2006).

▶ Invited review

Geipel, G.
Laser-Induced Fluorescence Spectroscopy
Handbook of Applied Solid State Spectroscopy (D.R. Vij, ed.), 577-593, Springer, New York (2006).

▶ Proceedings, reports

Baumann, N.; Brendler, V.; Arnold, T.; Geipel, G.; Bernhard, G.
Spectroscopic evidence of adsorbed U(IV) surface species onto gibbsite and quartz obtained by TRLFS
15th Radiochemical Conference, April 23-28, 2006, Mariánské Lázně, Czech Technical University in Prague, Prague, Czech Republic, 44 (2006).

Brockmann, S.; Mibus, J.; Nebelung, C.
Migration of cesium in bentonite: Influence of the pore water composition
15th Radiochemical Conference, April 23-28, 2006, Mariánské Lázně, Czech Technical University in Prague, Prague, Czech Republic, 50 (2006).

Chukalina, M.; Funke, H.
Wavelet transform usage to analyse the signals and images collected by the X-ray techniques
Proceedings of the International scientific Workshop "Modern techniques for the X-ray diffraction data analysis", May 22-25, 2006, Velikii Novgorod, Russia, 278-281 (2006).

Den Auwer, C.; Moisy, P.; Guillaumont, D.; Vidaud, C.; Funke, H.; Hennig, C.
Structural investigation of neptunium(V) in toxicological processes
Materials Research Society Symposium Proceedings 893, 315-323 (2006).

Deun, R. van; Cartuyvels, E.; Nikitenko, S.; Hennig, C.; Parac-Vogt, T. N.
EXAFS study of the phosphodiester bond cleavage by Mo-containing polyoxometallates
Acta Crystallographica A62, 206 (2006).

Deun, R. van; Hennig, C.; Cartuyvels, E.; Nikitenko, S.; Parac-Vogt, T. N.
Mo K-edge EXAFS investigation of the $[Mo_7O_{24}]^{6-}$ promoted phosphate ester hydrolysis
Acta Crystallographica A62, 206 (2006).

Ender, V.; Schumann, T.; Sachs, S.; Bernhard, G.
Untersuchungen zur Aufnahme von Organika aus natürlichen Wässern durch Ionenaustauscher mit C-14-markierten Modellsubstanzen
Proceedings VGB-Konferenz "Chemie im Kraftwerk 2006", TB 442/P11, October 11-12, 2006, Bad Neuenahr, Germany, 13 (2006).

Funke, H.; Chukalina, M.; Hennig, C.; Rossberg, A.; Scheinost, A.C.
Wavelet analysis of extended X-Ray absorption fine structure spectra
Speciation, Techniques and Facilities for Radioactive Materials at Synchrotron Light Sources (Agency, N.E., ed.), OECD, 149 (2006).

Geipel, G.
Influence of Mg, Ca, Sr and Ba on formation of geochemical relevant uranyl species
15th Radiochemical Conference, April 23-28, 2006, Mariánské Lázně, Czech Technical University in Prague, Prague, Czech Republic, 36 (2006).

Geipel, G.; Bernhard, G.
Alkaline earth uranyl compounds – From solution to mineral phases
Geochimica et Cosmochimica Acta 70, A196 (2006).

Geissler, A.; Reitz, T.; Tschikov, S.; Selenska-Pobell, S.
Influence of U(VI) and nitrate on microbial communities of uranium mining wastes
Biospektrum Sonderausgabe, Tagungsband zur VAAM-Jahrestagung 2006 (Brakhage, A., Diekert, G., Kothe, E., Straube, E., Wöstemeyer, J., eds.), Elsevier, Heidelberg, Germany, 69 (2006).

Geissler, A., Scheinost, A.C., and Selenska-Pobell, S.
Changes of bacterial community structure of a uranium mining waste pile sample induced by addition of U(IV)
Uranium in the Environment: Mining Impact and Consequences (Merkel, B.J.; Hasche-Berger, A., eds.), Springer, Berlin, 199-205 (2006).

Hennig, C.
Polarization effects at the uranium L_1 and L_3 edges – Theory and applications
Recent Advances in Actinide Science (May, I., Alvares, R., Bryan, N., eds.), RSC Publishing, Cambridge, UK, 716-718 (2006).

Hennig, C., Tutschku, J., Rossberg, A., Scheinost, A.C., Bernhard, G.
In situ speciation of actinides in solution with a newly developed spectro-electrochemical cell
Speciation, Techniques and Facilities for Radioactive Materials at Synchrotron Light Sources (Agency, N.E., ed.), OECD, 43-46 (2006).

Hübener, S.; Eichler, B.; Taut, S.
Thermochromatographic adsorption studies of curium and berkelium
Recent Advances in Actinide Science (May, I., Alvares, R., Bryan, N., eds.), RSC Publishing, Cambridge, UK, 287-289 (2006).

Křepelová, A.; Sachs, S.; Reich, T.; Roßberg, A.; Baumann, N.; Bernhard, G.
Influence of humic acid on U(VI) sorption onto kaolinite studied by TRLFS and EXAFS
15th Radiochemical Conference, April 23-28, 2006, Mariánské Lázně, Czech Technical University in Prague, Prague, Czech Republic, 45 (2006).

Křepelová, A.; Sachs, S.; Reich, T.; Roßberg, A.; Brendler, V.; Baumann, N.; Bernhard, G.
Influence of humic acid on U(VI) sorption onto kaolinite: Studies using extended X-ray absorption fine structure measurements and time-resolved laser-induced fluorescence spectroscopy
Humic Substances – Linking structure to functions, Proceedings of the 13th Meeting of the International Humic Substances Society (Frimmel, F.H.; Abbt-Braun, G., eds.), Karlsruhe, Germany, 733-736 (2006).

Merroun, M.; Nedelkova, M.; Rossberg, A.; Hennig, C.; Scheinost, A.C., Selenska-Pobell, S.
Interaction mechanism of uranium with bacterial strains isolated from extreme habitats
Recent Advances in Actinide Science (May, I., Alvares, R., Bryan, N., eds.), RSC Publishing, Cambridge, UK, 47-49 (2006).

Merroun, M., Rossberg, A., Hennig, C., Scheinost, A.C., Selenska-Pobell, S.
Structure and size of gold nanoparticles formed on cells and S-layers of *Bacillus sphaericus* JG-A12
Biospektrum Sonderausgabe, Tagungsband zur VAAM-Jahrestagung 2006 (Brakhage, A., Diekert, G., Kothe, E., Straube, E., Wöstemeyer, J., eds.), Elsevier, Heidelberg, Germany, 103 (2006).

Mibus, J.; Brendler, V.; Pfingsten, W.
Migration of uranium(VI) in a phosphate environment: Column experiments and modeling
15th Radiochemical Conference, April 23-28, 2006, Mariánské Lázně, Czech Technical University in Prague, Prague, Czech Republic, 238 (2006).

Mibus, J.; Sachs, S.; Křepelová, A.
Diffusion of humic acid in compacted clay
Bridging Clays, French Clay Group and The Clay Minerals Society, June, 03-07, 2006, Ile d'Oléron, France (2006).

Moll, H.; Bernhard, G.
Complex formation of curium(III) with the amino acids L2-aminobutyric acid and L-threonine and the corresponding phosphate ester O-phospho-L-threonine
15th Radiochemical Conference, April 23-28, 2006, Mariánské Lázně, Czech Technical University in Prague, Prague, Czech Republic, 223 (2006).

Nebelung, C.; Baraniak, L.
Uranium sorption and solubility under conditions relevant for the radioactive waste repository in Morsleben / Germany
Recent Advances in Actinide Science (May, I., Alvares, R., Bryan, N., eds.), RSC Publishing, Cambridge, UK, 110-112 (2006).

Nebelung, C.; Brendler, V.; Brockmann, S.; Mibus, J.
Uranium and cesium sorption on montmorillonite and bentonite
1st European Chemistry Congress, August 27-31, 2006, Budapest, Hungary, Abstract Book, 397 (2006).

Opel, K.; Hübener, S.; Weiß, S.; Zänker, H.; Bernhard, G.
Solubility studies of uranium by laser-induced breakdown detection (LIBD)
Recent Advances in Actinide Science (May, I., Alvares, R., Bryan, N., eds.), RSC Publishing, Cambridge, UK, 119-121 (2006).

Opel, K.; Hübener, S.; Weiß, S.; Zänker, H.; Bernhard, G.
Untersuchungen zur Löslichkeit verschiedener Urandioxidmodifikationen mittels LIBD und anderer spektroskopischer Methoden
72. Jahrestagung der Wasserchemischen Gesellschaft in der GDCh, May 22-24, 2006, Celle, Germany, 108-112 (2006).

Pollmann. K., Merroun, M., Herrmannsdörfer, T., Raff, J., Fahmy, K., Hennig, C., Selenska-Pobell, S.
Bacterial surface layers (S-layers) as biological templates for the synthesis of metal nanoparticles
Biospektrum Sonderausgabe, Tagungsband zur VAAM-Jahrestagung 2006 (Brakhage, A., Diekert, G., Kothe, E., Straube, E., Wöstemeyer, J., eds.), Elsevier, Heidelberg, Germany, 103 (2006).

Raff, J.; Berger, S.; Selenska-Pobell, S.
Uranium binding by cells and S-layers of *Bacillus* isolates recovered from uranium mining waste pile
Biospektrum Sonderausgabe, Tagungsband zur VAAM-Jahrestagung 2006 (Brakhage, A., Diekert, G., Kothe, E., Straube, E., Wöstemeyer, J., eds.), Elsevier, Heidelberg, Germany, 153 (2006).

Richter, A.; Brendler, V.
Sparse and uncertain SCM parameter sets – What are the consequences?
Abstr. Pap. Am. Chem. Soc. 231, 99-GEOC (2006).

Rossberg, A.; Scheinost, A
Actinide speciation based on EXAFS spectroscopy: From shell fitting to MCTFA
Speciation, Techniques and Facilities for Radioactive Materials at Synchrotron Light Sources (Agency, N.E., ed.), OECD, 134-135 (2006).

Sachs, S.; Bernhard, G.
Uranium(VI) adsorption onto synthetic humic substance-kaolinite sorbates
15th Radiochemical Conference, April 23-28, 2006, Mariánské Lázně, Czech Technical University in Prague, Prague, Czech Republic, 46 (2006).

Sachs, S.; Křepelová, A.; Schmeide, K.; Koban, A.; Günther, A.; Mibus, J.; Brendler, V.; Geipel, G.; Bernhard, G.
Joint project: Migration of actinides in the system clay, humic substance, aquifer – Migration behavior of actinides (uranium, neptunium) in clays: Characterization and quantification of the influence of humic substances
Final Report, BMWi Project No. 02 E 9673, FZD, Dresden, Germany (2006).

Sachs, S.; Mibus, J.
Migration behavior of humic acids in compacted clay and its influence on the uranium transport
Humic Substances – Linking structure to functions, Proceedings of the 13th Meeting of the International Humic Substances Society (Frimmel, F.H.; Abbt-Braun, G., eds.), Karlsruhe, Germany, 713-716 (2006).

Schabelnikova, S.; Funke, H.; Chukalina, M.
EXAFS spectra analysis: the mother wavelet choice
Proceedings of the International Science-Technical Conference "Fundamental problems of radioelectronic instrument-making industry", October 24-28, 2006, Moscow, Russia.

Schabelnikova, S.; Funke, H.; Chukalina, M.
Wavelet analysis of the EXAFS spectra: New wavelet function as a linear combination of two Morlet wavelets
Digest Reports of the XVI International Synchrotron Radiation Conference, July 11-14, 2006, Novosibirsk, Russia.

Scheinost, A.C.
The Rossendorf Beamline at the ESRF: An XAS experimental station for actinide research
Speciation, Techniques and Facilities for Radioactive Materials at Synchrotron Light Sources (Agency, N.E., ed.), OECD, 95-101 (2006).

Scheinost, A.C.; Hennig, C.; Somogyi, A.; Martinez-Criado, G.; Knappik, R.
Geochemical behavior of uranium in mine tailings at Freital, Germany: A µ-XRF, µ-XAFS and µ-XRD study.
Geochimica et Cosmochimica Acta 70, A560 (2006).

Scheinost, A.C.; Hennig, C.; Somogyi, A.; Martinez-Criado, G.; Knappik, R.
Uranium speciation in two Freital mine tailing samples: EXAFS, micro-XRD, and micro-XRF results
Uranium in the Environment: Mining Impact and Consequences (Merkel, B.J.; Hasche-Berger, A. eds.), Springer, Berlin, 117-126 (2006).

Schumann, T.; Ender, V.; Sachs, S.; Bernhard, G.
Verwendung von C-14-markierten Modellsubstanzen zur Untersuchung der Entfernung von Organika aus Wässern durch Ionenaustauscher
"Das CO_2-abgasfreie Kraftwerk" und "Analytik hochkonzentrierter Lösungen (REA)", Zittauer Kraftwerkschemisches Kolloquium, Hochschule Zittau/Görlitz, September 26-27, 2006, Zittau, Germany.

Ulrich, K.-U.; Rossberg, A.; Scheinost, A.C., Foerstendorf, H.; Zaenker, H.; Jenk, U.
Speciation of colloid-born uranium by EXAFS and ATR-FTIR spectroscopy
Uranium in the Environment: Mining Impact and Consequences (Merkel, B.J.; Hasche-Berger, A. eds.), Springer, Berlin, 137-148 (2006).

Ulrich, K.-U.; Rossberg, A.; Scheinost, A.; Reuther, H.; Zänker, H.
Interaction of uranium(VI) and colloidal iron(III) oxyhydroxide in an abandoned uranium mine
15th Radiochemical Conference, April 23-28, 2006, Mariánské Lázně, Czech Technical University in Prague, Prague, Czech Republic, 47 (2006).

Zänker, H.; Ulrich, K.-U.; Opel, K.; Brendler, V.
Influence of colloids on uranium transport in nuclear waste repositories and abandoned uranium mines – A critical comparison
Geochimica et Cosmochimica Acta 70, A731 (2006).

Zänker, H.; Weiß, S.
Einfluss von eisenreichen Kolloiden auf das Uran(VI) in Bergwerkshalden
72. Jahrestagung der Wasserchemischen Gesellschaft in der GDCh, May 22-24, 2006, Celle, Germany, 250-254 (2006).

Lectures, oral presentations

Arnold, T.; Scheinost, A.; Baumann, N.; Brendler, V.
Surface speciation of uranyl(VI) on gibbsite: A combined spectroscopic approach
2006 Fall Meeting, Materials Research Society, November 27-December 01, 2006, Boston, USA.

Baumann, N.
Uranmunition im Boden: Spektroskopische Untersuchungen zur Sekundärphasenbildung auf abgereichertem Uran
Vortragsreihe des Schwerpunktes Bio-Geo der Friedrich-Schiller-Universität Jena, November 07, 2006, Jena, Germany.

Baumann, N.; Brendler, V.; Arnold, T.; Geipel, G.; Bernhard, G.
Spectroscopic evidence of adsorbed U(IV) surface species onto gibbsite and quartz obtained by TRLFS
15th Radiochemical Conference, April 23-28, 2006, Mariánské Lázně, Czech Republic.

Bernhard, G.
Bindungsformen des Urans in umweltrelevanten Kompartimenten
Forschungszentrum Jülich GmbH, September 13, 2006, Jülich, Germany.

Brendler, V.
Grundlagen der geochemischen Modellierung
Dresdner Grundwasserforschungszentrum (DGFZ) e.V., September 15, 2006, Dresden, Germany.

Brendler, V.
Mechanistische Sorptionsmodelle – Gegenwärtiger Stand und Perspektiven für die Langzeitsicherheitsanalyse
GRS mbH Braunschweig, July 14, 2006, Braunschweig, Germany.

Brendler, V.
Overview of current thermodynamic databases
12th ISSP – International Symposia on Solubility Phenomena and Related Equilibrium Processes, Workshop on Quality Assurance in Thermodynamic Databases for Performance Assessment Studies in Waste Disposal, July 23-28, 2006, Freiberg, Germany.

Brendler, V.
Thermodynamische Datenbasis für das Nahfeld – Aktueller Stand
2. Fachgespräch zur Radionuklidmigration, PTKA, October 25-26, 2006, Karlsruhe, Germany.

Brendler, V.
Verlässliche Daten, Modelle und Codes für die Geochemie
Festkolloquium für PD Dr. M. Richter, IIF Leipzig, October 20, 2006, Leipzig, Germany.

Brendler, V.; Kienzler, B.; Lützenkirchen, J.
Sorption databases ("PA ready"): Proposed next steps towards a database
2nd Annual FUNMIG Workshop, November 21-23, Stockholm, Sweden.

Cannes, C.; Nikitenko, S.; Le Naour, C.; Trubert, D.; Hennig, C.; Moisy, P.
Uranium chloro complexes in hydrophobic room temperature ionic liquid: Structural investigation and redox properties
EuChem Conference on Molten Salts and Ionic Liquids 2006, September 16-22, 2006, Hammamet, Tunisia.

Chukalina, M.; Funke, H.
Wavelet transform usage to analyse the signals and images collected by the X-ray techniques
International scientific Workshop "Modern techniques for the X-ray diffraction data analysis", May 22-25, 2006, Velikii Novgorod, Russia.

Den Auwer, C.; Guilbaud, P.; Guillaumont, D.; Moisy, P.; Le Naour, C.; Trubert, D.; Simoni, E.; Digiandomenico, V.; Hennig, C.; Scheinost, A.
Molecular characterization of actinide oxocations from protactinium to plutonium
Actinides-XAS-2006, 4th Workshop on Speciation, Techniques, and Facilities for Radioactive Materials at Synchrotron Light Sources, Forschungszentrum Karlsruhe, September 18-20, 2006, Karlsruhe, Germany.

Ender, V.; Schumann, T.; Sachs, S.; Bernhard, G.
Untersuchungen zur Aufnahme von Organika aus natürlichen Wässern durch Ionenaustauscher mit C-14-markierten Modellsubstanzen
VGB-Konferenz "Chemie im Kraftwerk 2006", October 11-12, 2006, Bad Neuenahr, Germany (2006).

Funke, H.; Chukalina, M.; Voegelin, A.; Scheinost, A.
Improving Resolution in k and r Space: A FEFF-based Wavelet for EXAFS Data Analysis
XAFS-13, 13th International Conference on X-ray Absorption Fine Structure, July 09-14, 2006, Stanford, USA.

Gaillard, C.; Billard, I.; Mekki, S.; Ouadi, A.; Hennig, C.; Denecke, M.
Combined techniques for studying actinide complexes in room temperature ionic liquids
Actinides-XAS-2006, 4th Workshop on Speciation, Techniques, and Facilities for Radioactive Materials at Synchrotron Light Sources, Forschungszentrum Karlsruhe, September 18-20, 2006, Karlsruhe, Germany.

Geipel, G.
Alkaline earth elements in the uranium phosphate system - A TRLFS study
Nuclear Professional School, Graduate School of Engineering, University of Tokyo, August 01, 2006, Tokyo, Japan.

Geipel, G.
Influence of Mg, Ca, Sr and Ba on formation of geochemical relevant uranyl species
15th Radiochemical Conference, April 23-28, 2006, Mariánské Lázně, Czech Republic.

Geipel, G.
Interaction of Cu(II) with dendritic ligands studied by TRLFS
3rd SUPRAPHONE Meeting, May 04-06, 2006, Lisbon, Portugal.

Geipel, G.
Interaction of Cu(II) with dendritic ligands studied by TRLFS and some remarks on luminescence of uranium(V)
Tokyo Institute of Technology, August 01, 2006, Tokyo, Japan.

Geipel, G.
Speciation of actinides
Selected topics on nuclear methods for non-nuclear applications, September 27-30, 2006, Varna, Bulgary.

Geipel, G.
Uranium – An unique luminescent element – New observations in different oxidation states
Faculty of Nuclear Sciences and Physical Engineering, Czech Technical University in Prague, November 09, 2006, Prague, Czech Republic.

Geipel, G.
Uranium speciation in water – Lectures learned from the nature
Nuclear Professional School, Graduate School of Engineering, University of Tokyo, July 31, 2006, Tokyo, Japan.

Geipel, G.; Bernhard, G.
Uranium speciation of environmentally related waters
Western Pacific Geophysics Meeting, July 24-27, 2006, Beijing, China.

Geipel, G.; Bernhard, G.
Alkaline earth uranyl compounds – From solution to mineral phases
16th Annual V.M. Goldschmidt Conference 2006, August 27-September 01, 2006, Melbourne, Australia.

Geissler, A.; Reitz, T.; Tschikov, S.; Selenska-Pobell, S.
Influence of U(VI) and nitrate on microbial communities of uranium mining wastes
VAAM-Jahrestagung 2006, March 19-22, 2006, Jena, Germany.

Hennig, C.
Application of EXAFS spectroscopy for structural analysis of actinide compounds in solution
Chemistry Department of the Argonne National Laboratory, October 31, 2006, Chicago, USA.

Hennig, C.
Modified spectro-electrochemical cell for experiments with ionic liquids
ACTINET Meeting "Actinides and lanthanides solution chemistry in water stable room temperature ionic liquids", June 08-09, 2006, Strasbourg, France.

Hennig, C.
Structure analysis of actinide compounds in solution by X-ray absorption spectroscopy
23rd European Crystallographic Meeting, August 06-11, 2006, Leuven, Belgium.

Hennig, C.
Structure investigation of uranium in aqueous solution under reduced conditions
Research Reactor Institute, Kyoto University, January 19, 2006, Kyoto, Japan.

Hennig, C.
Study of U(IV), U(V), and U(VI) complexation using electrochemistry combined with XAFS spectroscopy
Speciation of Radionuclides in the Environment, Institute of Nuclear Chemistry, University of Mainz, September 21, 2006, Mainz, Germany.

Hennig, C.
The coordination of uranium in solution – What can we learn from EXAFS spectroscopy?
Molecular Design and Synthesis Group, Katholieke Universiteit Leuven, March 02, 2006, Leuven, Belgium.

Hennig, C.
What can we learn from diffuse scattering about actinide coordination in solutions?
ROBL Seminar, November 21, 2006, Grenoble, France.

Hennig, C.
X-ray absorption spectroscopy as tool for speciation and structure analysis of actinides in solution
Research Laboratory for Nuclear Reactors, Tokyo Institute of Technology, January 17, 2006, Tokyo, Japan.

Hennig, C.; Scheinost, A. C.; Funke, H.; Rossberg, A.; Strauch, U.; Ikeda, A.; Oehme, W.; Falkenberg, D.; Claußner, J.; Bernhard, G.
The Rossendorf beamline at ESRF
Actinides-XAS-2006, 4th Workshop on Speciation, Techniques, and Facilities for Radioactive Materials at Synchrotron Light Sources, Forschungszentrum Karlsruhe, September 18-20, 2006, Karlsruhe, Germany.

Hennig, C.; Schmeide, K.; Brendler, V.; Moll, H.; Tsushima, S.; Scheinost, A.C.
EXAFS investigation of U(VI), U(IV) and Th(IV) sulfato complexes in aqueous solution
Actinides-XAS-2006, 4th Workshop on Speciation, Techniques, and Facilities for Radioactive Materials at Synchrotron Light Sources, Forschungszentrum Karlsruhe, September 18-20, 2006, Karlsruhe, Germany.

Herrmannsdörfer, T.; Bianchi, A. D.; Papageorgiou, T. P.; Pobell, F.; Wosnitza, J.; Pollmann, K.; Merroun, M.; Raff, J.; Selenska-Pobell, S.
Magnetic properties of transition-metal nanoclusters on a biological substrate
17th International Conference on Magnetism (ICM 2006), August 20-25, 2006, Kyoto, Japan.

Křepelová, A.; Sachs, S.; Reich, T.; Roßberg, A.; Baumann, N.; Bernhard, G.
Influence of humic acid on U(VI) sorption onto kaolinite studied by TRLFS and EXAFS
15th Radiochemical Conference, April 23-28, 2006, Mariánské Lázně, Czech Republic.

Merroun, M.; Geissler, A.; Regenhardt, D.; Selenska-Pobell, S.
Response of bacterial strains isolated from a uranium mining waste to heavy metal stress
FEMS 2006, 2nd Congress of European Microbiologists, July, 04-08, 2006, Madrid, Spain.

Merroun, M.; Nedelkova, M.; Rossberg, A.; Hennig, C.; Selenska-Pobell, S.
Effect of pH on the speciation of uranium(VI) associated with bacterial strains isolated from extreme habitats: Spectroscopic and microscopic studies
ISME-11, 11th International Symposium on Microbial Ecology, August 20-25, 2006, Vienna, Austria.

Mibus, J.
Diffusion in compacted clay
Project Meeting NF-Pro, May 09-10, Hannover, Germany.

Mibus, J.; Sachs, S.; Křepelová, A.
Diffusion of humic acid in compacted clay
Bridging Clays, French Clay Group and The Clay Minerals Society, June 03-07, 2006, Ile d'Oléron, France.

Moll, H.
Interactions of microbes found at Äspö underground lab with actinides such as curium, plutonium and uranium
2nd Annual FUNMIG Workshop, November 21-23, 2006, Stockholm, Sweden.

Moll, H.; Bernhard, G.
Complex formation of curium(III) with the amino acids L2-aminobutyric acid and L-threonine and the corresponding phosphate ester O-phospho-L-threonine
15th Radiochemical Conference, April 23-28, 2006, Mariánské Lázně, Czech Republic.

Nebelung, C.
Simultanbestimmung von Nuklidgemischen durch Auswertung von Multielement LS-Spektren am Beispiel von Pb-210, Bi-210, Po-210 und Ra-226, U-233, Np-237
222. PTB-Seminar, Physikalisch-Technische Bundesanstalt, November 21, 2006, Braunschweig, Germany.

Nebelung, C.
Sorption of Cs and U(VI) on clay minerals
Project Meeting NF-Pro, May 09-10, Hannover, Germany.

Opel, K.; Hübener, S.; Weiß, S.; Zänker, H.; Bernhard, G.
Untersuchungen zur Löslichkeit verschiedener Urandioxidmodifikationen mittels LIBD und anderer spektroskopischer Methoden
72. Jahrestagung der Wasserchemischen Gesellschaft in der GDCh, May 22-24, 2006, Celle, Germany.

Pollmann, K.
Verwendung von Mikroorganismen zur Synthese von Nanopartikeln
Mikrobiologisches Kolloquium, Institut für Mikrobiologie und Weinforschung, Johannes Gutenberg University Mainz, July 03, 2006, Mainz, Germany.

Raff, J.
Bacteria from extreme environments and their interaction with uranium(VI)
Institut für Gewässerschutz/Wassertechnologie, EAWAG – Forschungszentrum für Limnologie, June 25-27, 2006, Kastanienbaum, Switzerland.

Raff, J.
Bakterien - die heimlichen Herrscher unserer Erde
Tag des offenen Labors, FZD, May 20, 2006, Dresden, Germany.

Raff, J.
Bio-nanotechnology
Besuch der japanischen Nanotechnologie-Delegation, FZD, September 26, 2006, Dresden, Germany.

Raff, J.
Innovationspool Natur: Bakterien und Bionik
Vortrag anlässlich des Besuches des Berufschulzentrum Technik, Bautzen und des Leistungskurses Physik des Vizthum-Gymnasiums Dresden, FZD, January 26 & June 19, 2006, Dresden, Germany.

Raff, J.
Nanocluster dank Bakterien
Innovationsforum "Nanobasierte Umwelttechnik", November 09-10, 2006, Jena, Germany.

Raff, J.
Uranabfallhalden als Reservoir für Bakterien mit hohem Anwendungspotential für die Bio- und Nanotechnologie
Vortrag anlässlich des Besuches von Mikrobiologie-Studenten der Universität Bayreuth (Prof. Dr. O. Meyer), FZD, June 27, 2006, Dresden, Germany.

Richter, A.; Brendler, V.
Sparse and uncertain SCM parameter sets – What are the consequences?
ACS National Meeting, American Chemical Society, March 26-30, 2006, Atlanta, USA.

Sachs, S.; Bernhard, G.
Uranium(VI) adsorption onto synthetic humic substance-kaolinite sorbates
15th Radiochemical Conference, April 23-28, 2006, Mariánské Lázně, Czech Republic.

Sachs, S.; Křepelová, A.; Schmeide, K.; Mibus, J.; Brendler, V.; Bernhard, G.
Einfluss von Huminstoffen auf die Migration von Uran und Neptunium im Ton
Workshop zum Forschungsvorhaben "Migration von Actiniden im System Ton, Huminstoff, Aquifer", March 28-29, 2006, Mainz, Germany.

Scheinost, A.
Environmental soil chemistry with synchrotron methods: Linking space, time, biology and hydrology
Institute of Environmental Technology - CTM, Universitat Politècnica de Catalunya, May 23, 2006, Barcelona, Spain.

Scheinost, A.C.; Charlet, L.
Biogeochemistry of iron and interacting metals in soils
XIII. International Symposium on Iron Nutrition and Interactions in Plants, July 3-7, 2006, Montpellier, France.

Scheinost, A.C.; Hennig, C.; Somogyi, A.; Martinez-Criado, G.; Knappik, R.
Geochemical behavior of uranium in mine tailings at Freital, Germany: A µ-XRF, µ-XAFS and µ-XRD study.
16th Annual V.M. Goldschmidt Conference 2006, August 27-September 01, 2006, Melbourne, Australia.

Schumann, T.; Ender, V.; Sachs, S.; Bernhard, G.
Verwendung von C-14-markierten Modellsubstanzen zur Untersuchung der Entfernung von Organika aus Wässern durch Ionenaustauscher
Zittauer Kraftwerkschemisches Kolloquium, Hochschule Zittau/Görlitz, September 26-27, 2006, Zittau, Germany.

Selenska-Pobell, S.
Changes in natural microbial community structure of a uranium mining waste pile induced by addition of sodium and uranyl nitrate
Institute of Molecular Biology, Bulgarian Academy of Science, May 29, 2006, Sofia, Bulgaria.

Selenska-Pobell, S.
Influence of bacteria on migration of uranium from uranium mining wastes
Fachdiskussion: "Mikrobiologie in Halden und Absetzanlagen", Bundesamt für Strahlenschutz, February 09, 2006, Berlin, Germany.

Steudtner, R.
Vorstellung des Instituts für Radiochemie und Erläuterungen zum Ablauf des Kernbrennstoffkreislaufes
Vortrag anlässlich des Besuches einer Schülergruppe, FZD June 13, 2006, Dresden, Germany.

Ulrich, K.-U.; Rossberg, A.; Scheinost, A.C.
Speciation of U(VI) in natural systems by advanced EXAFS analysis II. Application of MCTFA to solve the spatial structure of U(VI) sorption complexes on ferrihydrite
ACTINET Kick-off Meeting, ESRF, February 13-14, 2006, Grenoble, France.

Ulrich, K.-U.; Rossberg, A.; Scheinost, A.C.; Reuther, H.; Zänker, H.
Interaction of uranium(VI) and colloidal iron(III) oxyhydroxide in an abandoned uranium mine
15th Radiochemical Conference, April 23-28, 2006, Mariánské Lázně, Czech Republic.

Ulrich, K.-U.; Rossberg, A.; Scheinost, A.C.; Reuther, H.; Zänker, H.
Structural investigation on uranium mine water colloids and their interaction with UO_2^{2+}
232nd National ACS Meeting, September 10-14, 2006, San Francisco, USA.

Ulrich, K.-U.; Weiss, S.; Rossberg, A.; Foerstendorf, H.; Zänker, H.
Stability and molecular speciation of colloid-borne uranium
Water Quality SuperGroup Meeting, School of Engineering & Applied Science, Washington University, March 31, 2006, St. Louis, USA.

Zänker, H.
Investigation of environmental colloids/nano-particles at the FZD
1st Meeting of the working group "Aquatic Nanoscience and Nanotechnology", December 11-12, 2006, Vienna, Austria.

Zänker, H.; Opel, K.; Weiß, S.; Hübener, S.; Bernhard, G.
Investigations into the formation of intrinsic colloids and pseudocolloids of uranium(IV)
2nd Annual FUNMIG Workshop, November 21-23, 2006, Stockholm, Sweden.

Zänker, H.; Ulrich, K.-U.; Opel, K.; Brendler, V.
Influence of colloids on uranium transport in nuclear waste repositories and abandoned uranium mines – A critical comparison
16th Annual V.M. Goldschmidt Conference 2006, August 27-September 01, 2006, Melbourne, Australia.

Zänker, H.; Weiß, S.
Influence of colloids produced by the weathering of rock material on uranium(VI) behavior
36th Journées des Actinides, AWE Aldermaston, April 01-04, 2006, Oxford, UK.

Zänker, H.; Weiß, S.; Sachs, S.
Colloid generation and stability in simulated reduced groundwaters
2nd FUNMIG RTDC-2 Progress Meeting Karlsruhe, August 02, 2006, Karlsruhe, Germany.

▸ Posters

Brockmann, S.; Mibus, J.; Nebelung, C.
Migration of cesium in bentonite: Influence of the pore water composition
15th Radiochemical Conference, Czech Technical University in Prague, April 23-28, 2006, Mariánské Lázne, Czech Republic.

Deun, R. van; Hennig, C.; Cartuyvels, E.; Nikitenko, S.; Parac-Vogt, T. N.
Mo K-edge EXAFS investigation of the $[Mo_7O_{24}]^{6-}$ promoted phosphate ester hydrolysis
23rd European Crystallographic Meeting, August 06-11, 2006, Leuven, Belgium.

Funke, H.; Hennig, C.; Scheinost, A.
An EXAFS study of soddyite
ESRF Users' Meeting 2006, European Synchrotron Radiation Facility, February 07-08, 2006, Grenoble, France.

Funke, H.; Hennig, C.; Rossberg, A.; Scheinost, A.
The local structure of soddyite: EXAFS shell fitting and wavelet analysis
Actinides-XAS-2006, 4th Workshop on Speciation, Techniques, and Facilities for Radioactive Materials at Synchrotron Light Sources, Forschungszentrum Karlsruhe, September 18-20, 2006, Karlsruhe, Germany.

Glorius, M.; Moll, H.; Bernhard, G.
Actinides in biosystems - Complexation studies with relevant bioligands
ThUL-ACTINET School, May 15-20, 2006, Lille, France.

Großmann, K.; Arnold, T.; Krawczyk-Bärsch, E.
Detection of U(V) in *Pseudomonas stutzeri* biofilms by confocal laser scanning microscopy
Biofilm II, UFZ Centre for Environmental Research Leipzig-Halle, March 23-24, 2006, Leipzig, Germany.

Gürtler, S.; Rieck, S.; Ritter, A.
Synthese und Charakterisierung des Minerals Compreignacit ($K_2(UO_2)_6O_4(OH)_6 \cdot 7H_2O$) als ein Modell für typische Uransekundärphasen zur Untersuchung und Beurteilung der Schadstoffausbreitung in umweltrelevanten Geosystemen
8. Sächsischer Landeswettbewerb zur Umsetzung der Agenda 21 in der beruflichen Ausbildung 2005/06, September 19, 2006, Dresden, Germany.

Hennig, C.
Evidence for double-electron excitations in X-ray absorption spectra of actinides
Actinides-XAS-2006, 4th Workshop on Speciation, Techniques, and Facilities for Radioactive Materials at Synchrotron Light Sources, Forschungszentrum Karlsruhe, September 18-20, 2006, Karlsruhe, Germany.

Hennig, C.; Schmeide, K.; Brendler, V.; Moll, H.; Tsushima, S.; Scheinost, A. C.
Coordination of uranium aquo chloro and sulfato complexes under different redox conditions
XAFS-13, 13th International Conference on X-ray Absorption Fine Structure, July 09-14, 2006, Stanford, USA.

Hennig, C.; Tutschku, J.; Rossberg, A.; Bernhard, G.; Scheinost, A.
EXAFS investigation of U(VI) and U(IV) aquo chloro complexes with a newly developed spectro-electrochemical cell
ESRF Users' Meeting 2006, European Synchrotron Radiation Facility, February 07-08, 2006, Grenoble, France.

Ikeda, A.; Hennig, C.; Rossberg, A.; Scheinost, A.; Bernhard, G.; Mizuoka, K.; Ikeda, Y.
A comparative study of $U(V)O_2^+$- and $U(VI)O_2^{2+}$-carbonato complexes in aqueous solution
Actinides-XAS-2006, 4th Workshop on Speciation, Techniques, and Facilities for Radioactive Materials at Synchrotron Light Sources, Forschungszentrum Karlsruhe, September 18-20, 2006, Karlsruhe, Germany.

Křepelová, A.; Sachs, S.; Reich, T.; Roßberg, A.; Brendler, V.; Baumann, N.; Bernhard, G.
Influence of humic acid on U(VI) sorption onto kaolinte: Studies using extended X-ray absorption fine structure measurements and time-resolved laser-induced fluorescence spectroscopy
13th Meeting of the International Humic Substances Society, July 30-August 04, 2006, Karlsruhe, Germany.

Merroun, M.; Rossberg, A.; Hennig, C.; Scheinost, A.; Selenska-Pobell, S.
Structure and size of gold nanoparticles formed on cells and S-layers of Bacillus sphaericus JG-A12
VAAM-Jahrestagung 2006, March 19-22, 2006, Jena, Germany.

Mibus, J.; Brendler, V.; Pfingsten, W.
Migration of uranium(VI) in a phosphate environment: Column experiments and modeling
15th Radiochemical Conference, Czech Technical University in Prague, April 23-28, 2006, Mariánské Lázne, Czech Republic.

Nebelung, C.; Brendler, V.; Brockmann, S.; Mibus, J.
Uranium and cesium sorption on montmorillonite and bentonite
1st Europaen Chemistry Congress, August 27-31, 2006, Budapest, Hungary.

Pollmann, K.; Merroun, M., Herrmannsdörfer, T.; Raff, J.; Fahmy, K.; Hennig, C., Selenska-Pobell, S.
Bacterial surface layers (S-layers) as biological templates for the synthesis of metal nanoparticles
VAAM-Jahrestagung 2006, March 19-22, 2006, Jena, Germany.

Pollmann, K.; Merroun, M.; Raff, J.; Fahmy, K.; Hennig, C.; Selenska-Pobell, S.; Herrmannsdörfer, T.
Synthesis of metal nanoparticles using bacterial surface layers (S-layers) as biological templates
European Materials Research Society (E-MRS) 2006 Spring Meeting, May 29-June 02, 2006, Nice, France.

Raff, J.; Berger, S.; Selenska-Pobell, S.
Uranium binding by cells and S-layers of bacillus isolates recovered from uranium mining waste pile
VAAM-Jahrestagung 2006, March 19-22, 2006, Jena, Germany.

Rossberg, A.; Ulrich, K.-U.; Brendler, V.; Scheinost, A.
Influence of carbonate on U(VI) aqueous speciation and adsorption to ferrihydrite investigated by advanced EXAFS data analysis methods
XAFS-13, 13th International Conference on X-ray Absorption Fine Structure, July 09-14, 2006, Stanford, USA.

Rossberg, A.; Ulrich, K.-U.; Scheinost, A. C.
Spectroscopic studies on colloid-borne uranium(VI)
ESRF Users' Meeting 2006, European Synchrotron Radiation Facility, February 07-08, 2006, Grenoble, France.
16th Users Meeting, ESRF, 08.-11.02.2006, Grenoble, France, 06.-10.02.2006, Grenoble, France.

Rossberg, A.; Ulrich, K.-U.; Scheinost, A. C.
The molecular topology of uranium(VI) bonding to iron and aluminium oxyhydroxide nanoclusters revisited by EXAFS spectroscopy
Actinides-XAS-2006, 4th Workshop on Speciation, Techniques, and Facilities for Radioactive Materials at Synchrotron Light Sources, Forschungszentrum Karlsruhe, September 18-20, 2006, Karlsruhe, Germany.

Sachs, S.; Mibus, J.
Migration behavior of humic acids in compacted clay and its influence on the uranium transport
13th Meeting of the International Humic Substances Society, July 30-August 04, 2006, Karlsruhe, Germany.

Schabelnikova, S.; Funke, H.; Chukalina, M.
EXAFS spectra analysis: The mother wavelet choice
International science-technical Conference "Fundamental problems of radioelectronic instrument-making industry", October 24-28, 2006, Moscow, Russia.

Schabelnikova, S.; Funke, H.; Chukalina, M.
Wavelet analysis of the EXAFS spectra: New wavelet function as a linear combination of two Morlet wavelets
XVIth International Synchrotron Radiation Conference, July 11-14, 2006, Novosibirsk, Russia.

Servaes, K.; Hennig, C.; van Deun, R.; Görller-Walrand, C.
A comparative UV-vis and EXAFS investigation of the coordination of the uranyl ion UO_2^{2+} in solution
23rd European Crystallographic Meeting, August 06-11, 2006, Leuven, Belgium.

Servaes, K.; Hennig, C.; van Deun, R.; Görller-Walrand, C.
EXAFS and UV-vis investigation of the first coordination sphere of the uranyl ion in $UO_2(NO_3)_2(TBP)_2$
Actinides-XAS-2006, 4th Workshop on Speciation, Techniques, and Facilities for Radioactive Materials at Synchrotron Light Sources, Forschungszentrum Karlsruhe, September 18-20, 2006, Karlsruhe, Germany.

Tsushima, S.; Scheinost, A.
Hydration of U(VI,V) and Np(VI) ions revisited
Actinides-XAS-2006, 4th Workshop on Speciation, Techniques, and Facilities for Radioactive Materials at Synchrotron Light Sources, Forschungszentrum Karlsruhe, September 18-20, 2006, Karlsruhe, Germany.

Zänker, H.; Weiß, S.
Einfluss von eisenreichen Kolloiden auf das Uran(VI) in Bergwerkshalden
72. Jahrestagung der Wasserchemischen Gesellschaft in der GDCh, May 22-24, 2006, Celle, Germany.

▶ Theses

Opel, K.
Kolloid- und Löslichkeitsuntersuchungen an Uran(IV) mittels laserinduzierter Breakdown-Detektion
Dresden University of Technology, Dresden, Germany (2006).

▶ Diploma

Heller, A.
Untersuchung der Eignung bakterieller Hüllproteine zur Reinigung uranhaltiger Wässer
University of Applied Sciences, Dresden, Germany (2006).

Reitz, T.
Einfluss von Uran auf die *Archaea*-Diversität in Bodenproben aus der Haberlandhalde
Dresden University of Technology, Dresden, Germany (2006).

Steinborn, A.
Untersuchung der Ähnlichkeit von TRLFS-Spektren
Dresden University of Technology, Dresden, Germany (2006).

Trepte, P.
Sorption von Radionukliden an Tongestein: Spektroskopische Referenzdaten
University of Applied Sciences, Dresden, Germany (2006).

Awards / Research fellowships

Mibus, J.
Diffusion of nanoparticles in argillaceous media: Assessment of the pore structure
EURATOM – European Atomic Energy Community

Tsushima, S.
Complexation of Np and Pu ions with organic ligands: Combined quantum chemical and EXAFS study
Alexander-von-Humboldt Research-Fellowship

Scheinost, A.C.
Offer to take a faculty position (Professor of Environmental Mineralogy), declined.
University of Grenoble

Work placements

Gürtler, S.; Rieck, S.; Ritter, A.
Synthese und Charakterisierung des Minerals Compreignacit ($K_2(UO_2)_6O_4(OH)_6 \cdot 7H_2O$) als ein Modell für typische Uransekundärphasen zur Untersuchung und Beurteilung der Schadstoffausbreitung in umweltrelevanten Geosystemen
Beitrag zum 8. Sächsischen Landeswettbewerb zur Umsetzung der Agenda21 in der beruflichen Ausbildung, Dresden (2006).

- Seminars (Talks of visitors)
- Workshops
- Teaching activities

Seminars

*** Seminars in cooperation with the Institute of Radiopharmacy, FZD.**

Dr. C. Grüttner
micromod GmbH Rostock-Warnemünde
Target-spezifische Magnetpartikel für Anwendungen im Life Science- und Umweltbereich*
January 18, 2006

Prof. R. Bencheikh
Federal Institute of Technology, Lausanne, Switzerland
Uranyl-Pseudomonas fluorescence interactions: Implications for uranyl mobility in the subsurface
January 26, 2006

Dr. H. Claus
Mikrobiologe an der Uni Mainz
Zellwandstrukturen bei extremophilen Archaea
February 17, 2006

Dr. T. Neu
Microbiology of Interfaces, Dept. of River Ecology, UFZ Magdeburg, Germany
Confocal laser scanning microscopy of biofilms - Microorganisms, polymers and microhabitats
March 07, 2006

Prof. Dr. A. Eychmüller
Inst. f. Physikalische Chemie u. Elektrochemie, TU Dresden
Chemie und Physik von Halbleiternano-kristallen*
March 10, 2006

Dr. M. V. Sivaiah
Andrah University, India
Novel inorganic and inorganic-organic materials with reference to nuclear waste management*
April 20, 2006

Dr. A. Potthoff
Fraunhofer Institut für Keramische Technologien und Systeme, Dresden, Germany
Keramische Nanopartikel - Möglichkeiten und Grenzen
May 02, 2006

Prof. S. A. Banwart
Kroto Research Institute, Sheffield, United Kingdom
Attached microbial activity and natural attenuation of organic pollutants in groundwater: From lab- to field-scale
May 03, 2006

Prof. Dr. W. Brewitz
GRS Braunschweig
Ausrichtung und Ziele der deutschen Endlagerforschung 2006
May 10, 2006

Prof. Dr. R. Odoj
Institut für Sicherheitsforschung und Reaktortechnik, FZ Jülich GmbH, Jülich, Germany
Partitioning and transmutation - Eine alternative Entsorgungsstrategie?
July 07, 2006

Dr. T. Wagner
Institut für Technische Chemie, Forschungszentrum Karlsruhe, Karlsruhe, Germany
LIBD zum höchstempfindlichen Nachweis von Kolloiden - Möglichkeiten, aktuelle Entwicklungen und Grenzen
July 20, 2006

Prof. L. F. Lindoy
School of Chemistry,The University of Sydney, NSW 2006, Australia
New discrete and framework molecular structures formed by metal-ion directed self assembly*
July 25, 2006

Dr. A. Leonhardt
IFW Dresden
Synthese, Eigenschaften und Anwendungen von Kohlenstoffnanoröhren (Synthesis, properties and applications of carbon nanotubes)
November, 16, 2006

Prof. Dr. H. J. Bahl
Inst. f. Biowissenschaften/Mikrobiologie, Uni Rostock
Vorkommen und Funktion S-Layer homologer (SLH) Domänen
December 06, 2006

▸ Workshops (organized by the IRC)

Workshop of the joint project: Wechselwirkung und Transport von Actiniden im natürlichen Tongestein unter Berücksichtigung von Huminstoffen und Tonorganika

Mercure Hotel Newa, Dresden, Germany, November 7 – 8, 2006.

Acker, M.
Sachgebiet Strahlenschutz , Dresden University of Technology, Dresden
Temperaturabhängigkeit im System An(III)-Tongestein-NOM

Bauer, A.
Institute for Nuclear Waste Disposal, Forschungszentrum Karlsruhe
Aufarbeitung, Bereitstellung, Charakterisierung des Opalinus-Ton

Eidner, S.
Department of Chemistry – Physical Chemistry, University of Potsdam
Neuerliche Highlights in der spektroskopischen Charakterisierung von Actiniden-Humat-Komplexen

Eidner, S.
Department of Chemistry – Physical Chemistry, University of Potsdam
Spektroskopische Untersuchungen zum erweiterten Prozessverständnis in binären und ternären Huminstoff-Tongestein-Lanthanoid Systemen: Thermodynamische und kinetische Kenngrößen

Kautenburger, R.
Institute of Inorganic and Analytical Chemistry and Radiochemistry, Saarland University
Untersuchungen zur Migration von Lanthaniden und Radionukliden in natürlichen Tonformationen im Übergang von verdünnten Mineral-Suspensionen zu kompakten Tonen

Krüger, S.
Theoretical Chemistry, Technical University of Munich
Quantenmechanische Modellierung von Actinoidenkomplexen: Komplexierung durch Huminstoffe und Sorption an Tonmineralien

Kuczewski, B.
Institute of Analytical Chemistry and Radiochemistry, Graz University of Technology
Untersuchung des Umweltverhaltens des Elementes Iod - Wechselwirkung mit Huminstoffen und Kaolinit

Lippold, H.; Kulenkampff, J.
Institute of Interdisciplinary Isotope Research, Leipzig
Beiträge zur Modellierung des Actinidentransports in potentiellen Wirtsgesteinsformationen

Mansel, A.
Institute of Interdisciplinary Isotope Research, Leipzig
Bestimmung der Änderung des räumlichen und zeitlichen Ausbreitungsverhaltens von chemotoxischen Schwermetallen nach Wechselwirkung mit NOM in geologischen Formationen von Untertagedeponien

Marquardt, C.
Institute for Nuclear Waste Disposal, Forschungszentrum Karlsruhe
Einfluss von tonorganischen Substanzen auf die Rückhaltung von Actinoidionen in der Tonbarriere

Plischke, I.
Bundesanstalt für Geowissenschaften und Rohstoffe (BGR), Hannover
Vorstellung des Mont Terri Projekts sowie geologisch-mineralogischer und geomechanischer Daten zum Opalinus Ton

Reich, T.
Institute of Nuclear Chemistry, Johannes Gutenberg University Mainz
Wechselwirkung von Neptunium und Plutonium mit natürlichem Tongestein

Sachs, S.
Institute of Radiochemistry, FZD
Charakterisierung und Quantifizierung des Einflusses von Tonorganika auf die Wechselwirkung und die Diffusion von Uran und Americium im Ton

Stumpf, T.
Institute of Physical Chemistry, University of Heidelberg
Wechselwirkung von dreiwertigen Actiniden mit organischen Liganden und Mineraloberflächen

Workshop of the Institute of Radiochemistry (IRC) and the Paul Scherrer Institute (PSI), Villigen , Switzerland

FZD, Dresden, Germany,
October 5 – 6, 2006.

Baeyens, B. (PSI)
Metal sorption modeling on clay minerals: Overview and some recent developments

Bradbury, M. (PSI)
Status of radioactive waste management in Switzerland

Foerstendorf, H. (IRC)
Identifikation von Molekülkomplexen von Actinylionen: Photothermale Schwingungs-spektroskopie am Freie Elektronen Laser FELBE

Křepelová, A. (IRC)
Einfluss von HS auf die U(VI) Sorption an Kaolinit: TRLFS-Untersuchungen

Mibus, J. (IRC)
Experimente und Modellierung zum Radionuklidtransport in porösen Medien

Müller, K. (IRC)
Speziation von Uran(VI) in wäßrigen Lösungen mittels ATR-FTIR Spektroskopie

Pfingsten, W. (PSI)
Coupled modeling to transfer advanced process understanding into radionuclide transport calculations

Tits, J. (PSI)
Status and outlook for the LES-IRC on TRLFS investigations on the U(VI)/cement systems

Workshop of the Rossendorf-Beamline (ROBL) at the ESRF, Grenoble

FZD, Dresden, Germany,
December 19, 2006.

Baumann, N.; Arnold, T.; Scheinost, A.C.; Brendler, V.
Surface speciation of uranyl(VI) on gibbsite: A combined spectroscopic approach

Funke, H.
EXAFS studies of Zn-Al, Ni-Al, and Co-Al double layer hydroxides

Günther, A.; Roßberg, A.
Uranium species formed by monocellular algae - EXAFS investigations at 30K

Hennig, C.
Diffuse scattering as a new tool to get structural information on actinide coordination in solution

Ikeda, A.; Hennig, C.; Tsushima, S.; Rossberg, A.; Scheinost, A.C.; Bernhard, G.; Takao, K.; Ikeda, Y.
Comparative study of uranyl(VI) and uranyl(V) carbonato complexes in aqueous solution

Rossberg, A.; Tsushima, S.; Scheinost, A.C.; Ulrich, K.-U.
Carbonate effects on surface speciation of uranyl at the ferrihydrite-water interface: New insights from advanced EXAFS data analysis

Scheinost, A.C.; Charlet, L.; Gehin, A.; Sposito, G.
Abiotic Se reduction by Fe(II): Elucidation of reaction mechanisms and kinetics

Tsushima, S.; Rossberg, A.; Scheinost, A.C.
DFT study of the structure of uranyl complexes: Contribution from electronic and vibrational excitation

Meetings / Visitors

Students of University of Applied Sciences Dresden
FZD, February 06, 2006, Dresden, Germany

ISDA Project Meeting,
FZD, May 15, 2006, Dresden Germany

Students of the University of Bayreuth
FZD, September 27, 2006, Dresden Germany

ACTINET-Meeting
FZD, October 09-10, 2006, Dresden Germany

▸ Teaching activities

Lectures

Bernhard, G.
Radiochemistry – Radiochemical methods
Dresden University of Technology
Summer term 2006

Bernhard, G.
Environmental analysis (Trace analysis)
Dresden University of Technology
Summer term 2006

Bernhard, G.
Environmental chemistry (Environment – Substance – Energy)
Dresden University of Technology
Winter term 2006/2007

Merroun, M.
Lixiviación y Recuperación de Metales: Bioleaching and removal of metals
Centro de Ensenanzas Virtuales de la Universidad de Granada – Fundación Empresa Universidad de Granada & Escuela Superior de Ensenanza Abierta
Study course: Máster de Biotecnología – Master of Biotechnoogy

Courses

The IRC provided two experiments of the laboratory course "Instrumental Analysis" held by the Institute for Analytical Chemistry, Dresden University of Technology, during both summer and winter terms:

- Technetium analysis in environmental samples
- Alpha spectrometric isotope dilution analysis of uranium

Advisers:
Hübener, S.
Krogner, K.

Teaching Assistants:
Glorius, M.
Großmann, K.
Lehmann, S.
Müller, K.
Steudtner, R.
Weiß, S.

Prof. Dr. habil. G. Bernhard (Director)

Administration
Kirmes, C.; Kreusel, G.

Radiation Protection Technics
Heim, H.; Falkenberg, D.; Henke, S.; Hiller, B.; Rumpel, A.

D I V I S I O N S

BIOGEOCHEMISTRY

Dr. Geipel, G.

Dr. Arnold, T.
Dr. Barkleit, A. (geb. Koban)
Dr. Günther, A.
Dr. Ikeda, A.
Dr. Krawczyk-Bärsch, E.
Dr. Merroun, M.
Dr. Moll, H.
Dr. Pollmann, K.
Dr. Raff, J.
Dr. Regenhardt, D.
Dr. Sachs, S.
Dr. Schmeide, K.
Dr. Selenska-Pobell, S.
Dr. Viehweger, K.

Technical Staff

Dudek, M.
Eilzer, M.
Flemming, K.
Grambole, G.
Heller, S.
Rietig, A.
Ruske, R.

MIGRATION

Dr. Brendler, V.

Dr. Baumann, N.
Dr. Foerstendorf, H.
Dr. Hübener, S.
Dr. Krogner, K.
Dr. Mibus, J.
Nebelung, C.
Dr. Richter, A.
Dr. Richter, W.
Dr. Ulrich, K.-U.
Dr. Zänker, H.

Technical Staff

Eckhardt, C.
Eidner, I.
Fröhlich, C.
Heim, K.
Leckelt, M.
Müller, C.
Neubert, H.
Schaefer, U.
Weiß, S.

MOLECULAR STRUCTURES

(ROBL, ESRF, Grenoble, F)

PD Dr. habil. Scheinost, A.C.

Dr. Funke, H.
Dr. Hennig, C.
Dr. Roßberg, A.
Prof. Dr. Tsushima, S.

Strauch, M. (*Administration*)

Technical Staff

Strauch, U.

PH. D. STUDENTS

Geißler, A.
Glorius, M.
Großmann, K.
Hollenbach, B.
Joseph, C.
Křepelová, A.
Lehmann, S.
Li, B.
Opel, K.
Müller, K.
Raditzky, B.
Reitz, T.
Steudtner, R.
Tanh Jeazet, H.B.

DIPLOMA STUDENTS

Heller, A.
Trepte, P.

GRADUATE ASSISTANTS, STUDENT ASSISTANTS, TRAINEES

Dietrich, A.
Brockmann, S.
Heller, T.
Henke, F.
Jankowski, U.
Müller, C.
Philipp, C.
Raff, T.
Rentzsch, M.
Steinborn, A.

GUEST SCIENTISTS

Prof. E. Golovinsky	*Institute of Molecular Biology,* *Bulgarian Academy of Sciences, Sofia, Bulgaria*
Prof. Y. Ikeda	*Tokyo Institute of Technology,* *Tokyo, Japan*
A. Johnsson	*Department of Cell and Molecular Biology, Microbiology* *Göteborg University, Sweden*
Dr. E. Marsili	*Copernicus Institute,* *Utrecht University, The Netherlands*
F. Morcillo de Amueda	*Depertamento de Microbiología, Facultad de Ciencias,* *University of Granada, Spain*
Dr. G. Radeva	*Institute of Molecular Biology,* *Bulgarian Academy of Sciences, Sofia, Bulgaria*
Dr. J. Tits	*Laboratory for Waste Management* *Paul Scherrer Institute (PSI), Villigen, Switzerland*
V.V. Vilas	*Institute of Nuclear Chemistry,* *Johannes-Gutenberg-University Mainz, Germany*

ACKNOWLEDGEMENTS

The Institute of Radiochemistry is part of the Forschungszentrum Dresden-Rossendorf e. V. (FZD) which is financed in equal parts by the ***Federal Republic of Germany*** and the ***Free State of Saxony***.

The Commission of the European Communities (EU) supported the following projects:

- ACTINET Network for Actinide Sciences:
  Contract No.: FIR1-CT-2002-20211
  Contract No.: FI6W-CT-2004-508836
- ACTINET-6 Pooled Facility:
  Actinides and lanthanides solution chemistry in water stable room temperature ionic liquids(RTILs)
  Contract No.: 02-13
  Actinides and lanthanides solution chemistry in water stable room temperature ionic liquids(RTILs) – Part II
  Contract No.: 05-26
  Actinide selective recognition by bio mimetic molecules
  Contract No.: 05-01
  Batch experiments and spectroscopic studies of Np(V) sorption on montmorillonite
  Contract No.: 05-22
  Complexation of U, Np, and Pu ions with organic ligands: Combined quantum chemical and EXAFS study
  Contract No.: 05-10
  Coupling variable energy x-ray absorption spectroscopy and quantum chemistry: A new tool to investigate actinide molecules
  Contract No.: 04-02
  Development of advanced EXAFS analysis methods for speciation of radionuclides in natural systems
  Contract No.: 03-08
  Interaction of actinide cations with metalloproteins
  Contract No.: 02-05
  Investigation of U(VI)/U(V) carbonato complexes in aqueous solution by spectro-electrochemical and quantum chemical methods
  Contract No.: 01-19
  Probing the interaction of actinides with the functional species of mineral/electrolyte interfaces by sum frequency vibrational spectroscopy
  Contract No.: 5/11
  Spectroscopic approach of aqueous chemistry of protactinium(V)
  Contract No.: 02-19
  Structural defects in binary and ternary actinide oxides
  Contract No.: 01-15
  Studies of the chemical forms of actinides and fission products adsorbed on nanocrystalline magnetite
  Contract No.: 04-08
  Synthesis of actinide endmember solids and solid solutions of relevance for geologic storage
  Contract No.: 02-08
  Understanding the electronic structure of actinyl complexes
  Contract No.: 02-04
  Understanding the electronic structure of actinyl complexes, Part II
  Contract No.: 05-15
- ACTINET Sorption Board:
  Knowledge infrastructure and education
  Contract No.: 02-23
  Managing experiments, models and data
  Contract No.: 02-24
- Integrated project NF-Pro:
  Understanding and physical and numerical modelling of the key processes in the near-field and their coupling for different host rocks and repository strategies
  Contract No.: FI6W-CT-2003-002389
- Integrated project FUNMIG:
  Fundamental processes of radionuclide migration
  Contract No.: 516514

Six projects were supported by the ***Bundesministerium für Wirtschaft und Technologie (BMWi)*** and by the ***Bundesministerium für Bildung und Forschung (BMBF)***:

- Mobilisierung von Actiniden durch mikrobiell produzierte Liganden unter Berücksichtigung der Endlagerung von radioaktivem Abfall
  Contract No.: BMWi 02E9985
- Integriertes Sorptionsdatenbanksystem für Wechselwirkungen chemisch-toxischer und radioaktiver Kontaminanten mit mineralischen Systemen in geologischen Formationen (ISDA-FZR)
  Contract No.: BMBF 02C1144
- Thermodynamische Referenzdatenbasis THEREDA, Teilvorhaben FZR, gefördert durch das BMBF
  Contract No.: 02C1436
- Thermodynamische Referenzdatenbasis THEREDA, Teilvorhaben FZR, gefördert durch das BMWi
  Contract No.: 02E10136
- Verbundprojekt: Actinidenmigration im natürlichen Tongestein: Charakterisierung und Quantifizierung des Einflusses von Tonorganika auf die Wechselwirkung von U und Am im Ton
  Contract No.: BMWi 02E10156
- Verbundprojekt: Migration von Actiniden im System Ton, Huminstoff, Aquifer – Migrationsverhalten von Actiniden (Uran, Neptunium) in Tonen: Charakterisierung und Quantifizierung des Einflusses von Huminstoffen
  Contract No.: BMWi 02E9673

Five projects were supported by the ***Deutsche Forschungsgemeinschaft (DFG)***:

- Fluoreszenzspektroskopie von gelösten Uran(IV)-Komplexen – Aufklärung der Speziation im umweltrelevanten Konzentrationsbereich
  Contract No.: GE 1011/4-1
- Kolloidgetragener Transport von Uran und anderen radiotoxischen Schwermetallen in toxischen Bergwerkswässern
  Contract No.: ZA 238/2-2
- In-situ Speziation von Uran in Biofilmen
  Contract No.: AR 584/1-1
- Sorptionsprozesse von Np(V) an Alumosilikaten. Schwingungsspektroskopische Untersuchungen
  Contract No.: FO 619/1-1
- In situ-Strukturuntersuchungen von Neptunium-Spezies in wässriger Lösung unter reduzierenden Bedingungen
  Contract No.: HE 2297/2-1

One project was supported by ***Deutscher Akademischer Austauschdienst (DAAD)***:

- Bakterielle S-Layer als Templat für die Bildung von metallischen Nano-Partikeln für nanotechnologische Anwendungen
  Contract No. D/04/39988

The ***North Atlantic Treaty Organisation (NATO)*** supported the following project:

- Investigation of the short-rage structure of layered double hydroxides and phyllosilicates by EXAFS: Development of wavelet analysis
  Contract No.: CBP.NR.CLG.981353

The ***University of Manchester, Department of Chemistry***, Great Britain supported one project:

- Access to beamtime at Rossendorf Beamline at ESRF in the frame of a scientific collaboration

The ***Gesellschaft für Anlagen und Reaktorsicherheit Braunschweig*** supported one project:

- Entwicklung einer thermodynamischen Referenzdatenbasis (Teilprojekt Spaltprodukte und Zement: THEREDA-SZ)
  Contract-No.: VA3252 - AN550550 - UA2671

INDEX OF AUTHORS